2007 R&D 100 AWARDS ENTRY FORM:

1. Submitting Organization

Organization	Ernest Orlando Lawrence Berkeley National Laboratory (LBNL)
Address	1 Cyclotron Road
City, State, Zip	Berkeley, CA 94720-8125
Country	USA
Submitter	Pamela Seidenman
Phone	510/486-6461
Fax	510/486-6457
E-mail	PSSeidenman@lbl.gov

AFFIRMATION: I affirm that all information submitted as a part of, or supplemental to, this entry is a fair and accurate representation of this product.

Submitter's signature: _____

2. Joint entry with:

N/A

3. Product name:

TOUGH+HYDRATE

4. Briefly describe (25 words or less) what the entry is (e.g. balance, camera, nuclear assay, etc.)

TOUGH+HYDRATE is the first computer program that models the process and estimates the amount of gas production from natural hydrate accumulations in the permafrost and oceanic subsurface.

5. When was this product first marketed or available for order? (Must have been available in 2006.)

This product was first available on a restricted basis to organizations conducting hydrate research and funded by the U.S. Department of Energy in May 2005. It was marketed and made commercially available in 2006. It has been licensed by many academic and government

organizations, and by Chevron, ConocoPhillips, Shell Oil Co., and ENI (the national oil company of Italy).

6. Inventor or Principal Developer (List all developers from all companies)

Developer Name	George J. Moridis
Position	Staff Scientist and Research Area Leader
Organization	Ernest Orlando Lawrence Berkeley National Laboratory
Address	1 Cyclotron Road
City, State, Zip	Berkeley, CA 94720
Country	USA
Phone	(510)486-4746
Fax	(510)486-5686
E-mail	GJMoridis@lbl.gov

Key Contributor	Michael B. Kowalsky
Position	Scientist
Organization	Ernest Orlando Lawrence Berkeley National Laboratory
Address	1 Cyclotron Road
City, State, Zip	Berkeley, CA 94720
Country	USA
Phone	(510)486-7314
Fax	(510)486-5686
E-mail	MBKowalsky@lbl.gov

7. Product price

(a) For organizations conducting hydrate research supported by the U.S. Department of Energy: No cost for source code and/or executable code.

(b) For non-profit organizations : No cost for executable code.

(c) For commercial and for-profit organizations: U.S. $10,000 for executable code, U.S. $30,000 for source code.

8. Do you hold any patents or patents pending on this product?

No—however, copyright protection for TOUGH+HYDRATE software has been registered with the United States Patent and Trademark Office.

9. Describe your product's primary function as clearly as possible. What does it do? How does it do it? What theories, if any, are involved?

At a time when conventional fossil-fuel energy resources are dwindling, gas hydrates—ice-like solid crystalline compounds in which gas molecules are lodged within the lattices of ice crystals (Figure 1)—are being considered as a potential source of energy. While there has been no systematic effort to map and evaluate the size of this resource (and current estimates vary widely, ranging between 10^{15} to 10^{18} m^3), the consensus is that the worldwide quantity of gas hydrates is vast. Gas hydrates are predicted to contain at least twice as much energy, even by the most conservative estimate, as all of the total known fossil fuel reserves recoverable by current methods. Thus, the attractiveness of hydrates, augmented by the environmental desirability of gas (as opposed to solid and liquid) fuels, is undeniable.

Figure 1. Natural hydrates (white within the subsurface sample) retrieved from the Mallik field tests in Canada

Currently, we cannot produce gas from methane hydrates. While vast amounts of methane hydrate deposits exist in the earth's subsurface (Figure 2), the commercial production of methane gas from these hydrate deposits has not been successful, because the methane encapsulated in the hydrate must first be dissociated from the hydrate before it can be released and produced from a well. The processes that take place during dissociation are numerous, complex, and interlinked. Because these complex interactions were not understood, it has been impossible until now to predict how and how much gas might be produced from these deposits. There has been no tool up to now that could comprehensively model the processes that occur during dissociation, and thus reliably predict the behavior of hydrate deposits during gas production.

The TOUGH+HYDRATE program (hereafter frequently referred to in the text as **T+H**) is just such an investigative tool. Developed by Berkeley Lab's Dr. George Moridis, it is the first computer program to provide the capability to investigate hydrate-bearing systems (i.e., the hydrate and the geologic sediments in which they occur) during the process of dissociation or

during the opposite process of hydrate formation. With the advent of T+H, it is now possible to predict the behavior of such systems and, in turn, predict the feasibility of methane production from hydrate deposits.

The availability and capabilities of T+H provide the necessary tools to determine—for the first

a.

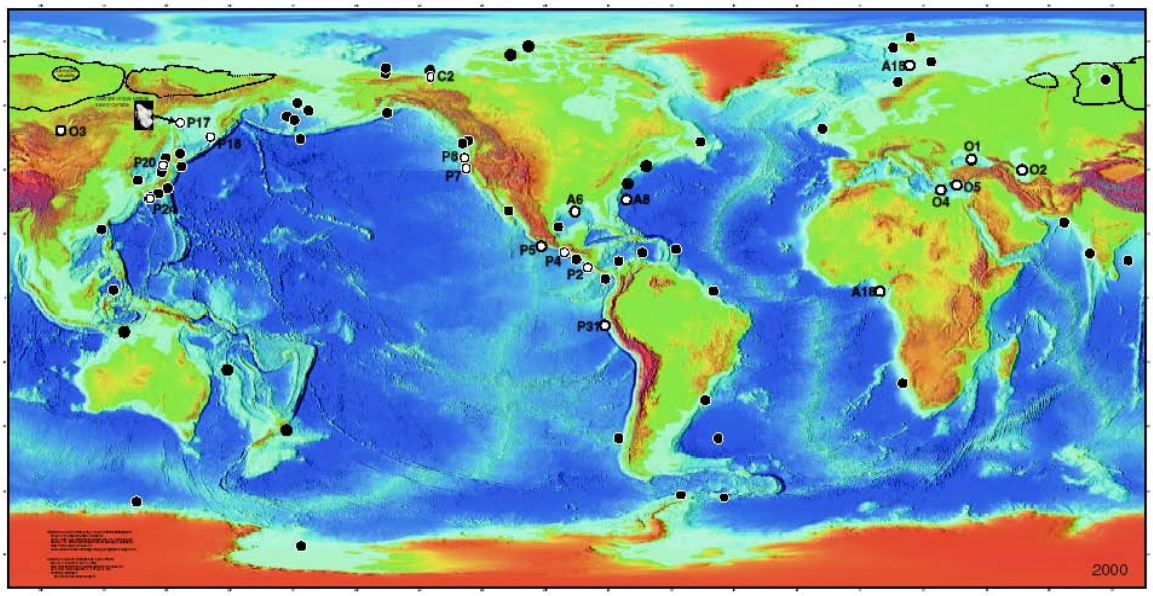

b.

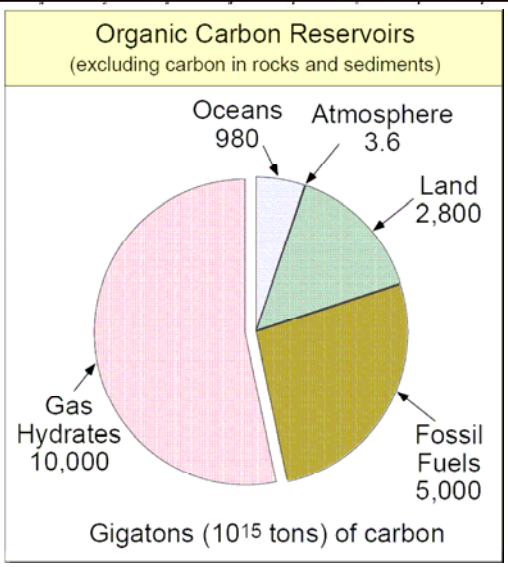

Figure 2. (a) Worldwide locations of hydrates, as confirmed from drilled wells (actual distribution of hydrates is known to be much wider), circles indicate location of hydrates; (b) Comparison of hydrate mass vs. the mass of all known fossil fuels (oil, gas, coal). T+H was the first program to allow the investigation of production from hydrates and unlock the potential of this enormous resource.

time—the technical feasibility of producing large amounts of methane from natural hydrates. As a consequence, this computer program has made accessible, and amenable to evaluation, a huge energy resource that was previously ignored and unexploited, for lack of knowledge about its behavior. The implementation of T+H has shown that production of large volumes of methane

from hydrate deposits is possible with current technology. Moreover, it has been able to determine the conditions and predict strategies to maximize production.

TOUGH+HYDRATE CAPABILITIES

TOUGH+HYDRATE is capable of modeling the following complex processes:

(1) The flow of methane and water through the porous medium in the subsurface. An example of such a flow is the arrival of these fluids at a production well. Additionally, the competition and interaction between gases and liquids during flow, as they move through the pores of the sediments that may also include solid hydrates and/or ice.

(2) The heat transfers that occur in the system. Several different methods of heat transfer occur simultaneously: heat conduction, heat carried by the moving fluids, heat changes due to chemical reactions, and heat changes due to H_2O state changes.

(3) The chemical reaction of hydrate dissociation into water and methane, and the opposite reaction of hydrate formation from water and methane. There are fifteen possible states of phase coexistence: the water and methane occur in various combinations of a gas phase, a liquid phase, and two solid phases: hydrate and ice. The program describes the pressure-temperature relationships in each of these states (Figure 3).

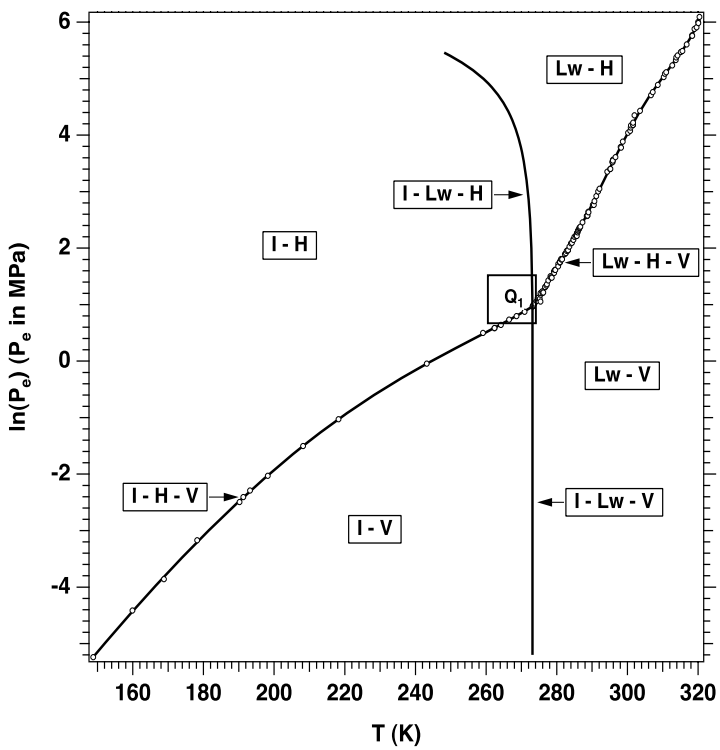

Figure 3. A phase diagram of one of the many hydrate dissociation processes that T+H is the first and only simulation program to capture: the pressure-temperature equilibrium relationship of the water-CH_4-hydrate system (Lw: liquid water, H: hydrate, V: vapor (i.e., gas phase), I: ice; Q_1: quadruple point [Lw +H+V+I]). This figure shows 9 (identified by rectangles) of the 15 possible phases captured by T+H, covering a wide pressure and temperature range.

(4). The physical properties of the hydrate. These include density, thermal conductivity, and energy and their dependencies on pressure and temperature, in addition to the relationship between the heat of dissociation and temperature.

(5) The properties of (a) the gas phase, and (b) of water in its various phases, i.e., vapor, liquid, and ice. These properties (e.g., density, viscosity, thermal conductivity, energy, latent heat, solubility of methane in water) are computed as functions of pressure and temperature.

(6) The effect of other materials on hydrate stability.

Importantly, all these processes are interdependent. Because of this, it is not possible to treat them separately. A predictive tool must account for all of them simultaneously. T+H was the first computer program to do this accurately. This capability allows the program (a) to verify the potential of the hydrates as an energy source (a mere hypothesis until now), (b) to investigate and predict the effectiveness of alternative methods to produce gas from hydrate deposits, and (c) to design well configurations and production processes to optimize fuel production. Figure 4 shows the rate of gas production from a single vertical well, as designed and investigated using T+H. In addition, Figure 4 shows the rate of methane release in the reservoir and depicts both the significant promise of hydrate deposits as an energy resource and the technical feasibility of recovering energy from them. Note that Figure 4 is the first such figure ever released, and was made possible only because of T+H.

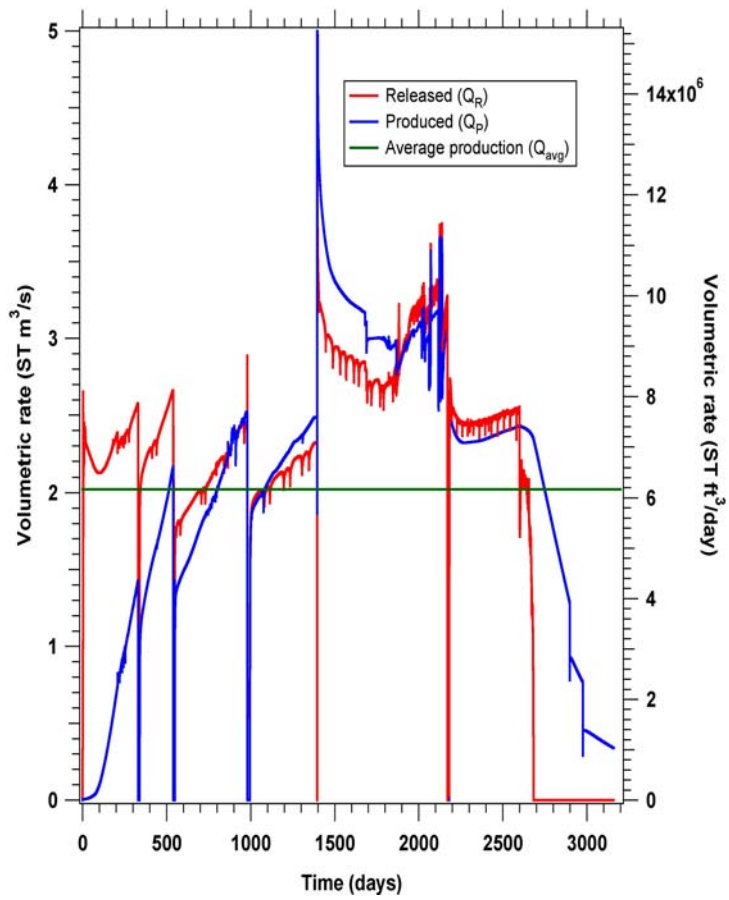

Figure 4. This is the first evidence of the very large gas production potential from hydrate deposits, made possible by the use of T+H. Shown are the rates of methane release in the reservoir (Q_R) and methane production at the well (Q_P) during production from a Class 2 (hydrate layer at the top, water zone underneath) permafrost hydrate deposit. The average production rate (Q_{avg}) over the simulation period (3160 days) is also shown.

TOUGH+HYDRATE VALIDATION, ACCOMPLISHMENTS, AND CONTRIBUTIONS

The TOUGH+HYDRATE code has met with significant success and wide acceptance in all the countries actively involved in hydrate research. In the period between May 2005 (when the code was first released to select research organizations) and September 15, 2006, noncommercial licenses for the T+H code had been granted to about 30 research organizations in 11 different countries (USA, Canada, UK, Germany, Italy, Japan, Russia, Turkey, Korea, Taiwan, India). Commercial licenses have also been granted to Chevron, ConocoPhillips, Shell Oil Co., and ENI (the national oil company of Italy). About 70 researchers worldwide are current users of T+H.

T+H was verified and validated against results from the Mallik field tests (Mackenzie Delta, Canada). The numerical predictions of the model turned out to be exceptionally close to the field observations. The accuracy of the model predictions is depicted in Figure 5, which shows their excellent agreement with the Mallik field data. This confirmed the validity of the processes modeled in the code, and allowed the determination of additional values for important parameters. In earlier work at Mallik, an earlier version of T+H was used to design the first-ever field test of gas production at the site (Figure 6), and analyze field tests results (Figure 7) with an unprecedented accuracy.

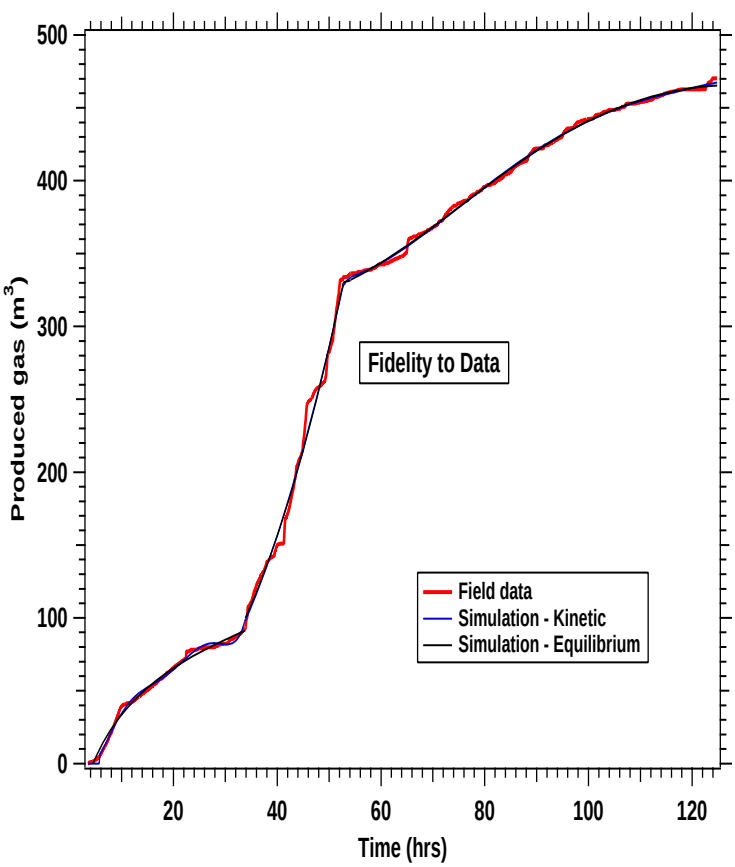

Figure 5. Comparison of field data (in red) and model predictions from the T+H code (with both an equilibrium and kinetic hydrate dissociation model). The proximity of observations and predictions validates the T+H model and provides evidence of its accuracy.

The Mallik work and other significant scientific advances made possible by T+H have been reported in numerous published journal papers (several of which can be found in Appendix C, Selected Scientific Publications). The following is a brief summary of the program's achievements.

Another earlier, experimental version of T+H was used to investigate, for the first time, potential gas production scenarios in the North Slope of Alaska from marine deposits and permafrost. The results suggested that these hydrate deposits have the potential of becoming significant sources of gas, and that gas production from permafrost hydrates was economically feasible. A 2004 review by the National Research Council of the National Academies of Science praised the Berkeley Lab hydrate project as "a small project with major technological impact" that "…incorporates the best independently measured physical property data into a fundamental reservoir model."

Figure 6. Flaring of the first gas produced entirely from hydrates during the Mallik field tests, which had been designed using T+H.

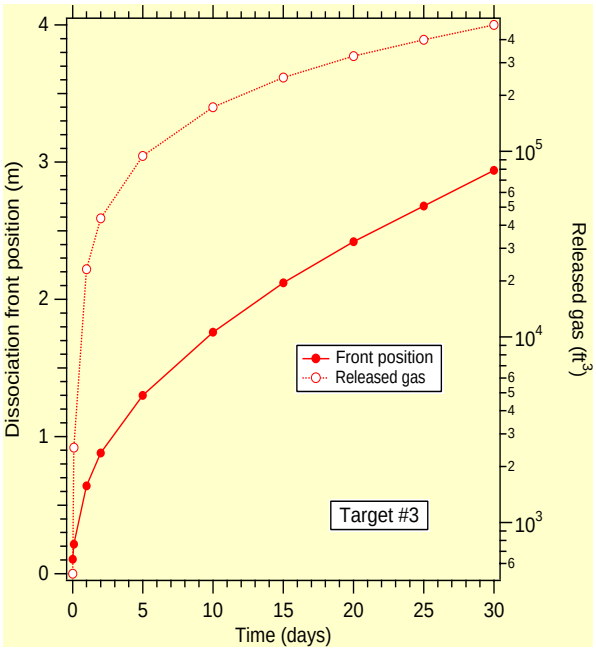

Figure 7. T+H predictions for the location of hydrate dissociation and released gas at the Mallik site. This figure was part of the design analysis, and was within an unprecedented 2% of field observations.

Accurate descriptions of the dissociation reaction within sediment pores were unknown before 2005, when Moridis and others used T+H and a set of laboratory data to analyze this reaction. This work showed that production of large volumes of methane from such deposits is possible with current technology, at high rates and over long times.

Also, natural hydrate samples, which are essential for laboratory research into the properties of hydrates, are very difficult to obtain. Hydrates exist under conditions alien to humans, and tend to become unstable and dissociate rapidly when exposed to a normal atmospheric pressure. To prevent dissociation, core samples containing hydrates must be preserved under pressure. Using T+H in a 2005 study, Moridis and others determined conclusively that, even under the best-

controlled conditions, only a small fraction of hydrates survive to the surface. These results indicated the need for retrieving pressurized cores and have served to define the conditions of the core acquisition process.

In 2005 and 2006, the T+H program was used to analyze, again for the first time, the methane production potential of specific oceanic deposits. This analysis demonstrated the limited production potential of such deposits, and are being used as guides by the Minerals Management Service of the U.S. Department of the Interior in the resource evaluation of oceanic hydrate deposits in the Gulf of Mexico.

Moreover, T+H has enabled scientists to study the extent to which oceanic hydrates (because of their instability) could interfere with offshore oil-drilling operations by fracturing geologic formations and possibly producing wellbore damage. These and other potentially harmful effects had been largely unknown, and none had been quantified, prior to these 2006 and 2007 studies based on T+H investigations.

10A. List your product's competitors by manufacturer, brand name and model number.

TOUGH+HYDRATE was the first model of its kind to be developed. Since its development and release, competing models have appeared. These include the following:

(1) **The MH21 Model**, developed by a Japanese consortium, with M. Kurihara of the Japan Oil Engineering Company as the lead developer. This code is proprietary, is not available for distribution, and its capabilities are unknown.

(2) The **STOMP-HYDRATE Model**, developed by Dr. Mark White of the Pacific Northwest National Laboratory (PNNL). This code has been shared with PNNL collaborators, but has seen limited public distribution.

(3) The **STARZ** commercial simulator, developed by the Canadian Modeling Group (CMG). The hydrate dissociation is not described by code specifically designed for the purpose. Instead, it is described by a generic chemical-reaction package. This code is proprietary, and is available for purchase or license.

(4) A semi-analytical model developed by Dr. Merhan Pooladi-Darvish of the University of Calgary. This in-house code (hereafter referred to as the MPD model) is proprietary and has not been distributed.

10B. Supply a matrix or table showing how the key features of your product compare to existing products or technologies. Include both numerical and descriptive comparisons.

System → / Feature ↓	**TOUGH+ HYDRATE**	*MH21*	*STOMP-H*	*STARZ*	*MPD*	**Competitive Advantage of TOUGH+HYDRATE**
Domain, coordinates and grids	1D, 2D, 3D Cartesian or cylindrical, structured or unstructured grids	1D, 2D, 3D Cartesian or cylindrical, structured grids only	1D, 2D, 3D Cartesian or cylindrical, structured grids only	1D, 2D, 3D Cartesian or cylindrical, structured grids only	2D, cylindrical coordinates, structured grids only	**Complete flexibility in describing any irregularly shaped formation in 1D, 2D or 3D, use of regular or irregular grids.**
Completeness of state description; Limitations in types of tractable problems	Describes the 15 possible states involving all coexistence scenarios of the four possible phases (gas, liquid, hydrate, ice) No problem limitations	Limited number of states; Limitations in range of tractable problems	Limited number of states (no possibility of liquid phase disappearance) Limitations in range of tractable problems	Limited number of states (no possibility of liquid phase disappearance or ice evolution) Limitations in range of tractable problems	Limited number of states, no possibility of liquid or gas phase disappearance Limitations in range of tractable problems	**Capable of describing the entire spectrum of possible conditions that can occur in a hydrate-bearing system;** **No limitation in type of tractable problems good summaries**
Expandability – coupling with ocean circulation and global climate models	Yes	No	No	No	No	**Can be used to determine greenhouse effects of marine hydrate dissociation on global climate**
Seamless inclusion of geomechanical effects	Yes	No	No	No	No	**Can fully describe geomechanical processes in hydrate-bearing media; can describe subsidence and fracturing of hydrate-bearing media**
Solution method (fully implicit vs. implicit-explicit); Property Updating CAN WE SAY THIS MORE SIMPLY? Perhaps "ability to handle dynamic processes"?	Fully implicit (can handle accurately and seamlessly extremely dynamic processes, e.g. phase changes; Continuous property/ parameter updating	Not known, possibly fully implicit	Fully implicit, continuous property and parameter updating	Implicit-explicit, leading to inaccuracies when dynamic processes such as phase changes and rapid dissociation occur	Semi-analytical, semi-constant parameters assumed	**Provides accurate solutions to even the most demanding problems**
Process description and approximations	Complete process description	Complete process description	Complete process description	Limited process description	Limited process description, important approximations	**Complete process description, no omissions or approximations of known processes**
Type of reaction (kinetic vs. equilibrium)	Kinetic and equilibrium	Kinetic only	Kinetic and equilibrium	Kinetic only	Kinetic only	**More options, enhanced stability and faster execution when reaction conditions approach equilibrium**
Types of Dissociation processes that can be modeled	Depressurization, thermal stimulation, inhibitor effects, any combination	Depressurization, thermal stimulation, limited combinations	Depressurization, thermal Stimulation, limited combinations	Depressurization, thermal stimulation, limited combinations	Depressurization only	**Can describe any combination of the possible dissociation mechanisms**
Availability, distribution and support	Available to the public (executable and/or source code), product support	Proprietary code, no public distribution, no support	Available to collaborating organizations, unknown level of product support	Proprietary code, public distribution, no hydrate-specific support	Proprietary in-house code, no public distribution, no support	**Only program that is enerally available to all researchers and fully supported**

10C. Describe how your product improves upon competitive products or technologies.

TOUGH+HYDRATE includes the following advantages over competing products:

- It can be used to describe any irregularly shaped domain such as those found in actual geologic formations. Flexibility in describing geometrical features is crucial, for example, in refining grids near reservoir production wells, or in incorporating topographic features (e.g., geological boundaries). Users of codes lacking geometrical flexibility must resort to uniformly spaced grids with extremely fine grid spacing, resulting in simulations that are computationally prohibitive.
- It can describe any of the 15 possible states of phase coexistence (i.e., combinations of the four possible phases: gas, liquid, hydrate, and/or ice). Thus, its application is not limited to specific classes of problems or geologic settings, and it can be used to describe any condition that may arise in the process of simulation, thus producing accurate scenarios.
- It describes all the known processes (physical, chemical, thermodynamic) that occur during hydrate dissociation/formation. That is, there is no approximation through the omission of any process. This provides a physically correct basis for the analysis of the hydrate problems at hand.
- It can be seamlessly integrated with a geomechanical model to describe the effect of hydrate dissociation/formation on the strength and integrity of the hydrate-bearing sediment. This is a unique capability of T+H, providing a means by which to investigate how best to locate and anchor structures, such as production platforms, on the ocean floor.
- By using a fully implicit formulation, it can accurately describe all the complex interacting processes that occur during hydrate dissociation/formation. Without fully implicit formulation (e.g., by limiting the simultaneous solution to a subset of the original equations), inaccurate solutions are almost inevitable, given the strongly dynamic nature of the hydrate dissociation/formation process.
- It is available to the public (source code and executable). Its distribution is on a no-cost basis to any nonprofit organization conducting hydrate research, while commercial outfits are charged a relatively low fee for the executable and the source code.
- Its distribution is accompanied by code support proffered by the program development team.

11A. Describe the principal applications of this product.

Assessment of Gas Production from Natural Hydrate Deposits

The main application of TOUGH+HYDRATE (and the main reason underlying its development) is for determining the technical feasibility of producing methane from a wide variety of hydrate deposits in a range of geological formations. Having established the technical feasibility through simulation studies, T+H was and is used for the following purposes:

(a) Design of well configurations, production strategies, and methods to maximize gas production from the various types of deposits in a wide range of geological systems;

(b) Design of laboratory and field tests; and

(c) Sensitivity analysis to determine the dominant processes and parameters in laboratory and field studies (without these types of studies, it would not be possible to design production strategies).

One of the most important contributions of the T+H model is that it opened up for evaluation and exploration a potentially huge energy resource, one that had been ignored up to now for lack of appropriate analytical tools. Exploitation of this resource may have tremendous economic and energy security implications, in addition to providing an environmentally "cleaner" form of energy.

11B. List all other applications for which your product can now be used.

Prediction of Geomechanical Stability of Oceanic Hydrate Deposits

Before **TOUGH+HYDRATE**, the available information was insufficient for designing seafloor platforms or wells in the vicinity of hydrate deposits—considering the safety, environmental, and economic risks posed by unstable seafloor behavior. By coupling T+H with a geomechanical model, we developed a computational tool that allows us to determine the envelope of safe conditions (a) when locating and operating an offshore production platform, (b) for production from gas hydrates, and (c) for evaluation of the performance and structural integrity of wellbore assembly systems in hydrate deposits under stress.

Interrelation between Global Climate and Oceanic Hydrate Accumulations

Vast amounts of methane are trapped in oceanic hydrate deposits. Because methane is a formidable greenhouse gas (about 26 times more powerful in trapping heat than CO_2), there is considerable concern that a rise in ocean water temperature will induce dissociation of oceanic hydrates, potentially releasing very large amounts of CH_4 (methane) into the atmosphere. Such a release could have dramatic climatic consequences, because it could lead to further atmospheric and oceanic warming and accelerate dissociation of the remaining hydrates.

By coupling T+H with a geochemical/biochemical model of ocean warming, and an ocean circulation and global climate model, we are developing a model that can assess the role of dissociating hydrates in contributing to climate change.

12. Summary. State in layman's terms why you feel your product should receive an R&D 100 Award. Why is it important to have this product? What benefits will it provide?

As domestic demand for energy continues to rise, so does our dependence on imported sources of energy, and our need to find alternatives. Recent studies have shown that methane hydrates, previously overlooked, could be an important new source of energy. Frozen compounds of flammable methane gas trapped inside water molecules, methane hydrates were once believed to exist only on the outskirts of the solar system. Over the last 20 years, however, large formations of methane hydrates have been discovered within the earth, and in deepwater marine and permafrost sediment. If this resource were to be recoverable on a large scale, it could more than double the U.S. natural gas resource base.

The availability of TOUGH+HYDRATE has made investigating the feasibility of methane production from hydrates possible. It has also provided a tool by which to design the processes and facilities needed to facilitate and optimize production. As stated in one of the letters of support for this submission, by E.D. Sloan, Director of the Center for Research on Hydrates at the Colorado School of Mines, “Hydrate deposits will play a significant role in world energy security. Countries like China, Japan, India, and the USA have multimillion dollar hydrate related projects to make gas production from hydrate deposits a reality in the next 10 years.” Because of TOUGH+HYDRATE, we can finally assess the vast potential of methane hydrates and determine the path forward in our exploration of this energy source.

ORGANIZATION DATA

13. Contact person to handle all arrangements on exhibits, banquet, and publicity.

Name	Pamela Seidenman
Position	Marketing Manager, Technology Transfer
Organization	Ernest Orlando Lawrence Berkeley National Laboratory (LBNL)
Address	1 Cyclotron Road, 90R1070
City, State, Zip	Berkeley, CA 94720-8125
Country	USA
Phone	510/486-6461
Fax	510/486-6457
E-mail	PSSeidenman@lbl.gov

Appendix
List of Attachments
2007 R&D 100 AWARDS
ENTRY—TOUGH+HYDRATE (Berkeley Lab)

A. Letters of Support

- Center for Research on Hydrates and Other Solids, Colorado School of Mines
- National Energy Technology Laboratory
- Chevron Energy Technology Company
- U.S. Geological Survey

B. Technical Notes

- TOUGH+HYDRATE: Physical Basis, Mathematical Representation, and Solution Approach
- About Gas Hydrates
- Hydrates and the Environment

C. Selected Scientific Publications

- Moridis, G.J., T.S. Collett, S.R. Dallimore, T. Satoh, S. Hancock, and B. Weatherill, Numerical Studies of Gas Production from Several CH4 Hydrate Zones at the Mallik Site, Mackenzie Delta, Canada, Journal of Petroleum Science and Engineering (Elsevier), 43, 219–238, 2004.
- Moridis, G.J., Numerical Studies of Gas Production from Class 2 and Class 3 Hydrate Accumulations at the Mallik Site, Mackenzie Delta, Canada, SPE 88039, SPE Reservoir Evaluation & Engineering, 2004.
- Moridis, G.J., M. B. Kowalsky, and K. Pruess, Depressurization-Induced Gas Production from Class 1 Hydrate Deposits, SPE 97266, Journal of the Society of Petroleum Engineers, October 9–12, 2005.
- Moridis, G.J., and M.B. Kowalsky, Response of Oceanic Hydrate-Bearing Sediments to Thermal Stresses, OTC 18193, Publication of the Offshore Technology Conference, May 1–4, 2006.
- Moridis, G.J., and M.B. Kowalsky, Gas Production from Unconfined Class 2 Hydrate Accumulations in the Oceanic Subsurface, In: Economic Geology of Natural Gas Hydrate, M.D.Max, A.H. Johnson, and W.P. Dillon, eds., Coastal Systems and Continental Margins series, Springer, The Netherlands, pp. 249–266, 2006.

D. Selected Press Coverage

- "Gas Hydrate Resource: Smaller But Sooner," Science, February 13, 2004
- "From Athens to Mallik—In the Name of Science," NETL Methane Hydrate Newsletter, Winter 2004.
- "Model Evaluates Production Potential of Methane Hydrates," Energy & Petrochem Engineering Standards News, April 21, 2006
- "The National Methane Hydrates R&D Program," DOE/NETL Projects, August, 2006.
- "TOUGH-Fx/HYDRATE V2.4 Announcement," NETL Methane Hydrate Newsletter, Spring 2005.
- "Workshop on Integrating Modeling and USGS Laboratory Studies of Gas Hydrates," USGS Sound Waves Monthly Newsletter, September 2005.

2007 R&D 100 AWARDS
ENTRY—TOUGH+HYDRATE (Berkeley Lab)

Appendix A

Letters of Support

Center for Research on Hydrates and Other Solids, Colorado School of Mines

National Energy Technology Laboratory

Chevron Energy Technology Company

U.S. Geological Survey

E. Dendy Sloan, Jr., Director
Center for Research on Hydrates
Colorado School of Mines
Golden, Colorado 80401-1887
303 273-3723 FAX 303 273-3730
esloan@mines.edu
www.mines.edu/research/chs

January 30, 2007

% Ms. Pamela Seidenman
Lawrence Berkeley Laboratory
1 Cyclotron Road
Berkeley, California 94720-8125

RE: Nomination of numerical simulator, TOUGH-Fx/HYDRATE for the RD100 award

Dear Members of the 2006 RD100 Award Selection Committee,

My highest recommendation goes to the innovative numerical simulator, TOUGH-Fx/HYDRATE, developed by Dr. George. J. Moridis. This unique program enables both industry and researchers to develop methane hydrates – the largest natural gas resource.

Natural hydrate deposits contain twice as much methane as the remainder of the fossil fuel reserves. Hydrate deposits will play a significant role in world energy security. Countries like China, Japan, India, and the USA have multimillion dollar hydrate related projects to make gas production from hydrate deposits a reality in next 10 years.

TOUGH-Fx/HYDRATE is the most sophisticated numerical simulator available to enable gas production from hydrate reservoirs. TOUGH-Fx/HYDRATE simulates the behavior of hydrate-bearing geological systems and enables evaluation of production strategies and economic viabilities of the hydrate-related projects.

The strength of the code lies in its wide-ranging application from laboratory to reservoir scale studies. According to the US Department of Energy, the TOUGH-Fx/HYDRATE program is used by 25 academic and industrial organizations in 11 countries.

In summary, I strongly support and endorse nomination of TOUGH-Fx/HYDRATE for 2006 R&D 100 awards. Please contact me if I can provide any further information. Thank you for the opportunity to write this letter on behalf of Dr. Moridis and his useful TOUGH-Fx/HYDRATE invention.

Best Wishes,

E. D. Sloan, Jr.
Weaver Distinguished Professor,
Director of Center for Hydrate Research,

U.S. Department of Energy

National Energy Technology Laboratory

January 26, 2007

RD 100 Award Selection Committee
ATTN: Ms. Pamela Seidenman
Marketing Manager, Technology Transfer
Lawrence Berkeley National Lab
One Cyclotron Road, MS 90-1070
Berkeley, CA 94720

Dear RD 100 Award Committee Members:

We are writing in regards to the nomination of Lawrence Berkley National Laboratory's (LBNL) TOUGH+/HYDRATE reservoir simulator for an RD 100 award in 2007.

TOUGH+/HYDRATE is an innovative simulation program developed by LBNL over the past four years with funding from the U.S. Department of Energy (DOE). The first publicly available simulator of its kind, the TOUGH+/HYDRATE program allows researchers and industry to better understand an emerging natural gas resource: methane hydrates. Methane hydrate systems are currently the subject of great interest worldwide because of their potential as a future energy resource and their possible role in global climate change throughout time.

TOUGH+/HYDRATE's strength lies in its wide-ranging scope, scale, and applicability. The model can be used by laboratory scientists for fundamental research from the molecular to the reservoir level. It can also be run by industrial operators to conduct large-scale production studies using actual field data.

Since its public release in 2005, there has been considerable interest in TOUGH+/HYDRATE, both domestically and abroad. Program licenses have been granted to over 25 non-commercial organizations in 11 countries. Two major oil and gas companies have also purchased licenses-the first steps into industry application. In all, more than 80 researchers are estimated to now have access to the TOUGH+/HYDRATE program.

Prompted by the Methane Hydrate R&D Act, DOE's Methane Hydrate R&D Program has funded LBNL's development of the simulator since 2002. Already the most advanced reservoir simulator dedicated specifically to methane hydrates, TOUGH+/HYDRATE is slated for ongoing support and development through 2007.

Sincerely,

Kelly Rose
Office of Research & Development
National Energy Technology Laboratory

Ray Boswell, PhD
Methane Hydrates Technology Manager
National Energy Technology Laboratory

3610 Collins Ferry Road, P.O. Box 880, Morgantown, WV 26507

Emrys Jones, Ph.D.
Research Consultant

Chevron Energy
Technology Company
100 Chevron Way, 10-3453
Richmond, CA 94802
Tel 510 242 1006
EJones@chevron.com

January 25, 2007

R & D 100 Award Selection Committee
c/o Ms. Pamela Seideman
Marketing Manager, Technology Transfer
Lawrence Berkeley National Laboratory
One Cyclotron Road, MS 90-1070
Berkeley, CA 94720

Dear R & D 100 Award Selection Committee:

I am pleased to write this letter to support the nomination of the TOUGH-Fx/HYDRATE code for the R & D 100 Award. Chevron has been active member of the Gulf of Mexico (GOM) Hydrate Joint Industry Project (JIP), in collaboration with NETL/DOE. The JIP participants consist of major oil and gas producers and service companies, such as ConocoPhillips, Halliburton, JOGMEC, Reliance Industries Ltd., Schlumberger, TOTAL and another federal agency the Mineral Management Service (MMS) .

As chairman of this JIP, we are committed to steering technology advances through collaborative research. One of the outcomes of the DOE sponsored research is the successful development and implementation of the Hydrate model in TOUGH-Fx simulator by the dedicated scientists at the Lawrence Berkeley National Laboratory (LBNL). To date, this is the only simulator endorsed by the DOE and used by multiple industrial companies including Chevron.

Briefly, this simulator uses fully implicit formulation to model non-isothermal hydrate reaction, phase behavior, fluid flow, and heat transfer in complex methane hydrate deposits in geologic formation. It includes both equilibrium and kinetic models of hydrate formation and dissociation. The model accounts for heat and up to four mass components (water, methane, hydrate, and water-soluble inhibitors such as salts or alcohols) that are partitioned among four possible phases, namely gas, liquid, ice, and hydrate. Furthermore, the code can handle any of the possible hydrate dissociation mechanisms including depressurization, thermal stimulation, and inhibitor-induced effects.

Simulation is an essential part of the field development studies. It is probably the least expensive way to scope projects and conduct feasibility study. Needless to mention with ample uncertainties in geological models, flow simulation is one way if not the only way to identify major uncertainties and provide a range of production forecast. Hence, a reliable simulator with accurate representation of the physics of hydrate dissociation and formation coupled with an efficient algorithm to solve multi-phase multi-component systems is needed to advance methane gas production modeling of hydrate formations. The TOUGH-Fx/HYDRATE code is well known and well thought of among the hydrate community. And I believe TOUGH-Fx/HYDRATE code deserves such praise and your favorable consideration is much appreciated.

Please do not hesitate to contact me if you have any questions.

Sincerely,

Emrys Jones, Ph.D.
Research Consultant, Chevron Energy Technology Company

United States Department of the Interior
U.S. Geological Survey

In Reply Refer To:
Mail Stop 939

January 28, 2007

C/O: Dr. George Moridis
Research Area Leader, Transport and Thermodynamics
Lawrence Berkeley National Laboratory
University of California
Earth Sciences Division
1 Cyclotron Rd., MS 90-1116
Berkeley, CA 94720, USA

Dear Committee Members:

I was pleased when I was informed that Lawrence Berkeley National Laboratory had decided to submit the TOUGH-Fx/HYDRATE computer code as one of its five annual entries for the R&D100 Awards. I was also humbled when I was asked to provide a letter of support for this nomination. I would like to take this opportunity to strongly support the nomination of the TOUGH-Fx/HYDRATE computer code for the R&D100 Awards.

Over the last 25 years, I have the good fortune to participate and in several cases manage some of the most important gas hydrate research and development programs in the World. With a highlight being the Co-Chief Scientist of the Mallik 2002 Gas Hydrate Production Research Program, which featured the use of an earlier version of the TOUGH-Fx/HYDRATE computer code to design the Mallik production testing program.

Gas hydrates, an ice-like mixture of natural gas and water, are believed to contain more potential energy than all of the other known fossil fuels in the World. However, very little is known about how to produce this vast untapped energy resource. The TOUGH-Fx/HYDRATE computer code and its predecessors were the first and still the most advanced computer code available to predict the response of in-situ gas hydrate to external changes. In the case of the Mallik 2002 effort, the code was used to predict how the inferred in-situ gas hydrate accumulation at Mallik would respond to temperature and pressure stimulation. These predictions were used to design the Mallik 2002 testing program, the cost of which exceeded 16 million USD. The Mallik 2002 test results were than used to further develop and calibrate the TOUGH-Fx/HYDRATE computer code. Since this effort, the calibrated TOUGH-Fx/HYDRATE computer code has been used in projects ranging from Alaska, the Gulf of Mexico, China, and many other countries to evaluate the producibility of delineated gas hydrate accumulations.

I again greatly appreciate the opportunity to support the nomination of the TOUGH-Fx/HYDRATE computer code for the R&D100 Awards.

Sincerely,

Timothy S. Collett
Confirmed Signature 01/28/07

Dr. Timothy S. Collett
US Geological Survey
Denver Federal Center, MS-939
Box 25046
Denver, Colorado 80225 USA
Email tcollett@usgs.gov

2007 R&D 100 AWARDS
ENTRY—TOUGH+HYDRATE (Berkeley Lab)

Appendix B

Technical Notes

TOUGH+HYDRATE: Physical Basis, Mathematical Representation, and Solution Approach

About Gas Hydrates

Hydrates and the Environment

TOUGH+HYDRATE: PHYSICAL BASIS, MATHEMATICAL REPRESENTATION, AND SOLUTION APPROACH

George Moridis

Lawrence Berkeley National Laboratory

TOUGH+HYDRATE (**T+H)** accounts for all the processes that occur during hydrate dissociation and/or formation. These processes are well-known physical phenomena that have been investigated in theoretical analyses, laboratory settings and/or field tests, and are described mathematically as functions of several parameters and conditions.

For example, in **T+H**, the flow of fluids (liquids or gases) through porous media is described by the Darcy equation, which has been developed and verified in theoretical, laboratory, and field studies. According to this equation, the flow of a fluid between two points is a function of the pressure difference between these two points within a porous medium (e.g., a sediment), the characteristics of the sediment (how permeable and porous it is), and the properties of the fluid (how dense and how viscous it is). The interaction of the gas and liquid flow within the same pores is described by a "relative permeability" function, which is related to the fraction of the pore space occupied by the fluid, the pore characteristics, and the other phases in the pores. The description of the 15 states of phase coexistence is based on pressure-temperature relationships that define the range of phase coexistence (see Figure 3).

Similarly, all the processes described in the previous section have mathematical representations (expressed in equations) involving relationships between various parameters. These equations are all included in **T+H**, which predicts the system behavior by solving simultaneously the equations of mass and heat balance. These are based on the simple principle that the total mass and energy within a closed system are conserved, and the state of the system at any time and place is defined by how mass and energy are distributed. In other words, given a certain mass of methane and water and a certain energy content, the system is uniquely defined. Any change in the total mass and/or energy in the system will be reflected in changes in the composition and/or state.

Within **T+H**, mass-balance equations represent each one of the substances, i.e., methane, water and heat (and possibly salt). Each mass-balance equation involves the flow through, and accumulation in, any given part of the system. The heat-balance equation sums up the heat changes caused by the flow of fluids, by conduction, and by the heat exchanged during phase changes and/or dissociation.

The strong interdependence of the various processes makes it difficult (if not impossible) to address each one of them independently (or in groups) and to combine the results. Such an approach involves significant approximations and is inherently inaccurate. To obtain an accurate solution, we need to maintain the interdependence of processes—accomplished by accounting simultaneously (as **T+H** does) for all these processes in the balance equations, in an approach that is called a "fully implicit solution."

ABOUT GAS HYDRATES

George Moridis

Lawrence Berkeley National Laboratory

Gas hydrates are ice-like solid crystalline compounds in which gas molecules (referred to as guests) are lodged within the lattices of ice crystals (called hosts). Under suitable conditions of low temperature and high pressure, a gas will react with water to form hydrates. Of particular interest are hydrates formed by hydrocarbon gases. Natural hydrates deposits are composed mainly of methane, a valuable energy source. Methane hydrates have the appearance of ice, but they can be much warmer. When they dissociate (decompose), they provide water and methane. Thus, it is possible to set these ice-like substances on fire that is fueled by the methane, and which releases remarkably cold water.

Such deposits occur in two distinctly different geologic settings where the necessary favorable pressure and temperature conditions exist for their formation and stability: in the permafrost and in deep ocean sediments. The hydrates in the permafrost were created during the last ice age (which lasts until today), when natural gas reservoirs became progressively cooler. As this happened, the combination of high pressure and low temperature evolved into the conditions that promote the reaction of water and methane to form hydrates. The mechanism of hydrate formation in the oceans is very different. There, hydrates are formed when methane (that is produced deeper in the subsurface from biological reactions or from escaping gas reservoirs) rises toward the ocean floor and combines with the ocean water when the pressure and temperature are amenable to such a reaction.

Although there has been no systematic effort to map and evaluate this resource and current estimates vary widely (ranging between 10^{15} to 10^{18} m^3), the consensus is that the worldwide quantity of hydrocarbon gas hydrates is vast. Even the most conservative estimate surpasses by a factor of two the energy content of the total known fossil fuel reserves recoverable by conventional methods. The sheer magnitude of this resource commands attention as a potential energy resource, even if a limited number of hydrate deposits are attractive production targets and/or only a fraction of the trapped gas may be recoverable. Even if the move to a “hydrogen economy” (i.e., involving the use of hydrogen rather than carbon-based fuels as an energy resource) becomes a reality, methane production from hydrates remains an attractive proposition as a prime source for hydrogen. This is because the energy needed for electrolysis (i.e., breaking down water into its constituents hydrogen and oxygen) far exceeds that needed to strip the hydrogen from the methane.

Gas from hydrates is produced by inducing dissociation (i.e., decomposition) by one of the following three main methods (or combinations thereof):

(1) Depressurization, which involves lowering the pressure below the equilibrium hydration pressure (i.e., the pressure at which hydrates are stable at the

prevailing temperature). This can be accomplished by withdrawing fluids from a hydrate deposit.

(2) Thermal stimulation, in which the temperature is raised above the equilibrium hydration temperature (i.e., the temperature at which hydrates are stable at the prevailing pressure). This can be accomplished by heating the hydrate, e.g., by injecting hot water.

(3) The use of hydration inhibitors (such as salts and alcohols). Inhibitors are substances that destabilize the hydrates and lead to their dissociation.

Although the methods to destabilize hydrates have been known for several decades, there was no quantitative tool before **TOUGH+HYDRATE** to investigate gas production from natural hydrate deposits in the permafrost or in the oceans, and their behavior during any such attempt was unknown.

Note that many processes occurring within hydrates are coupled, i.e., dependent on each other. For example, hydrate dissociation releases methane, and leads to higher pressures. Additionally, the dissociation reaction requires heat to proceed. This heat is absorbed from its surroundings, and leads to cooling. The evolution of gas reduces the flow of water because some of the pore space is now occupied by gas. If the cooling is very strong, it is possible to drop the temperature so much that ice forms. The formation of ice can drastically affect the flow behavior. The cooling affects the properties of all the phases (liquid, gas, hydrate and ice), which in turn modify the flow behavior. Meanwhile, the lower temperature and higher pressure affect the solubility of methane in the water (also affected by the rising temperature). If ice is formed, the latent heat of fusion (i.e., the energy released as water turns into ice) stabilizes the temperature (albeit temporarily). Because dissociation has resulted in a lower temperature and a higher pressure, it is more difficult to continue at a constant pace, and it slows down until more heat (flowing from the surroundings) becomes available.

If an inhibitor (such as salt) is present in the system, then the situation becomes even more complicated. The presence of salt reduces the solubility of methane in the water, so gas evolves easier. Additionally, the effect of the inhibitor is to destabilize the hydrate, allowing easier dissociation, i.e., at a higher pressure or lower temperature than what happens without salt. However, large amounts of fresh water are released during dissociation (when the water trapped in the solid hydrate is freed), which dilutes the salt and attenuates its strong effect on hydrate stability. Thus, as the water becomes progressively less salty, it becomes more difficult to induce hydrate dissociation. Conversely, if hydrate is formed in salty water (e.g., the ocean), it expels salt and makes the surrounding water saltier. This is turn inhibits further hydrate formation.

HYDRATES AND THE ENVIRONMENT

George Moridis

Lawrence Berkeley National Laboratory

Even when no gas is produced is produced from hydrates, their response is very important when heat from hot reservoir fluids (produced from deeper reservoirs) flows into the hydrates through uninsulated pipes. Even before dissociation, the rising temperature weakens the mechanical strength of the hydrate-bearing sediments. When dissociation begins, the rapid release of large amounts of gas can result in high pressures that can fracture the geologic formation and its boundaries, and can even lead to wellbore damage. Additionally, the loss of hydrate (a very strong cementing agent) during dissociation can lead to the deterioration of the structural stability of the geologic formation in the vicinity of the wellbore and substantial subsidence, with possibly catastrophic consequences on the wellbore assembly (the substantial weight of which cannot be supported by the sediment which has a "soupy" consistency after dissociation). Finally, during dissociation, the base of the gas hydrate becomes under-consolidated and possibly over-pressurized because of the newly released gas, leading to a zone of weakness that can result in submarine landslides. Several of these effects were unknown, and none had been quantified prior to the study of *Moridis and Kowalsky* [2006] that was based on **TOUGH+HYDRATE (T+H)** investigations.

This work was significantly expanded with the coupling of **T+H** with a commercial state-of-the-art geomechanical model [*Rutqvist and Moridis*, 2007] to predict the interrelationship between (a) changes in pressure, temperature and saturation of the hydrate-bearing sediment and (b) changes in the permeability, porosity and strength of the system, which, under certain conditions, can lead to substantial subsidence, fracturing, and oceanic landslides. The general perception of instability of hydrate-bearing sediments, coupled with the lack of knowledge on the overall geomechanical behavior of such sediments, have resulted in a general strategy of avoidance of such sediments when locating offshore production platforms (considering the tremendous safety, environmental, and economic risks posed by unstable seafloor behavior), and are certain to impede the development of hydrate deposits as gas production targets. By locating production platforms at sites not selected for optimum operation but dictated by the need to avoid the hydrate accumulations, the cost of production can increase significantly. The new coupled program is the first of its kind, and can be used to determine the envelope of safe conditions when locating and operating an offshore production platform for either conventional oil or gas production, or for production from gas hydrates. This knowledge also provides the necessary tools to evaluate the expected stability performance of hydrate-bearing sediments, and to select optimal sites for production facility installation.

Because of the vast amounts of methane trapped in ocean hydrates and the fact that methane is a powerful greenhouse gas (about 26 times more effective than CO_2), there is considerable concern that a rise in the temperature of the ocean water will induce dissociation of oceanic hydrate accumulations, potentially releasing very large amounts

of methane into the atmosphere. Such a release could have dramatic climatic consequences because it could lead to cascading effects including further atmospheric and oceanic warming and amplification of the problem by accelerating dissociation of the remaining hydrates. The Clathrate Gun Hypothesis (stipulating that the global reservoir of marine hydrates undergoes repeated cycles of reloading and discharge, accumulating during cold glacial intervals and dissociating when temperatures rise) has been proposed as the main culprit for a repeated, remarkably rapid sequence of global warming effects that occurred in less than one human life span during the late Quaternary period. By coupling **T+H** with (a) a code describing the geochemical and biochemical reactions that follow the release of methane in the oceanic sediments after dissociation, and (b) the Parallel Ocean Program (POP), a 3D, global-scale ocean general circulation model that is used as the ocean component of the Community Climate System Model (based at the National Center for Atmospheric Research), it is possible to (1) investigate the effect of rising water temperatures on the stability of oceanic hydrate accumulations and to determine the conditions under which CH_4 releases are likely to occur, (2) to estimate the global quantity of hydrate-originating carbon that could reach the upper atmosphere, (3) to quantify the interrelationship between hydrate-originating carbon (CH_4 and CO_2) and global climate, and (4) to test the Clathrate Gun Hypothesis. This work is currently in progress.

Moridis, G., and M.B. Kowalsky, Response of Oceanic Hydrate-Bearing Sediments to Thermal Stresses, *OTC 18193* (in press), Publication of the Offshore Technology Conference, Society of Petroleum Engineers, 2007.

Rutqvist, J. and G.J. Moridis, Numerical Studies of Geomechanical Stability of Hydrate-Bearing Sediments, *OTC 18860* (in press), Publication of the Offshore Technology Conference, Society of Petroleum Engineers, 2007.

2007 R&D 100 AWARDS
ENTRY—TOUGH+HYDRATE (Berkeley Lab)

Appendix C

Selected Scientific Publications

Moridis, G.J., T.S. Collett, S.R. Dallimore, T. Satoh, S. Hancock, and B. Weatherill, Numerical Studies of Gas Production from Several CH4 Hydrate Zones at the Mallik Site, Mackenzie Delta, Canada, Journal of Petroleum Science and Engineering (Elsevier), 43, 219–238, 2004.

Moridis, G.J., Numerical Studies of Gas Production from Class 2 and Class 3 Hydrate Accumulations at the Mallik Site, Mackenzie Delta, Canada, SPE 88039, SPE Reservoir Evaluation & Engineering, 2004.

Moridis, G.J., M. B. Kowalsky, and K. Pruess, Depressurization-Induced Gas Production from Class 1 Hydrate Deposits, SPE 97266, Journal of the Society of Petroleum Engineers, October 9–12, 2005.

Moridis, G.J., and M.B. Kowalsky, Response of Oceanic Hydrate-Bearing Sediments to Thermal Stresses, OTC 18193, Publication of the Offshore Technology Conference, May 1–4, 2006.

Moridis, G.J., and M.B. Kowalsky, Gas Production from Unconfined Class 2 Hydrate Accumulations in the Oceanic Subsurface, In: Economic Geology of Natural Gas Hydrate, M.D.Max, A.H. Johnson, and W.P. Dillon, eds., Coastal Systems and Continental Margins series, Springer, The Netherlands, pp. 249–266, 2006.

Available online at www.sciencedirect.com
SCIENCE DIRECT®
Journal of Petroleum Science and Engineering 43 (2004) 219–238
JOURNAL OF PETROLEUM SCIENCE & ENGINEERING
www.elsevier.com/locate/petrol

Numerical studies of gas production from several CH_4 hydrate zones at the Mallik site, Mackenzie Delta, Canada

George J. Moridis[a,*], Timothy S. Collett[b], Scott R. Dallimore[c], Tohru Satoh[d], Steven Hancock[e], Brian Weatherill[e]

[a] *Earth Sciences Division, Lawrence Berkeley National Laboratory, University of California, 1 Cyclotron Road, Berkeley, CA 94720, USA*
[b] *United States Geological Survey, Denver, CO 80225-0046, USA*
[c] *Geological Survey of Canada, Sidney, British Columbia, Canada V8L 4B2*
[d] *Japan National Oil Corporation, Chiba 261-0025, Japan*
[e] *Adams Pearson Associates Inc., Calgary, Alberta, Canada T2P 3T6*

Received 30 August 2002; accepted 10 February 2004

Abstract

The Mallik site represents an onshore permafrost-associated gas hydrate accumulation in the Mackenzie Delta, Northwest Territories, Canada. A gas hydrate research well was drilled at the site in 1998. The objective of this study is the analysis of various gas production scenarios from five methane hydrate-bearing zones at the Mallik site. In Zone #1, numerical simulations using the EOSHYDR2 model indicated that gas production from hydrates at the Mallik site was possible by depressurizing a thin free gas zone at the base of the hydrate stability field. Horizontal wells appeared to have a slight advantage over vertical wells, while multiwell systems involving a combination of depressurization and thermal stimulation offered superior performance, especially when a hot noncondensible gas was injected. Zone #2, which involved a gas hydrate layer with an underlying aquifer, could yield significant amounts of gas originating entirely from gas hydrates, the volumes of which increased with the production rate. However, large amounts of water were also produced. Zones #3, #4 and #5 were lithologically isolated gas hydrate-bearing deposits with no underlying zones of mobile gas or water. In these zones, thermal stimulation by circulating hot water in the well was used to induce dissociation. Sensitivity studies indicated that the methane release from the hydrate accumulations increased with the gas hydrate saturation, the initial formation temperature, the temperature of the circulating water in the well, and the formation thermal conductivity. Methane production appears to be less sensitive to the specific heat of the rock and of the hydrate, and to the permeability of the formation.
© 2004 Published by Elsevier B.V.

Keywords: Gas hydrates; Hydrate dissociation; Depressurization; Thermal stimulation; Numerical modeling

1. Introduction

1.1. Background

Gas hydrates are crystalline substances composed of water and gas, in which a solid water lattice

* Corresponding author.
E-mail address: gjmoridis@lbl.gov (G.J. Moridis).

0920-4105/$ - see front matter © 2004 Published by Elsevier B.V.
doi:10.1016/j.petrol.2004.02.015

accommodates gas molecules in a cage-like structure, or clathrate. The estimated amount of gas in the hydrate accumulations of the world greatly exceeds the volume of known conventional gas resources (Sloan, 1998). However, the role that gas hydrates may play in contributing to the world's energy requirements will depend ultimately on the availability of producible gas hydrate resources and the cost to extract them.

The three main methods of hydrate dissociation for gas production include: (1) depressurization, in which the pressure is lowered to a level lower than the hydration pressure P_H at the prevailing temperature; (2) thermal stimulation, in which the temperature is raised above the hydration temperature T_H at the prevailing pressure; and (3) the use of inhibitors (such as salts and alcohols), which causes a shift in the P_H–T_H equilibrium (Fig. 1) through competition with the hydrate for guest and host molecules (Sloan, 1998).

The Mallik gas hydrate field, located at the northeastern edge of Canada's Mackenzie Delta, occurs within a sequence of Tertiary sediments in an area underlain by over 600 m of permafrost. With data available from the original Mallik discovery well in 1971 and 1972 (Bily and Dick, 1974), and a scientific research well program in 1998, the geology and gas hydrate occurrences at the site have been well documented (Dallimore et al., 1999a). Quantitative well log determinations and core studies reveal at least 10 discrete gas hydrate layers (exceeding 110 m in total thickness) with high gas hydrate saturation values, which, in some cases exceed 80% (Collett et al., 1999; Miyairi et al., 1999). These attributes establish the Mallik field as one of the most concentrated gas hydrate reservoirs in the world. Thus, Mallik represented an ideal site for a field test of gas production from a natural gas hydrate accumulation. This would be the first ever such test, primarily aiming to observe and analyze the unknown field behavior of natural hydrates during dissociation under controlled conditions, and leading to the determination and quantification of the corresponding processes and parameters that affect hydrate-originating CH_4 production, as well as to preliminary estimates of the gas production potential from such deposits.

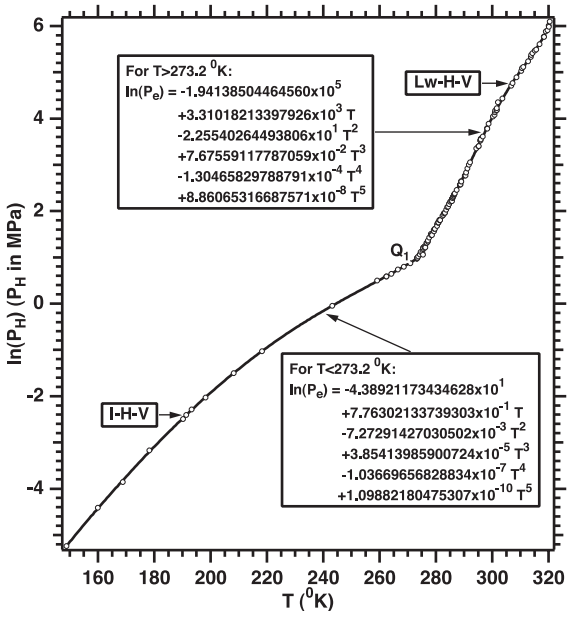

Fig. 1. Pressure–temperature equilibrium of the simple methane hydrate (Moridis, in press (a,b)). The quadruple point Q_1 is denoted.

1.2. Objectives of the study

In preparation of such a field test, various scenarios of gas production from the several hydrate-bearing stratigraphic layers at the Mallik site were investigated by means of numerical simulation. The main objectives of this numerical study were to provide a scientific basis for the selection of both a promising hydrate-bearing zone and the corresponding appropriate production strategy, and to provide scoping calculations for the design of the field test. This was accomplished by (a) evaluating the suitability and effectiveness of alternative production strategies (involving different dissociation mechanisms) from several potential hydrate-bearing target zones (Fig. 1), (b) assessing the performance of production systems employing different well geometries and configurations, and (c) determining the sensitivity of gas production to important conditions and parameters (field, physical, well, and operational). The numerically predicted contribution of dissociating hydrate to the total gas production represents the first attempt to evaluate the Mallik hydrate accumulations (and other permafrost hydrate deposits

with similar characteristics) as a potential energy resource. The results of this scoping and design study are presented in this paper.

1.3. The numerical model

The analysis of the production scenarios in this paper were conducted using the EOSHYDR2 model (Moridis et al., 1998; Moridis, in press (a)), a member of the TOUGH2 (Pruess et al., 1999) family of codes for the simulation of multicomponent, multiphase fluid and heat flow and transport in the subsurface. By solving the coupled equations of mass and heat balance, EOSHYDR2 can model the nonisothermal hydrate formation or dissociation, gas release, phase behavior, and flow of fluids and heat under conditions typical of common natural hydrate deposits (i.e., in the permafrost and in deep ocean sediments) in complex formations. The binary hydrate systems that can be studied by EOSHYDR2 involve methane and a second hydrate-forming gaseous compound G. Their formation and dissociation are described by the general reaction equation

$$\chi_m[CH_4 \cdot N_m H_2O] \cdot \chi_G[G \cdot N_G H_2O] = \chi_m CH_4 + \chi_G G + (\chi_m N_m + \chi_G N_G)H_2O$$

where the subscripts m and G denote the methane and the second hydrate-forming gas, respectively, χ is the mole fraction in the binary hydrate, and N is the hydration number. The second gas G can be another hydrocarbon C_vH_{2v+2} ($v = 2, 3, 4$), or $G \equiv CO_2$, H_2S, or N_2. It is obvious that $\chi_m + \chi_G = 1$. Depending on the prevailing temperature T, CH_4 and G are gases during dissociation, but H_2O can be either liquid water (when T exceeds the temperature of the hydrate quadruple point T_Q, Fig. 1) or ice (when $T < T_Q$).

EOSHYDR2 includes both equilibrium and a kinetic model of gas hydrate formation and dissociation, and can describe gas hydrate dissociation involving any combination of the possible dissociation mechanisms (i.e., depressurization, thermal stimulation, and inhibitor effects salting-out effects). A detailed description of EOSHYDR2 can be found in Moridis (in press (a)).

2. Site geology and simulation zones

2.1. Geological system

In 1998, the Mallik 2L-38 gas hydrate research well was drilled in 1998 by an international consortium involving North American and Japanese organizations (Dallimore et al., 1999a). This project was the first targeted study of the occurrence of natural gas hydrate accumulations in the Mallik area of the Mackenzie River Delta, Northwest Territories, Canada, and involved detailed scientific and engineering studies (Dallimore et al., 1999b). After an extensive review process (Dallimore and Collett, 1999), the site of the well was selected in the vicinity of the Mallik L-38 well, an earlier industry exploration well (Bily and Dick, 1974) that had indicated the advantages of this location because of the occurrence of significant gas hydrate deposits (in addition to its relative accessibility).

The geology of the Mackenzie Delta–Beaufort Sea region (where the Mallik site is located) has been extensively described (Dallimore and Collett, 1999; Jenner et al., 1999). The structural basement of this region is formed by highly faulted Lower Cretaceous strata that underlie the delta. A regional unconformity separates these strata from 12 to 16 km of Late Cretaceous to Holocene deltaic, shelf, slope, and deep-water deposits. The Mallik 2L-38 well penetrated the upper 1150 m of Oligocene to Holocene sediments. The Mallik gas hydrate field is restricted to the crest of a large anticlinal feature and is estimated to hold between 2.93×10^9 and 4.15×10^9 m^3 of gas (at standard conditions) in the 1 km^2 area surrounding the drill site (Collett et al., 1999).

While drilling the Mallik 2L-38 well, major emphasis was placed on coring the log-inferred gas hydrate intervals identified in the earlier Mallik L-38 well. Approximately 37 m of core was recovered from gas hydrate zones in the interval between −886 and −952.6 m (Ohara et al., 1999, 2000). Visual observations at the drill site identified a predominance of pore space gas hydrates in coarse-grained sandy layers interbedded with low- to nonhydrate-bearing fine-grained silty sediments, and indicated a strong lithological control (Collett et al., 1999). Thin veins and clasts or nodules of hydrates were also observed, although these occurred rarely (Uchida et al., 1999a).

Analysis of recovered cores and downhole log data from the Mallik 2L-38 well has confirmed the occurrence of approximately 113 m of gas hydrate-bearing strata in the interval from −897.25 to −1109.8 m (Collett et al., 1999), mainly in unconsolidated to weakly cemented sediments of the Kugmallit, Mackenzie Bay, and Ipek sequences. Fig. 2 presents important geophysical log data and properties from the Mallik site subsurface, shows the dominant geologic sequences, indicates inferred hydrate saturation distributions, and identifies five major hydrate-bearing zones. Analysis of the log data confirmed the existence of a thin two-phase layer of mobile gas (free gas) at the base of the deepest downhole gas hydrate accumulation (1108.4–1109.8 m). The hydrate-free gas interface marked the bottom of the stability zone, below which the elevated temperature (caused by geothermal fluxes from deeper strata) does not allow the occurrence of hydrates. The presence of free gas in contact with gas hydrates is an important consideration in terms of identifying potential production targets and designing corresponding production strategies. Such hydrate accumulations are desirable targets for exploitation because of the thermodynamic proximity to the hydration equilibrium at the highest possible temperature (necessitating only small changes in pressure and temperature to induce dissociation).

2.2. General simulation parameters and conditions

Five zones were investigated. The regional plunge along the crest of the Mallik structure was not considered in the simulations because of the very shallow dip angle (2° to the northwest) and the limited extent of the affected hydrate accumulations during dissociation. The properties used in the simulations were based on data published by Uchida et al. (1999b), Winters et al. (1999), Collett et al. (1999), and Wright et al. (1999a,b), and were assumed the same in all the zones: porosity (ϕ=0.28), intrinsic permeability ($k=2\times10^{-14}$ m^2), composite thermal conductivity of the rock hydrate reservoir fluids system ($k_\theta=1.5$ W/m/°C), rock specific heat ($C_R=800$ J/kg/°C), and hydrate specific heat ($C_H=1600$ J/kg/°C). Even when no-flow boundaries were involved, the simulation domains were appropriately extended to adequately describe the thermal fluxes between the hydrate-bearing formation and the bounding impermeable strata. Note that k_θ does not remain constant during the simulations, but changes according to the Bejan (1984) parallel model as the hydrate, water and gas saturations change. The thermal conductivity of water is computed internally in EOSHYDR2 as described by Pruess et al. (1999), while that of the methane hydrate is 0.45 W/m/°C (Sloan, 1998).

The following assumptions were involved in all simulations: (1) the pressure distribution was hydrostatic, (2) a heat flux corresponding to the geothermal gradient ($dT/dz=0.03$ °C/m) was applied between the top and bottom boundaries of the simulated domain, and (3) the gas hydrate was a simple methane hydrate ($\chi_m=1$), with the native gas, when present, 100% methane. In addition, the dissociation of gas hydrate was assumed to follow the equilibrium process described in Fig. 1, as affected by the water salinity (Wright et al., 1999a; Moridis, in press (a). The heat fluxes at the boundaries resulted in realistic, nonuniform temperature distributions across the formation profiles, with temperature increasing with depth. Relative permeabilities and capillary pressures were computed from the Parker et al. (1987) three-phase model, in which the immobile hydrate was the third "organic" phase. The wettability parameters used by the Parker et al. (1987) model to estimate both relative permeabilities and capillary pressures were typical of porous media with the same level of k, while the irreducible water and gas saturations of the were $S_{wr}=0.2$ and $S_{gr}=0.05$, respectively, and were assumed to be the same in all zones.

The planned new field test at the Mallik site could only be conducted in winter, when it is possible to build and maintain ice roads allowing access to the site. The limited duration of such conditions (not exceeding 4–6 weeks) and the high cost of operating under Arctic conditions resulted in a very narrow operational window (≤30 days), within which both the well drilling and the field test would have to be accommodated. Thus, the production simulations were limited to short periods. A particular effort was made to minimize water production in the scoping calculations and the design of the field test. This need was driven by economic, environmental and regulatory concerns (which make the handling and disposal of large volumes of reservoir water difficult and expensive in the challenging Arctic conditions of Mallik), as well as by the desire to maximize gas production. Gas

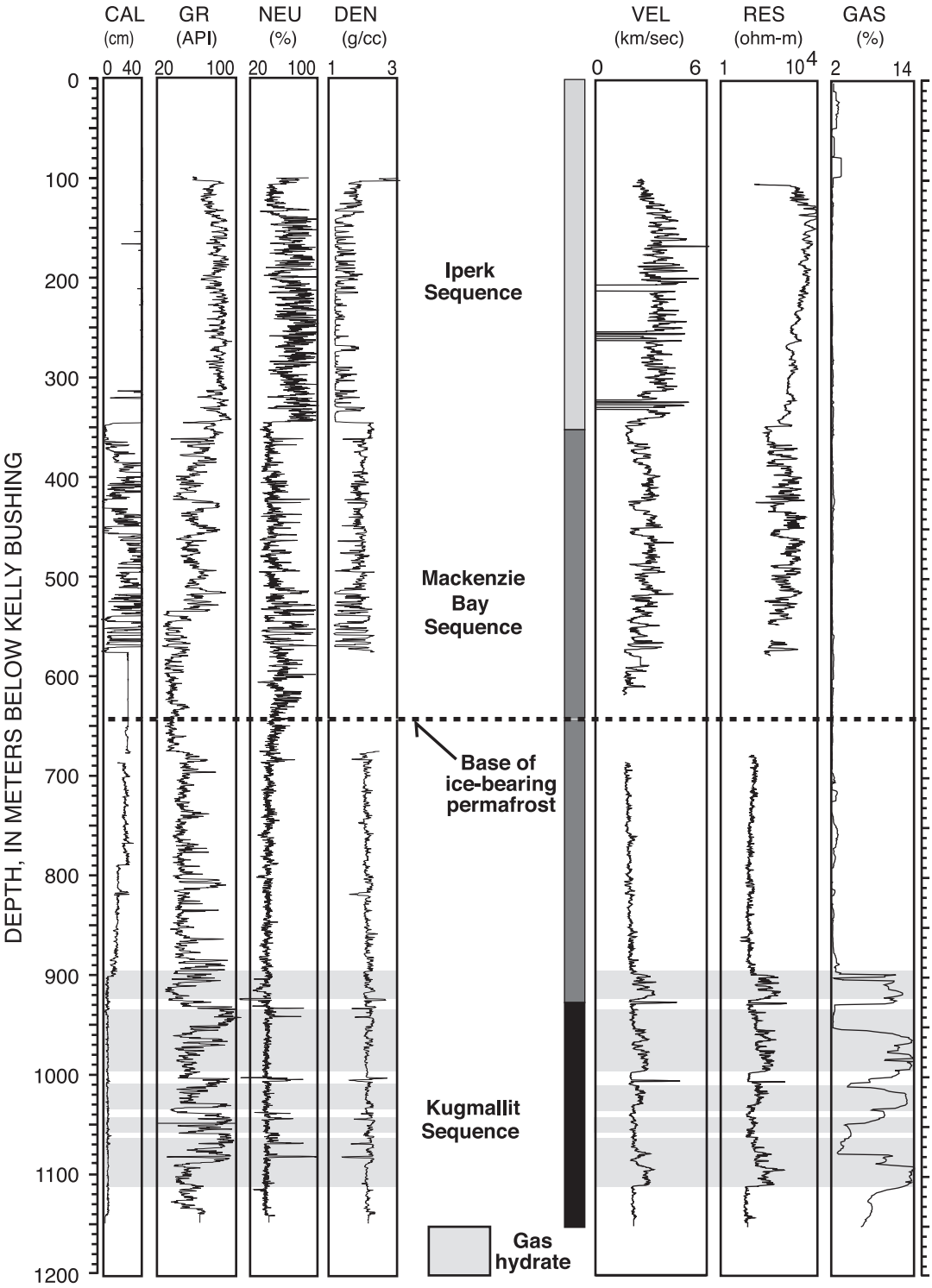

Fig. 2. Geological structure, geophysical well log data and deduced hydrate saturations at the Mallik site (Collett et al., 1999).

production was already expected to be low because of the short duration of the field test. Given the unknown (at the time of this study) level of difficulty of gas production through dissociation from natural gas hydrates, it was important to minimize uncertainty by maximizing the production of hydrate-originating CH_4 (hereafter referred to as "H-methane").

3. The simulation zones

3.1. Hydrate Zone #1

3.1.1. Properties and characteristics in Zone #1

Zone #1 is the deepest hydrate accumulation and is characterized by a 20-m-thick hydrate-bearing sediment, the base of which (at a depth of -1108.4 m) marks the bottom of the hydrate stability zone. The initial temperature at the bottom of the hydrate layer is $T = 13.18$ °C, which is the gas hydrate equilibrium temperature T_H at the formation pressure of $P = 10.8$ MPa and at the native salinity of 4% (Wright et al., 1999a). The gas hydrate interval has a uniform hydrate saturation $S_H = 0.8$ and a water saturation $S_w = 0.2$.

The hydrate-impregnated interval is capped by a water-saturated siltstone/mudstone sequence that acts as a no-flow boundary, and is underlain by a thin (1.4 m thick) two-phase layer in which gas and liquid water (a brine) coexist. The water and gas saturations in the two-phase layer are shown in Fig. 3, and clearly indicate the presence of large amounts of water. The two-phase layer is underlain by a 15-m-thick water-saturated sandstone unit bounded at the bottom by a tight (no flow) unit. The water-saturated layer, coupled with the high initial S_w in the overlying thin free gas layer, make upconing a potentially serious problem.

Zone #1 and its boundaries extend uniformly over a large area. Because hydrates at the hydrate gas interface occur at thermodynamic equilibrium at the highest possible temperature limit of stability under natural conditions, relatively small pressure and/or temperature changes can induce gas hydrate formation or dissociation. Gas production from the thin two-phase layer effects depressurization over a relatively large area in contact with the practically impermeable overlying gas hydrates. This, in turn, can induce gas production through gas hydrate dissociation, but can also lead to a decline in gas production at later times because of water upconing.

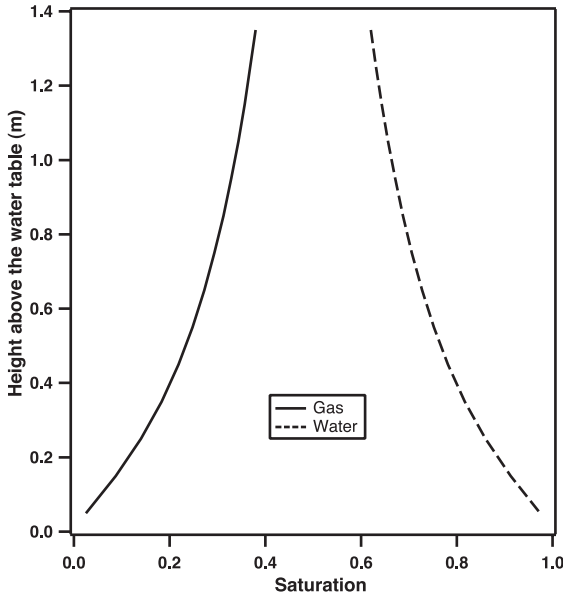

Fig. 3. Water and gas saturation in the two-phase layer in Zone #1.

3.1.2. Case 1: depressurization-induced dissociation, single vertical well

Case 1 involved simple depressurization of the hydrate interval through a single vertical well completed in the entire two-phase interval. The cylindrical 2D semiinfinite reservoir domain in this set of simulations was discretized into 57 and 65 nonuniform grid blocks in r and z, respectively, for a total of 3705 grid blocks, of which 3584 were active (the rest are inactive boundary grid blocks). To capture the dissociation profile in detail and avoid numerical artifacts in the production curves, a very fine discretization scheme was employed in the vicinity of the well, (i.e., $\Delta r = 0.02$ m and $\Delta z = 0.05$ m), but the grid became progressively coarser away from the well.

To obtain an accurate estimate of the contribution of methane originating from gas hydrate dissociation to the total gas production, the native methane was considered separately from the H-methane. Five mass components (hydrate, water, native methane, H-methane, and salt) and heat were described in the simulations, resulting in a system of 21,504 simultaneous

equations. Accounting for the salt is important in this zone because a previous study (Wright et al., 1999a) has shown that salinity at the site was sufficiently large to reduce T_H at the prevailing pressure by 1.4 °C. Given the thermal inertia of the system, such a decrease in the hydration temperature can have a significant effect on the volume of the produced gas. Thus, the dilution of the salt in the native water by the water released during dissociation could not be ignored.

Fluids were produced from the well at a cumulative mass flow rate of $Q = 1.67 \times 10^{-3}$ kg/s, determined through trial and error to allow significant gas production without a very early water flooding in the first 30 days of the production (Section 2.2). Brine and gas (principally methane with minor water vapor) were distributed in the production stream according to their mobilities in the vicinity of the well. The very low rate (corresponding to a volumetric flow rate of 225 m^3/day when only gas is produced) in no way compromised the validity of the planned field test, because the test objective was not the demonstration of the feasibility of large-scale production from hydrate deposits, but rather the study of hydrate dissociation and behavior in porous media under field conditions.

To quantify the effects of the dissociating gas hydrates, two sets of simulations were conducted. In the first set, the gas hydrate layer was assumed to be inert (i.e., nondissociating), while hydrate dissociation was accounted for in the second set. This approach was implemented to determine whether the two systems had a markedly different response.

The evolution of pressure and temperature at the production interval midpoint for the two simulation sets are shown in Fig. 4. The pressure and temperature are generally uniform and do not exhibit significant vertical variation because of the limited thickness of this interval. The simulations suggest that the pressure in the two-phase interval underlying Zone #1 is significantly higher when gas hydrate dissociation is considered. This is consistent with expectations because of the contribution of the H-methane to the total gas pressure.

For nondissociating gas hydrates, the temperature initially rises very slowly (practically imperceptibly), and is then followed by a rapid and monotonic temperature increase as warmer water from deeper in the aquifer is drawn to the well. For

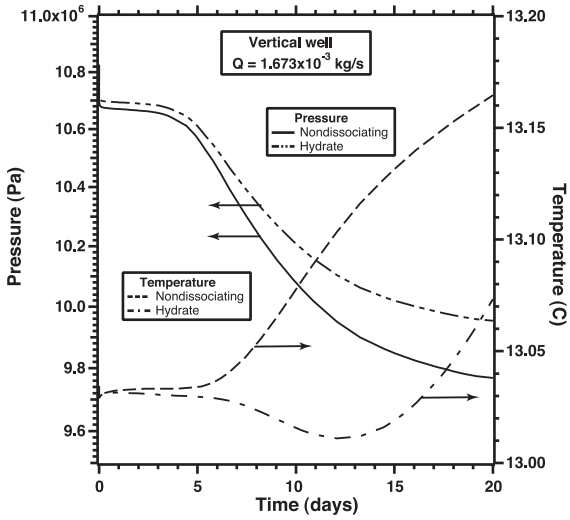

Fig. 4. Evolution of pressure and temperature at the vertical well in Zone #1.

dissociating gas hydrates, a temperature drop is first observed. This is consistent with gas hydrate dissociation and the strongly endothermic nature of this reaction, which leads to water cooling in the vicinity of the dissociating gas hydrate interface. However, the temperature begins to increase after the initial drop as deeper, warmer water moves toward the well.

Fig. 5 shows the evolution of F, the mass fraction of gas in the production stream, during the production period. By maintaining a low total mass production rate, gas is practically the only phase produced for about 6 days (indicated by $F \simeq 1$), at which time the gas production rate begins to decline because of increasing water production. Note that maintaining high gas production is challenging in Zone #1 because of (1) the limited thickness of the two-phase layer, (2) the proximity to the underlying infinite aquifer, (3) the large amounts of water released in the course of gas hydrate dissociation, and (4) an adverse gas relative permeability in the presence of so much native and released water. The effect of released water during dissociation is reflected in the F (compared to that for no dissociation) in the produced stream near the end of the 100-day production period.

As shown in Fig. 6, the mass fraction of H-methane in the produced gas rises from 0 to approx-

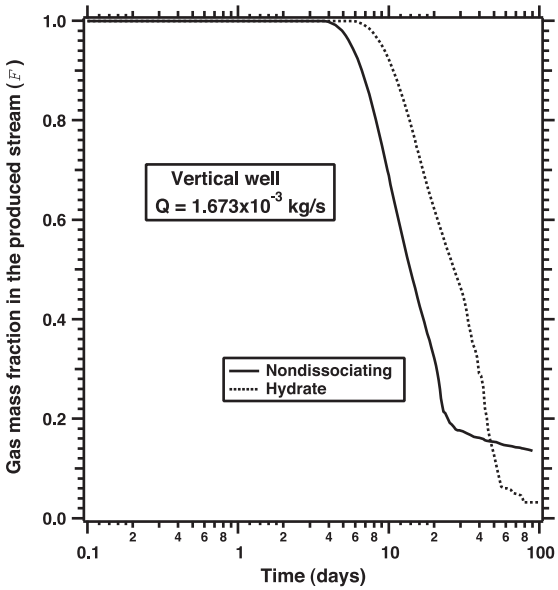

Fig. 5. Gas mass fraction in the production stream of the vertical well in Case 1, Zone #1.

imately 0.45 in about 60 days. For $t>60$, f rises very slowly and appears to stabilize at $t \simeq 90$ days. This indicates that, under the conditions of Case 1, gas hydrate dissociation is a significant source of gas, contributing about half of the produced gas when f stabilizes.

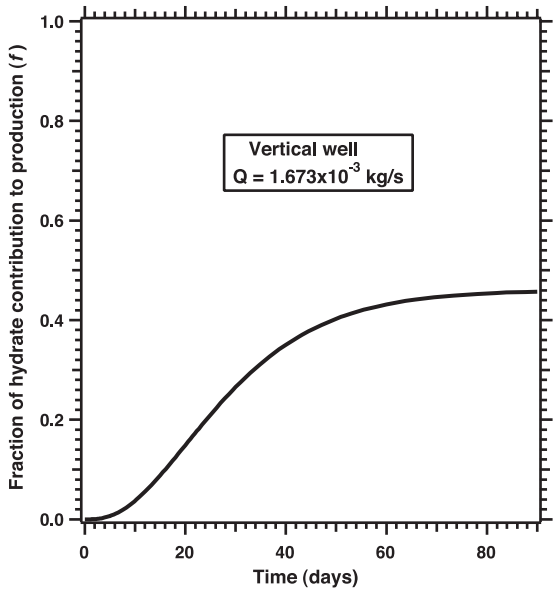

Fig. 6. Hydrate contribution to gas production stream in Case 1, Zone #1 (vertical well).

3.1.3. Case 2: depressurization-induced dissociation, single horizontal well

Case 2 involved hydrate dissociation (through depressurization) induced by gas production from a single horizontal well. The center axis of the horizontal well was in the two-phase layer 0.25 m below the bottom of the hydrate layer of Zone #1, and the perforated interval had a length of 20 m. Fluids were produced from the well at the same rate as in the single vertical well (Section 3.1.2), resulting in lower pressure drops that were more uniformly distributed along the length of the perforated interval. The different geometry of the system dictated a different grid. Because of symmetry along the (x,z) plane, only half the domain was discretized. The 3D Cartesian grid comprised $30 \times 30 \times 26 = 23{,}400$ grid blocks in (x,y,z), of which 17,864 were active.

Fig. 7 shows the evolution of F (the mass fraction of gas in the production stream) and f (the mass fraction of H-methane in the produced gas) over time in Case 2. By distributing the production over the 20-m interval, the pressure changes are

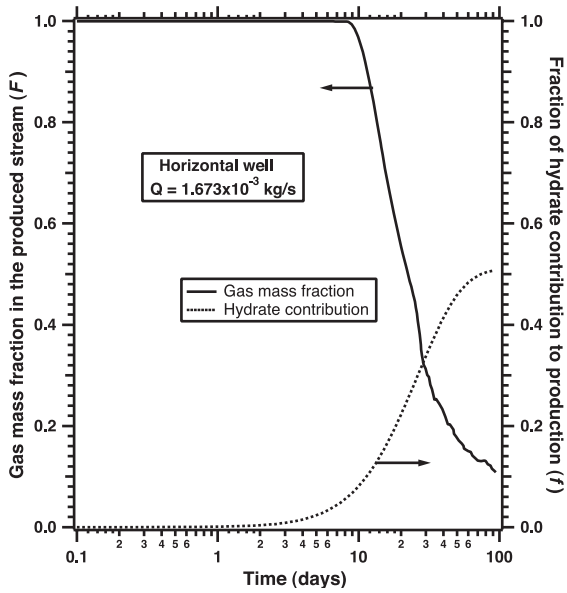

Fig. 7. Gas mass fraction in the production stream and hydrate contribution to gas production stream in Case 2, Zone #1 (horizontal well).

significantly lower and result in a delay in the onset of rapid water production from about 6 days to about 9 days. By virtue of its proximity to a larger area of the hydrate interface and the more favorable gas relative permeability regime in the upper part of the two-phase layer (where the horizontal well is located), the contribution of CH_4 from dissociation to the produced gas is larger than that for the vertical well in Fig. 4. At the end of the 100-day production period, more than half (52%) of the produced gas originates from methane hydrate dissociation. Although these results tend to indicate that horizontal wells may be more effective means of gas production from hydrates, no definitive conclusion can be reached because, even if economic issues of well construction are ignored, the incremental improvement in performance over that of a vertical well is not substantial.

3.1.4. Cases 3 and 4: depressurization and thermal stimulation, vertical two-well systems

The production/injection two-well systems employed in Cases 3 and 4 induced dissociation of the methane hydrates through a combination of depressurization (at the production well) and thermal stimulation (at the injection well). The distance between the two vertical wells was 50 m. The injection and production intervals were located in the upper 0.5 m of the two-phase layer immediately below the hydrate interface.

In Case 3, steam with a specific enthalpy of $H = 3200$ kJ/kg (corresponding to $T = 420$ °C and sufficiently high to remain superheated steam at the injection $P \simeq 11$ MPa) was injected. The steam injection rate and the fluid production rate were the same, and equal to $Q = 1.67 \times 10^{-3}$ kg/s. Although much higher injection and production rates are possible in such a well configuration, the rates were kept at this low level to allow a meaningful performance comparison to those in Cases 1 and 2.

Case 4 involved the injection of hot methane with a specific enthalpy equal to that of the steam in Case 3. The injection rate of CH_4 was $Q_i = 8.35 \times 10^{-4}$ kg/s (half that of the injected steam), while fluids were produced at a rate of $Q_p = 2.51 \times 10^{-3}$ kg/s (thus maintaining an effective production rate of $Q = Q_p - Q_i = 1.67 \times 10^{-3}$ kg/s). The practical problems and safety concerns of the heating and injection of CH_4 were not addressed because the study focused on general strategies that can maximize production.

The Cartesian 3D grid used in the simulation of Cases 3 and 4 involved domain discretization into $76 \times 31 \times 36 = 84{,}816$ nonuniform grid blocks in (x,y,z), of which 75,480 were active. To accurately capture the dissociation profiles, a very fine discretization was used in the vicinity of the two wells. The simulations solved for the same six components involved in the single well studies (Section 3.1.2), resulting in a system of 452,880 equations.

In Fig. 8, the review of the evolution of F over time in the two-well system shows that, when steam is injected (Case 3), the onset of significant water production is delayed to about 12 days. Additionally, after a rapid initial decline, the rate of decline in F is substantially reduced, and the F at $t = 100$ days is much higher than that for the single vertical or horizontal wells. This occurs despite the fact that the injection of steam inevitably adds water to the system (after condensation), thus adversely affecting the gas relative permeability.

When hot CH_4 in injected (Case 4), the onset of water production is delayed to about 14 days, but F declines only to about 0.7 at $t = 30$ days, after which time it rises very slowly. The slow rise coincides with

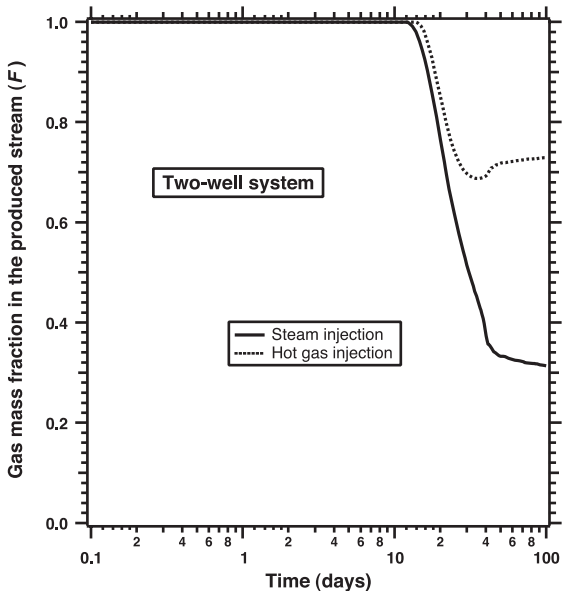

Fig. 8. Gas mass fraction in the production stream of the two-well system in Zone #1 (Cases 3 and 4).

the arrival at the production well of the hot gas stream from the injection well. The behavior of F indicates that, despite producing from a very thin two-phase layer underlain by a large aquifer, it is possible to maintain a relatively high F in the production stream. This is attributed to the favorable gas relative permeability regime. The buoyancy of the injected hot CH_4 directs it to the top of the two-phase layer, where it displaces native water while ensuring maximum contact with the hydrate, i.e., the intended target. Thus, aided by the pressure differential between the two wells, a high gas saturation zone is established underneath the hydrate interface. This zone keeps expanding upward as the interface recedes. The fact that the injected CH_4 (unlike steam) is noncondensible reduces adverse relative permeability, maximizing production and performance in the process.

More encouraging results are provided by Fig. 9, which shows the evolution of f in the two-well system; f rises continuously (although very slowly after $t = 60$ days) to as high as 0.61 in Case 3, and to an even higher level ($f \simeq 0.72$) in the case of hot CH_4 injection (Case 4). These results indicate that, in two-well configurations (and, by extension, in five-spot arrangements), the majority of the produced gas originates from the dissociation of the methane hydrates. As indicated by Figs. 8 and 9, the injection of hot CH_4 appears to have an advantage (in terms of limiting water upconing) steam injection.

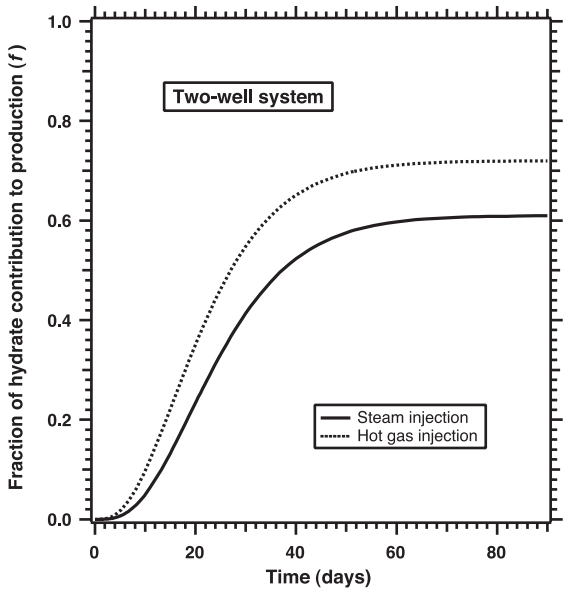

Fig. 9. Hydrate contribution to gas production stream of the two-well system in Zone #1 (Cases 3 and 4).

3.2. Hydrate Zone #2

3.2.1. Properties and characteristics in Zone #2

Zone #2 is characterized by a 16-m-thick hydrate-bearing interval (from -899 to -915 m, with $T = 7.5$ °C, $P = 9$ MPa at the base of the hydrate interval) capped by a relatively thick sandstone (with minor hydrate saturation) that acts as an impermeable flow boundary. This gas hydrate accumulation has a uniform $S_H = 0.5$ and is underlain by a 2-m-thick water-saturated layer, followed by a 2-m-thick low-porosity ($\phi < 0.02$) sandstone that behaves as a no-flow boundary. Because of its shallower depth, Zone #2 is cooler than Zone #1. Zone #2 and its boundaries are assumed to extend uniformly over a large area.

3.2.2. Production approach and numerical system in Zone #2

As in Zone #1, the only dissociation method we considered was depressurization of the gas hydrate accumulation through fluid withdrawals from the underlying water-saturated zone. The very low compressibility of water was expected to provide conditions conducive to dissociation through depressurization, because the pressure decline is transmitted more effectively (compared to a free gas zone) over a larger area of the hydrate interface.

The cylindrical 2D grid involved 65 and 38 non-uniform grid blocks in r and z, respectively, for a total of 2210 grid blocks. The simulations accounted for heat and four components (hydrate, water, H-methane, and salt), resulting in a system of 12,350 simultaneous equations. Fluids were produced from the well (completed in the entire 2-m water-saturated layer) at a mass flow rate of $Q = 0.578$ kg/s, corresponding to an initial volumetric rate of water production $Q_w = 50$ m^3/day. This rate does not exceed the capacity of the system to deliver water at the well (as controlled by the formation permeability and the pressure drop) and can be sustained without cavitation. The corresponding rate of CH_4 production was computed internally by the model from the aqueous- and gas-phase mobilities near the well bore.

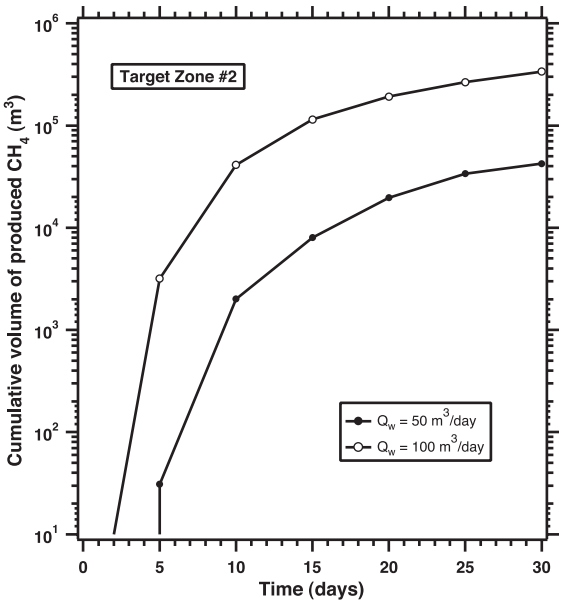

Fig. 10. Cumulative gas production in Zone #2.

3.2.3. Production predictions and analysis in Zone #2

Fig. 10 shows the cumulative gas production over time in the 30-day simulation period. The gas phase emerges only after about 5 days of continuous water production. There are two reasons for the delay in gas appearance. The first is the adverse relative permeability conditions (emergence of a gas phase in a previously fully saturated formation, coupled with the release of large amounts of water during dissociation) that necessitate a gas saturation S_g>0.05 for gas mobility. The second reason is the low initial temperature (at the formation pressure of 9 MPa, the hydrate dissociation temperature is 11.5 °C), which requires a larger pressure drop (and, thus, longer fluid withdrawal) to effect dissociation through depressurization. The shape of the cumulative gas production curve indicates a continuously declining gas production rate as the pressure approaches a steady-state distribution (with the boundaries replenishing the withdrawn water) and the gas hydrate reaches a new pressure–temperature equilibrium point at a lower temperature. Generally, gas production through depressurization in deposits such as the one represented in Zone #2 results in a mild temperature decline because the water moving from the boundaries through the water-saturated layer to the well provides the necessary heat to sustain the dissociation of the hydrate.

The sensitivity of gas production to the production rate is also demonstrated in Fig. 10, which includes the cumulative gas production when the fluid mass production rate is doubled to $Q = 1.156$ kg/s (initial $Q_w = 100$ m^3 of water per day). Doubling the well production rate leads to an increase in the cumulative volume of produced gas by almost an order of magnitude, and to an earlier onset of gas appearance at the well. This response is attributed to the faster and more pronounced (in terms of magnitude and areal extent) pressure drop associated with the larger rate, which leads to correspondingly earlier and faster dissociation through depressurization from a larger portion of the hydrate layer.

An important observation from Fig. 10 is that a large volume of gas can be produced from Zone #2, and all of it originates from gas hydrate dissociation. While this is promising, the potential of this single-well approach is limited by the large volume of produced water. This is demonstrated by the very low gas mass fraction in the production stream (Fig. 11), which does not exceed 0.017 over the simulation period when $Q = 0.58$ kg/s. In addition to the adverse economics of lifting and disposing of the large

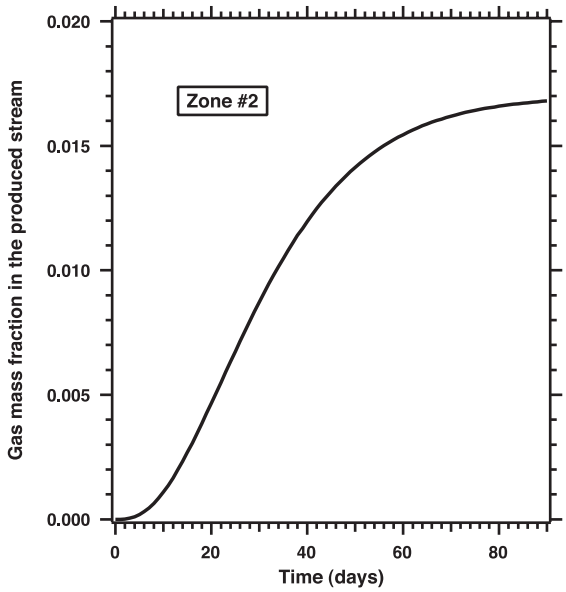

Fig. 11. Gas mass fraction F in the production stream of Zone #2 ($Q_w = 50$ m^3/day).

volumes of produced water, the environmental challenges posed by the disposal of this water (usually a brine) in the sensitive Arctic environment at the Mallik site cast an unfavorable light on production from Zone #2.

3.3. Hydrate Zones #3, #4 and #5

3.3.1. Properties and characteristics in Zones #3–5

These three zones are discussed together because they are similar, in that they do not have underlying layers of mobile gas or water. In these zones, the pore space is occupied by gas hydrate and water (mostly immobile), and the hydrate interval occupies the entire zone thickness.

Zone #3 extends from a depth of about −1081 to −1091 m, with $S_H = 0.8$, $T = 12.8$ °C, and $P = 10.74$ MPa at the base of the hydrate interval. It is the deepest and warmest of these three zones, and, as such, the most promising of the three as a potential production target zone because of its proximity to thermodynamic equilibrium. The other two zones are deeper within the hydrate stability zone and, consequently, stabler and more difficult to dissociate. Zone #3 is capped by a relatively thick siltstone sequence and is underlain by a relatively thick gas hydrate-bearing sandstone sequence with varying gas hydrate saturations. Both boundaries are treated as impermeable to flow, but allowing heat fluxes consistent with the prevailing geothermal gradient.

Zone #4 extends from a depth of −1007 to −1017 m, and is capped and underlain by relatively thick sandstone sequences with varying gas hydrate saturations. This zone has a lower hydrate saturation ($S_H = 0.5$) and, at the base of the hydrate interval, $T = 10.5$ °C and $P = 10.0$ MPa. Zone #5 ($S_H = 0.8$ and $P = 8.9$ MPa at the bottom of the hydrate layer) is shallower (from a depth of −905 to −915 m) and colder ($T = 7.5$ °C) because of its proximity to the permafrost, and its top and bottom boundaries are similar to those of Zone #4.

3.3.2. Production approach and numerical systems in Zones #3–5

Because of the high S_H in all three zones and the absence of an initial gas phase, the relative permeability to both the aqueous and the gas phases—computed in EOSHYDR2 using the model of Parker et al. (1987) for wettability parameters consistent with the intrinsic permeability k of the formation—are very small. Coupled with the absence of free gas or water zones underlying or overlying the hydrate interval, this creates an adverse permeability environment that severely restricts flow, confines pressure changes to a very small portion of the hydrate deposit, and severely limits (if it does not preclude) the use of a depressurization to hydrate dissociation. Because of the dearth of information on the subject, no hydrate fracturing was considered in this analysis.

Thermal stimulation was selected as the mechanism for hydrate dissociation because of the aforementioned limitations to the depressurization approach in Zones #3–5. The main production strategy involved the circulation of hot water in a single vertical well completed in the entire hydrate interval. The hot water column maintained constant pressure (hydrostatic) and temperature conditions at the well, and the heat for the hydrate dissociation was provided through conduction and, to a far lesser extent and later in the simulation period, advection.

The same cylindrical 2D grid was used in the simulations of gas hydrate dissociation in Zones #3, #4 and #5. The hydrate zones were subdivided into $82 \times 20 = 1640$ nonuniform grid blocks in (r,z), respectively. The simulations accounted for heat and three mass components (hydrate, water, and H-methane), resulting in a system of 6560 equations. In all simulations, the well radius was $R_w = 0.036$ m, the well bore temperature was maintained at $T_w = 50$ °C, and the well was kept at the hydrostatic pressure corresponding to the elevation at the bottom of the respective zone.

3.3.3. Production predictions and analysis

Fig. 12 shows the evolution of pressure at the midpoint of the hydrate interval as Zone #3 is exposed to the hot water. The observed pressure surge exceeds the hydrostatic fluid pressure by a factor of as high as 2.5. The reason for the very high pressure is the sudden release of a large volume of methane from the dissociating gas hydrate (1 m^3 of hydrate releases 164 m^3 of methane under standard conditions) in response to the thermal stimulation, and the ease of dissociation because of the proximity of initial formation temperature T to the

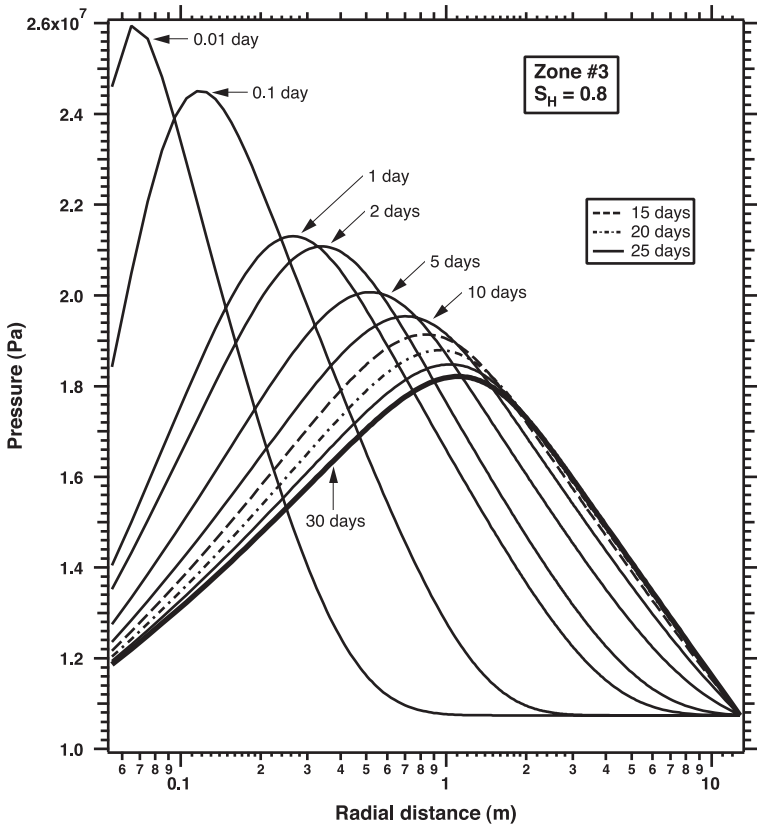

Fig. 12. Formation pressure during thermal dissociation of hydrates in Zone #3 ($R_w = 0.036$ m).

equilibrium hydration temperature T_H at the prevailing pressure.

Under these conditions of limited flow, thermal stimulation appears to be a more effective mechanism than depressurization, as indicated by the gas hydrate equilibrium pressure–temperature relationship (Fig. 2). The large methane volume is released into the limited pore space that was previously occupied by only the nearly incompressible water. This, coupled with the extremely low effective permeability of the gas hydrate-bearing formation (a result of $S_H = 0.8$), which does not allow the gas to move radially away from the well and the pressure to dissipate, causes the pressure spike. The peak pressure decreases over time as the released gas escapes through the well and the dissociation front advances (with a corresponding increase in the permeable pore space).

Fig. 13 shows the distribution of temperature over time during the same period. Note the absence of a discernible temperature drop at the leading edge of the advancing temperature front. This indicates that the system thermal conductivity (probably the grain-to-grain contact of the more conductive solid grains) is sufficiently large to provide the needed dissociation heat. In addition, Fig. 13 shows that the reach of the temperature front during the 30-day simulation period is only about 4 m. This is indicative of the position of the dissociation front, although of limited accuracy because of the shifting dissociation temperature (because of the increase in pressure, Fig. 12).

The position of the dissociation fronts in Zones #3, #4, and #5 over time is shown in Fig. 14. In Zone #3, the dissociation front at $t = 30$ days is at a radius of only about 3 m, confirming the indications of the temperature profile. The dissociation radius is significantly smaller in Zone #4, and even smaller in the much colder Zone #5. This is consistent with expect-

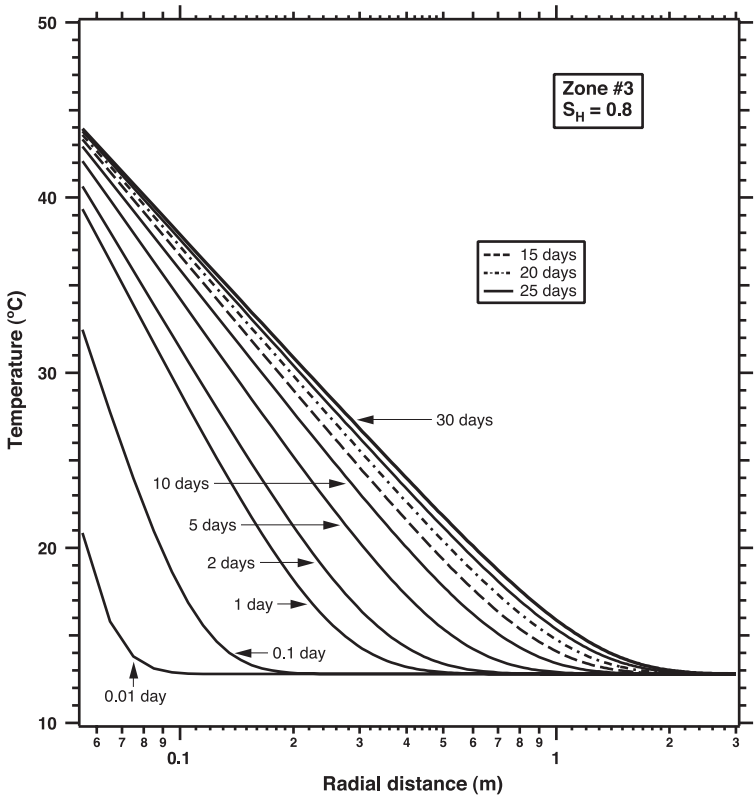

Fig. 13. Temperature distribution during thermal dissociation of hydrates in Zone #3 ($R_w = 0.036$ m).

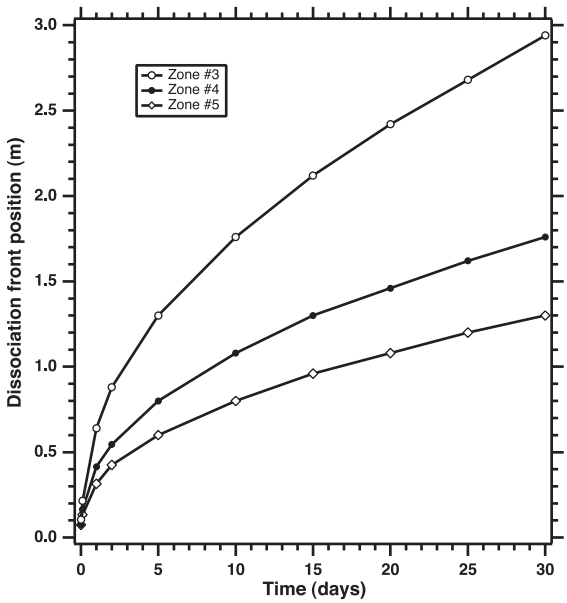

Fig. 14. Radii of the dissociation fronts in Zones #3–#5.

ations because of the large thermal inertia of the subsurface, which requires substantial amounts of heat to reach the dissociation temperature at the prevailing pressure, thus reducing the heat available for dissociation and limiting the dissociation radius in the colder zones.

The cumulative gas production in Zones #3, #4 and #5 is shown in Fig. 15, and is consistent with the results of Fig. 14. The volume of the H-methane from Zone #3 is about five times larger than the corresponding volumes from Zone #5. This significant difference results from the higher temperature, which is close to the dissociation temperature at the pressure of Zone #3. Thus, heat addition is used mostly for dissociation, without being consumed to raise the temperature of the hydrate (a relative insulator). This is demonstrated by the gas production from the colder Zone #5, which is smaller by a factor of five than that from Zone #3, despite having the same $S_H = 0.8$. Al-

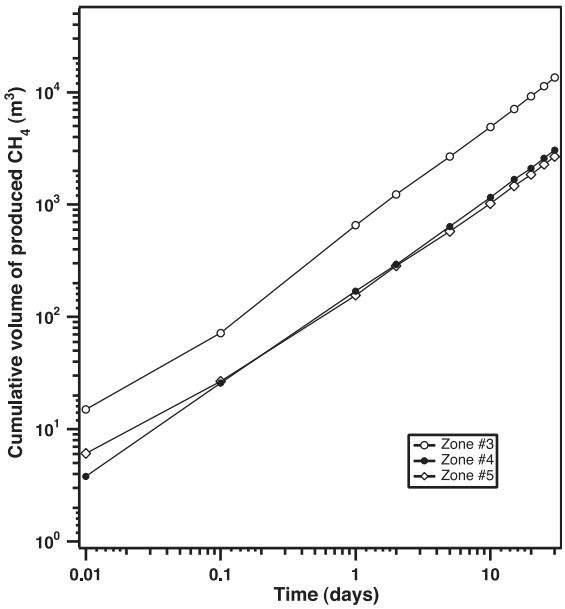

Fig. 15. Cumulative gas production in Zones #3, #4 and #5 (volumes in standard conditions).

though the dissociation front advances much further in Zone #4 (Fig. 14), the volume of the released gas is about the same as that from Zone #5 because of the lower $S_H = 0.5$.

4. Sensitivity analysis of thermal dissociation

Sensitivity analyses of CH_4 production from thermally induced dissociation were conducted to determine the governing parameters and assess their relative importance. The effect of S_H, T, k_θ, k, C_H and C_R, as well as the impact of the boundary conditions at the well during thermal stimulation were investigated. These sensitivity analyses involved a single vertical production well and assumed a uniform spatial distribution of the various parameters of interest.

4.1. Effect of S_H

For a constant temperature, T_w, of the hot circulating water at the well, a higher S_H is expected to correspond to larger volumes of produced CH_4 because of larger hydrate abundance. The substantial increase in the volume of the released gas when S_H in Zone #4 increases from 0.5 to 0.8 in Fig. 16 confirms this expectation; however, the increase in the released gas volume is sublinear. This is attributed to the larger thermal insulating effect of a larger S_H, because of the low thermal conductivity t_θ of the hydrate-impregnated porous medium—computed in EOSHYDR2 using the parallel model of Bejan (1984). Thus, the heat fluxes within the hydrate-bearing formation are lower and the corresponding rise in temperature is slower, limiting the released gas volumes in a given fixed production period.

4.2. Effect of T and k_θ

Fig. 17 compiles the effect of formation temperature and thermal conductivity on gas release vs. time using the gas production from the colder Zone #5 (in which the hydrate is stable because of its departure from hydration equilibrium) as a baseline. The initial formation temperature T appears to have a dramatic effect on gas production. Thus, a 3.5 °C temperature difference (between the initial $T = 7.5$ °C in Zone #5 and the hydration temperature $T_H = 11$ °C at the formation pressure) is shown to reduce production

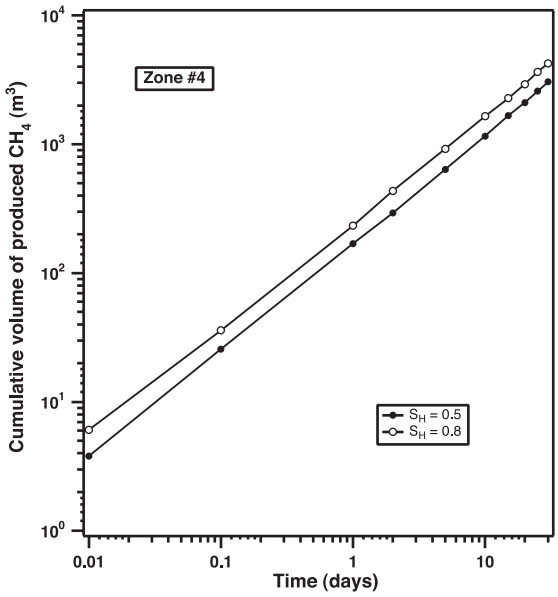

Fig. 16. Sensitivity of gas production to S_H in Zone #4 (volumes in standard conditions).

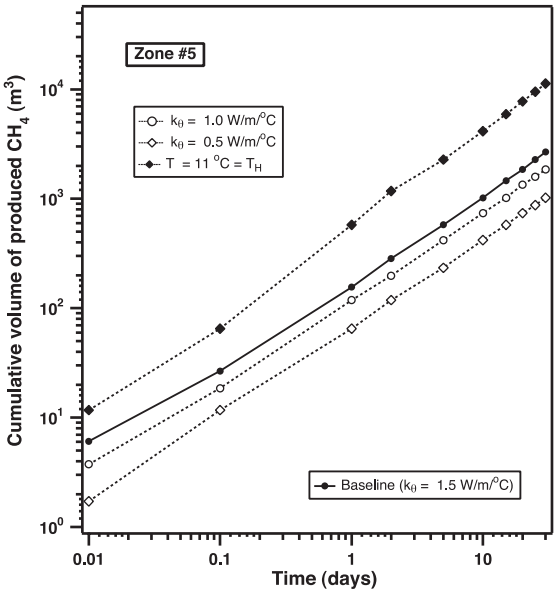

Fig. 17. Sensitivity of gas production to the thermal conductivity k_θ and to the hydrate initial temperature T.

by a factor of about 4. This behavior results from the substantial amount of heat needed to raise the temperature of the hydrate (a relative thermal insulator) to the dissociation temperature T_H.

Fig. 17 also shows the strong dependence of gas production from dissociating hydrates on the thermal conductivity k_θ. When the composite k_θ (including the contributions of the rock and all the phases in the pores) decreases from the baseline value of 1.5–1.0 and 0.5 W/m/°C (the conductivity of pure hydrate), the corresponding reduction in the volume of the produced gas appears to be linear. This conforms with expectations, because a decrease in conductivity leads to a linear decline in the rate at which heat is supplied to the dissociating front.

4.3. Effect of the boundary conditions at the production well

When the well temperature, T_w, increases from 50 to 70 °C, the produced gas volume increases by about 25% (Fig. 18). The reason for this modest increase is the dependence of the heat flux into the hydrate interval on the temperature differential between the circulating hot water and the formation adjacent to the well. This temperature differential decreases continuously over time, and the higher well temperature is insufficient to counteract this decline.

The pressure conditions at the well, combined with the manner of heat addition, appear to have the most dramatic effect on gas production. Thus, heat addition at a constant rate of $Q_H = 6$ kW increases gas production by 40% when the well bore is kept at the hydrostatic pressure of the circulating water (denoted by 'a' in Fig. 18). For comparison, the change of Q_H over time at a constant T_w is shown in Fig. 19, which indicates that a constant power input at the well alleviates the problem of continuous Q_H decline as the temperature differential at the well decreases. Although about double the heat is added when Q_H is a constant 6 kW, gas production increases only by about 40% because of the large thermal inertia of the system.

When, however, heat is added at a rate of $Q_H = 6$ kW and the well is kept at atmospheric pressure (e.g., by artificial lift production of the water released during dissociation), then gas production increases by about an order of magnitude (denoted by 'b' in Fig. 18). This is caused by the combined effect of thermal stimulation of the gas hydrate and depressur-

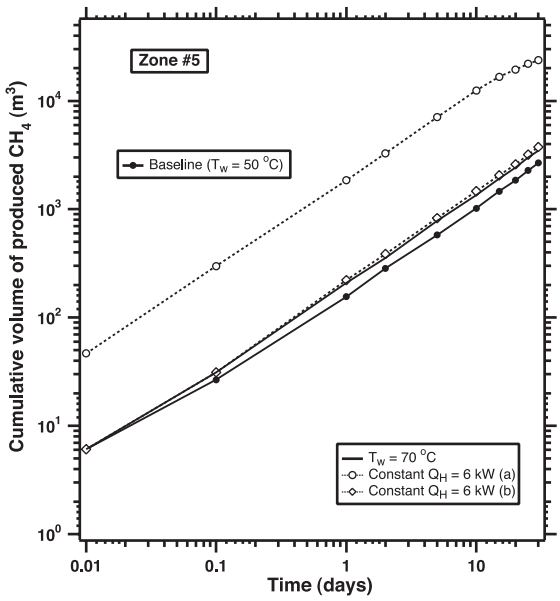

Fig. 18. Sensitivity of gas production to the method of heat addition and to the well boundary conditions.

ization (as the hydrate interval is exposed to the atmospheric rather than the hydrostatic pressure), which appears multiplicative rather than additive.

4.4. Effect of k, C_H, and C_R

Fig. 20 shows that gas production appears to be practically insensitive to the formation permeability k when k increased from 2×10^{-14} m^2 (20 mD) to 10^{-13} m^2 (100 mD). This is attributed to the very high pressures that develop after the gas release (see Section 3.3.3) and the very limited radius of the dissociated hydrate zone that the released gas has to cross before reaching the well.

Fig. 20 also indicates that gas production appears insensitive to the specific heat of the gas hydrate C_H, because the released volumes barely differ when C_H is reduced from 1600 to 1300 J/kg/°C. This is probably because, unlike the porous medium, the hydrate has a low density and occupies only a portion of the pore volume; thus, it is not the dominant component per unit volume and unit mass of the system. Conversely, the dominance of the porous medium in the mass and heat balance affects gas production. Thus, the volume of released CH_4 decreases (albeit mildly) as C_R increases from 800 to 1000 J/kg/°C (Fig. 20). This is consistent with expectations, because a larger C_R indicates more energy stored in the rock per unit temperature and unit mass, with a corresponding reduction in the energy available for hydrate dissociation.

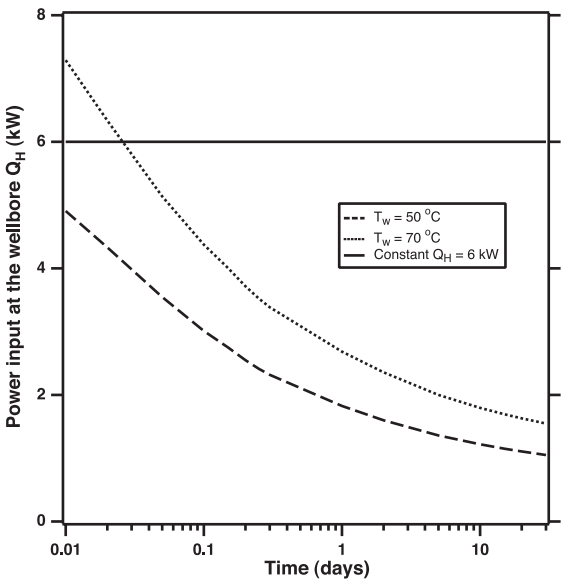

Fig. 19. Power addition Q_H at the well for the different heating schemes.

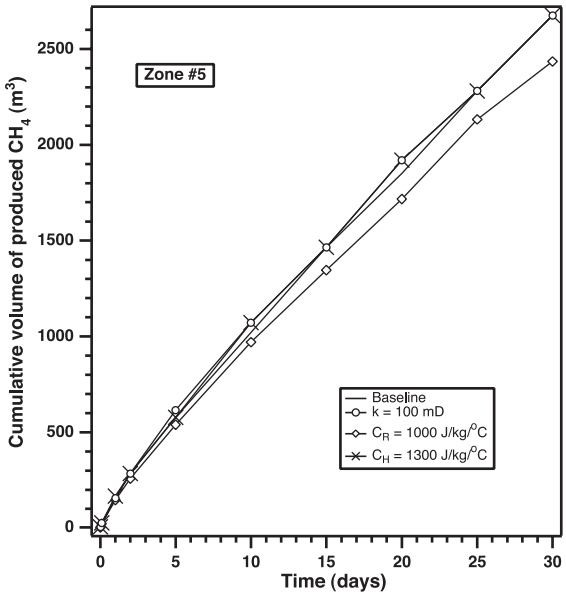

Fig. 20. Sensitivity of gas production to the formation intrinsic permeability k, rock specific heat C_R and hydrate specific heat C_H.

5. Conclusions and discussion

The following conclusions were drawn from the numerical simulation study of gas production from the five zones at the Mallik site:

(1) Production from Zone #1 (with a free gas zone underlying the gas hydrate deposit) by depressurization is possible. Single horizontal wells appear to have an advantage over single vertical wells by delaying water upconing and leading to higher contributions of CH_4 from dissociation to the production gas stream. Two-well systems, involving a combination of depressurization (at the production well) and thermal stimulation (at the injection well, where hot fluids are injected), appear to be substantially superior to single-well

systems, and their advantages are more evident if hot noncondensible gases are injected.

(2) Depressurization of Zone #2 (a gas hydrate underlain by an aquifer) can result in significant gas production, but it also leads inevitably to the production of large amounts of water.

(3) In Zones #3–5 (gas hydrates with no underlying free gas or water zones, and a gas hydrate saturation of at least 50%) thermal stimulation yields measurable amounts of H-methane.

(4) Under the conditions of Zones #3–5, sensitivity studies indicate that the gas production from the hydrate accumulations increases with the gas hydrate saturation, the hydrate initial temperature, and the temperature of the circulating water in the well, as well as the thermal conductivity of the system, the method of heat addition, and the pressure at which the well is kept. Gas production appears to be less sensitive to the rock and gas hydrate specific heat and the permeability of the formation.

Note that the goal of the planned field test is to establish the scientific basis for gas production from natural hydrate deposits, and not to investigate the feasibility of large-scale production from such deposits. Consequently, the aim of the numerical study in this paper is not the development of a viable long-term production strategy, but instead the evaluation of a number of hydrate-bearing zones produced using appropriate methods. The scoping calculations in support of the design for this short-term field experiment focus on the behavior of hydrates during dissociation, make possible the identification of the controlling processes and the corresponding parameters (to be determined in the course of the actual field test), and provide technical criteria for the selection of promising zones as candidates for the field test of gas production.

For the aforementioned reasons, the results presented in this paper should not be extrapolated to large-scale gas production from natural hydrate accumulations and cannot be used to reach conclusions on the subject of feasibility of commercial production. The reason for caution is further reinforced by the considerable knowledge gaps in basic hydrate science, the dearth of field data on the magnitude of important parameters, and the significant uncertainty concerning the ability to describe the behavior of hydrate-impregnated natural systems during dissociation, as discussed in detail by Moridis (in press(a,b)). Because the planned Mallik field test is the first ever attempt at investigating production from natural hydrates, there is no previous similar experience upon which to draw. This numerical study provides some basic information on the relative importance of the various factors and parameters affecting dissociation, and a scientific basis for the selection of appropriate zones as targets for the field test.

Nomenclature

C_H	Specific heat of hydrate (J/kg/°C)
C_R	Specific heat of rock (J/kg/°C)
f	Mass fraction of H-methane in the produced gas stream (kg/kg)
F	Mass fraction of gas in the production stream (kg/kg)
k	Intrinsic permeability of the porous medium (m^2)
k_θ	Composite thermal conductivity (W/m/°C)
N	Hydration number, dimensionless
P	Pressure (Pa)
P_H	Equilibrium hydration pressure at a given temperature (Pa)
Q	Mass flow rate (kg/s)
Q_w	Volumetric flow rate of water production (kg/s)
Q_i	Mass flow rate at the injection well (kg/s)
Q_p	Mass flow rate at the production well (kg/s)
Q_H	Rate oh heat addition (W)
R_w	Well radius (m)
S_{gr}	Irreducible gas saturation, dimensionless
S_w	Water saturation, dimensionless
S_{wr}	Irreducible water saturation, dimensionless
S_H	Hydrate saturation, dimensionless
t	Time (s)
T	Temperature (°C)
T_w	Temperature of the circulating water at the well (Section 4.3) (°C)
T_H	Equilibrium hydration temperature at a given pressure (°C)
T_Q	Equilibrium hydration temperature at the hydrate quadruple point Q_1 (°C)
r	Radial cylindrical coordinate (m)
x	Cartesian coordinate (m)
y	Cartesian coordinate (m)
z	Cartesian or axial cylindrical coordinate (m)

Greek letters

ϕ Porosity of the porous medium (m^3/m^3)

χ_m, χ_G Mole fraction of the methane hydrate and of the second gas hydrate, respectively, in the binary hydrate (Section 1.3), dimensionless

Acknowledgements

This work was supported by the Assistant Secretary for Fossil Energy, Office of Natural Gas and Petroleum Technology, through the National Energy Technology Laboratory, under the US Department of Energy Contract No. DE-AC03-76SF00098. The authors are indebted to Stefan Finsterle and John Apps for their insightful review comments.

References

Bejan, A., 1984. Convection Heat Transport. Wiley, New York, NY.

Bily, C., Dick, J.W.L., 1974. Natural occurring gas hydrates in the Mackenzie Delta, Northwest Territories. Bulletin of Canadian Petroleum Geology 22, 340–352.

Collett, T.S., Lewis, R.E., Dallimore, S.R., Lee, M.W., Mroz, T.H., Uchida, T., 1999. Detailed evaluation of gas hydrate reservoir properties using, JAPEX/JNOC/GSC Mallik 2L-38 gas hydrate research well downhole well-log displays. In: Dallimore, S.R., Uchida, T., Collett, T.S. (Eds.), Scientific Results from the JAPEX/JNOC/GSC Mallik 2L-38 Gas Hydrate Research Well, Mackenzie Delta, Northwest Territories, Canada. Geological Survey of Canada Bulletin, vol. 544, pp. 295–311.

Dallimore, S.R., Collett, T.S., 1999. Regional hydrate occurrences, permafrost conditions, and Cenozoic geology, Mackenzie Delta area. In: Dallimore, S.R., Uchida, T., Collett, T.S. (Eds.), Scientific Results from the JAPEX/JNOC/GSC Mallik 2L-38 Gas Hydrate Research Well, Mackenzie Delta, Northwest Territories, Canada. Geological Survey of Canada Bulletin, vol. 544, pp. 31–43.

Dallimore, S.R., Collett, T.S., Uchida, T., 1999a. Overview of science program, JAPEX/JNOC/GSC Mallik 2L-38 gas hydrate research well. In: Dallimore, S.R., Uchida, T., Collett, T.S. (Eds.), Scientific Results from the JAPEX/JNOC/GSC Mallik 2L-38 Gas Hydrate Research Well, Mackenzie Delta, Northwest Territories, Canada. Geological Survey of Canada Bulletin, vol. 544, pp. 11–17.

Dallimore, S.R., Uchida, T., Collett, T.S. (Eds.), 1999b. Scientific Results from the JAPEX/JNOC/GSC Mallik 2L-38 Gas Hydrate Research Well, Mackenzie Delta, Northwest Territories, Canada. Geological Survey of Canada Bulletin, vol. 544.

Jenner, K.A., Dallimore, S.R., Clark, I.D., Paré, D., Medioli, B.E., 1999. Sedimentology of gas hydrate host strata from the JAPEX/JNOC/GSC Mallik 2L-38 gas hydrate research well. In: Dallimore, S.R., Uchida, T., Collett, T.S. (Eds.), Scientific Results from the JAPEX/JNOC/GSC Mallik 2L-38 Gas Hydrate Research Well, Mackenzie Delta, Northwest Territories, Canada. Geological Survey of Canada Bulletin, vol. 544, pp. 57–68.

Miyairi, M., Akihisa, K., Uchida, T., Collett, T.S., Dallimore, S.R., 1999. Well-log interpretation of gas-hydrate-bearing formations in the JAPEX/JNOC/GSC Mallik 2L-38 gas hydrate research well. In: Dallimore, S.R., Uchida, T., Collett, T.S. (Eds.), Scientific Results from the JAPEX/JNOC/GSC Mallik 2L-38 Gas Hydrate Research Well, Mackenzie Delta, Northwest Territories, Canada. Geological Survey of Canada Bulletin, vol. 544, pp. 281–293.

Moridis, G.J., 2003. Numerical Studies of Gas Production From Methane Hydrates. SPE Journal 32 (8), 359–370 (SPE 87330).

Moridis, G.J., 2004. Numerical simulation studies of thermally-induced gas production from hydrate accumulations with no free gas zones at the Mallik site, Mackenzie Delta, Canada. SPE 77861, 2002, Asia Pac. Oil and Gas Conf. and Exhib., Melbourne, Australia, October 8–10. (in press, SPE Res. Eval. Eng., 2004).

Moridis, G.J., Apps, J., Prues, K., Myer, L., 1998. EOSHYDR: A TOUGH2 module for CH_4-hydrate release and flow in the subsurface. Report LBNL-42386, Lawrence Berkeley National Laboratory, Berkeley, CA.

Ohara, T., Dallimore, S.R., Fercho, E., 1999. Drilling operations, JAPEX/JNOC/GSC Mallik 2L-38 gas hydrate research well. In: Dallimore, S.R., Uchida, T., Collett, T.S. (Eds.), Scientific Results from the JAPEX/JNOC/GSC Mallik 2L-38 Gas Hydrate Research Well, Mackenzie Delta, Northwest Territories, Canada. Geological Survey of Canada Bulletin, vol. 544, pp. 19–30.

Ohara, T., Dallimore, S.R., Fercho, E., 2000. GSC Mallik 2L-38 gas hydrate research well, Mackenzie Delta, N.W.T.: overview of field operations. SPE 59795, Gas Technol. Symp., Calgary, Alberta, Canada, April 3–5.

Parker, J.C., Lenhard, R.J., Kuppusamy, T., 1987. A parametric model for constitutive properties governing multiphase flow in porous media. Water Resources Research 23 (4), 618–624.

Pruess, K., Oldenburg, C., Moridis, G., 1999. TOUGH2 User's Guide—Version 2.0. Report LBL-43134, Lawrence Berkeley National Laboratory, Berkeley, CA.

Sloan, E.D., 1998. Clathrate Hydrates of Natural Gases. Marcel Dekker, New York, NY.

Uchida, T., Dallimore, S.R., Mikami, J., Nixon, F.M., 1999a. Occurrences and X-ray computerized tomography (CT) observations of natural gas hydrate, JAPEX/JNOC/GSC Mallik 2L-38 gas hydrate research well. In: Dallimore, S.R., Uchida, T., Collett, T.S. (Eds.), Scientific Results from the JAPEX/JNOC/GSC Mallik 2L-38 Gas Hydrate Research Well, Mackenzie Delta, Northwest Territories, Canada. Geological Survey of Canada Bulletin, vol. 544, pp. 197–204.

Uchida, T., Matsumoto, R., Waseda, A., Okui, T., Yamada, K., Uchida, T., Okada, S., Takano, O., 1999b. Summary of physicochemical properties of natural gas hydrate and associated gas-hydrate-bearing sediments, JAPEX/JNOC/GSC Mallik 2L-38 gas hydrate research well. In: Dallimore, S.R., Uchida, T., Col-

lett, T.S. (Eds.), Scientific Results from the JAPEX/JNOC/GSC Mallik 2L-38 Gas Hydrate Research Well, Mackenzie Delta, Northwest Territories, Canada. Geological Survey of Canada Bulletin, vol. 544, 205–228.

Winters, W.J., Dallimore, S.R., Collett, T.S., Katsube, T.J., Jenner, K.A., Cranston, R.E., Wright, J.F., Nixon, F.M., Uchida, T., 1999. Physical properties of sediments from the JAPEX/JNOC/GSC Mallik 2L-38 gas hydrate research well. In: Dallimore, S.R., Uchida, T., Collett, T.S. (Eds.), Scientific Results from the JAPEX/JNOC/GSC Mallik 2L-38 Gas Hydrate Research Well, Mackenzie Delta, Northwest Territories, Canada. Geological Survey of Canada Bulletin, vol. 544, pp. 95–100.

Wright, J.F., Dallimore, S.R., Nixon, F.M., 1999a. Influence of grain size and salinity on pressure–temperature thresholds for methane hydrate stability in JAPEX/JNOC/GSC Mallik 2L-38 gas hydrate research-well sediments. In: Dallimore, S.R., Uchida, T., Collett, T.S. (Eds.), Scientific Results from the JAPEX/JNOC/GSC Mallik 2L-38 Gas Hydrate Research Well, Mackenzie Delta, Northwest Territories, Canada. Geological Survey of Canada Bulletin, vol. 544, pp. 229–239.

Wright, J.F., Taylor, A.E., Dallimore, S.R., Nixon, F.M., 1999b. Estimating in situ gas hydrate saturation from core temperature observations, JAPEX/JNOC/GSC Mallik 2L-38 gas hydrate research well. In: Dallimore, S.R., Uchida, T., Collett, T.S. (Eds.), Scientific Results from the JAPEX/JNOC/GSC Mallik 2L-38 Gas Hydrate Research Well, Mackenzie Delta, Northwest Territories, Canada. Geological Survey of Canada Bulletin, vol. 544, pp. 101–108.

Numerical Studies of Gas Production From Class 2 and Class 3 Hydrate Accumulations at the Mallik Site, Mackenzie Delta, Canada

G.J. Moridis, SPE, Lawrence Berkeley Natl. Laboratory, U. of California

Summary

The Mallik site represents an onshore permafrost-associated methane hydrate accumulation in the Mackenzie Delta, Northwest Territories, Canada. This study focuses on gas production at the Mallik site from hydrate deposits that are underlain by either a free-water zone (Class 2) or an impermeable boundary (Class 3). The production analysis was conducted with a numerical simulator that can model the nonisothermal CH_4 release, phase behavior, and flow under conditions typical of CH_4-hydrate deposits by solving the coupled equations of mass and heat balance. Accumulations with a CH_4-hydrate saturation of at least 50% were studied. Dissociation was induced mainly by a combination of thermal stimulation and depressurization as hot fluids circulated between injection and production wells. The effects of salinity and of pressure changes at the wells were also accounted for. The production strategy resulted in a zero net water production. The simulation results indicated that the amount of CH_4 released from the dissociating hydrate deposits is sensitive to the hydrate saturation, the initial temperature, the specific enthalpy, and the flow rate of the circulating fluids.

Introduction

Background. Gas hydrates are solid crystalline compounds in which gas molecules are encaged inside the lattices of ice crystals. Vast amounts of hydrocarbons are trapped in hydrate deposits.[1] Such deposits exist under favorable thermodynamic conditions that occur in two distinct types of geologic formations in which the necessary low temperatures and high pressures exist: in permafrost and in deep ocean sediments.

Current estimates of the worldwide quantity of hydrocarbon gas hydrates range between 10^{15} and 10^{18} m^3. Even the most conservative estimates of the total quantity of gas in hydrates may surpass by a factor of two the energy content of the total fuel fossil reserves recoverable by conventional methods.[1] The magnitude of this resource could make hydrate reservoirs a substantial future energy resource. Although the current energy economics cannot support gas production from hydrate accumulations, their potential clearly demands evaluation.

Gas from hydrates is produced by inducing dissociation. The three main methods of hydrate dissociation are: (1) depressurization, in which the pressure is lowered to a level lower than the equilibrium hydration pressure at the prevailing temperature; (2) thermal stimulation, in which the temperature is raised above the equilibrium hydration temperature at the prevailing pressure; and (3) the use of inhibitors (such as salts and alcohols).[1]

The Mallik site represents an onshore permafrost-associated methane hydrate accumulation in the Mackenzie Delta, Northwest Territories, Canada. A significant body of literature[2] on both the geology and the hydrate accumulations at the site became available following an 1150-m-deep gas hydrate research well that was drilled in 1998.

The Numerical Model. The numerical studies of gas production in this paper were conducted with the EOSHYDR2 model,[3] which is a member of the TOUGH2[4] family of codes for multicomponent, multiphase fluid and heat flow and transport in the subsurface. By solving the coupled equations of mass and heat balance, EOSHYDR2 models the behavior of methane-bearing binary hydrates that are formed or dissociate in porous media according to the general reaction equation:

$$\chi_m(CH_4 \cdot n_m H_2O) \cdot \chi_G(G \cdot n_G H_2O) = \chi_m CH_4 + \chi_G G + (\chi_m n_m + \chi_G n_G)H_2O, \quad (1)$$

where G is the second hydrate-forming gas, n is the hydration number, χ is the mole fraction in the binary hydrate, and the subscripts m and G denote the methane and the second gas, respectively. Obviously, $\chi_m+\chi_G=1$. The gas G can be CO_2, H_2S, N_2, or another gaseous alkane $C_\nu H_{2\nu+2}$ ($\nu=2, 3, 4$).

Classification of Hydrate Deposits. Natural hydrate accumulations are divided into three main classes.[5,6] Class 1 accumulations comprise two layers: the hydrate interval and an underlying two-phase fluid zone with free (mobile) gas. In this class, the bottom of the hydrate stability zone (i.e., the location above which the formation of hydrates becomes thermodynamically possible) coincides with the bottom of the hydrate interval. On current evidence, this appears to be the most desirable class for exploitation, necessitating only small changes in pressure and temperature to induce dissociation.[6]

Class 2 deposits feature two zones: a hydrate-bearing interval, overlying a mobile water zone with no free gas (e.g., an aquifer). Class 3 accumulations are composed of a single zone, the hydrate interval, and are characterized by the absence of an underlying zone of mobile fluids. In Classes 2 and 3, the entire hydrate interval may be well within the hydrate stability zone and can exist under equilibrium or stable conditions.

Objective and Approach. Class 2 and Class 3 hydrate deposits are more challenging production targets than Class 1 hydrates because of adverse permeability conditions, which limit the effectiveness of depressurization and increase the appeal of thermal stimulation as production strategies.[5,7] Previous studies of gas production from Class 2 and Class 3 hydrates involved the production and/or circulation of large amounts of water.[5,7] The main objective of this study is to evaluate the potential of Class 2 and Class 3 accumulations when using production strategies that result in zero net water withdrawals. This approach eliminates the environmental and economic problems posed by the disposal of water in the sensitive Arctic environment.

The Hydrate Zones of Study

Although this study focuses on gas production from deposits at the Mallik area, the analysis is not site-specific; it is applicable to any other hydrate accumulation with similar initial phase-distribution (i.e., water and hydrate saturation) characteristics. The Mallik hy-

Copyright © 2004 Society of Petroleum Engineers

This paper (SPE 88039) was revised for publication from paper SPE 77861, first presented at the 2002 SPE Asia Pacific Oil and Gas Conference and Exhibition, Melbourne, Australia, 8–10 October. Original manuscript received for review 27 March 2004. Revised manuscript received 15 January 2004. Paper peer approved 25 February 2004.

drate zones were selected because the Mallik area is practically the only site for which sufficiently reliable field data are available.[2] The two hydrate zones investigated in this study are referred to as Zones A and B.

Zone A. The hydrate layer in Zone A is 16 m thick, extends from –899 m to –915 m, and is underlain by a 2-m-thick water-saturated layer. The hydrate and water saturations in the hydrate interval are $S_H = 0.8$ and $S_w = 0.2$, respectively (i.e., there is no free gas in this system). At the bottom of the hydrate interval, the pressure $p = 9$ MPa and the temperature $T = 7.5$°C. The hydrate interval is capped by a tight and relatively thick gas-hydrate-bearing sandstone sequence with varying gas-hydrate saturations that act as a no-flow boundary. Similarly, the water-saturated interval is underlain by a 2-m-thick low-porosity (ϕ<2%) sandstone that is assumed to act as a flow boundary. Zone A and its top and bottom boundaries are assumed to extend uniformly over a large area.

Zone B. This zone is characterized by the absence of any layers of mobile gas or water, the pore space being occupied primarily by gas hydrate and water (mostly immobile). Thus, this zone consists entirely of a hydrate system that is not in contact with a flowing water or gas interval. The hydrate layer extends from –1081 m to –1091 m, is assumed to be areally uniform, and has a uniform $S_H = 0.8$ (the rest being water). The pressure and temperature at the bottom of Zone B are $p = 10.74$ MPa and T=7.5°C. Zone B is capped by a relatively thick siltstone sequence, and it is underlain by a relatively thick gas-hydrate-bearing sandstone sequence with varying gas-hydrate saturations. These two bounding formations are both considered no-flow boundaries.

Properties and Characteristics. In both zones, the porosity ($\phi = 0.28$), the intrinsic permeability ($k = 20$ md), the thermal conductivity ($k_\theta = 1.5$ W/m/°C), the rock specific heat ($C_R = 800$ J/kg/°C), and the hydrate specific heat ($C_H = 1600$ J/kg/°C) were assumed to be the same. The regional plunge along the crest of the Mallik structure was not considered in the simulations because of the very shallow dip angle (2° to the northwest). Relative permeabilities and capillary pressures were computed from the Parker *et al.* model,[8] in which the irreducible aqueous and gas saturations were assumed to be $S_{wr} = 0.2$ and $S_{gr} = 0.03$, respectively. Because of the lack of a mobile gas phase and the adverse permeability to gas (intrinsic and relative), gas production from Zones A and B poses serious challenges.

Assumptions. Some general assumptions were made in all the simulations. The temperature distribution was determined by using the known temperature at particular points in the profile and applying a heat flux corresponding to the geothermal gradient of 0.03°C/m to the bottom of the simulated domain. The pressure distribution followed the hydrostatic gradient. The gas hydrate was assumed to be a simple methane hydrate (i.e., $\chi_m = 1$), an assumption supported by the gas-composition studies from the site[2] that indicate $\chi_m \geq 0.98$. Finally, the dissociation of the hydrates was described by an equilibrium process. This is a valid assumption in cases of significant dissociation driving forces, such as a large depressurization or a strong thermal stimulation (both of which are involved in the proposed approach). Under these conditions, dissociation can be very rapid (and even explosive).[7]

It is important to indicate that the results discussed here should not be viewed as an attempt to provide definitive predictive answers to the problem of gas production from dissociating hydrates. The focus of the analysis is the determination of the relative importance and contributions of the various processes involved in dissociation and the sensitivity of gas production to various reservoir conditions and operating parameters. This cautious approach of concentrating more on the relative rather than the absolute system performance is more appropriate, given the considerable uncertainties in the quantitative description of some fundamental processes involved in the dissociation of naturally occurring hydrates.[3,9]

Simulation of Production From Zone A

The Numerical System. In all the simulations of production from Zone A, production and injection wells were arranged in a conventional five-spot pattern **(Fig. 1).** The injected fluid was hot water because the parametric study of McGuire[10] indicated that when steam is injected, the amount of produced gas is less than the estimated fuel consumption. Hot water was injected into the center well of the five-spot pattern, and reservoir fluids (i.e., water and gas from dissociation) were produced from the four production wells at rates determined by the prevailing relative permeabilities. The obvious advantage of this scheme is that it combines the two most important mechanisms of hydrate dissociation (i.e., depressurization at the production well and thermal stimulation at the injection well). The lack of any free gas in Zone A guaranteed that the hydrate was the only possible source of any produced gas.

In an effort to focus the thermal stimulation and depressurization effects in the vicinity of the hydrate interface, the injection and production wells were completed in the top 1 m of the free-water zone underlying the gas-hydrate layer. This configuration offered the additional advantage of limiting mixing of the injected hot water with the colder native reservoir water while maximizing the thermal advantages of buoyancy that tended to concentrate the warmer water immediately below the hydrate interface. To take advantage of the gas buoyancy and the receding hydrate interface in its vicinity, the production well was also completed in the entire hydrate interval. However, this well interval contributed practically no fluids in the early stages of gas production because of adverse relative permeability conditions.

The selection of the five-spot multiwell production scheme was based on earlier work[6,7] that had indicated the advantages of multiwell systems over single wells. An additional reason was provided by the potential of this scheme to minimize water production, the disposal of which may pose environmental and economic challenges. In the proposed scheme, the injection and production rates were initially equal, and the produced fluid was initially 100% water. As dissociation progressed and gas began to appear in the production stream, the injection rate of the hot water was maintained equal to that of the produced water. Thus, the produced water was heated to the desired temperature and then reinjected, and the water-injection rate was less than the rate of fluid produc-

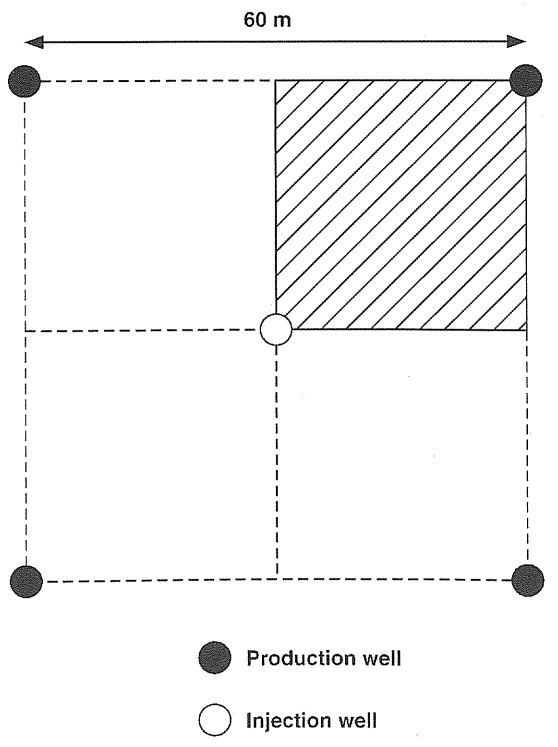

Fig. 1—Five-spot well pattern for modeling a ¼ symmetry subdomain (shaded) in the simulations of Zone A.

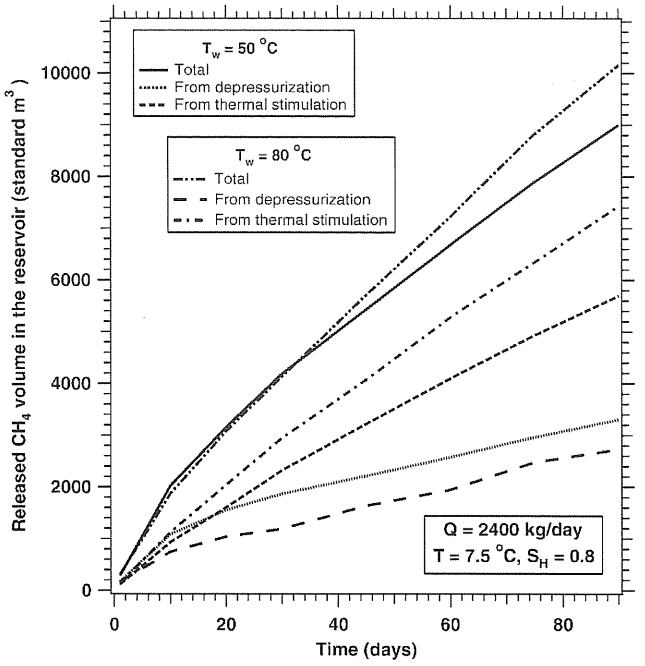

Fig. 2—Zone A: cumulative gas release for T_w=50°C (base case) and T_w=80°C. The contributions of gas from depressurization- and thermally induced hydrate dissociation are described.

tion. This approach eliminated the potential environmental (and the corresponding economic) problems posed by the production of undesirable water while minimizing the energy costs for the heating of the warmer reinjected water.

The water released during dissociation continuously dilutes the salinity of the native reservoir water. Because this is a localized phenomenon concentrated where flow (and, under the conditions of the proposed scheme, maximum dissociation) occurs, and the flowing water is recirculated through reinjection, salinity could not be ignored in this analysis. Note that the salinity level in the pore water can be significant, causing a 1.4°C decrease in the dissociation temperature[2] at the prevailing pressure in Zone A.

The Numerical Grid. Because of symmetry, only a quarter of the domain was simulated with a 3D Cartesian system. The side of the simulated quadrant was 30 m. The domain was discretized in 46×46×33 unequally spaced subdivisions in (x,y,z), resulting in a total of 69,828 gridblocks. Five equations (i.e., components) were considered (CH_4, H_2O, hydrate, salt, and heat) in each gridblock, leading to a system of 349,140 simultaneous equations. The large size and the complexity of the simulated system made the solution of the problem of production from Zone A very demanding computationally.

The Base Case. In this section and in all subsequent discussions, production and injection rates are based on the simulated quadrant of the five-spot pattern in Fig. 1 (corresponding to one-fourth of the rates in the full system). In the base case, the initial water injection and production rate was $Q = 2400$ kg/D, and the injection temperature $T_w = 50$°C.

There are two possible sources of the evolving gas: CH_4 originating from the depressurization-induced dissociation of hydrates in the vicinity of the production well (hereafter referred to as D-gas), and CH_4 from the thermally induced dissociation of hydrates in the vicinity of the hot-water-injection well (hereafter referred to as T-gas). These two gas streams are tracked separately. Note that it is impossible to completely separate pressure and thermal effects during dissociation: thermal changes will occur during depressurization-induced dissociation in response to the endothermic nature of the reaction, and the dissociation temperature will change in the vicinity of hot-water injection in response to the elevated pressure.

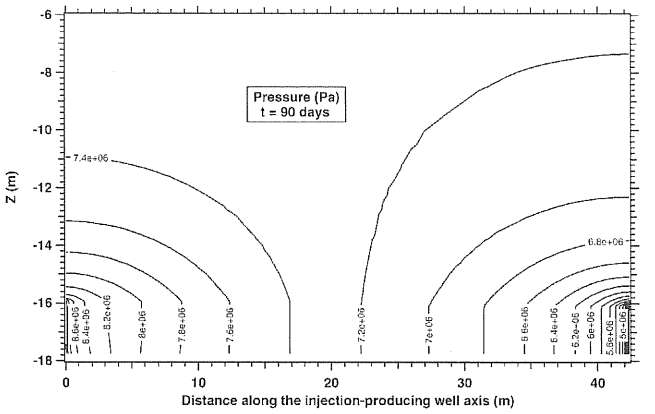

Fig. 3—Pressure distribution on the injection/production well plane at t=90 days (base case, Zone A).

Fig. 2 shows the cumulative gas release in Zone A over a 90-day period, and it describes explicitly the contributions of depressurization and thermal stimulation. As expected, D-gas emerges earlier than T-gas because of the speed of propagation of the pressure wave and the significant thermal inertia of hydrate-impregnated media (hydrate being a relative thermal insulator). However, the pressure drop caused by fluid withdrawal (the driving force of depressurization-induced hydrate dissociation) is relatively small and is further hampered by a temperature decline in the vicinity of the production well (steeper before the hot-water front arrives at the production well). This is caused by the endothermic nature of the hydrate dissociation reaction and leads to an increase in the hydrate dissociation pressure, thus making hydrate dissociation progressively more difficult. The result is that the contribution of T-gas overtakes that of D-gas at an early stage.

The pressure distribution in Zone A on the plane that passes by the injection and production wells at $t = 90$ days is shown in **Fig. 3.** The low-pressure region in the vicinity of the production well is clearly identified. The corresponding temperature distribution near the injection well is shown in **Fig. 4a,** which indicates limited

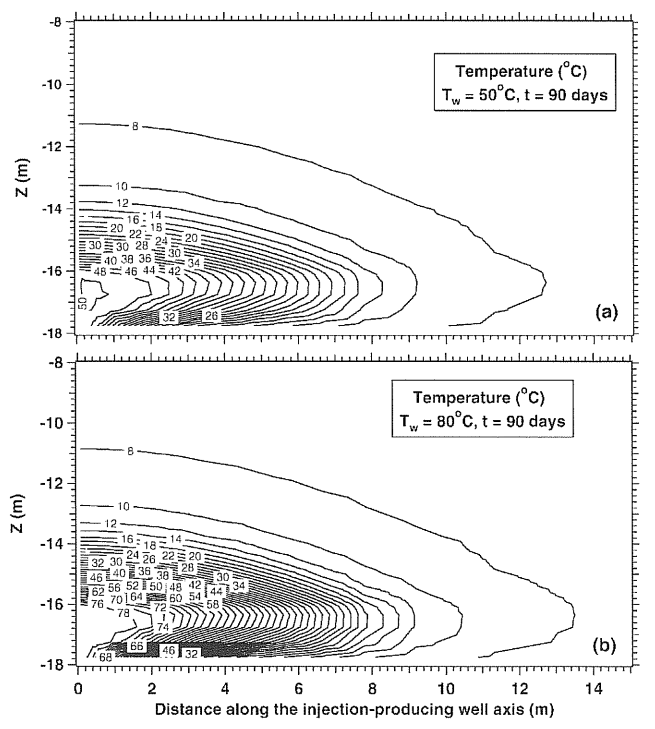

Fig. 4—Temperature distribution on the injection/production well plane at t=90 days: (a) base case, T_w=50°C, (b) T_w=80°C (vicinity of the hot-water-injection well, Zone A).

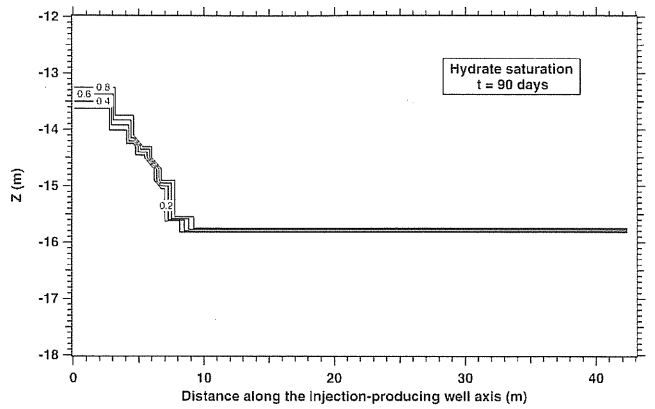

Fig. 5—Hydrate saturation distribution on the injection/production well plane axis at t=90 days (base case, Zone A).

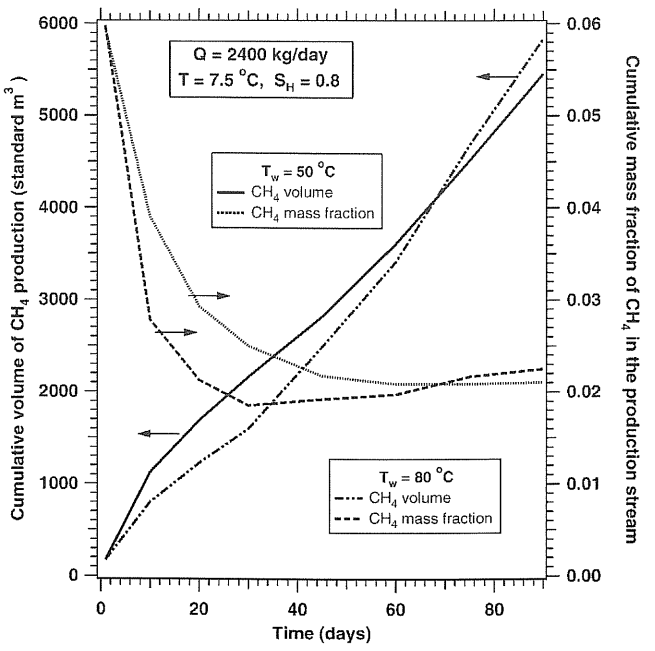

Fig. 6—Zone A: cumulative gas production and gas mass fraction in the production stream for T_w=50°C and T_w=80°C.

penetration of the thermal front into the hydrate layer because of the thermal inertia of the hydrate-impregnated porous medium.

The hydrate-saturation distribution in **Fig. 5** is characterized by a sharp hydrate interface (demonstrated by the bunching of the saturation contour lines). This was expected because the high initial hydrate saturation results in a very low relative permeability. Thus, for thermal dissociation, advection-driven heating is limited, conduction (a slow process) is important, and the corresponding thermal dissociation occurs over a very narrow zone at the hydrate interface. Additionally, the very low permeability limits the depressurization effect to a narrow zone at the interface. The result is dissociation that has the characteristics of an interface process. Lower hydrate saturations lead to higher fluid permeabilities and a more volume-based dissociation process. The hydrate saturation distribution in Fig. 5 is consistent with the pressure and temperature distributions in Figs. 3 and 4. Note the flatness of the bottom of the receding hydrate interface near the production well, which corresponds to an expanded (after the hydrate dissociation) free-water zone.

The cumulative gas production from the production well and the corresponding mass fraction of the gas in the production stream appear in **Fig. 6.** Note that these are different from Fig. 2 because of gas storage in the reservoir after dissociation. Comparison of Figs. 6 and 2 indicates that the gas production and D-gas release are approximately equal at early times, but they begin to deviate as T-gas begins arriving at the production well. The arrival of T-gas is marked by a change in the slope of the cumulative gas-production curve.

An important observation is that the produced gas represents a small fraction of the total produced mass (the rest being water) and does not exceed the 6% level during the 90-day simulation period. The gas mass fraction declines from an initial high and then appears to stabilize at a level close to 2%. This behavior was expected because of the short distance the D-gas has to cover to reach the production well at early times. The possibility of this level rising after a longer injection/production period cannot be dismissed (as the expanding gas front from thermal dissociation reaches the production well), especially because the curve in Fig. 6 shows faint signs of an upward trend. Unfortunately, the extremely demanding computational requirements dictated by the size and complexity of the problem did not allow expansion of the study beyond the 90-day period.

Effect of the Injection Temperature T_w. These simulations differ from the ones for the base case in that the injection temperature $T_w = 80$°C. Fig. 2 shows the evolution of gas over time in Zone A. As in the base case, the volume of T-gas exceeds that of D-gas. The T-gas volume is substantially larger than that in the base case (also shown in Fig. 2). The increase is caused by the larger specific enthalpy of the warmer water, leading to a deeper penetration of the thermal front (see Fig. 4b). However, the dependence of released gas on the injection temperature is sublinear because the large thermal inertia of the system results in higher temperatures in the vicinity of injection and larger temperature gradients, but not substantially deeper penetration. Conversely, the D-gas volume is lower than that in the base case (also shown in Fig. 2). This is attributed to the larger T-gas volume, which leads to higher pressures and thus reduces dissociation by limiting depressurization at the production well. After an initial period of near parity, the total gas release exceeds that in the base case (consistent with expectations).

The cumulative gas production and the corresponding gas mass fraction are shown in Fig. 6. Thus, at early times the gas production is roughly the same as the rate of D-gas release in the reservoir and is later augmented by gas from thermal dissociation. The T-gas contribution to production is more substantial than in the base case because of the availability of larger volumes of such gas. The gas mass fraction shows a distinct upward trend that coincides with the arrival of T-gas at the production well.

Effect of the Hydrate Saturation S_H. These simulations differ from the ones for the base case in that the initial hydrate saturation $S_H = 0.5$. The cumulative gas volume release in **Fig. 7** shows the same pattern as in Fig. 2, with the T-gas volume exceeding that of D-gas. The volume of the released CH_4, however, is lower than that in the other cases (in which $S_H = 0.8$). This is consistent with expectations. The difference is caused by the smaller amounts of the gas source (i.e., the hydrate saturation).

Effect of the Production Rate Q. A change in the injection/production rate Q affects both the amount of heat available for thermal dissociation of the hydrate (at the injection well) and the pressure differential that drives depressurization (at the production well). This is evident in **Fig. 8,** which shows a reduction in the gas released in zone A when Q is reduced to 1,200 kg/D. In this case, the contribution of D-gas to the total gas release decreases because the lower fluid-withdrawal rate affects depressurization more severely.

Further reduction of Q to 240 kg/D (one-tenth the rate in the base case) results in the commensurate reduction in the released volume shown in Fig. 8. Note that, unlike all previous cases (in which gas appears practically immediately), it takes almost 5 days for gas to begin evolving. This is because of the low rate Q, which is insufficient to provide the necessary heat (at the injection well) and pressure differential (at the production well) immediately upon the beginning of the operation.

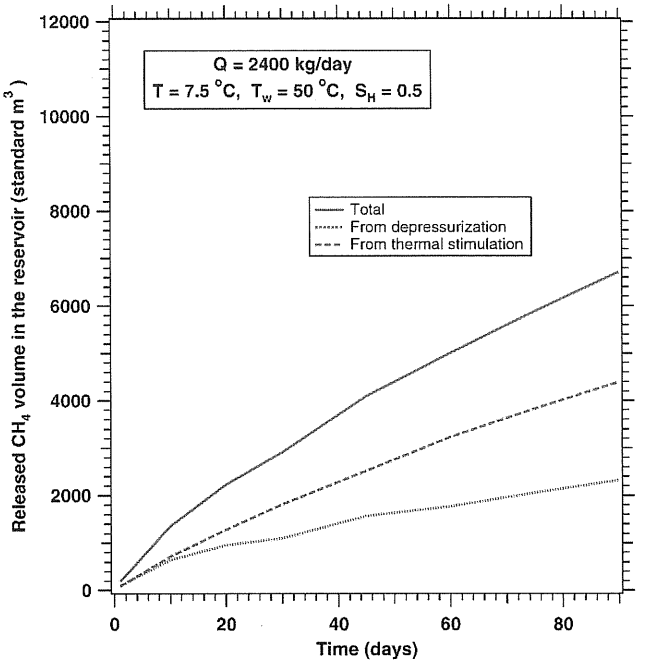

Fig. 7—Cumulative gas release in Zone A when S_H=0.5.

Effect of the Initial Hydrate Temperature *T*. Under the conditions of the proposed gas-production scheme, higher initial hydrate (formation) temperature T is expected to lead to larger amounts of released gas because both thermal and depressurization dissociation will be easier to attain. This is because a higher T reduces the considerable amount of heat needed in the wasteful process of raising the temperature of the hydrate (which has high heat capacity and low thermal conductivity) to the dissociation temperature. Additionally, a higher T allows depressurization-induced hydrate dissociation to proceed more effectively and for longer because (a) it corresponds to higher dissociation pressures (thus dissociating more easily) and (b) provides a larger heat reservoir to cover the needs of the endothermic dissociation reaction (thus taking longer for the dissociation to decline because of cooling).

This is amply demonstrated by the simulation results of gas production when the temperature at the base of the hydrate interval is set to the hydration temperature $T_H = 10°C$ at the prevailing reservoir pressure. From **Fig. 9,** it is evident that the effect on the released gas volume is rather dramatic. The cumulative released gas remains practically constant after 3 to 4 days, indicating complete dissociation of the hydrate in the five-spot quadrant. The released volumes are very large, almost two orders of magnitude larger than the ones in all previous cases. Additionally, the contributions from depressurization and thermal stimulation show a different pattern: depressurization is by far the dominant contributor to gas release.

This is further confirmed by the evolution of the gas-hydrate saturation on the injection/production well plane over time in Fig. 9. The effect of depressurization is evident even at very early times. The depressurization-induced dissociation front propagates rapidly from the production well toward the injection well. It is remarkable that the last remaining intact hydrate region in **Fig. 10** at t = 1.5 days is located in the vicinity of the hot-water-injection well. This is rather counterintuitive and is caused by the higher pressures near the injection well (which necessitate higher temperatures for dissociation) and the insulating thermal properties of the hydrates. The implication of these observations is that hydrate intervals at or in the vicinity of the dissociation temperature (i.e., the boundary of the hydrate stability zone) should be the obvious targets for hydrocarbon gas recovery because of the efficiency and speed of dissociation.

The proposed process rapidly transforms the simulated hydrate and water system into a gas and water system, from which fluids are withdrawn at a rate much slower than the gas-generation rate. The cumulative gas production and the corresponding gas mass fraction in the production stream are shown in **Fig. 11,** which indicates that far more gas is produced than in any other case. Additionally, the gas mass fraction follows the same general pattern as in Fig. 6 but is significantly higher. This was expected because of the substantially larger amounts of released gas in the reservoir.

Production From Zone B

Flow-induced dissociation in Zone B is very difficult (and almost impossible initially) because of (a) the absence of a free- (mobile) water or free-gas zone in contact with the hydrate interval and

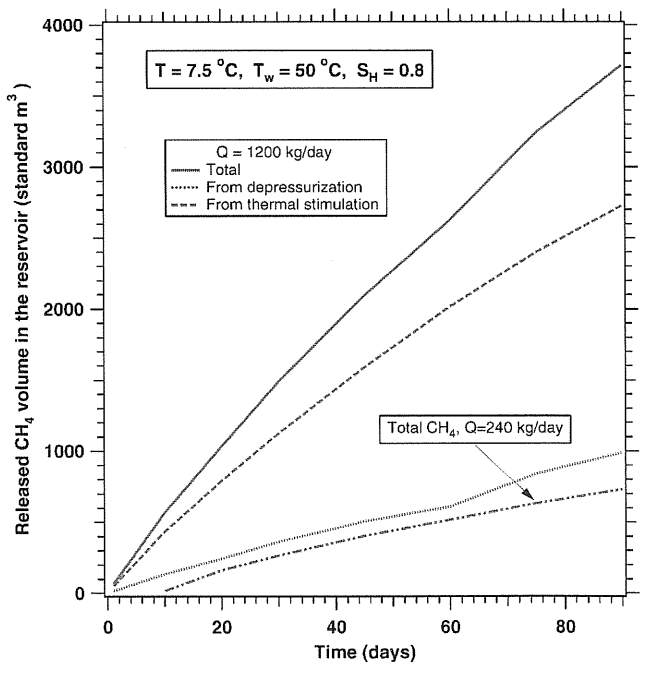

Fig. 8—Cumulative gas release in Zone A when *Q*=1,200 kg/D and *Q*=240 kg/D.

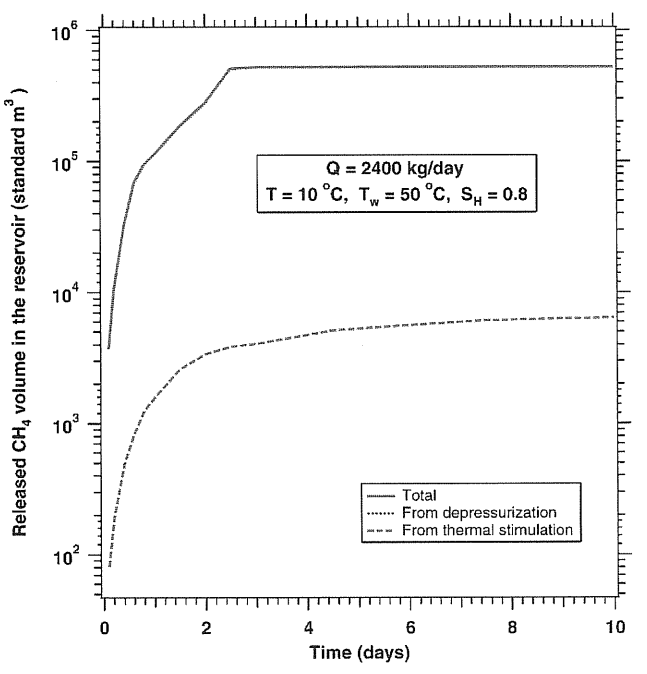

Fig. 9—Cumulative gas release in Zone A when *T*=10°C (the curve for the D-gas release practically coincides with that for the total released gas).

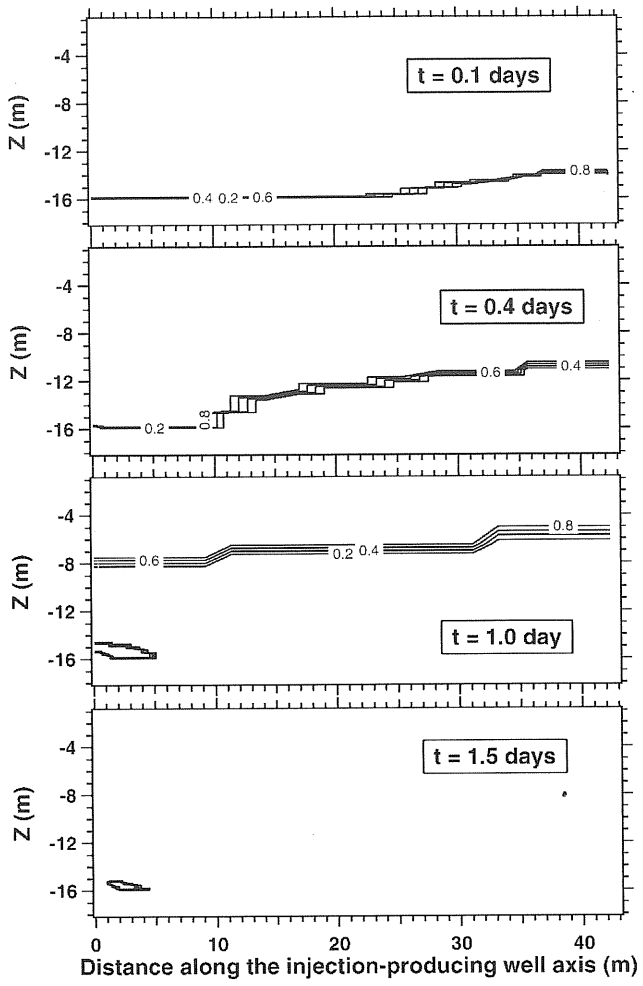

Fig. 10—Evolution of the hydrate saturation on the injection/production plane when *T*=10°C (Zone A).

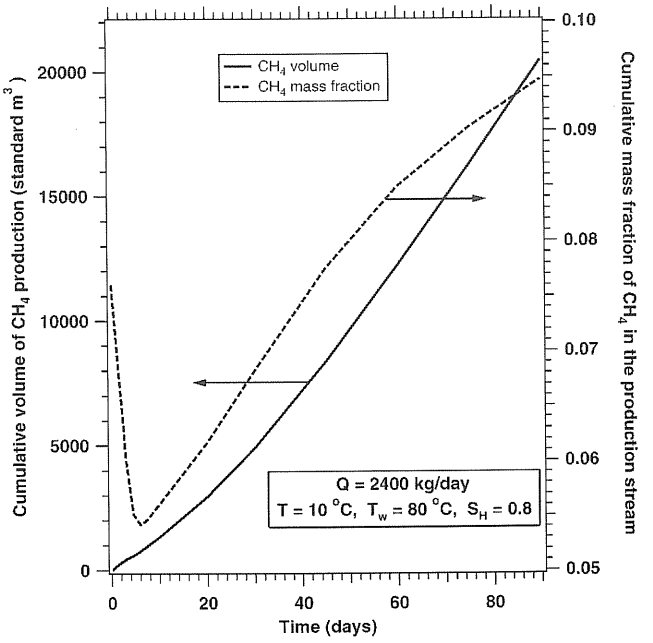

Fig. 11—Cumulative gas production and gas mass fraction in the production stream when *T*=10°C (Zone A).

(b) the very low permeability to the native water within the hydrate interval. At the initial $S_H = 0.8$, the water saturation $S_w = 0.2$ is at the irreducible level, and the water relative permeability is zero. Under these conditions, the effectiveness of both depressurization and thermal stimulation as dissociation mechanisms is severely restricted because the pressure front cannot advance deeply into the hydrate zone, and heat transfer is limited to conduction only (a slow process in the insulating hydrates). Production from such nonflowing systems using hot-water circulation in the wellbore was studied by Moridis *et al.*,[7] who investigated the relative importance of various reservoir properties and operation parameters on gas recovery.

In the present study, the effort is focused on enhancing gas production through dissociation by adding the component of flow and heat advection to the process. This is possible only if the hydrate layer is fractured. Single-well systems in continuous depressurization or huff 'n' puff processes (that combine thermal, inhibitor, and depressurization effects) were not addressed because of their limited effectiveness (a result of the very low volume of the fractures) and the possibility of self-healing fractures in the hydrates during cooling in depressurization-induced dissociation.

Thus, the studies of gas recovery from Zone B involved two-well systems (an injection and a production well) connected through fractures. In all the simulation of production from Zone A, the production and injection wells were located on the same fracture plane. Note that this and all other fracture-related properties in this study are significant assumptions, the validity of which is currently unknown given the existing knowledge gaps in the characteristics of hydrate fracturing.

Hot water was injected into the injection well, and reservoir fluids (i.e., water and gas) were produced from the production well at rates determined by the prevailing relative permeabilities. As in the case of Zone A, this scheme aimed to combine the advantages of the two most important mechanisms of hydrate dissociation (i.e., depressurization at the production well and thermal stimulation at the injection well). The initial phase distribution guaranteed the hydrates to be the exclusive source of any CH_4 gas evolving during the study.

In the simulations of Zone B, the injection and production wells were completed in the entire gas-hydrate interval and were spaced 30 m apart. The fractures were assumed to have a uniform aperture, to be fully saturated with mobile water ($S_w = 1$), to extend throughout the 10-m thickness of the hydrate layer without extending into the top and bottom bounding formations, and to extend 4 m past the wells in the x direction (see **Fig. 12**). The fracture intrinsic permeability was k = 1,000 md. The production approach was the same as in Zone A. The injection and production rates were initially equal (and the produced fluid was initially 100% water). The water-injection rate was equal to the time-variable rate of water production. Thus, the produced water was heated to the desired temperature and then reinjected, and the water-injection rate was less than the rate of fluid production.

The Numerical Grid. Because of symmetry, only half the domain was simulated with a 2D Cartesian areal system with a uniform thickness of $\Delta z = 10$ m. The dimensions of the simulated domain are shown in Fig. 12. The domain was discretized in 120×44

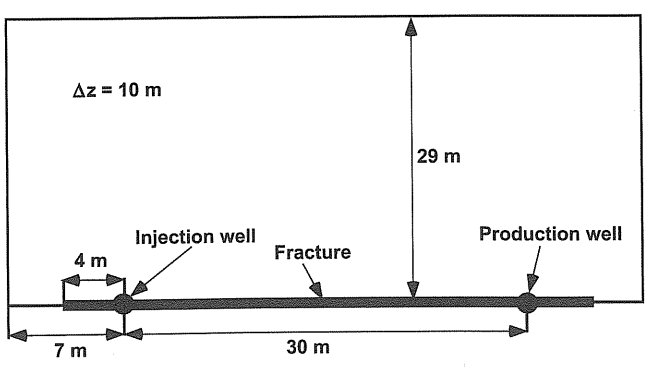

Fig. 12—A schematic of the areal configuration of the injection/production system in Zone B (not to scale).

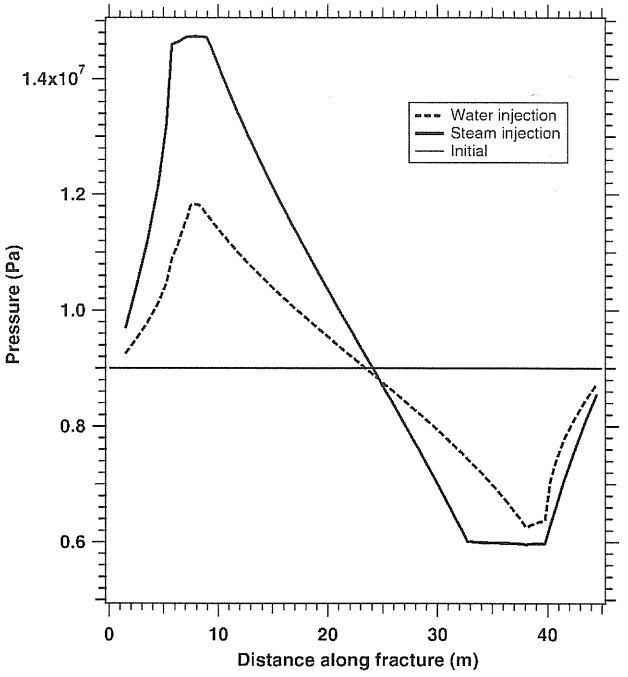

Fig. 13—Pressure distribution in the fracture of Zone B during water and steam injection (*t*=10 days).

unequally spaced subdivisions in (x,y), resulting in a total of 5,720 gridblocks, of which 5,504 were active and the remaining represented constant conditions at the x and y boundaries of the domain. The first subdivision in y corresponded to the fracture, which was assumed to have an aperture of 5×10^{-4} m.

The same five components discussed in Zone A (CH_4, H_2O, hydrate, salt, and heat) were considered here, leading to a system of 27,520 simultaneous equations. Heat losses into the underlying and overlying boundaries were accounted for using the semianalytical solution option available in TOUGH2.[4] Note that although the number of equations involved in Zone B was less than one-tenth of that in Zone A, the execution times were considerably longer because of the mathematical challenges posed by the fracture and the initial absence of flowing zones.

Water Injection. In the simulations of Zone B, production and injection rates are based on the half-domain shown in Fig. 12 (corresponding to half the rates in the full system). For the reasons discussed in Zone A, the initial injection fluid was hot water at a rate of $Q=120$ kg/D and at a temperature $T_w=50$°C. Water was initially produced at the same rate from the production well. This low injection/production rate was selected to avoid possible (a) fracturing of the bounding formations (caused by excessive pressures at the injection well) and subsequent fluid loss and (b) cavitation (at the production well) if the system is incapable of supplying the flow rate imposed in the simulations. Both of those potential problems can arise because of the near-impermeability of the system and the very low fracture volumes.

Fig. 13 shows the pressure distribution in the fracture at $t=10$ days (at which time pressure has stabilized) and indicates that the selected rate is not expected to cause any serious problems. The corresponding temperature distribution in the reservoir in **Fig. 14** shows the limited extent of the volume affected by the hot-water injection. This limited extent was expected because of the low injection rate, the relatively low specific enthalpy of the injected water, and the insulating behavior of the hydrates. The obvious implication is that, for effective dissociation, higher specific enthalpies are needed.

This is further confirmed by **Fig. 15,** which shows the cumulative gas release in Zone B over a 90-day period. The released volumes are significantly smaller than those released in the hydrate dissociation from Zone A. All the gas evolving in the system

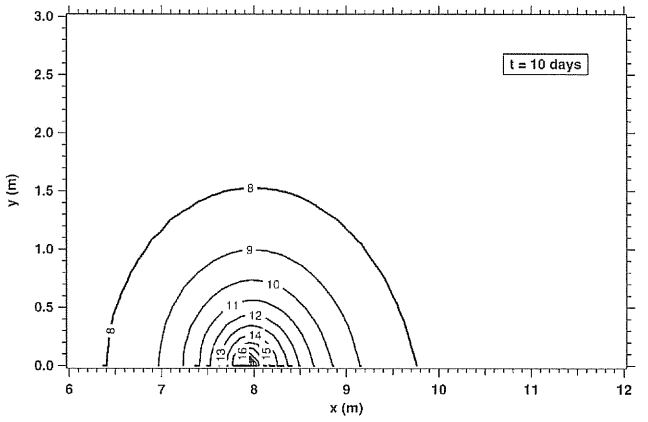

Fig. 14—Areal temperature distribution at *t*=10 days in the vicinity of the injection well during water injection (Zone B).

originates from thermal dissociation because the production rate is insufficient to effect any depressurization-induced gas production. Thus, in this approach, higher injection/production rates are desirable, but the possibility of fracturing the bounding formations has to be considered.

The cumulative gas production at the well in Fig. 15 shows a delay in the appearance of gas. This was expected because of the absence of any depressurization-originating CH_4 and the distance the thermally released gas has to travel along the fracture before appearing at the production well.

Steam Injection. In these simulations, the conditions were different from the water-injection case in two respects. The injected fluid was superheated steam with a specific enthalpy corresponding to a pressure of 10 MPa and a temperature of 400°C. Additionally, the initial injection/production rate was increased to $Q=240$ kg/D.

Fig. 13 shows the pressure distribution in the fracture. Note the reduction in depressurization (indicated by a flattening of the pressure distribution in the vicinity of the production well) caused by dissociation-driven gas release. The increase in the pressure at the injection well is much smaller than what the doubling of the in-

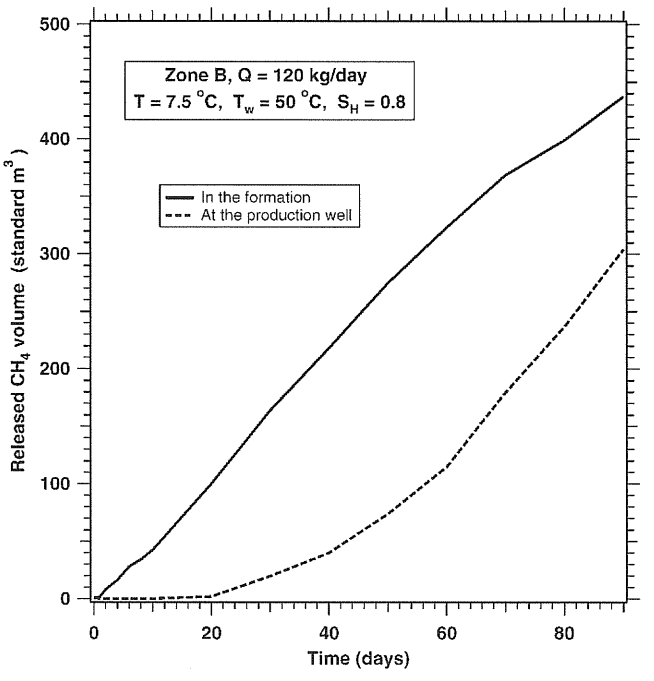

Fig. 15—Cumulative gas release in the reservoir and at the well during water injection (Zone B). Note that all the gas is originating from thermal dissociation.

jection rate would suggest (though it is unknown if it exceeds the fracture pressure of the bounding layers). The effect can be further mitigated if the compressibility of naturally occurring hydrates (assumed zero in the simulations) is significant.

The cumulative gas release in **Fig. 16** shows a drastically different behavior from that for the water injection in Fig. 15. In this case, the released volumes are large, and depressurization is the main contributor to gas production. This was made possible by the larger production rate, which lowers pressure below the dissociation threshold.

Discussion

Remaining Challenges. To complete this study, it is important to assess the impact of a number of other factors on gas release and recovery. These include the formation intrinsic permeability, the fracture area (in Zone B), the system thermal properties (conductivity and specific heat), and the relative permeability. Of those, relative permeability poses a particular challenge because no quantitative information exists on its behavior in hydrate-impregnated media. The thermal conductivity of the hydrate-bearing medium is known to have a significant effect on gas recovery[7] in conduction-driven dissociation, but its importance remains to be determined in advection-driven processes. It is expected that production is less sensitive to the rock and hydrate specific heats, and to the irreducible gas saturation, but this has not yet been demonstrated. Additionally, operational parameters (such as time-variable injection/production rates in fractured hydrates, to take advantage of the increased hydrate-free volume and the corresponding larger permeability after dissociation) merit investigation.

Note that, while the pathway for a thorough study of hydrate behavior is rather evident, there are significant practical difficulties that slow the pace of such investigations. Among the most challenging are the extraordinarily large computational requirements for the study of such systems, necessitated by the complexity of the underlying physics and the need for fine discretization. Thus, even when using some of the most powerful computers, the simulations of the various production cases in Zones A and B can easily take several days to entire weeks.

Knowledge Gaps. The most serious limitation, however, is the dearth of information on the fundamental properties of hydrate reservoirs and their field thermodynamic behavior. There are very few reliable measurements of the permeability, porosity, and saturation of natural hydrate deposits, and the understanding of the hydrate kinetic behavior is at a very early stage.[1] Additionally, there are significant scientific challenges and knowledge gaps that must be addressed for numerical simulation to provide reliable predictions of gas production.[3,9] These include the type of formation/dissociation reactions occurring in natural accumulations (equilibrium vs. kinetic), the values and temperature dependence of the corresponding parameters under field conditions, the hysteretic behavior between the formation and dissociation *p-t* equilibrium curves, the relative permeability in hydrate formations, hydrocarbon solubility near the hydration point, hydrate thermal properties, and the effect of the hydration number on the properties and behavior of hydrates. The fact that no representative undisturbed sample of natural hydrates has been obtained to date indicates the magnitude of the problem.

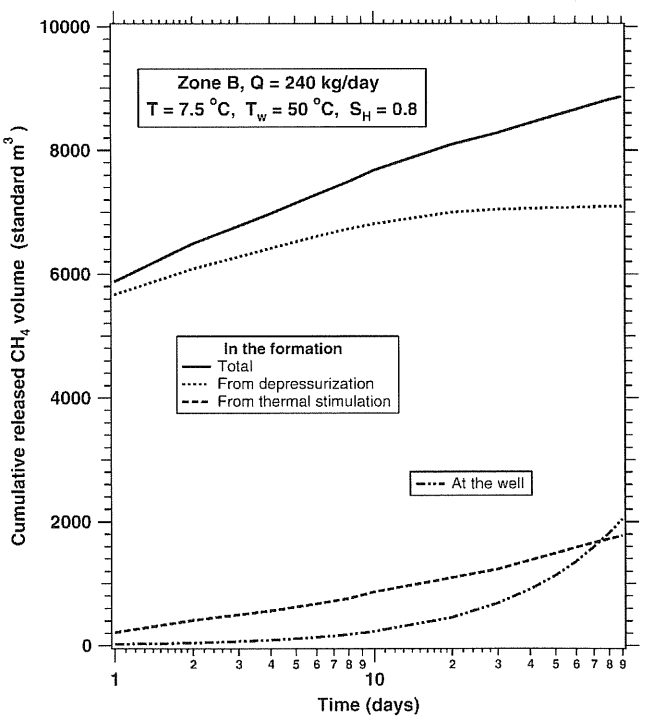

Fig. 16—Cumulative gas release in the reservoir and at the well during steam injection (Zone B).

Scope of Simulations. Thus, at this stage, our ability to describe the hydrate system mathematically exceeds our knowledge of some basic processes that control its behavior. This should not be interpreted as lack of confidence in the role of numerical simulation. Even with the current lack of data, numerical simulation makes it possible to determine technical feasibility, establish envelopes of possible solutions, and identify promising target zones of hydrates for development. This is the light in which the current study must be considered. With this approach in mind, the results discussed here should not be viewed as an attempt to provide definitive predictive answers to the problem of gas production from dissociating hydrates. Instead, the emphasis here is on determining the relative importance and contributions of the various processes involved in dissociation, and the sensitivity of gas production to various reservoir conditions and operating parameters, rather than on the absolute system performance. Thus, although some of the production results obtained in this study appear intriguing (especially when the initial reservoir temperature is that at the base of the stability zone), the question of commercial feasibility cannot yet be answered because of the aforementioned uncertainties and because the subject of developing techniques for effective hydrate dissociation has barely been researched.

Conclusions

The Mallik site represents an onshore permafrost-associated methane hydrate accumulation in the Mackenzie Delta, Northwest Territories, Canada, and is characterized by several hydrate intervals. This study focuses on gas production from two hydrate accumulations: Zone A, a Class 2 deposit, and Zone B, a Class 3 deposit. These are some of the most challenging targets for gas recovery because of adverse permeability and the thermal properties of hydrates. Gas produced from these deposits is certain to originate from the dissociation of hydrates.

In Zone A, hot water was injected into the underlying water zone through injection wells, and reservoir fluids were withdrawn from the production wells of a five-spot pattern. The water produced from the production well was heated and reinjected into the injection well, resulting in a net zero withdrawal of water. Thus, the potentially adverse environmental impacts of the produced water were eliminated, and the corresponding economic considerations were alleviated.

The results of the simulations indicate that, in Zone A, gas release in the reservoir increases with the specific heat of the injected water (a function of its temperature) because this increases the amount of heat available for dissociation. An increasing injection rate leads to larger gas releases because of increased thermal and depressurization-induced dissociation. Larger initial hydrate saturations lead to larger releases because of the availability of larger gas sources. The initial formation temperature may have a dramatic effect on the volume of the released gas. Hydrates at higher temperatures require substantially smaller depressurization and far less heat for dissociation.

Because of high hydrate saturation, flow is impossible without fracturing in Zone B. In this case, a system of two wells connected

through a common fracture was used. The approach in Zone B was similar to that in Zone A and involved a zero net water withdrawal. Hot water and superheated steam were injected into the injection well, and reservoir fluids were withdrawn from the production well.

The limited study of production from Zone B indicates that, despite the relatively large fracture permeabilities, the small fracture volumes in such systems may pose challenges. In the balanced injection/production regime proposed in this study, by minimizing injection rates to prevent potential fracturing of the bounding formation, it is possible to inhibit depressurization (an unwelcome development) if the pressure fails to fall below the dissociation threshold. To avoid this problem, the highest safe level of injection rate and the highest possible specific enthalpy of the injected fluid (e.g., by resorting to superheated steam) are possible mitigation strategies.

Nomenclature

C = specific heat (J/kg/°C)
G = hydrate-forming gas (Eq. 1)
k = intrinsic permeability (m^2)
k_θ = thermal conductivity (W/m/°K)
n = hydration number
p = pressure (Pa)
Q = total fluid mass flow rate at a well ($kg/m^3/s$)
S = phase saturation
t = time (s)
T = temperature (°K)
x,y,z = coordinates (m)
χ = mole fraction of constituent hydrates in composite hydrate
ϕ = porosity

Subscripts and Superscripts

G = gas phase
H = solid hydrate phase
m = methane component
R = rock
gr = irreducible gas
wr = irreducible water
w = water component
ν = number of carbons in alkanes

Acknowledgments

This work was supported by the Assistant Secretary for Fossil Energy, Office of Natural Gas and Petroleum Technology, through the Natl. Energy Technology Laboratory, under the U.S. Dept. of Energy, Contract No. DE-AC03-76SF00098. The author is indebted to John Apps and Stefan Finsterle for their insightful review comments.

References

1. Sloan, E.D.: *Clathrate Hydrates of Natural Gases*, Marcel Dekker Inc., New York City (1998).
2. Dallimore, S.R., Uchida, T., and Collett, T.S. (eds.): "Scientific Results from JAPEX/JNOC/GSC Mallik 2L-38 Gas Hydrate Research Well, Mackenzie Delta, Northwest Territories, Canada," Geological Survey of Canada Bull. 544, Ottawa, Canada (1999).
3. Moridis, G.J.: "Numerical Studies of Gas Production From Methane Hydrates," *SPEJ* (December 2003) 359.
4. Pruess, K., Oldenburg, C., and Moridis, G.: "TOUGH2 User's Guide—Version 2.0," Report LBL-43134, Lawrence Berkeley Laboratory, Berkeley, California (1999).
5. Moridis, G.J. and Collett, T.S.: "Strategies for Gas Production From Hydrate Accumulations Under Various Geologic Conditions," Report LBNL-52568, Lawrence Berkeley Natl. Laboratory, Berkeley, California (2003).
6. Moridis, G.J. and Collett, T.S.: "Gas Production from Class 1 Hydrate Accumulations," Report LBNL-61003, Lawrence Berkeley Natl. Laboratory, Berkeley, California (2004); in press, in *Recent Advances in the Study of Gas Hydrates*, C. Taylor and J. Qwan (eds.), Kluwer Academic, New York City (2004).
7. Moridis, G.J. *et al.:* "Numerical Studies of Gas Production Scenarios From Several CH_4-Hydrate Accumulations at the Mallik Site, Mackenzie Delta, Canada," Report LBNL-50257, Lawrence Berkeley Natl. Laboratory, Berkeley, California (2002); in press, *J. Petrol. Sci. Eng.* (2004).
8. Parker, J.C., Lenhard, R.J., and Kuppusamy, T.: "A Parametric Model for Constitutive Properties Governing Multiphase Flow in Porous Media," *Water Resour. Res.* (1976) **12,** No. 1, 57.
9. Swinkels, W.J.A.M. and Drenth, R.J.J.: "Thermal Reservoir Simulation Model of Production From Naturally Occurring Gas Hydrate Accumulations," *SPEREE* (December 2000) 559.
10. McGuire, P.L.: "Methane Hydrate Gas Production: An Assessment of Conventional Production Technology as Applied to Hydrate Recovery," Report LA-9102-MS, Los Alamos Natl. Laboratory, Los Alamos, New Mexico (1981).

SI Metric Conversion Factors

atm × 1.013 250*		E + 05	= Pa
eV × 1.602 19		E − 19	= J
ft × 3.048*		E − 01	= m
ft^2 × 9.290 304*		E − 02	= m^2
ft^3 × 2.831 685		E − 02	= m^3
°F	(°F − 32)/1.8		= °C
°F	(°F + 459.67)/1.8		= K

*Conversion factor is exact.

George Moridis has been a staff scientist with the Hydrology and Reservoir Dynamics Dept. in the Earth Sciences Division of the Lawrence Berkeley Natl. Laboratory (LBNL), Berkeley, California, since 1991. e-mail: GJMoridis@lbl.gov. He is the Research Area Leader for Transport and Thermodynamics, is in charge of the LBNL hydrate research program, and is responsible for the LBNL radionuclide transport studies for the Yucca Mountain High Level Radioactive Waste Repository. Moridis is the author or coauthor of 30 papers in peer-reviewed journals, more than 100 LBNL reports and book articles, and two patents. He holds MS and PhD degrees from Texas A&M U. and BS and ME degrees in chemical engineering from the Natl. Technical U., Athens.

SPE 97266

Depressurization-Induced Gas Production From Class 1 Hydrate Deposits

George J. Moridis, SPE, Michael B. Kowalsky and Karsten Pruess, SPE,
Lawrence Berkeley National Laboratory, University of California

Copyright 2005, Society of Petroleum Engineers

This paper was prepared for presentation at the 2005 SPE Annual Technical Conference and Exhibition held in Dallas, Texas, U.S.A., 9 – 12 October 2005.

This paper was selected for presentation by an SPE Program Committee following review of information contained in a proposal submitted by the author(s). Contents of the paper, as presented, have not been reviewed by the Society of Petroleum Engineers and are subject to correction by the author(s). The material, as presented, does not necessarily reflect any position of the Society of Petroleum Engineers, its officers, or members. Papers presented at SPE meetings are subject to publication review by Editorial Committees of the Society of Petroleum Engineers. Electronic reproduction, distribution, or storage of any part of this paper for commercial purposes without the written consent of the Society of Petroleum Engineers is prohibited. Permission to reproduce in print is restricted to a proposal of not more than 300 words; illustrations may not be copied. The proposal must contain conspicuous acknowledgment of where and by whom the paper was presented. Write Librarian, SPE, P.O. Box 833836, Richardson, TX 75083-3836, U.S.A., fax 01-972-952-9435.

Abstract

Class 1 hydrate deposits are characterized by a hydrate-bearing layer underlain by a two-phase zone involving mobile gas. Two kinds of deposits are investigated. The first involves water and hydrate in the hydrate zone (Class 1W), while the second involves gas and hydrate (Class 1G). We introduce new models to describe the effect of the presence of hydrates on the wettability properties of porous media. We determine that large volumes of gas can be readily produced at high rates for long times from Class 1 gas hydrate accumulations by means of depressurization-induced dissociation using conventional technology. Dissociation in Class 1W deposits proceeds in distinct stages, while it is continuous in Class 1G deposits. To avoid blockage caused by hydrate formation in the vicinity of the well, wellbore heating is a necessity in production from Class 1 hydrates. Class 1W hydrates are shown to contribute up to 65% of the production rate and up to 45% of the cumulative volume of produced gas; the corresponding numbers for Class 1G hydrates are 75% and 54%. Production from both Class 1W and Class 1G deposits leads to the emergence of a second dissociation front (in addition to the original ascending hydrate interface) that forms at the top of the hydrate interval and advances downward. In both kinds of deposits, capillary pressure effects lead to hydrate lensing, i.e., the emergence of distinct banded structures of alternating high-low hydrate saturation, which form channels and shells and have a significant effect on production.

Introduction

Background. Gas hydrates are solid crystalline compounds in which gas molecules (referred to as guests) are lodged within the lattices of ice crystals (called hosts). Under suitable conditions of low temperature and high pressure, a gas G will react with water to form hydrates according to

$$G + N_H H_2O = G \bullet N_H H_2O,$$

where N_H is the hydration number. Of particular interest are hydrates formed by hydrocarbon gases when G is an alkane.

Gas hydrate deposits occur in two distinctly different geologic settings where the necessary favorable thermodynamic conditions exist for their formation and stability: in the permafrost and in deep ocean sediments. Because of different formation processes, these two types of accumulations have distinctly different attributes.

Although there has been no systematic effort to map and evaluate this resource and current estimates vary widely (ranging between 10^{15} to 10^{18} m^3), the consensus is that the worldwide quantity of hydrocarbon gas hydrates is vast[1]. Even the most conservative estimate surpasses by a factor of two the energy content of the total fossil fuel reserves recoverable by conventional methods. The sheer magnitude of this resource commands attention as a potential energy resource, even if a limited number of hydrate deposits are attractive production targets and/or only a fraction of the trapped gas may be recoverable. As current energy economics make gas production from unconventional resources increasingly appealing (or, at a minimum, less prohibitive), the potential of hydrate accumulations clearly demands technical and economic evaluation. The attractiveness of hydrates is further augmented by the environmental desirability of gas (as opposed to solid and liquid) fuels.

Gas from hydrates is produced by inducing dissociation by one of the following three main methods[1] (or combinations thereof): (1) depressurization, which involves pressure lowering below the equilibrium hydration pressure at the prevailing temperature, (2) thermal stimulation, in which the temperature is raised above the equilibrium hydration temperature at the prevailing pressure, and (3) the use of hydration inhibitors (such as salts and alcohols).

Classification of hydrate deposits. Natural hydrate accumulations are divided into three main classes[2,3]. Class 1 accumulations are composed of two layers: the hydrate interval and an underlying two-phase fluid zone with free (mobile) gas. In this class, the bottom of the hydrate stability zone (i.e., the location above which hydrates are stable because of thermodynamically favorable P and T conditions) coincides with the bottom of the hydrate interval. On current evidence, this class appears to be the most promising target for gas production, because the thermodynamic proximity to the hydration equilibrium at the highest possible temperature requires only small changes in pressure and temperature to induce dissociation[3]. Additionally,

the existence of a free gas zone provides a significant economic advantage because it guarantees gas production even when the hydrate contribution is small. The three-phase coexistence (gas, aqueous and hydrate) at the bottom of the hydrate interval is a unique characteristic of Class 1 deposits, which indicates that such accumulations have about the same P and T at the hydrate interface if the geothermal gradient does not exhibit significant local variations.

Class 2 deposits comprise two zones: (1) a hydrate-bearing interval, overlying (2) a mobile water zone. Class 3 accumulations are composed of a single zone, the hydrate interval, and are characterized by the absence of an underlying zone of mobile fluids. In Classes 2 and 3, the entire hydrate interval may be well within the hydrate stability zone and can exist under equilibrium or stable conditions. Production from Class 2 and Class 3 accumulations is burdened with long lead times before substantial gas release from the hydrates can be established, in addition to unfavorable initial permeability regimes.

Objective and approach. The problem of production from Class 2 and Class 3 hydrate deposits has been discussed in past studies[4,5,6] that determined their potential and identified the challenges they pose. Gas production from Class 1 accumulations has been investigated in earlier studies[3,7] that did not have the benefit of recent advances in our understanding of the thermal and hydraulic behavior of hydrate-bearing geologic media[8,9].

The main objective of this study is to evaluate the production potential of Class 1 accumulations under depressurization (to induce hydrate dissociation), and to determine the factors and conditions affecting it. We investigate two kinds of Class 1 deposits. The first one has hydrate and water in the upper hydrate zone, and is hereafter referred to as a Class 1W deposit; the second involves hydrate and gas, and is referred to as a Class 1G accumulation. Depressurization-based production strategies appear well suited to the conditions of Class 1 deposits because of their simplicity, technical and economic effectiveness, and the fast (practically immediate) response of hydrates to the rapidly propagating pressure wave (as opposed to the much slower response to thermal stimulation). Because of the strongly endothermic nature of the dissociation reaction and the rapidity of dissociation under depressurization, care must be taken to limit the formation of solid phases (i.e., hydrate and ice) in the vicinity of the producing well, which may have adverse effects on the fluid permeability regime and, consequently, on gas production.

Numerical and Conceptual Issues

The numerical model. The numerical studies in this paper were conducted using the TOUGH-Fx/HYDRATE model[9], the successor to the earlier EOSHYDR2 code[7] for the simulation of hydrate-bearing geologic media. TOUGH-Fx/HYDRATE can model the nonisothermal hydration reaction, phase behavior and flow of fluids and heat under conditions typical of natural CH_4-hydrate deposits in complex formations. It includes both an equilibrium and a kinetic model[10,11] of hydrate formation and dissociation. The model accounts for heat and up to four mass components (i.e., water, CH_4, hydrate, and water-soluble inhibitors such as salts or alcohols) that are partitioned among four possible phases: gas phase, liquid phase, ice phase, and hydrate phase. A total of 12 states (phase combinations) can be described by the code (of which 8 are shown in Figure 1), which can handle any combination of the possible hydrate dissociation mechanisms (i.e., depressurization, thermal stimulation, and inhibitor-induced effects). TOUGH-Fx/HYDRATE involves a fully implicit formulation, continuous property updating, and the Newton-Raphson iteration for the solution of the nonlinear coupled equations of fluid and heat flow. The resulting Jacobian matrix equation is capable of handling the phase changes and steep solution surfaces that are typical of hydrate problems.

Composite thermal conductivity of hydrate-bearing media. The presence of interstitial solid phases (such as hydrate and/or ice) can have significant effects on the properties and behavior of the porous medium. Recent studies[8] have indicated that the commonly used linear model[12] (based on the saturation-weighted contributions of the phases and of the solid matrix) is inadequate, and that a more representative estimate of the composite thermal conductivity of hydrate-bearing media is given by

$$\theta_C = \theta_{dry} + (S_A^{1/2} + S_H^{1/2})\,(\theta_{wet} - \theta_{dry}) + \phi\, S_I\, \theta_I \quad \text{.....} \quad (1)$$

Equation (1) represents an extension of the model of Somerton et al.[13], which is used extensively in geothermal studies.

Effect of the presence of interstitial solid phases. The presence of solid phases can profoundly alter the ability of the porous medium to transmit fluids through reduction in porosity, giving rise to a reduction in permeability as well. We have proposed two alternative models[9] to describe the hydraulic and wettability effects in hydrate-bearing media. The first model, hereafter referred to as the *Original Porous Medium* (OPM) model, considers the hydrate phase in analogy to other fluid phases, except that, being solid, it is immobile. Accordingly, hydrate is characterized by its saturation S_H, and changes in effective permeability to the fluid phases due to the presence of hydrate are modeled as relative permeability effects.

The second model, hereafter referred to as the *Evolving Porous Medium* (EPM) model, considers the evolution of the solid phases (hydrate and ice) as tantamount to the creation of a new porous medium with continuously changing porosity and intrinsic permeability, the pore space of which is occupied only by the two fluid phases (aqueous and gas). In the absence of any information on the behavior of hydrate-bearing media, the current hypothesis is that models developed for solid precipitation in porous media are valid in the description of the EPM model.

Relative permeability issues. The simpler OPM model does not require any new parameters to be introduced. This model assumes that in the presence of solid phase(s), relative permeability to each fluid phase is given by the same function $k_r\beta(S\beta)$ as in the absence of solids, and $k_r\beta$ can be given by any of the commonly used two-phase relative permeability models[14,15]. Thus, the aqueous phase relative permeability $k_{rA} = k_{rA}(S_A)$ depends only on the aqueous saturation S_A, and is the

same, regardless of how the remaining fraction ($1- S_A$) of the pore space is divided between gas and solid phases. A similar comment applies to the gas relative permeability $k_{rG} = k_{rG}(S_G)$. Permeability reduction for the fluid phases then occurs simply because, when $S_S = S_H + S_I$ increases, fluid phase saturations S_A and S_G generally must decrease also, as dictated by the constraint in the sum of saturations. This approach is tantamount to asserting that liquid phase flow behaves as though solids deposition occurs entirely in what would otherwise be gas-filled pore space, while gas phase flow behaves as though solids deposition occurs entirely in what otherwise would be liquid-filled pore spaces. An obvious limitation of the OPM model is that solids deposition cannot simultaneously occur only in liquid- and only in gas-filled pore spaces.

The EPM model attempts to overcome the limitations of the OPM model. The same relative permeability models are used, but saturations are adjusted to reflect the changes in the porous medium. The fraction of pore space available to fluid phases is $S_A + S_G$, and the active porosity available to fluid is

$$\phi = (S_A + S_G)\ \phi_0 \Rightarrow \frac{\phi}{\phi_0} = (S_A + S_G) \quad \text{(2)}$$

where ϕ_0 is the original porosity. Referring to the total *active* (hydrate- and ice-free) pore space, an aqueous saturation S_A in a medium with solid saturation S_S then corresponds to an adjusted saturation

$$S_A^* = \frac{S_A}{S_A + S_G} \quad \text{(3)}$$

The gas saturation is similarly adjusted, and the adjusted values are used in the estimation of the relative permeabilities.

Considering the permeability reduction when the fluid-available pore space is either entirely liquid-filled or entirely gas-filled, a plausible estimate of the "new" intrinsic permeability of the porous medium is given by

$$\frac{k}{k_0} = \frac{1}{2}\left[k_{rA}\left(S_A = 1 - S_S\right) + k_{rG}\left(S_G = 1 - S_S\right)\right] \quad \text{(4)}$$

in which k_0 is the intrinsic permeability of the OPM (i.e., ice- and hydrate-free medium), and the estimation of k_{rA} and k_{rG} depends only on the solid saturation S_S. Equation (4) is referred to as the EPM #1 model. An alternative model (referred to as the EPM #2 model) is based on solids precipitation studies[16,17], in which

$$\frac{k}{k_0} = \left(\frac{\phi - \phi_c}{\phi_0 - \phi_c}\right)^n \quad \text{(5)}$$

where ϕ_C is the critical porosity (at which permeability is reduced to zero), and n can vary from 2 to 3 (for mild dependence of permeability on porosity[18]), to as high as 10 or more[19]. Note that, in the absence of any data on the subject, the irreducible aqueous and gas phase saturations in the EPM models are assumed to remain as in the OPM.

Capillary pressure issues. Our understanding of the role and importance of capillary pressure in hydrate-bearing media has dramatically evolved since our first studies of the subject[7]. Our current evaluation is that P_{cap} plays a critical role in gas production from hydrate deposits, and even more so in Class 1 accumulations.

The presence of the solid phases and the interaction of the fluid phases in the pore-space of hydrate-bearing media require adjustment of the capillary pressures even in the OPM model. Such scaling is based on the Leverett[20] model, which relates P_{cap} to changes in the intrinsic permeability and porosity according to:

$$P_{cap}(S_A) = \sqrt{\frac{k_0}{k} \cdot \frac{\phi}{\phi_0}}\ P_{cap,0} \quad \text{(6)}$$

where $P_{cap,0}$ is the capillary pressure of the ice- and hydrate-free porous medium (i.e., corresponding to k_0 and ϕ_0) and can be computed from any of several available models[14,21]. The most basic scaling involves the use of the adjusted saturations of Equation (3) to estimate $P_{cap,0}$. For additional OPM (and for EPM #1) scaling, the ratios of porosities and intrinsic permeabilities are provided by Equations (2) and (4). For capillary pressure scaling according to the EPM #2 model, the ratio of intrinsic permeabilities is estimated from Equation (5).

Gravity equilibration and initialization process. Gravity equilibration and initialization for the simulation of Class 1 hydrate deposits is a challenging task. Correct initialization requires (and results in) hydraulic, thermal, thermodynamic, and chemical equilibrium. The initialization process for Class 1 hydrates is in essence a solution of the inverse problem, through which we determine the proper conditions that result in the correct location of the hydrate interface at known equilibrium P and T.

Thus, gravity equilibration and initialization proceed as follows: The domain is subdivided into two subdomains, one corresponding to the hydrate-bearing zone and the other corresponding to the mobile gas two-phase zone. The bottom layer of the overlying (hydrate) subdomain and the top layer of the underlying (free gas) subdomain are treated as boundaries representing the hydrate interface, i.e., three-phase conditions of coexistence of gas, liquid water, and solid hydrate.

Starting with the lower subdomain, initial P, T, and saturation conditions in this two-phase (gas and water) zone are determined by running a simulation to steady state, assuming (a) uniform initial saturations (using average values obtained from geophysical or well log studies) and (b) a uniform geothermal gradient (usually dT/dz = 0.029 K/m). A bottom constant-temperature boundary is located at a sufficient distance to ensure that the temperature disturbance does not reach it during the simulation period.

Working with the upper subdomain next, initial P, T, and S conditions in this two-phase (hydrate and water or hydrate and gas) zone are determined by running a simulation to steady state, assuming (a) uniform initial saturations (using values obtained from geophysical or well log studies) and (b) a geothermal gradient that results in steady-state heat fluxes that are identical to those estimated in the lower subdomain. (Note that the presence of a hydrate layer is invariably associated with a discontinuity in the geothermal gradient.) The top constant-temperature boundary should be sufficiently removed from the moving hydrate-free gas interface to ensure that the temperature disturbance does not reach it during the simulation period. To determine the proper geothermal gradient, the temperature in the upper boundary is adjusted to result in the desired heat fluxes.

Finally, the two subdomains are joined, with the interface no longer treated as a boundary. Having ensured identity of the heat fluxes in the two subdomains, the simulation to steady state in the combined domain is very fast, and results in very small changes of the conditions in the profile.

The problem of gravity equilibration in Class 1W deposits. The problem of gravity equilibration and initialization poses particular challenges in Class 1W deposits (by far the most common condition). The difficulties stem from the inability to reconcile conventional approaches and theories with the limited data from hydrate field experiments. One of the most puzzling issues is the lack of drainage from the hydrate zone even when S_A is well in excess of the irreducible aqueous phase saturation S_{irA} for that formation[22]. The observed fact that water does not drain from the hydrate layer implies that either water is not mobile, or that there is no net force that would cause the water to move downward. We now discuss various possibilities that may give rise to such conditions.

Hypothesis #1: Changes in the S_{irA}. The presence of hydrate may change the irreducible aqueous saturation S_{irA}, which increases with S_H. While this may seem plausible, it is contradicted by pressure tests during the Mallik field experiment[23] that indicated surprisingly high (relatively speaking) permeability in the presence of S_H as high as 80%. The mobility of the water in the hydrate zone is a strong argument against the hypothesis of S_{irA} increasing with S_H.

Hypothesis #2: Permeability barrier to drainage. This hypothesis postulates that a thin zone of high S_H is formed at or near the hydrate-gas zone interface, in which water is near the S_{irA} level. The rationale for this approach is provided by the assumption of maximum co-existence of gas and water at this point of hydrate stability, hence the possibility for a continuing hydration reaction that creates this permeability barrier. The formation of this barrier does not allow gas flow and more hydrate formation in the upper hydrate zone.

This hypothesis allows the formation of a permeability barrier to downward flow, which prevents water drainage from above the interface. Numerical simulations with conventional capillary pressure models lend support to this approach. It is not possible to allow fluid saturations (gas and/or aqueous) to reach their irreducible levels at the interface because of practical numerical problems: the use of upstream weighting (the standard in multiphase flow simulations, which prevents the emergence of nonphysical conditions) does not allow any pressure drop in the hydrate zone because of the immobile fluid saturations, thus completely inhibiting dissociation. Although it is known that even nonporous hydrate begins dissociating when exposed to low pressures, this process has not yet been studied and quantified, and, consequently, is not described in the current generation of numerical simulators. The important implications of this numerical challenge are discussed in detail in later sections of this paper.

The initialization approach under Hypothesis #2 involves setting at least one fluid saturation slightly above its irreducible level at the three-phase interface, allowing very slow drainage. In other words, instead of initial equilibrium, we have conditions of "quasi- equilibrium" that involve very slow drainage. Considering that it is not unusual for permafrost deposits to be 10,000 to 20,000 years old, we can estimate an initial S_A or S_G resulting in fluxes that are significant at this time frame. This is the approach we have been employing in describing initial conditions in Class 1 deposits up to now[2,7]. It is a plausible scenario, but has not been confirmed or disproved by field evidence. Numerically speaking, this approach allows a reasonable representation of the system, and has been used successfully in the past.

Following the dissociation of the barrier layer, the water in the hydrate zone starts draining freely, and gas production from dissociation can be quite high at relatively early times because of the increased mobility of the fluid phases. This approach works well if the barrier dissociation proceeds faster than hydrate formation in the hydrate zone, as gas seeping through the disintegrating layer into the hydrate zone can react with the free water and form new hydrate. If, however, the production rate is relatively slow, the formation of new hydrate above the interface seals the zone, hydrate dissociation drops substantially (and may even cease), and we are faced with the numerical problems of dealing with an immobile, non-dissociating hydrate interface (described earlier in this section).

Hypothesis #3: Capillary pressure barrier to drainage. The last hypothesis invokes capillary pressure effects to explain why liquid water cannot drain from the water-hydrate region to the gas-water region below. The field data from the Mallik[23] test are consistent with this hypothesis. We note that the presence of hydrate in the pore space will effectively reduce the size of pores available to the water, so that for a given water content of the porous medium, capillary suction effects should be stronger than they would be in the absence of hydrate. This is analogous to the strengthening of capillary suction in partially frozen soils, which has been established as a key mechanism in the phenomenon of *frost heave*[24,25,26]. Frost heave is a well-known process in which the surface of a partially frozen soil undergoes upward displacement. Usually associated with seasonal cycles of freezing and thawing, frost heave is caused by the development of banded patterns with alternating layers of large and small ice concentrations. Layers of large ice concentration, called *ice lenses*[25,26], typically have thicknesses and spacings of the order of a few centimeters, and form due to a peculiar kind of fluid dynamics instability, that gives rise to self-enhancing feedback for ice formation. In a partially frozen porous medium, capillary suction will be stronger in regions with larger ice content, owing to the smaller effective pore sizes there. This causes water to be drawn towards regions with larger ice saturation, causing additional ice formation there at the expense of neighboring regions. As will be seen below, our simulations give rise to the evolution of alternating layers of increasing and decreasing hydrate saturation (referred to as *hydrate lensing*), in analogy to the formation of ice lenses during frost heave.

Under Hypothesis #3, water stays immobile (although S_A significantly exceeds S_{irA}) because the capillary pressure is so strong that it prevents drainage. Thus, P_{cap} at the interface must be sufficiently strong to exceed the gravitational body force of the water in the hydrate zone. Additionally, the P_{cap} function must yield large values even at low gas saturations at the interface (large gas saturations at the interface lead to the formation of a very high S_H barrier immediately above the interface because of gas mobility and water availability), indi-

cating a high gas-entry pressure for the hydrate-bearing sediment. The functional requirements of P_{cap} lead us to propose a variant of the Brooks-Corey[21] function to estimate the capillary pressure of hydrate-water systems in Class 1 hydrates:

$$P_{cap}(S_H,S_{aA}) = H(S_H)\cdot F\cdot P_e\,(S_{aA})^c \quad \text{.....(7)}$$

where P_e (< 0) is the gas entry pressure, c is a negative exponent ($|c| < 1$), $S_{aA} = (S_A - S_{irA})/(1 - S_{irA})$, and F is a smoothing factor to avoid discontinuities in the estimation of the derivatives in the Jacobian of the fully implicit method employed in TOUGH-Fx/HYDRATE. We found that the expression

$$F = \text{erf}[60(1- S_{aA})] \quad \text{.....(8)}$$

preserves the steep entry pressure while preventing discontinuities in the derivatives. The function H describes the augmenting effect of the hydrate saturation on P_{cap}. A general and flexible form of H is given by the relationship

$$H = H(S_H) = 1 + w\cdot B_x(a,b,S_S) \quad \text{.....(9)}$$

where w is a constant (that can be estimated from laboratory data or the height of the water column above the interface), B_x is the incomplete beta function, and a and b are shape parameters. B_x is a functional form that has been shown to represent the general shape of capillary pressure curves[14]. By varying a and b it is possible to describe the entire range of possible S_S effects (hydrate and/or ice) on the system capillary pressure. Equation (7), an example of which is shown in Figure 3, can easily describe the inability of water in the hydrate zone to drain. If valid, the functional form of equation (7) can have profound implications for gas production from hydrates. It results in increasing P_{cap} with an increasing S_H, and can lead to initial difficulty in the drainage of water from dissociation, and rapid (and accelerating) hydrate formation in the vicinity of the wellbore. Note that, with the effects of S_H accounted for by Equation (7), there is no further need for P_{cap} scaling or for invoking the OPM/EPM model.

Also note that the capillary pressure function of equation (7), as well as the other hypotheses and the OPM and EPM models discussed earlier, are reasonable assumptions based on physical analogs and conceptual constructs. Currently there is no information to prove or disprove any of these models.

Problem 1: Class 1W, Reference Case

Problem description. The geometry and initial conditions of the system in Problem 1 are shown in Figure 2 and are listed in Table 1. While the geometry is based on an early study of Holder *et al.*[24] (later also investigated by Moridis[7]), the conditions and parameters are representative of those in a permafrost accumulation[22,23] and are substantially different from the ones used by Holder *et al.*[27] because the current state of knowledge indicates that the original P and T were substantially higher than the maximum values encountered in the natural permafrost system (in which the deepest interface occurs at a depth of 1150 m, with corresponding P and T not exceeding 11.3 MPa and about 14 °C, respectively).

The reservoir radius was R_{max} = 567.5 m, and its thickness was 30 m (98.4 ft), with the hydrate layer and the free gas zone being 15 m each. Based on scoping calculations, the confining formations of the deposit (i.e., the no-flow but heat-exchanging upper and lower boundaries) were 30 m thick. This thickness is sufficient to allow accurate representation of heat exchange with the hydrate deposit during a 30-yr long production period. Gas was produced through a single well located at the center of the reservoir, and its production rate was constant at 0.81944 ST m^3/s (2.5x10^6 ST ft^3). To alleviate hydrate formation problems in the vicinity of the wellbore, at the beginning of the simulation the z = -41 m to -57 m interval of the wellbore (with z = 0 set at the top of the upper boundary) was heated at a rate of 500 W per wellbore meter. This heating rate was arrived at from earlier scoping calculations. Note that wellbore heating plays a critical role in making long-term production from hydrates possible. After about 3 years of production, hydrate formation near the well in the vicinity of the hydrate-gas interface at the top of the heated zone (which occurred despite the wellbore heating) threatened to "choke" the well by creating a nearly impermeable barrier to flow. Extending the heated zone to cover the –30 m to –57 m interval eliminated the problem.

The producing interval was from –46 m to –56 m, i.e., 1 m below the initial hydrate interface. This was based on earlier calculations that demonstrated convincingly the necessity of having the production interval removed from the immediate vicinity of the nearly impermeable interface, because the resulting steep P and T gradients can lead to hydrate formation, which can choke the well. Although this may appear counterintuitive in a depressurization process, it is necessary because, as we will discuss in following sections, spatially uniform and gentle P and T gradients (as opposed to steep localized fronts) can significantly enhance long-term production from gas hydrates.

In the hydrate zone, S_H = 0.7 and S_A = 0.3, which are consistent with saturation levels encountered in permafrost deposits[22,23]. Relative permeabilities were estimated from a modified Stone[28] equation (Table 1) and the OPM model. The capillary pressure was computed from Equation (7), and appears in Figure 3 along with the corresponding H-factor.

Grid and simulation specifics. The system was simulated using a 2-D cylindrical grid. Its dimensions result in a reservoir with a volume identical to the Cartesian system of Holder *et al.*[24]. The domain was discretized in 90 x 94 = 8,460 gridblocks in (r,z), of which 8,280 were active and the remaining were boundary cells. The top and bottom layers corresponded to constant temperature, no-flow boundaries, while the layers corresponding to the 30-m-thick top and bottom confining layers were impermeable but allowed heat exchange with the deposit. In the radial direction, after 5 subdivisions of Δr = 0.25 m, the remaining 85 Δr were computed using a logarithmic distribution. The 15 m hydrate-bearing formation was subdivided uniformly along the z-direction into 60 segments of Δz = 0.25 m each. For reasons explained later, such a fine discretization of the hydrate zone is important (and possibly necessary) for accurate predictions. The conditions of the free gas zone allowed a coarser discretization in z of mostly Δz = 1 m, although Δz = 0.25 m and 0.5 m subdivisions were used near the initial hydrate interface. This fine discretization provided a high level of detail near the wellbore and in the entire hydrate-bearing zone.

Using the equilibrium hydration reaction option in TOUGH-Fx/HYDRATE[9], the grid resulted in 24,840 coupled equations that were solved simultaneously.

We determined the initial conditions in the reservoir (associated with the location of the hydrate-gas interface, and the corresponding P and T) by following the initialization process described earlier. The initial conditions can be gleaned from Figure 11 (discussed later) as the distributions at $t = 0$.

Hydrate contribution to production and system performance. To quantitatively describe gas production from Class 1 hydrates, we introduce the concepts of *Rate Replenishment Ratio* (RRR or R3) and *Volume Replenishment Ratio* (VRR or VR2). RRR is defined as the fraction of the gas production rate at the well(s) that is replenished by CH_4 released from hydrate dissociation. VRR is defined as the fraction of the cumulative gas volume produced at the well(s) that is replenished by hydrate-originating CH_4. These two parameters provide a measure of the hydrate system response and the effectiveness of dissociation as a gas-producing method. Obviously, VRR is the integral of RRR over time.

The evolution of the gas production rate and of the corresponding volumetric rate of CH_4 release from the hydrate (fueled by depressurization-induced dissociation) are shown in Figure 4(a). The evolution of VRR in Figure 4(b) closely follows that of the CH_4 release rate from dissociation, because the gas production rate remains nearly constant for a very long time (and slightly declines later because of increasing water in the production stream).

Of interest are the spikes at early times. Study of the simulation output indicated that the corresponding gas-release bursts are caused by dissociation (caused by pressure drop) and corresponding gas evolution in the hydrate-bearing layers moving upward toward the upper boundary of the system. Thus, there is gas in the entire 15-m thick hydrate zone after less than 45 days of production, attesting to the effectiveness of depressurization as a dissociation mechanism. Each of the gas release spikes corresponds to a distinct event that corresponds to rapid dissociation along a particular layer.

A very interesting feature in Figures 4(a) and 4(b) is the local minima (troughs) that are identified as feature #1. These reflect discretization effects and indicate the depletion of hydrate in a particular layer. Dissociation leads to a localized increase in pressure (caused by the evolving gas and the resistance to flow in the porous medium) and a drop in temperature (caused by the endothermic nature of the hydrate reaction). The increase in the pressure and the temperature drop cause a reduction of the subsequent rate of dissociation, a situation that is significantly accentuated when hydrate is exhausted. Pressure dissipation and heat flux later restore the rate of dissociation.

Note that our simulations indicate a very strong tendency for lateral propagation of processes (such as hydrate dissociation or hydrate formation) along distinct layers, resulting in laterally uniform distributions of properties and conditions in the reservoir. While there is an element of discretization effect in this behavior, there is strong evidence that this is also a physical (in additional to numerical) process, caused by the significant permeability, P, and T contrast between a dissociating layer and its adjacent layer(s). This condition enhances the lateral propagation of fronts (along the dominant direction of flow), and is accentuated by the presence of high S_H in hydrate lenses.

Review of Figure 4 and study of the corresponding simulation results lead us to identify four stages – marked in Figure 4(b) – in the course of gas production from Class 1W deposits. These are discussed below.

Stage I. The initial Stage I corresponds to dissociation from two main zones: the initial horizontal hydrate interface and a cylindrical interface that expands radially around the well. A third dissociation zone also develops slowly, involving the evolution of a second horizontal hydrate interface (in addition to the original one at the bottom of the hydrate zone) that first appears at the top of the hydrate interval and then advances downward. This appears to be a unique and universal characteristic of production from hydrate deposits. Kurihara et al.[29] observed the evolution of such interfaces in the study of Class 2 hydrate deposits. The reason for the emergence of the second horizontal interface is a combination of depressurization (enhanced by the proximity to the impermeable top boundary) with heat exchange with the overburden. This realization underlines the importance of adequate discretization for accurate heat-exchange estimation at the boundaries. Note that the emergence of the upper interface can have very important implications in the Stage IV gas production from Class 1W hydrates, and in production from marine deposits in which the hydrate zone is the gas cap of an underlying gas reservoir (where it can lead to fast deterioration of the gas confining structure).

An additional phenomenon observed in Phase I is the beginning of evolution of a *hydrate channeling* system, i.e., a system of narrow conductive channels alternating with impermeable high-S_H bands that advance into the body of the hydrate in a 'wormhole-like" manner aligned with the general direction of flow. The hydrate channels are a direct consequence of the hydrate lensing process (caused by capillary pressure) discussed earlier, with the alternating high-low S_H bands formed along the direction of fluid flow as hydrate forms or dissociates. They provide access to the interior of the hydrate body and an additional diffuse dissociation venue. Hydrate channels appear to be enhanced by mild production regimes (i.e., lower production rates, spatially uniform depressurization, and appropriate well location), can be effective in providing fluid flow between different parts of the hydrate zone, and appear to play an important role in production. The issue will be addressed in the later detailed discussion of Figures 6 to 10 (in which the hydrate channels are evident). Note that hydrate lensing begins practically immediately after the inception of production, and becomes more pronounced with time.

Hydrate channels are dynamic features, in which the high-S_H bands can continue to expand at the expense of the area (aperture) available for flow. The end of Stage I is marked by the drop in RRR in Figure 4(b), which occurs when the effects of hydrate channeling and lensing begin to have a significant effect on flow and hydrate dissociation. At the end of Stage I, the cylindrical dissociation zone is roughly uniform and extends to the upper boundary. The time at which the front reaches the upper boundary is marked as #2 in Figure 4(b).

Note that the physical processes and conditions that determine the scale of hydrate interfaces, lenses and channels have not necessarily been adequately resolved in these simulations. Thus, while the authors believe that the occurrence of such features is real, they have insufficient information to claim that the discretization (quite fine for standard reservoir simulations) is adequate to describe them with quantitative accuracy.

Stage II. In Stage II, dissociation continues along the two horizontal interfaces (upper and lower) and the cylindrical interface. This stage is characterized by full development of the hydrate channels (and maximum flow through them), which represent an additional dissociation zone within the main body of the hydrate. Through the important additional communication they provide (between the cylindrical hydrate-free dissociated zone and the upper interface), they enhance dissociation at the upper boundary and along the channels with the main body of the hydrate zone. In the absence of such channels, dissociation in the upper interface can occur only in response to depressurization fueled by radial flow toward the well through the very narrow cross-sectional area of the hydrate-free layer above the upper interface. Additionally, there would be very limited dissociation within the main body of the hydrate zone (as defined by the three interfaces). After its decline at the end of Phase I, RRR begins to increase because of the increased pressure drop brought about by the evolution of the hydrate channels and the permeability of these structures.

Hydrate lensing continues during Stage II. The end of Stage II is marked by a precipitous drop in RRR, caused by the "sealing" of the entire bottom (horizontal) boundary by the effects of hydrate lensing, which leads to hydrate formation to very high S_H, with concurrent reduction of the S_A and S_G to below their irreducible levels. The hydration reaction can continue in such static systems even when the gas and aqueous phases are immobile. Thus, the hydrate above the bottom horizontal interface is occluded (isolated) by a thin high-S_H shell that is impermeable to gas and water flow.

It is important to indicate that, while the model[9] is capable of describing the physical phenomena of hydrate lensing, hydrate channeling, and formation of the hydrate shell, the current state-of-the-art numerical approach is very conservative (in terms of prediction of gas release from dissociation) because of reliance on "upstream weighting", in which flow between two adjacent elements is controlled by the mobility of the cell at the higher pressure from which flow emanates. This approach eliminates the possibility of non-physical behavior in conventional multiphase simulations, but is insufficient in the case of hydrate simulations because it cannot describe dissociation at very high S_H and immobile gas and aqueous phases. Laboratory experiments have demonstrated conclusively that even nonporous (and practically impermeable) hydrates dissociate in response to low pressure, a fact that indicates the limitation of the conventional "upstream weighting" approach. Currently, there is no alternative model to address this issue.

Consequently, the simulation results provide the lower limit of the gas production estimate ("worst case scenario"), with a large fraction of the hydrate mass being treated as inert because of the inability of the current approach to describe dissociation in immobile hydrate systems. This approach may underpredict estimates of recoverable hydrocarbons.

Stage III. In Phase III, only the cylindrical and the upper horizontal interfaces are active dissociation fronts. The dissociation zone created by the hydrate channels is also active, but hydrate lensing continues to accumulate hydrates, increasing S_H and decreasing the aperture of the "wormholes" crisscrossing the main body of the hydrate. In this stage, the hydrate channels play a critical role in providing hydraulic communication between the upper hydrate interface, the overlying hydrate-free layer, and the interior of the hydrate zone.

Compared to Stages I and II, RRR is lower in Stage III and has a downward trend because (a) the total area of dissociation is reduced by the very large bottom horizontal boundary (now inactive), (b) the remaining dissociating regions are more distant from the well, and (c) are connected to the hydrate-free zone (the main flow region) mainly through the limited cross-sectional area of the progressively less conductive hydrate channels.

Stage IV. The onset of Stage IV is marked by another precipitous drop in the RRR value to levels that are consistently less than 0.1. This indicates a dramatic reduction in dissociation activity and is caused by occlusion of the upper interface by a hydrate shell or through closure of the hydrate channels, which also stops dissociation within the main hydrate body. Additionally, hydrate lensing has occluded the majority of the hydrates along the outer perimeter of the cylindrical interface, with lenses occurring radially in the grid layers. At this stage, dissociation occurs in only a few isolated gridblocks either on the vertical wall of the cylindrical interface or served by still-open channels within the main hydrate body.

Note that while a reduction in RRR is expected because of the blockage of the hydrate channels and the occlusion of the majority of the remaining hydrate body, the practical cessation of dissociation is a numerical exaggeration caused by the "upstream weighting" approach. Thus, the RR prediction should be viewed only as an estimator of the lower limit of expected gas production.

The evolution of the upper interface offers interesting possibilities for gas production using enhanced hydrate dissociation in Stage IV. The presence of a hydrate-free zone above the main hydrate body allows consideration of complex dissociation strategies. These could involve injection of warm brines immediately above the upper hydrate interface, thus integrating depressurization at the well with a combination of thermal stimulation and inhibitor effects at the upper interface.

Because of the very limited contribution of dissociation to gas production in Stage IV, and in light of the very large computational requirements of hydrate simulations (about 65,000 timesteps to cover the 10 years in Figure 4), the simulations of production from Class 1W deposits was stopped when Stage IV was reached.

General observations. The most important observations from Figure 4 are that (a) the rate of CH_4 release from dissociation attains high levels early, and (b) it increases with time in Stage I and II. Thus, after less than 3 months of production, over 25% of the production rate is replenished from hydrate dissociation. The RRR continues to increase. At

the end of Phase II (at about 6.2 years), dissociation proceeds at a rate of 0.533 ST m^3/s (= 1.6 x 10^6 ST ft^3/day) and replenishes about 65% of the production rate. Even with the decline in dissociation in Stage III, RRR averages about 40%.

Comparison of (a) the cumulative volume of CH_4 released from dissociation to (b) the produced gas volume leads to (c) the VRR shown in Figure 5, which confirms the early contribution of hydrates to gas production in addition to the hydrate potential for the production of very large amounts of gas. VRR continues to increase rapidly through Stages I and II and indicates that 47% of the produced volume the end of Stage II has been replenished from hydrate dissociation. Because of decreasing contribution of dissociation to gas production, VRR declines during Stage III and more rapidly in Stage IV. However, at the end of the 10-year production period, the VRR value indicates that about 42% of the total gas volume produced up to that point (i.e., 1.08 x 10^8 ST m^3 = 3.81x10^9 ST ft^3) had been replenished from dissociation.

These results indicate the technical feasibility and the effectiveness of using dissociation to readily produce large amounts of gas at high rates using conventional technology. Note that the depressurization process described in this paper does not have any technical requirements that cannot be addressed with current state-of-the-industry capabilities.

Dissociation of impermeable hydrates. It is important to clarify that stopping the simulations after reaching Stage IV should not be interpreted as an implicit conclusion that gas production from hydrate dissociation is negligible past that point. While the increasing S_H in the hydrate channels and lenses is certainly expected to reduce the rate of dissociation (because of the reduction in the fluid relative permeabilities and occlusion) in Stage IV, it will just as certainly not stop it completely, as our models currently assume. The fundamentals of dissociation from immobile hydrate systems are not well understood, and our models reflect this lack of knowledge. It is entirely possible that dissociation from impermeable hydrates proceeds as a slower surface reaction (as opposed to the earlier faster volume process), the rate of which increases as dissociation leads to an increase in the fluid saturations. If this is case, then the severe reduction in dissociation is reversible, and it is possible to have a cyclical dissociation regime of alternating slow and rapid rates.

Evolution of system conditions during production. The evolution of P, T, and saturation distributions in the reservoir are shown in Figures 6 to 10. In these figures, (a) corresponds to the initial distribution, (b) to Stage I, (c) to Stage II, (d) to Stage II immediately before the onset of Stage III, (e) to Stage III, and (f) to Stage IV.

Pressure distribution. Review of the simulation results indicates that the P distribution conforms to expectations, with maximum pressure drops near the well and overall pressure decline in the reservoir over time. In Figure 6, we show the deviation P^* of pressure from a reference level (changing temporally), which is the P at the top layer of the hydrate zone and near R_{max}. The hydrate body begins to differentiate from the background in the P^* distribution in Figures 6b, and is demarcated by the higher-pressure region that is caused by the lower fluid permeability. The evolution of hydrate lensing and the resulting hydrate channels, denoted by the higher P^*, are evident in Figure 6c, which also shows faint signs of evolution of a hydrate shell at the lower hydrate interface. Because of the high S_H in the hydrate channels, permeability is significantly lower, and consequently the pressure is higher. The S_H rises very fast to levels that render the water and gas phases immobile in the hydrate channels, causing the high-S_H bands of the hydrate channels to become occluded, and the pressure in them to stay "frozen" at about the P level at the time of occlusion. Thus, they appear as higher-pressure regions in the P^* distribution as time advances and the pressure in the reservoir declines.

Figure 6d shows the continuous evolution of the hydrate channels, as well the hydrate shell responsible for the occlusion of the lower horizontal interface at the bottom of the hydrate body. The high-S_H bands of the hydrate lenses, channels and shells continue to expand in Stage III (Figure 6e) because of continuous hydrate accumulation fueled by P_{cap}, eventually becoming impermeable boundaries that occlude the main hydrate body (as depicted in Figure 6f). Because there is no hydraulic communication, depressurization is not felt within the occluded hydrate body, thus no dissociation takes place. Within the isolated main body of the hydrate, P remains constant at about the level at the time of final occlusion, while the permeable surroundings continue to depressurize.

Temperature distribution. Review of the temperature profile in Figure 7 shows a generally uniform radial distribution. Localized effects such as the influence of the heat sources near the wellbore and the cooling in dissociating hydrate-bearing layers are easily recognizable. The expanding and sagging cool zone is caused by continuing dissociation, Joule-Thomson cooling, and drainage of the cooler water released from dissociation. Of interest is the shrinkage of the cool zone in the main hydrate body at t = 8 years in Figure 7e, when compared to that at t = 6 years in Figure 7d. This indicates warming, caused by reduction in the endothermic dissociation activity because of the occlusion of the lower dissociation interface during Stage III. The expanding colder zone adjacent to the upper boundary in Figure 7e is caused by dissociation in the hydrate in the main hydrate body and fluid flow through the channels, as Figures 8 to 10 confirm.

Hydrate distribution. Some of the most interesting observations can be made from the distribution of the S_H, S_G and S_A saturations in Figures 8, 9, and 10, respectively. Figure 8b reveals the expansion of the cylindrical interface radially from the wellbore during Stage I.

The evolution of the upper horizontal hydrate interface begins in Stage I, as a review of the simulation outputs indicates. In Figure 8, imaging limitations do not allow the upper interface to become discernible before t = 2 years. The upper interface casts an unmistakable (and strengthening with time) signature after t = 4 years.

The most striking feature in Figure 10 (and also present with different levels of intensity in Figures 6 to 10) is the emergence of the banded S_H distribution of the hydrate channels, which becomes more pronounced with time as they advance into the hydrate body. The hydrate channels are evident at t = 4 years, i.e., at the beginning of Stage II (Figure 8c). These "wormhole-like" structures appear to permeate a large portion of the main hydrate body during Stage III (t = 8 years, Figure 8e) and an even larger one in Stage IV (Figure

8f, t = 10 years). An interesting feature of the hydrate channels is that they are formed at an angle to the horizontal that is roughly aligned with the flow lines to the well.

Along with the hydrate channels, hydrate lenses (and a hydrate shell occluding the bottom hydrate interface) evolve at the lower horizontal hydrate interface, which continues to dissociate and to move upward until the end of Stage III. The alternating high-low S_H bands are evident at t = 4 years (Figure 8c), and continue to expand until the end of Stage III, after which time they no longer change. In Stage IV, dissociation has ceased in the bulk of the hydrate body because of occlusion, and only proceeds in isolated subregions mainly on the cylindrical hydrate interface. One such pocket with the appearance of an intrusion into the hydrate body is evident in Figure 8f. The drastic decline in hydrate dissociation in Stage IV is due to reductions in (a) the extent of the active dissociation regions, in (b) their permeability and in (c) their cross-sectional area available to flow.

The increasing hydrate saturation in the high-S_H bands in the hydrate lenses, channels, and shells as time advances is evidenced by the progressively darker shade of these structures in Figure 8. Note the difference between the hydrate saturation distributions at the upper and lower horizontal interfaces. While the lower one shows a clear preference for horizontal uniform lensing, the upper one is crisscrossed by hydrate channels, which allow communication with the main reservoir during Stage III. Because (a) the cross-sectional area of the channels is limited, (b) lateral access to the wellbore appears blocked (see Figure 8e and 8f, at z = -30 m and at r = 5-6 m), (c) the permeability of the hydrate channels is limited, and (d) the upper hydrate interface is physically far from the well, hydrate dissociation declines in Stage III (see Figure 4b). It appears that the hydrate channels remain conductive at the point where they cross the upper hydrate interface even in Stage IV, but they are blocked by hydrate accumulation at their other end, i.e., at the outer edges of the main hydrate body. Figures 9 and 10 tend to support this thesis.

Gas phase saturation distribution. The evolution of the S_G distribution in Figure 9 is consistent with expectations, and mirrors the S_H distribution. The gas zone is seen to expand with time, reflecting gas emergence from dissociation. Because of (a) preferential downward flow during dissociation along the bottom of the hydrate body and (b) hydrate lensing (which consumes CH_4 to form new hydrate), no banded S_G signature appears near the lower horizontal interface. Conversely, the upper dissociated zone (between the upper hydrate interface and the overburden) shows high S_G.

S_G registers only in hydrate channels located predominantly in the upper reach of the cylindrical hydrate interface. It appears that these hydrate channels remain conductive to gas even in Stage IV, during which they appear to provide hydraulic communication between the upper horizontal dissociation zone and the main reservoir. However, the cross section of the hydrate channels is limited (as evidenced by the narrowness of the high-S_G bands in Figure 9), making flow and further dissociation difficult within the main body of the hydrate.

Figures 9d and 9e offer some intriguing insights. The S_G saturation appears at its maximum (in terms of magnitude and extent) at t = 6 years, and declines afterward. The gradual shrinking of the high-S_G region in Stage III (Figure 9e) and in Stage IV (Figure 9f) in the dissociated cylindrical zone around the well (and below the upper boundary) can only be caused by a combination of water releases and reduction of dissociation as the hydrate becomes increasingly occluded. In the absence of hydrate in this region, the water has to come from the main hydrate body through the hydrate channels. Figure 10 confirms this hypothesis. Note the gradual expansion of the low-S_G zone at the bottom of the reservoir, which is indicative of water accumulation resulting from drainage. The drastic reduction of the high-S_G region in Figure 9f is attributed to the occlusion of the hydrate, which precludes further dissociation and gas release.

Aqueous phase saturation distribution. The evolution of the S_A distribution in Figure 10 shows clearly the emergence of the hydrate channels and lenses. The S_A distributions appear complementary to those of S_H in Figure 8. Because hydrate saturations are generally low in the hydrate body, the S_A signature is much fainter than the S_H signature in Figure 8. Figure 10 also shows the process of drainage of water released from the hydrate dissociation and the emergence of a water-saturated zone at the bottom of the free-gas zone.

The S_A distribution at t = 8 years shows clear signs of water flow from the upper dissociated zone through the hydrate channels. This flow of this colder water (originating from earlier dissociation – otherwise a commensurate increase in S_G would have been observed) is the reason for the lower temperatures at the same location observed in Figure 7. This flow and drainage appears to continue (indicating water conductive channels) until t = 10 years in Figure 10f, which also shows high S_A in the upper dissociated zone.

Profiles at select locations. The processes discussed up to now are clearly indicated in Figures 11, 12, and 13, which show the evolution of conditions at the three cross sections r = 0.5 m, r = 5 m and r = 50 m. The P profiles in Figure 13 show the decline in pressure over time, and the T profiles in Figure 13 show the effect of the wellbore heating source. The S_H profile shows the relative exhaustion of hydrate at this distance from the well after t = 2 years because of the combined thermal and depressurization effects. The hydrate is replaced mainly by gas (S_G profile). Because of drainage, S_A shows only a small increase in the region previously occupied by the hydrate, but increases to full saturation at the bottom of the domain, with the draining water accumulates and a rising water level is observed.

The r = 5 m cross section is located at an area of intense concentration of hydrate channels (Figure 8). Their banded saturation pattern in the hydrate zone is clearly evident in Figures 12, which also shows that (a) the saturation in the high-S_H bands exceeds the original saturation as lensing leads to hydrate accumulation, (b) S_H shows the largest variations and steepest increases in decreases in the zigzag pattern of the banded structure, and (c) $S_A < S_{irA}$ and $S_G < S_{irG}$ when S_H is at its highest, i.e., fluids are immobile at these locations. The emergence of the upper horizontal hydrate interface is clearly shown as a receding S_H front, with the space above it filled with water and gas following dissociation. Figure 12 also shows the receding lower hydrate interface, which moves upward with time. The occlusion of the high-S_H hydrate bands in the hydrate channels is responsible for the increase of P

above the initial level. As T increases in response to wellbore heating, the fluids in these cells are immobile and their pressure rises (after a slight readjustment of phase saturation) to maintain equilibrium. Note the slight decline in T at t = 2 years (caused by the endothermic dissociation reaction and Joule-Thomson cooling), which is quickly reversed when wellbore heating begins to affect this location. Progressive cooling is observed at regions unaffected by the wellbore heating, i.e., at the bottom of the free-gas zone and at the top of the hydrate interval.

The effect of occlusion is evident in the P profile in Figure 13, which remains "frozen" in the main hydrate body at the t = 8 years level (Stage III). Progressive cooling because of dissociation and Joule-Thomson effects is clearly demonstrated in the T profile, which shows a minimum at t = 8 years associated with the water drainage through the hydrate channels at that time (see Figure 10e). A very important observation is that the T in the hydrate declines by less than 2.5 K after about 10 years of production. This indicates that, under the conditions in this study, the temperature drops are mild and the risk of ice evolution (with adverse effects on the fluid relative permeability and the rate of dissociation) is minimal.

The receding S_H fronts at the bottom and the top of the hydrate interval show advancing hydrate destruction at the two horizontal hydrate interfaces (active dissociation fronts) until hydrate lensing inhibits the reaction. While hydrate lensing does not exhibit the dramatic S_H zigzag pattern seen in Figure 12, S_H rises to a level that results in $S_A < S_{irA}$ and $S_G < S_{irG}$ (i.e., immobile fluids) at the lower hydrate interface (development of the occluding hydrate shell) and at the upper hydrate interface (closure of the hydrate channels). The S_G and S_A profiles show the rising water level at the bottom of the domain in response to accumulation of drainage water.

Water production at the well. A very positive result of this study is that water production is limited over the 10-year production period. The water production rate and the cumulative mass of produced water in Figure 14 are very low, and are at no time below generally accepted economic threshold levels.

Problem 1: Class 1W, Sensitivity Analysis

We investigated the sensitivity of gas production from hydrate dissociation to reservoir properties and operating conditions that earlier scoping studies had determined to be important. These include the reservoir intrinsic permeability k, the gas production rate Q at the well, and the thickness Z_G of the free-gas zone. Note that the extended wellbore heating discussed in the reference case was applied in all the sensitivity studies.

Case 1: Sensitivity to the reservoir intrinsic permeability. When we used the k of the Holder et al.[27] study, (k = $4.325\text{x}10^{-14}$ m^2 = 43 mD), the simulation ceased at about t = 4 days despite the very substantial wellbore heating because of cavitation (*well choking*) caused by the formation of hydrate in the vicinity of the wellbore (Figure 15a). Hydrate reaches saturations in excess of 0.9 and creates a barrier to flow that cannot be reconciled with the prescribed production rate. The hydrate formation contributes to the low permeability, which causes a significant pressure drop, very fast dissociation (Figure 14a), and rapid cooling near the well bore. Because of the fast cooling rate, the porous medium does not have sufficient heat to prevent hydrate formation, and conduction is too slow to counter the problem.

We conducted an additional simulation with k = $4.325\text{x}10^{-13}$ m^2 (= 433 mD), and with all the other properties and conditions as in the reference case. There was no evidence of well "choking" at this k level.

Case 2: Sensitivity to the production rate. An increasing production rate is expected to result in faster depressurization and, consequently, to a faster and more efficient dissociation. To test the effect of the production rate Q, we conducted a simulation in which Q = 1.6389 ST m^3/s (= 5 x 10^6 ST ft^3), i.e., double the Q in the reference case. All other properties, parameters, and conditions remained as in the reference case.

Case 3: Sensitivity to the thickness of the free gas zone. For the same production rate, a narrower free gas zone Z_G is expected to enhance dissociation because mass is being removed at the same rate from a smaller system. We conducted a simulation in which Z_G was reduced to 10 m (from the original 15 m). All other properties, parameters, and conditions remained the same as in the reference case.

Results of the sensitivity analysis. The Rate Replenishment Ratios (RRRs) for the three sensitivity analysis cases are shown in Figure 16. Compared to the reference case, the RRR in Stage I is about the same in Case 1 (Figure 16a) despite a k that is about 2.5 times smaller. The insensitivity of hydrate dissociation to the very significant change in k is explained by the competition between stronger and localized depressurization from a smaller hydrate volume (a consequence of lower k), and a milder, more uniform depressurization affecting a larger volume of hydrate (resulting from a higher k). There is rough parity between the two, hence the similarity in the RRR values in Stage I.

There is a distinct decline in Stage II, during which the RRR in Case 1 evolves in a manner roughly parallel to that in the reference case and for a shorter time. Comparison of the S_H distributions in Case 1 and in the reference case at the beginning of Stage II (Figure 17) indicates the lack of early development of hydrate channels in Case 1. This is attributed to the lower k, which creates steeper pressure and temperature fronts that do not promote hydrate channel development.

There appears to be no Stage III in Case 1, with dissociation moving directly from Stage II to Stage IV. The corresponding S_H distribution at the beginning of Stage IV (Figure 18a) provides an explanation because it demonstrates an underdeveloped hydrate channel system, as a comparison to the extensive distribution of the wormhole-like structures in Figure 8f of the reference case demonstrates. It is obvious that production from hydrates in Case 1 significantly lags behind that in the reference case, with an early decline in Phase II and an early emergence of Stage IV (during which hydrate contributions to production fall below the 10% level).

Compared to the reference case (Figure 16a), the RRR in Stage I is about the same in Case 2 (despite the doubling in the production rate) for the same reasons discussed in Case 1. Of particular interest is the observation that dissociation moves directly from Stage I to Stage IV in Case 2. This transition is

explained by the relative absence of hydrate channels in Figure 18b, which does not allow hydraulic communication with the interior of the hydrate mass, thus inhibiting dissociation. The obvious conclusion is that higher production rates may have a strong adverse effect on gas release from hydrates, which appears to be favored by milder processes that keep dissociation fueled for long times.

In Case 3 (Figure 16b), the reduction in Z_G to 10 m appears to have a profound effect. The RRR during Stage I is higher than in the reference case, indicating that a larger portion of the produced gas is being replenished by CH_4 from hydrate dissociation. The same is observed during Stage II (which is shorter than in the reference case) and in Stage III (during which RRR is higher than in the reference case). Note that at the end of Stage II, over 70% of the production rate is being replenished by hydrate dissociation in Case 3. Although we expected the effect of a smaller Z_G to be similar in general to that of a larger Q in Case 2, it appears that hydrate channel development is greatly promoted in Case 3, leading to the very favorable RRR pattern of Figure 16b.

Comparison of (a) the cumulative volume of CH_4 released from dissociation to (b) the produced gas volume leads to (c) the VRRs shown in Figure 19. As implied by the rough parity of the RRRs in Figure 16a, the VRRs for Cases 1 and 2 are very similar, indicating that the contribution of hydrates to the production stream during Stage I appears to be insensitive to reservoir properties or production rates. This, coupled with the VRR for Case 3, leads to speculation that RRR and VRR depend only on the geometric features of the system during Stage I. The VRR begin differentiating from the reference case in Stage II.

Figure 19 shows the superiority of mild processes (favored by high k and lower Q) in terms of total CH_4 volume released from dissociation. Such conditions (encountered in the reference case) allow dissociation to proceed far longer and to release much larger amounts of hydrate-originating CH_4 than in Cases 1 and 2.

Note that the VRR in Case 3 reaches the 50% level at the end of Stage II, indicating that half the produced CH_4 volume has been replaced by gas from dissociation. An early conclusion from this observation is that Class 1W hydrate deposits with thin free gas zones are desirable targets for gas production. It is important, however, to determine the optimal Z_G that allows maximum production while avoiding the evolution of (a) an adverse water/gas ratio in the production stream and (b) unfavorable relative permeability regimes (expected to be more pronounced in narrow Z_G deposits) as water from dissociation drains.

Review of the water production data in Figure 20 indicates that the water production rate increases in Cases 1 and 2 (because of faster dissociation near the well), although the rates are expected to rapidly decline after the occlusion of the hydrate in Stage IV when dissociation stops. In Case 3, although the water production rate is somewhat larger than that for the reference case, the two become roughly equal after about 3 years. This provides further indication of the desirability of Class 1W hydrate deposits with narrow Z_G as production targets.

Problem 2: Class 1G, Reference Case

Problem specifics. The system configuration, geometry, and properties in Problem 2 are very similar to those in Problem 1, from which it differs in the following aspects:

(1) The intrinsic permeability k is that of the Holder et al.[27] study, i.e., $k = 4.325\text{x}10^{-14}$ m^2 (= 43 mD). Thus, k is lower than in the reference case of Problem 1.
(2) In the hydrate zone, $S_H = 0.7$ and $S_G = 0.3$ (i.e., $S_A = 0$). This is consistent with a gas-rich, H_2O-poor system.
(3) The OPA and EPS #1 models were employed in the computations of relative permeability and capillary pressure, respectively.
(4) The rate of wellbore heating to prevent hydrate formation was 200 W, and followed the initial (as opposed to the later) heat application regime discussed in Problem 1
(5) The capillary pressure is now given by the van Genuchten[14] model as,

$$P_{cap} = -P_0\left[\left(S^*\right)^{-1/\lambda} - 1\right]^{-\lambda}, \quad S^* = \frac{\left(S_A - S_{irA}\right)}{\left(S_{mxA} - S_{irA}\right)} \quad \text{..... (10)}$$

with $S_{mxA} = 1$, $\lambda = 0.6$, and $P_0 = 1890$ Pa.

Hydrate contribution to production and system performance. The (a) volumetric rate of depressurization-induced CH_4 release from the hydrate, (b) the production rate at the well, and (c) the corresponding RRR over the 30-year simulation period appear in Figure 21 and exhibit a drastically different pattern than that in Problem 1. The RRR in Figure 21 does not show any sign of the distinct stages identified in Problem 1 (Figure 4), and seems to indicate that dissociation from hydrates in Class 1G deposits is a continuous process. This is attributed to the high gas mobility in the hydrate zone. The steep, short-duration drops in the CH_4 release rate and the RRR are related to discretization effects, and occur when dissociation (which proceeds very quickly along a given layer) is complete. The exhaustion of the hydrate removes a source of gas (in addition to causing a T drop in adjacent layers because of the endothermic nature of the reaction) and results in the temporary steep drop in the release rate.

An important observation from Figure 21 is that hydrate contribution to production increases monotonically (the short temporal fluctuations notwithstanding) during production. In other words, hydrates keep improving (as a gas source) with time. At the end of the 30-year production period, an impressive 75% of the rate of gas production is being replenished by gas releases from hydrate dissociation. Compared to the RRR pattern in the reference case of Problem 1, it is evident that the hydrate contribution to production increases significantly at a much slower pace in Class 1G deposits. Thus, hydrate contributions reach the RRR = 0.2 level after 580 days of production in the Class 1G deposit, while the same level is attained in about 53 days in Problem 1. The difference is caused by the much larger free gas volume available for production in Class 1G deposits, in addition to the much larger gas compressibility. These observations lead to the conclusion that long-term production is needed to realize the full potential of the very promising Class 1G hydrate deposits.

Comparison of (a) the cumulative volume of CH_4 released from dissociation to (b) the produced gas volume leads to (c) the VRR shown in Figure 22, which provides another measure

of the hydrate potential for the production of very large amounts of gas. VRR rises rapidly early, increases continuously with time, and shows that 54% of the produced volume at the end of the 30-year production period has been replenished from hydrate dissociation. By that time, 4.13×10^8 ST m^3 (= 1.46×10^{10} ST ft^3) have been released from dissociation in this relatively small deposit.

These results further confirm the technical feasibility and the effectiveness of using dissociation to readily produce large amounts of gas at high rates using conventional technology. The attractiveness of Class 1G deposits is further underlined by the water production data shown in Figure 23, which demonstrate that water production remains very low during the entire 30-year production span.

Evolution of system conditions during production. The evolution of P, T, and saturation distributions in the reservoir are shown in Figures 24 to 28.

Pressure distribution. Review of the simulation results indicates that the P distribution conforms to expectations, with an overall pressure decline in the reservoir over time. In Figure 24, we show the deviation P^* of pressure from a reference level (changing temporally) that was selected to prominently display the localized variations. The P^* distribution indicates that the pressure decline during production is quite uniform in the entire domain, with the exception of thin structures with predominantly horizontal alignment. These structures, better illustrated in Figure 26, are hydrate lenses and channels. The evolution of hydrate lensing and the resulting hydrate channels, denoted by the higher P^*, becomes evident in the sequence after Figure 24d (t = 10 years). The hydrate lenses and channels become more extensive with time, and eventually hydrate sheets develop, occluding a region in the upper part of the formation (Figures 24f to 24h). As in Problem 1 (Figure 6), the fluid phases are immobile in the high-S_H bands of the hydrate channels and lenses become occluded, and the pressure in them stays "frozen" at about the P level at the time of occlusion. Thus, they appear as higher-pressure regions in the P^* distribution as time advances and the pressure in the reservoir declines. The same occurs when an occluded region loses hydraulic communication with its surroundings after encapsulation by hydrate shells.

Temperature distribution. The influence of the heat sources near the wellbore is easily recognizable in the T profile in Figure 25, which shows a generally uniform radial distribution. As expected, the T distribution indicates progressive cooling of the entire reservoir, consistent with the endothermic dissociation reaction, Joule-Thomson cooling, water evaporation near the well, and drainage of the cooler water released from dissociation. Inspection of Figure 25 allows tracking the active zones of dissociation (as the low-T regions) and the dissociation fronts (as the outer boundaries of the low-T regions). The most interesting observation is that, in addition to the upward-moving original hydrate-gas interface (i.e., the lower horizontal interface), a second horizontal interface appears to develop at the top of the hydrate interval. The second interface is entirely analogous to the one observed in the study of the Class 1W deposit (Figures 6 to 13), and will be thoroughly analyzed in the ensuing discussion of the S_H distribution.

Hydrate saturation distribution. There are significant differences in the evolution of the S_H distribution between the Class 1G deposit of Problem 2 (Figure 26) and the Class 1W deposit of Problem 1(Figure 8). These are caused by the differences in the fluid permeability in the hydrate interval, which is much higher in the Class 1G deposit and results in the preponderance of horizontal flow through the hydrate-bearing interval toward the well. As a result, the development of horizontal hydrate lenses is evident in the formation (Figures 26e to 26h). Additionally, hydrate channels aligned with the flow lines develop closer to the well, and become distinctive at later times (Figures 26f to 26h). For the reasons already discussed in Problem 1, the hydrate saturation in the high-S_H bands of the lenses, channels, and sheets becomes progressively larger, as evidenced by the darkening shades.

Figure 26 depicts a pattern of continuous destruction of hydrates that is consistent with the observations of Figures 21 and 22. The upward movement of the receding lower hydrate interface is evident in the sequence of Figure 26, as is the downward movement of the second horizontal hydrate interface that develops at the top of the hydrate interval in response to depressurization and heat fluxes from the overburden.

Gas phase saturation distribution. The distribution in Figure 27 shows a halo of low S_G along the dissociation fronts during the early phase of production. This is caused by dissociation, which releases large amounts of water. As time advances, gas flow from the main hydrate body through the hydrate channels and along the permeable bands of the hydrate lenses becomes evident. The very high S_G region near the well corresponds to drying, caused by wellbore heating and water evaporation. The lower S_G zones that appear after t = 25 years (Figures 27g and 27h) below the remaining hydrate can be attributed to (a) water flow to the well through the hydrate channels near the well and (b) drainage away from the well.

Aqueous phase saturation distribution. Figure 28 shows a S_A distribution that is consistent with expectations. Higher S_A regions appear below the hydrate and denote draining water released from dissociation. The higher S_A zone expands with time, but does not reach the bottom of the free gas zone. Consequently, we do not observe water accumulation and a rise of the water table. Simple scoping calculations indicate that such a pattern is consistent with the low intrinsic permeability of this system. Flow through the hydrate channels at later times is evident in Figures 28g and 28h, which also show typical drainage patterns at distinct locations away from the well. The latter appears to indicate drainage through breaks in the hydrate lenses, which can be easily located in Figure 26.

Profiles at select locations. Figures 29, 30, and 31 show the evolution of conditions at the three cross sections r = 0.5 m, r = 5 m and r = 50 m. The P profiles in Figure 29 show an overall decline in pressure over time (consistent with continuous production), with the exceptions of (a) the high-S_H bands of the hydrate sheets, channels, and shells (evient from the zigzag pattern), and (b) the occluded region (centered around the –35 m mark). The T profiles in Figure 30 show warming where wellbore heating has an effect, and continuous cooling (to a minimum of about 9°C at t = 30 years) in the rest of the profile. Compared to Problem 1 (Figure 11), a smaller

portion of the hydrate interval is heated, leading to the non-zero S_H distributions in the vicinity of the well that persist during the 30-year production period.

The S_H profile shows the receding horizontal hydrate interfaces at the top and bottom of the hydrate interval. Because of the abundance of gas in the hydrate zone, hydrate lensing and channeling at this location (depicted by a distinctive zigzag appearance) leads to very high S_H that approaches 1; i.e., practically all the pore space is occupied by hydrate in the high-S_H bands of the lenses. It is easy to identify the occluded region discussed in Figure 26, which is hydrate-free and is isolated by the very high-S_H hydrate shells above and below the –35 m mark.

The S_G profile shows a zigzag pattern complementary to the S_H pattern (with the S_G highs corresponding to the S_H lows) in the hydrate channels and lenses. The receding upper horizontal hydrate interface and the evolving upper dissociated zone are demarcated by the high-S_G region (> 0.5) at the top of the hydrate interval. Note that S_G is also high within the occluded region. Hydrate is replaced mainly by gas as the lower hydrate interface moves upward. The S_A saturations in the upper dissociated zone and in the occluded region are complementary to the S_G at these locations. While some evidence of drainage is obvious, there is no water accumulation at the bottom of the free gas zone because of low permeability and preferential flow to the well.

The r = 5 m cross section is located at an area of intense concentration of hydrate channels (Figure 8). Their banded saturation pattern in the hydrate zone is very distinct in Figure 30, which also shows that (a) the saturation in the high-S_H bands reaches almost 1 as lensing leads to hydrate accumulation, (b) S_H shows the largest variations and steepest increases in the zigzag pattern of the banded structure, and (c) $S_A < S_{irA}$ and $S_G < S_{irG}$ when S_H is at its highest, i.e., fluids are immobile at these locations. Note the occurrence of multiple occlusions, marked by high (and mobile) S_G and S_A regions confined between bounding lenses of impermeable hydrates in which S_H is almost 1. It is at these locations that pressure "anomalies" are observed for the reasons already discussed. The receding upper and boundary interfaces can be easily tracked from the S_H, S_G, and S_A profiles. Because the wellbore heating rate is much lower than in Problem 1, the effect of temperature at this location does not show any direct influence from the well, although this can be deduced when compared to the T distribution further away into the formation (Figure 31). Dissociation, Joule-Thomson effects, and the flow of cooler water from the dissociating hydrate result in continuous cooling that reaches about 8 ^{o}C at t = 30 years.

The profiles at r = 50 m (Figure 31) are a good descriptor of the average reservoir behavior. We observe progressive depressurization, and only limited evidence of pressure "freezing," despite the severe hydrate lensing and occlusions defined by the S_H, S_G and S_A distributions. This points to formation of the lenses very late (i.e., after t = 25 years) in the production period (an indication supported by the evolution of the S_H profile). This is a favorable situation because it signifies that the bulk of the hydrate remains open to hydraulic communication, thus making depressurization and the continuation of dissociation possible for practically the entire 30-year production period.

Figure 31 shows increasing S_G and S_A where the upper and lower hydrate interfaces recede. As in Figures 29 and 30, there is no evidence of a rising water table, with the S_A remaining practically stable near the bottom of the free gas zone. This is attributed to the low intrinsic permeability of the reservoir and the preferential flow toward the well.

Cooling is more pronounced at this location, for the reasons discussed earlier. The minimum T in the profile is about 6 ^{o}C and occurs within the hydrate interval (where dissociation takes place). A very important observation is that the T in the hydrate declines by 7.5 ^{o}C (from its original 13.5^{o}C) after 30 years of uninterrupted production. This indicates that, under the conditions in this study, the temperature drops are mild and the risk of evolution of ice (with adverse effects on the fluid relative permeability and the rate of dissociation) is minimal.

Problem 2: Class 1G, Sensitivity Analysis

Note that the results presented here cover, at most, 5 years of production (instead of the 30-year period of the reference case) because the simulations had not been concluded at the time of the submission of this paper.

We investigated the sensitivity of gas production from Class 1G deposits in the following cases:

(1) Case 1: To test the effect of the intrinsic permeability k, we conducted a simulation in which $k = 4.325\text{x}10^{-13}$ m^2 (= 433 md), i.e., an order of magnitude larger than in the reference case.

(2) Case 2a: To test the effect of the production rate Q, we conducted a simulation in which Q = 1.6389 ST m^3/s (= 5 x 10^6 ST ft^3), i.e., double the Q in the reference case.

(3) Case 2b: When well "choking" was experienced in the simulation of Case 2a, the simulation was repeated with a wellbore heating rate of Q_H = 500 W per wellbore meter (i.e., 2.5 times the original one).

Results of the sensitivity analysis. The Rate Replenishment Ratios (RRRs) for the three sensitivity analysis cases are shown in Figure 32. A striking observation is that the rate of hydrate dissociation (as quantified by RRR) appears to be completely insensitive to a tenfold increase in k, at least during the first 5 years of production. A possible explanation is that, during this period, the competition between stronger and localized depressurization from a smaller hydrate volume (a consequence of lower k), and a milder, more uniform depressurization affecting a larger volume of hydrate (resulting from a higher k) are evenly matched. A more likely explanation is that the rate of gas release from dissociation is small at this relatively early time, and the two predictions will begin to deviate at a later time.

As is a common occurrence in gas production wells, hydrate begins to develop in the vicinity of the production interval in Case 2a, leading to well "choking" at about t = 615 days (Figure 15). The larger Q in this case was expected to result in faster depressurization, and, consequently in a faster and more efficient dissociation. Consistent with expectations, the corresponding RRR up to the time of well "choking" consistently exceeds that in the reference case. The increased wellbore heating in Case 2b allowed continuation of production and hydrate dissociation past that point, but the RRR curve for

Case 3b coincides with that of Case 3a up to the point of well "choking" (Figure 32). Beyond that point, the RRR in Case 3b continues to increase and to consistently exceed that for the reference case.

Comparison of (a) the cumulative volume of CH_4 released from dissociation and (b) the corresponding VRRs are shown in Figure 33. As implied by the practical identity of the RRRs in Figure 32, the VRR for Case 1 is practically indistinguishable from that in the reference case. Similarly, the VRRs for Cases 3a and 3b coincide prior to the well "choking" in Case 3a, substantially exceeding the VRR for the reference case. As we discussed earlier (Figure 21), depressurization-induced dissociation begins slowly in Class 1G deposits, its efficiency increases with time, and its full benefits are realized in long-term production regimes. The period covered in the sensitivity analysis calculations is short, and consequently the RRR and VRR levels do not rise to the levels seen during the 30-year simulation of the reference case. Thus, after 5 years, 25% of the produced volume of CH_4 has been replaced by gas from hydrate dissociation, and 3.1×10^7 ST m^3 (= 1.1×10^9 ST ft^3) have been produced. It is obvious that, barring recurrence of well "choking", Case 3b will result in much larger released volumes and VRR at the same time.

Numerical Challenges and Limitations

Timestep evolution and duration of simulations. A very important feature of hydrate simulations is their long durations and the large number of timesteps Δt they require. The Class 1W simulations necessitated between 30,000 to 65,000 Δt to cover the simulation period to Stage IV (10 years at most), while the simulation of the numerically "better-behaving" Class 1G problem required about 50,000 Δt to cover the 30-year production period. The reasons for these extraordinarily long simulations are (a) the extreme nonlinearity of the problem, (b) the steepness of the dissociation fronts, (b) the continuous property updating at every time step and every Newtonian iteration, (c) the fine discretization required for accurate results (see discussion below), and (d) the necessity to employ a fully implicit scheme and fully coupled equations. The resulting long execution times are the necessary price to pay for stable solutions that are free of mass-balance problems in the face of phase changes and steep fronts. The steepness of the dissociation fronts is a unique characteristic of hydrate simulations, as is the persistence of the sharpness of these fronts over time. Unlike conventional multiphase flow problems, the solution surfaces in hydrate simulations do not become progressively more diffusive with time, but appear to propagate through the domain without any attenuation. The persistent steepness of the solution front imposes severe restrictions on the evolution of the Δt. Even near the end of the better-behaved (numerically speaking) 30-year simulation of the Class 1G reference problem, the Δt rarely exceeded a fraction of a day.

In Class 1W problems, an additional reason for the lengthy simulations is the numerical difficulty of treating the capillary pressures described in Equation (7). This is more pronounced at the early stages of the simulation when the lower hydrate-bearing layer in the discretized domain begins to dissociate. This creates competition between the declining S_H (which reduces P_{cap}) and the increasing S_G (which, conversely, tends to increase P_{cap}). The result is a "confusing" regime with fluid fluxes alternating from Newtonian iteration to Newtonian iteration and from timestep to timestep.

Grid discretization. The persistence of the sharp fonts necessitates fine discretization for accurate numerical simulations of the behavior of hydrate-bearing media. The conventional approach in the study of conventional oil and gas systems involves progressively larger gridblocks as distance from producing boundaries (i.e., wells) increases, and made possible by the increasingly diffusive solutions of systems as time advances. This approach is inadequate for hydrate simulations because coarser grids cannot accurately capture the steep fronts of the hydrate solutions. The very long execution times are another consequence of the need for fine discretization.

In Figure 34, we compare the rate of CH_4 release from dissociation for Case 1 of Problem 1 (involving a Class 1W deposit) using two different discretizations: the discretization used in Problems 1 and 2, and a grid that was substantially coarser in the z-direction. The coarser grid involved 99 x 48 = 4,752 gridblocks in (r,z), of which 4554 were active and the remaining were boundary cells. While fine near the initial bottom of the hydrate interval, discretization along the z-axis became increasingly coarse, with a large number of Δz = 1 m gridblocks away from the interface.

The deviations between the two solutions are very large. The larger Δz discretization results in an erroneous RRR that indicates a lower rate of dissociation and a longer duration of Stages I and II, in addition to an extra Stage III (not observed in the finer discretization solution). This occurs because hydrate lensing occurs over a larger Δz that is slower to respond and to attain the high-S_H levels that restricts flow. Consequently, flow and dissociation continue for longer. Additionally, the thickness of the top hydrate-bearing layer prevents the evolution of the upper hydrate adjacent to the overburden. Instead, the upper dissociation front develops within the body of the hydrate, because the grid coarseness does not allow accurate resolution of the heat fluxes at the top of the hydrate interval in the presence of the steep fronts. Essentially, the coarse discretization causes a portion of the hydrate interval to behave thermally as the upper boundary. Comparison of the S_H distributions in Stage IV for the coarser (Figure 35) and the finer (Figure 18b) discretizations demonstrates the distortion in the solution effected by the coarser grid.

Treatment of immobile hydrate-bearing cells. In previous sections we discussed the challenge of estimating dissociation in gridblocks in which the aqueous and gas phases are immobile, and the need for models (to be incorporated into our numerical codes) to describe the process. We are currently considering alternative approaches to address the problem.

The most obvious possibility is to consider hydrate dissociation as a surface process, described by a gas generation term using the kinetic equation of Kim et al. (1987). In this approach, instead of considering the surface area of the hydrate "grains" in the entire gridblock volume, we restrict the reaction surface to the limited area of direct contact of the impermeable hydrate with its adjacent free gas. The challenge

in this case is the inevitability of dealing with directional permeabilities and localized gas saturations within subdomains of the affected cells, which somehow have to be averaged in a representative and mathematically consistent way over the discretized gridblock. Additionally, this approach requires developing a technique that will provide a smooth transition from the initial surface process to a volume process once the fluid saturations have risen above their irreducible levels. A significant complicating factor is the need for the surface-to-volume process to work seamlessly in 2-D and 3-D systems.

Alternative approaches are also being considered. For example, a model that shows some potential is based on the concept of secondary "matrix" permeability, which allows the flow of gas through the solid hydrate clathrates and gradual emptying of the cavities (with concurrent change in the hydration number). One particular challenge for this approach is describing the energy requirement for this type of process as a function of the changing hydration number (a subject on which no information is available). Another model to examine prevents the relative or intrinsic permeability of the hydrate-bearing systems from dropping below a certain level.

We have not yet implemented any of these models in the TOUGH-Fx/HYDRATE simulator[9] because of incomplete conceptual development, and because supporting laboratory studies for confirmation and calibration are still in progress. In the mean time, our predictions of gas production from hydrate dissociation represent the lower limit of the possible solutions.

Conclusions

The following conclusions can be drawn from this study:

1. Large volumes of gas can be readily produced at high rates for long times from Class 1 gas hydrate accumulations, by means of depressurization-induced dissociation using conventional technology.
2. To avoid blockage caused by hydrate formation in the vicinity of the well, wellbore heating of the entire production interval and a substantial part of the hydrate interval (and possibly all of it) is a necessity in production from Class 1 hydrates. Additionally, the production interval should be placed at a sufficient distance from the hydrate interface to avoid steep pressure fronts.
4. A unique and universal characteristic of depressurization-induced production from Class 1 hydrate deposits is the evolution of a second horizontal hydrate interface (in addition to the original one at the bottom of the hydrate zone) that first appears at the top of the hydrate interval and advances downward. The evolution of this interface has important implications for late-stage production from Class 1 hydrates and from marine accumulations.
3. Capillarity plays a critical role in gas production from hydrates. It is responsible for hydrate lensing, an instability that gives rise to self-enhancing feedback for hydrate formation, and results in the development of banded patterns with alternating layers of large and small hydrate saturations.
4. To describe the contributions of hydrate dissociation to production, we introduced the concepts of Rate Replenishment Ratio (RRR, defined as the ratio of the CH_4 release rate from dissociation to the production rate at the well) and Volume Replenishment Ratio (VRR, defined as the ratio of the CH_4 volume produced from dissociation to the cumulative volume of produced CH_4).
5. There are up to four stages of system response in Class 1W hydrates under production. Stage I involves dissociation from the initial lower horizontal hydrate interface and a cylindrical interface that expands radially around the well. The upper horizontal hydrate interface and hydrate lenses also begin to develop in Stage I. Stage II is characterized by dissociation at the three interfaces, and the full development of a system of hydrate channels that penetrate the hydrate body (thus defining an additional dissociation zone). Furthermore, hydrate lensing continues. In Stage III, only the cylindrical and the upper horizontal interfaces are active dissociation fronts, while the entire lower horizontal interface is occluded by hydrate shells resulting from lensing. This sealing leads to a rapid decline in dissociation at the beginning of Stage III, during which the hydrate channels are mostly conductive and active in dissociation. Stage IV is marked by a precipitous drop in the dissociation activity resulting from occlusion of the remaining hydrate body by hydrate shells and/or through closure of the hydrate channels.
6. In gas production from Class 1W hydrate deposits, the rate of CH_4 release from dissociation (a) attains high levels early, (b) increases with time in Stages I and II, (c) exhibits a declining trend in Stage III, and (d) declines drastically in Stage IV.
7. In Class 1W deposits, up to 65% of the production rate and 45% of the produced volume are replenished with gas from hydrate dissociation.
8. Short-term (i.e., Stage I) gas release from hydrate dissociation in Class 1W accumulations appears to be practically insensitive to the intrinsic permeability of the formation and the gas production rate, but is enhanced by thinner free gas zones.
9. Long-term gas release from hydrate dissociation Class 1W accumulations is enhanced by relatively mild depressurization processes and uniform pressure distributions in the reservoir, which generally involve higher permeabilities and lower production rates. Such milder processes promote the development of hydrate channels that play a significant role in accessing the interior of the hydrate body and promoting dissociation. Thinner free gas zones also appear to enhance gas production from dissociation.
10. Production from Class 1G deposits is continuous and free of the stages identified in Class 1W accumulations. Hydrate channels, lenses, and sheets also develop in such hydrates and lead to occlusions, but these are more limited in extent, and do not have the serious impact that such structures have on Class 1W deposits because of higher permeability.
11. In Class 1G deposits, the hydrate contribution to production increases monotonically with time, and the full benefits of depressurization-induced dissociation are realized in long-term production regimes. Up to 75% of the rate of gas production and 54% of the produced volume are replenished by gas releases from hydrate dissociation. Class 1G accumulations are slower to respond than Class 1W deposits, but their efficiency increases with time.

12. Short-term gas release from hydrate dissociation in Class 1G accumulations appears to be practically insensitive to the intrinsic permeability of the formation, but increases with the gas production rate.
13. Water production remains very low during the long-term gas production from Class 1 hydrate deposits.
14. Long-term production from Class 1 deposits causes the temperature to decline in the reservoir in response to the endothermic hydrate dissociation reaction, Joule-Thomson cooling, and the flow of colder water released from the hydrate. However, the temperature drops are mild even after as many as 30 years of uninterrupted production, indicating that the risk of evolution of ice (with adverse effects on the fluid relative permeability and the rate of dissociation) is minimal.
15. Relative permeability and capillary pressures in hydrate-bearing media are complex processes that play a critical role in production from gas hydrates, but which are not well understood. We introduced new models to describe the effect of the presence of hydrates on the wettability properties of porous media.
16. Because of sharp fronts that persist with little attenuation during long production periods, fine discretization is very important for accurate solutions in hydrate simulations.
17. Because of limitations in the ability to describe hydrate dissociation at very high saturations under conditions impermeable to fluids, our predictions should be viewed as the lower limit of the possible solutions.

Nomenclature

Δr = Radial increment (sec)
Δt = Timestep size (sec)
Δz = Vertical discretization in the z-direction (m)
a,b = incomplete beta function shape parameters
B_x = incomplete beta function
c = Brooks-Corey exponent – equation (7)
C = specific heat (J/kg/^{o}C)
e = parameter – equation (9)
H = capillary pressure factor – equation (9)
k = intrinsic permeability (m^2)
N_H = hydration number
P = pressure (Pa)
Q = total fluid mass flow rate at a well (kg/m^3/s)
Q_H = Wellbore heating rate (W/m)
S = phase saturation
t = time (s)
T = temperature (^{0}K)
r,z = coordinates (m)
R_{max} = reservoir radius (m)
Z_G = thickness of the free gas zone (m)

Greek Symbols

λ = van Genuchten exponent—Equation (10)
ϕ = porosity
$\phi_{\square}$ = critical porosity
θ = thermal conductivity (W/m/s)

Subscripts and Superscripts

0 = denotes initial state
β = denotes phase
A = aqueous phase
cap = capillary
G = gas phase
H = solid hydrate phase
I = ice phase
n = permeability reduction exponent –equation (5)
R = rock
S = solid
irG = irreducible gas
irA = irreducible aqueous phase
$r\beta$ = denotes relative permeability of phase β
rA = aqueous phase relative permeability
rG = gas relative permeability

Acknowledgment

This work was supported by the Assistant Secretary for Fossil Energy, Office of Natural Gas and Petroleum Technology, through the National Energy Technology Laboratory, under the U.S. Department of Energy, Contract No. DE-AC03-76SF00098. The authors are indebted to Stefan Finsterle, John Apps and Dan Hawkes for their thorough review and their insightful comments.

References

1. Sloan, E.D.: *Clathrate Hydrates of Natural Gases*, Marcel Dekker, Inc., New York, NY (1998).
2. Moridis, G.J., and Collett, T.S.: "Strategies for Gas Production From Hydrate Accumulations Under Various Geologic Conditions", Report LBNL-52568, Lawrence Berkeley National Laboratory, Berkeley, CA (2003).
3. Moridis, G.J., and Collett, T.S.: "Gas Production from Class 1 Hydrate Accumulations", in *Recent Advances in the Study of Gas Hydrates*, Taylor, C., and Qwan, J., Eds., Kluwer Academic, New York, pp. 75–88 (2004).
4. Moridis, G.J., Collett, T.S., Dallimore, S.R., Satoh, T., Hancock, S., and Weatherhill, B.: "Numerical Studies of Gas Production Scenarios From Several CH_4-Hydrate Accumulations at the Mallik Site, Mackenzie Delta, Canada", *J. Petr. Sci. Eng.* (2004), **43**, 219.
5. Moridis, G.J.: "Numerical Studies of Gas Production from Class 2 and Class 3 Hydrate Accumulations at the Mallik Site, Mackenzie Delta, Canada", *SPEREE*, (2004), **7**(3), 175.
6. Moridis, G.J., and Kowalsky, M.B.: "Gas Production from Unconfined Class 2 Hydrate Accumulations in the Oceanic Subsurface", Report LBNL-57299, Lawrence Berkeley National Laboratory, Berkeley, CA (2005).
7. Moridis, G.J.: "Numerical Studies of Gas Production From Methane Hydrates", *SPEJ*, (2003), **32**(8), 359.
8. Moridis, G.J., Seol, Y., and T. Kneafsey: "Studies of Reaction Kinetics of Methane Hydrate Dissociation in Porous Media", Report LBNL-57298, Lawrence Berkeley National Laboratory, Berkeley, CA (2005).
9. Moridis, G.J., Kowalsky, M.B., and K. Pruess: "TOUGH-Fx/HYDRATE v1.0 User's Manual: A Code for the Simulation of System Behavior in Hydrate-Bearing Geologic Media", Report LBNL-58950, Lawrence Berkeley National Laboratory, Berkeley, CA (2005).
10. Kim, H.C., Bishnoi, P.R., Heidemann, R.A., and Rizvi, S.S.H.: "Kinetics of Methane Hydrate Decomposition", *Chem. Eng. Sci.*, **42**(7), 1645 (1987).

11. Clarke, M.A., and Bishnoi, P.R.: "Determination of the Intrinsic Rate of Ethane Gas Hydrate Decomposition", *Chem. Eng. Sci.* (2000), **55**, 4869
12. Bejan, A.: *Convection Heat Transfer*, John Wiley & Sons, New York (1984).
13. Somerton, W.H., et al.: "Thermal Behavior of Unconsolidated Oil Sands", Paper SPE-4506, 48th Annual Fall Meeting of the Society of Petroleum Engineers, Las Vegas, NV (1973).
14. van Genuchten, M.Th.: "A Closed-Form Equation for Predicting the Hydraulic Conductivity of Unsaturated Soils", *Soil Sci. Soc.*, **44**, 892 (1980).
15. Brooks, R.H., and Corey, A.T.: "Properties of Porous Media Affecting Fluid flow", *J. Irrig. Drain. Div. ASCE*, **IR2**, 61 (1966).
16. Verma, A., and Pruess, K.: "Thermohydrologic Conditions and Silica Redistribution Near High-Level Nuclear Wastes Emplaced in Saturated Geological Formations", *J. of Geophys. Res.*, (1988), **93**(B2), 1159.
17. Xu, T., Ontoy, Y., Molling, P., Spycher, N., Parini, M., and Pruess, K.: "Reactive Transport Modeling of Injection Well Scaling and Acidizing at Tiwi Field, Philippines", *Geothermics,* (2004), **33**(4), 477.
18. Phillips, O.M.: *Flow and Reactions in Permeable Rocks,* Cambridge University Press, Cambridge, New York (1991).
19. Pape, H., Clauser, C., and Iffland, J.: "Permeability Prediction Based on Fractal Pore-Space Geometry", *Geophysics,* (1999), **64**(5), 1447.
20. Leverett, M.C.: "Capillary Behavior in Porous Solids", *Trans. Soc. Pet. Eng. AIME*, (1941), **142**, 152.
21. Brooks, R.H., and Corey, A.T.: "Properties of Porous Media Affecting Fluid Flow", *ASCE J. Irrig. Drain. Div.*, **IR2**, 61, (1966).
22. Dallimore, S.R., Uchida, T., and Collett, T.S. (eds.): "*Scientific Results from JAPEX/JNOC/GSC Mallik 2L-38 Gas Hydrate Research Well, Mackenzie Delta, Northwest Territories, Canada*", Geological Survey of Canada Bulletin 544 (1999).
23. Kurihara, M., Funatsu, K., Kusaka, K., Yasuda, M., Dallimore, S.R., Collett, T.S., and Hancock, S.H.: "Well-Test Analysis for Gas Hydrate Reservoirs: Examination of Parameters Suggested by Conventional Analysis for the JAPEX/JNOC/GSC et al. Mallik 5L-38 Gas Hydrate Production Test Results", in *Scientific Results from the Mallik 2002 Gas Hydrate Production Research Well Program, Mackenzie Delta, Northwest Territories, Canada*, S.R. Dallimore and T.S. Collett, eds., Geological Survey of Canada, Bulletin 585, 1–31 (2005).
24. O'Neill, K. and R.D. Miller. "Exploration of a Rigid Ice Model of Frost Heave", *Water Resour. Res.,* **21**(3), 281 (1985).
25. Noon, C.: *Secondary Frost Heave in Freezing Soils,* Ph.D. Thesis, University of Oxford, England (1996).
26. Rempel, A.W., Wettlaufer, J.S. and Worster, M.G.: "Premelting Dynamics in a Continuum Model of Frost Heave", *J. Fluid Dynamics,* **498**, 227, DOI: 10.1017/S0022112003006761 (2004).
27. Holder, G.D., Angert, P.F., John, V.T., and Yen, S.L.: "Simulation of Gas Production From a Reservoir Containing Both Gas Hydrates and Free Natural Gas", paper SPE 11105, SPE Meeting, New Orleans, LA, 26–29 September (1982).
28. Stone, H.L.: "Probability Model for Estimating Three-Phase Relative Permeability", *Trans. SPE of AIME.*, **249**, 214 (1970).
29. Kurihara, M., Funatsu, K., Ouchi, H., Masuda, Y., and Narita, H.: "Investigation of Applicability of Methane Hydrate Production Methods to Reservoirs With Diverse Characteristics", Paper 3003, in *Proceedings of the 5th International Conference on Gas Hydrates,* June 13–16, Trondheim, 714 (2005).

Table 1 – Reservoir Properties

Parameter	Value
Gas zone thickness	15 m
Hydrate zone thickness	15 m
Initial pressure (at interface)	1.067×10^{7} Pa
Initial temperature	286.65 K
Gas composition	100% CH_4
Permeability $k_r=k_z$	1.0×10^{-12} m^2 (= 1 D)
Gas production rate	0.82 m^3/s (= 2.5 MMSCFD)
Dry thermal conductivity	0.5 W/m/K
Wet thermal conductivity	3.1 W/m/K
Relative permeability	
Capillary pressure model	Equation (7)
c	-0.65
P_e	1.55×10^{4} pa
w	9.28
a	2.1
b	2.2
Relative permeability model	$k_{rA} = (S_A^*)^n$ $k_{rG} = (S_G^*)^n$ $S_A^*=(S_A-S_{irA})/(1-S_{irA})$ $S_G^*=(S_G-S_{irG})/(1-S_{irA})$ OPM model
n	3
S_{irG}	0.02
S_{irA}	0.25

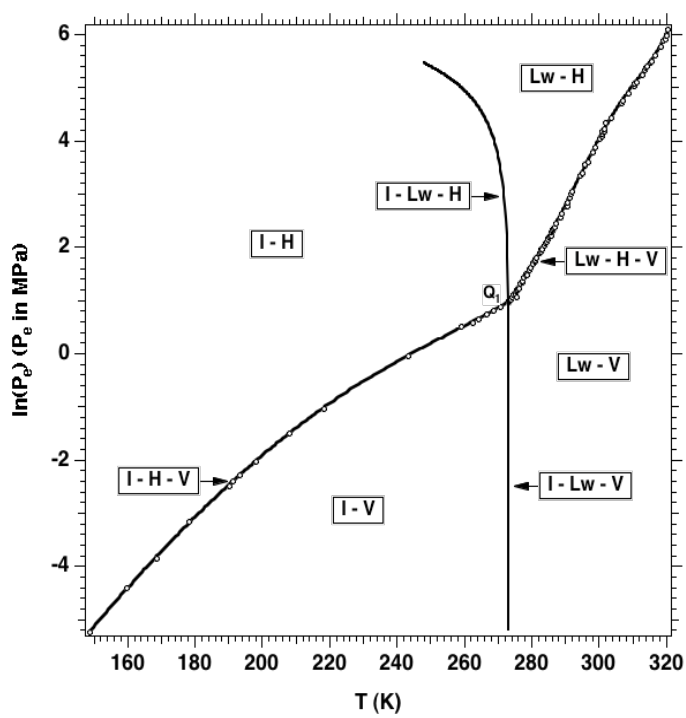

Figure 1 - Pressure-temperature equilibrium relationship in the phase diagram of the water--CH_4--hydrate system (Moridis et al.[9]).

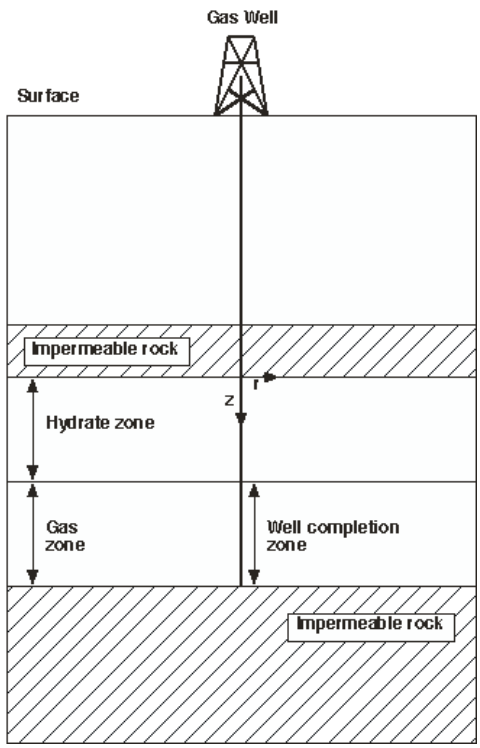

Figure 2 – Depressurization-induced production from a Class 1 hydrate deposit in Problem 1.

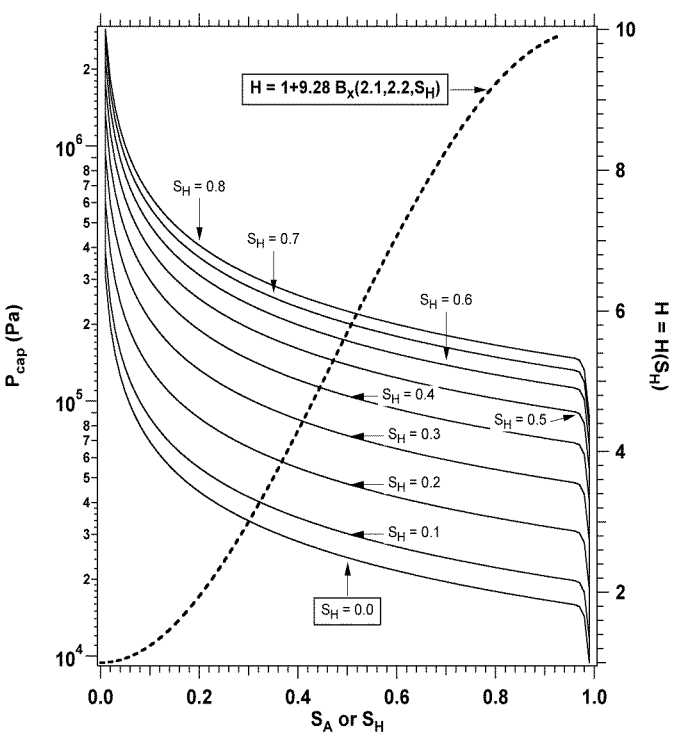

Figure 3 – Capillary pressure (as a function of S_{aA} and S_H) and H-factor of the hydrate-bearing formation in Problem 1.

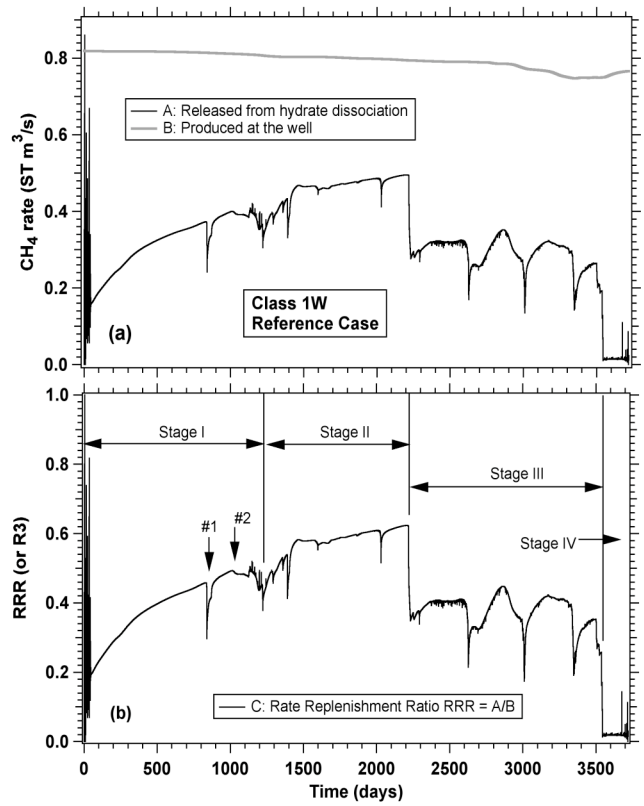

Figure 4 – Problem 1, reference case: Evolution of (A) the rate of CH_4 release from hydrate dissociation, (B) the rate of CH_4 production at the well, and (C) the corresponding RRR during long term production from a Class 1W hydrate deposit.

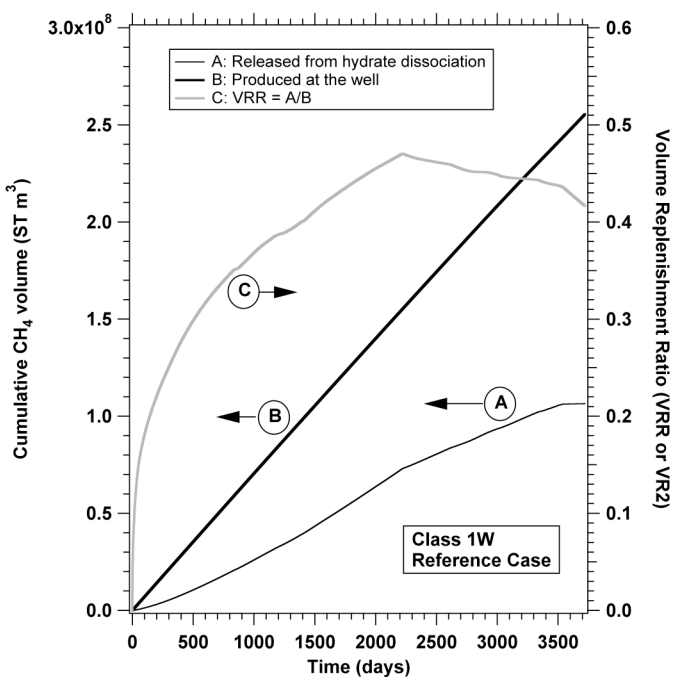

Figure 5 – Problem 1, reference case: Evolution of (A) the CH_4 volume released from hydrate dissociation, (B) the CH_4 volume produced at the well, and (c) the corresponding VRR during long term production.

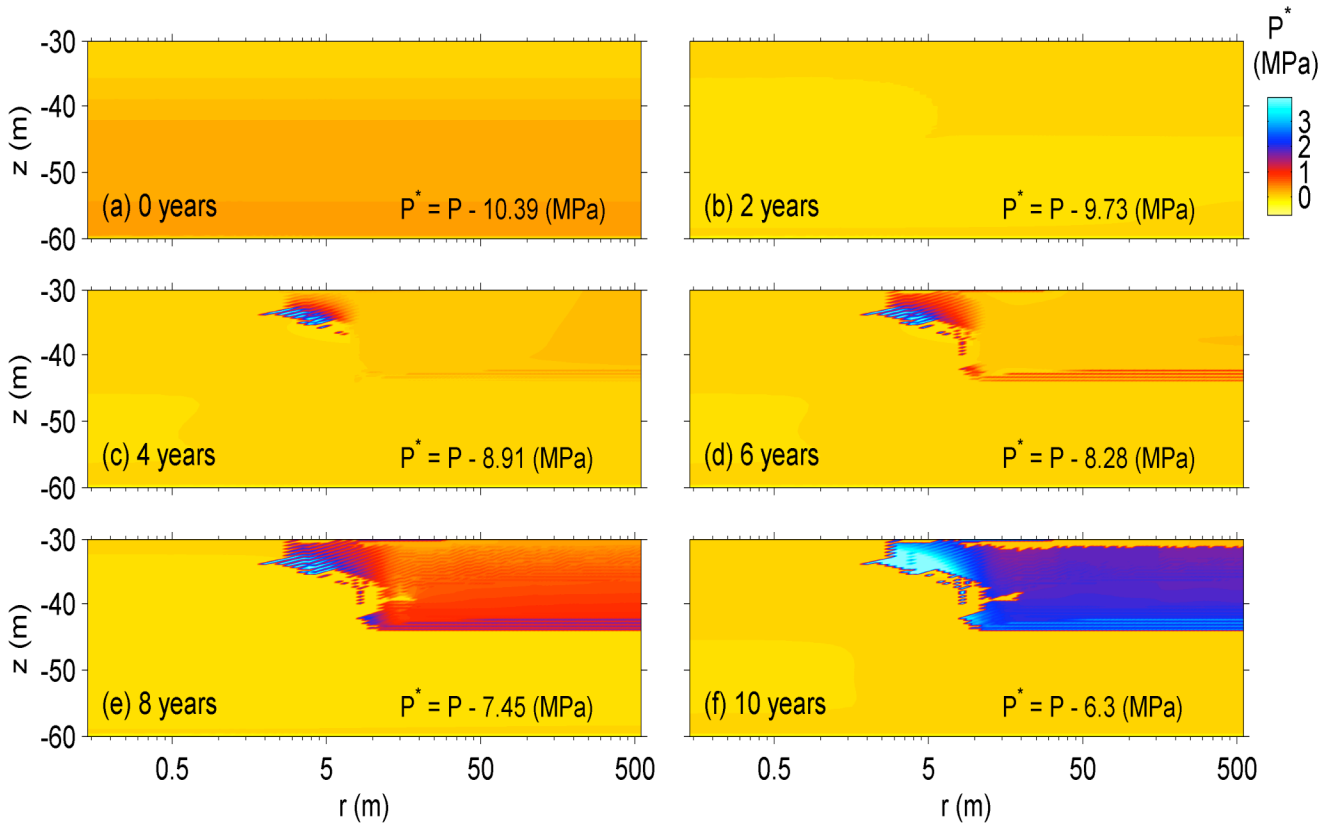

Figure 6 – Evolution of the pressure distribution in the Class 1W hydrate deposit of Problem 1 during depressurization.

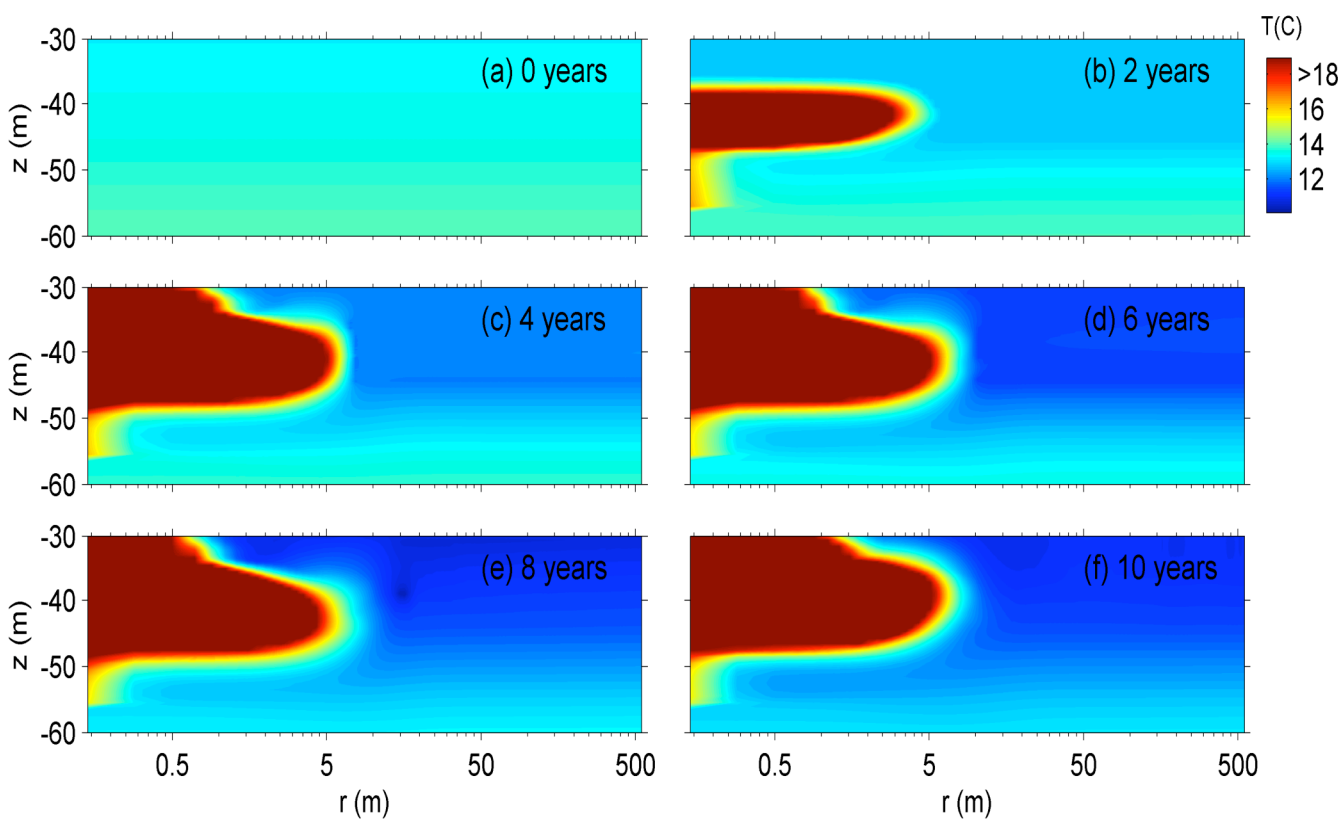

Figure 7 – Evolution of the temperature distribution in the Class 1W hydrate deposit of Problem 1 during depressurization.

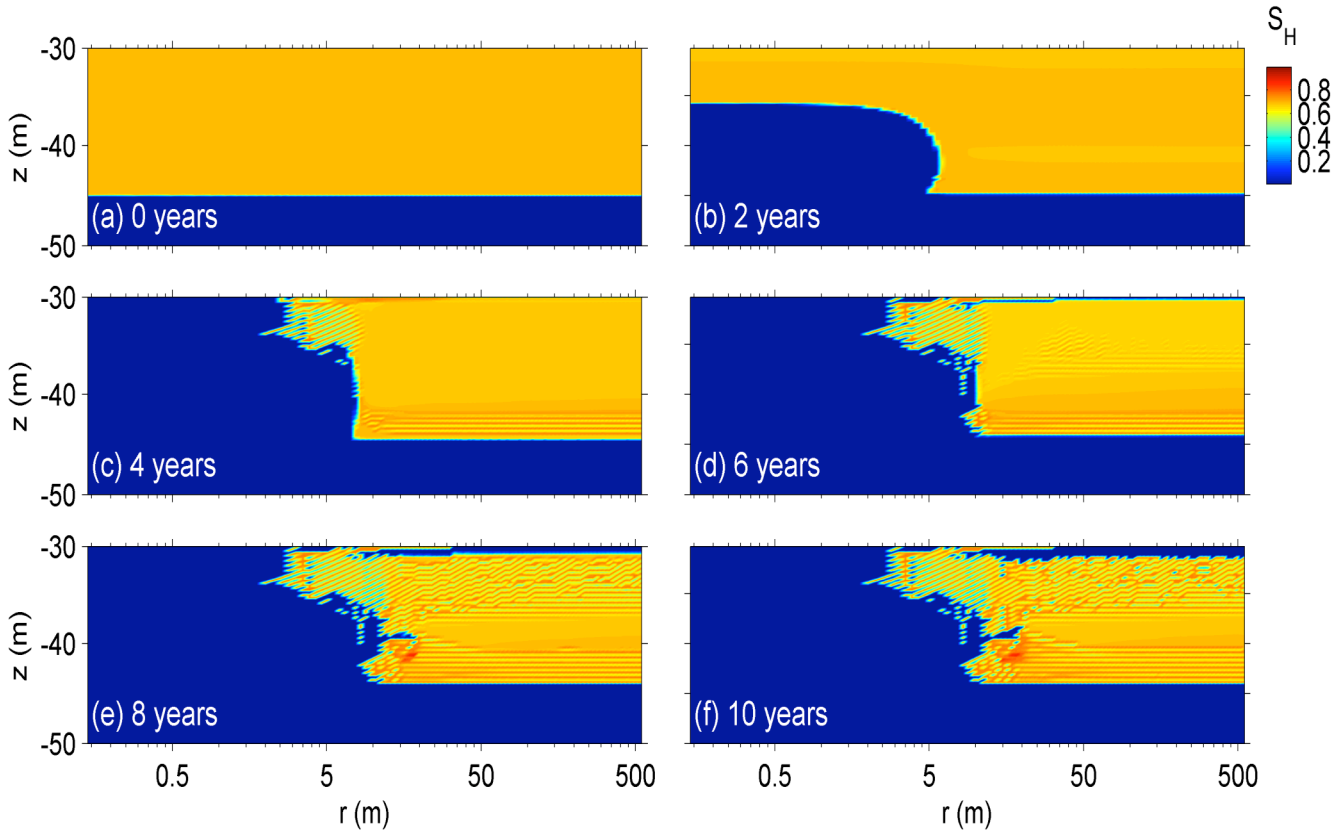

Figure 8 – Evolution of the hydrate saturation distribution in the Class 1W hydrate deposit of Problem 1 during depressurization.

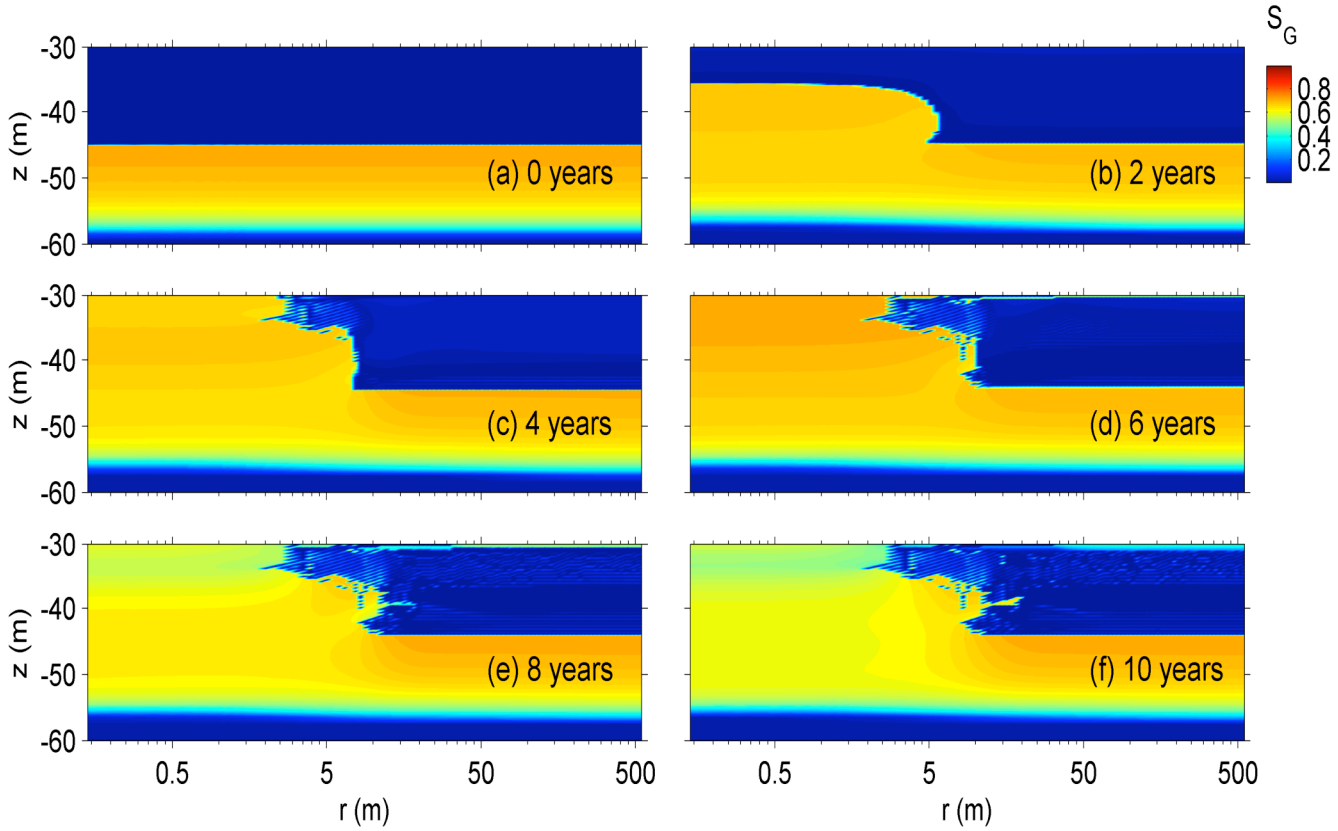

Figure 9 – Evolution of the gas saturation distribution in the Class 1W hydrate deposit of Problem 1 during depressurization.

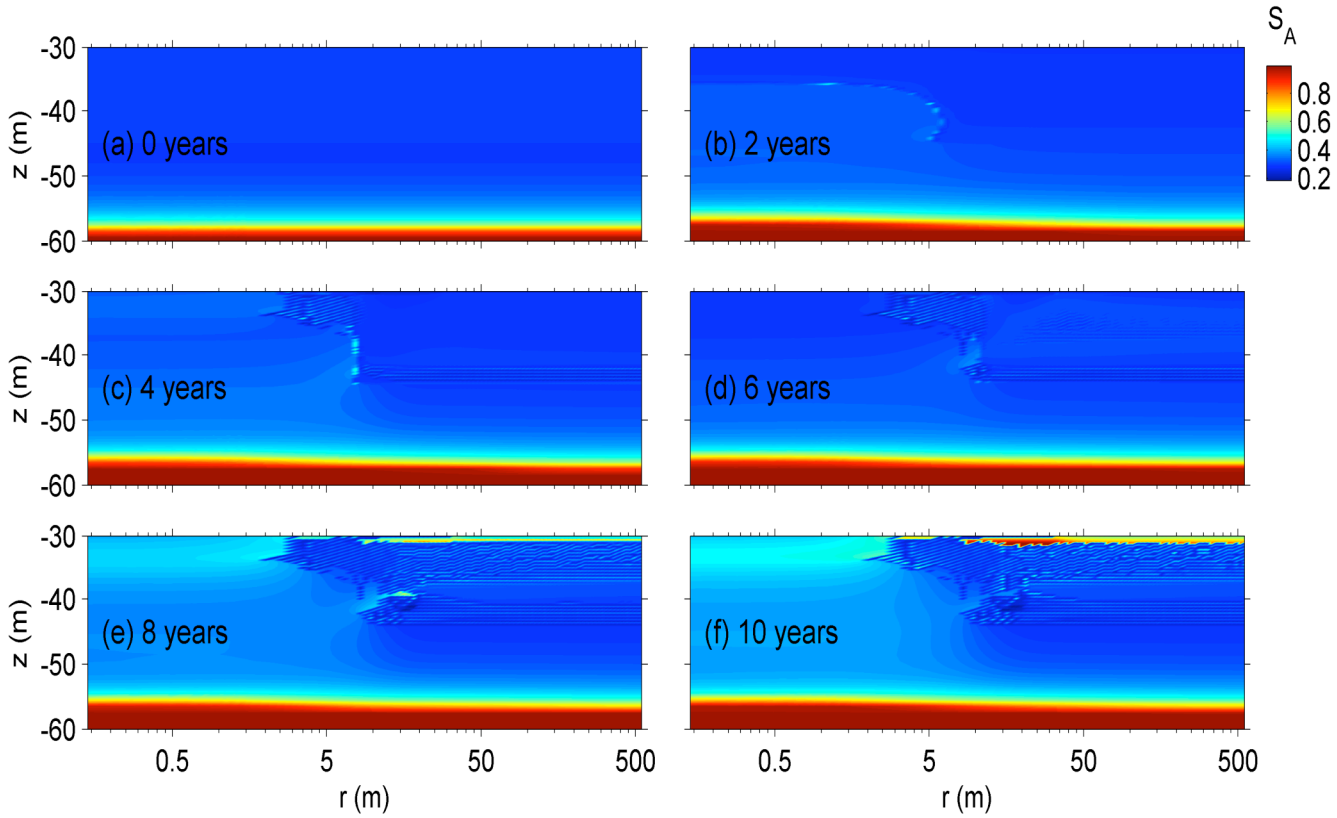

Figure 10 – Evolution of the aqueous phase saturation distribution in the Class 1W hydrate deposit of Problem 1 during depressurization.

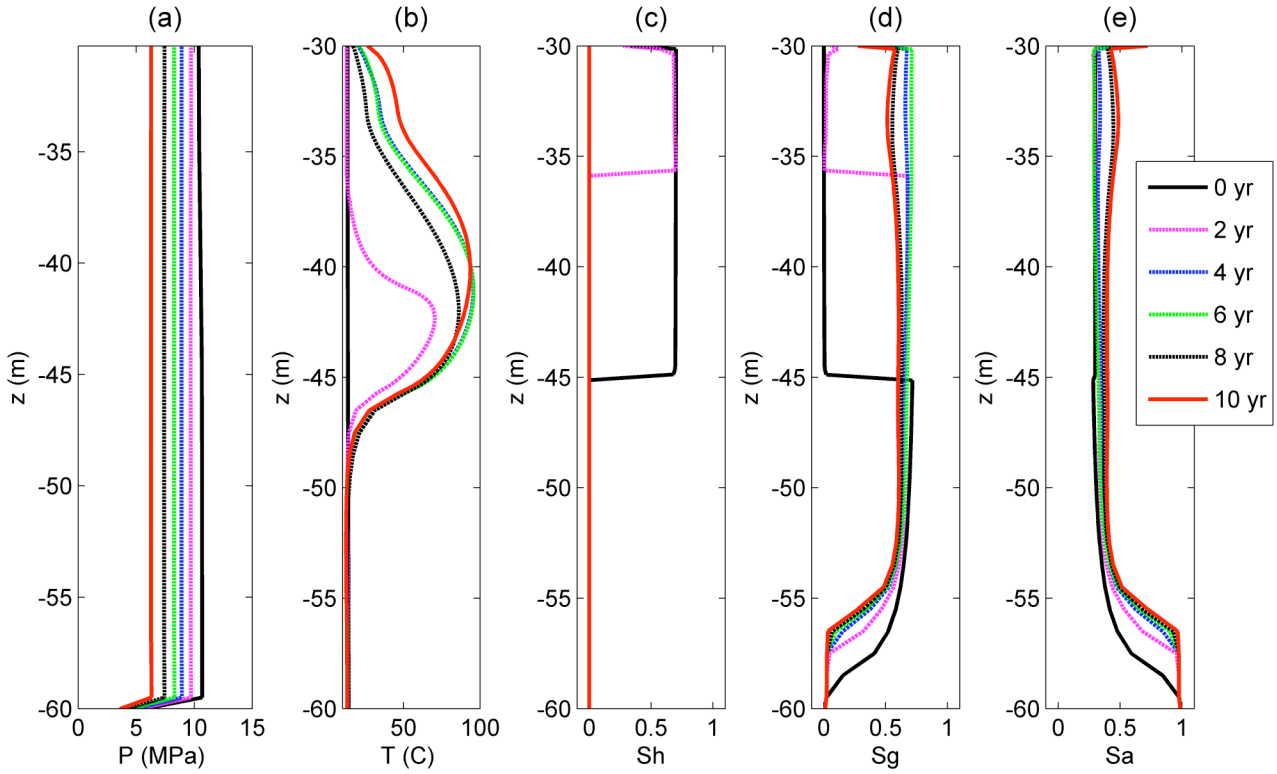

Figure 11 – Problem 1, Class 1W deposit: Evolution of the properties and conditions at r = 0.5 m.

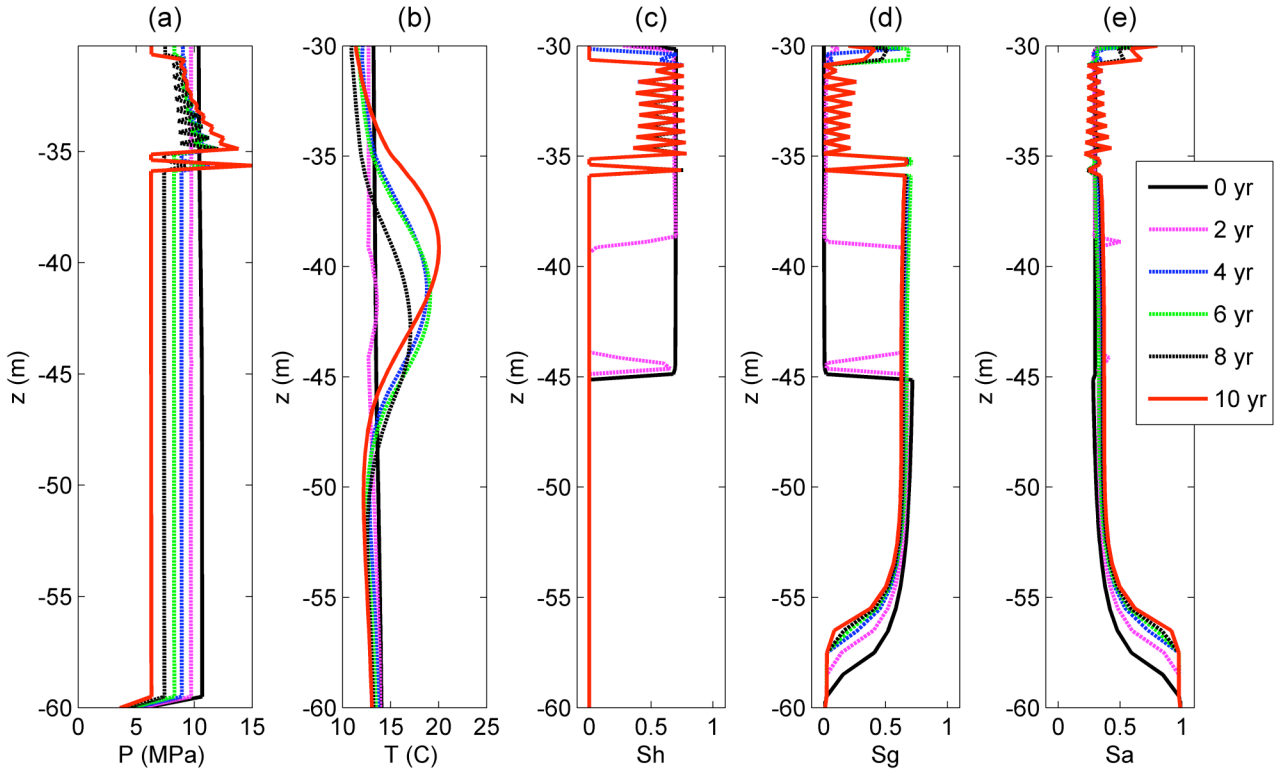

Figure 12 – Problem 1, Class 1W deposit: Evolution of the properties and conditions at r = 5 m.

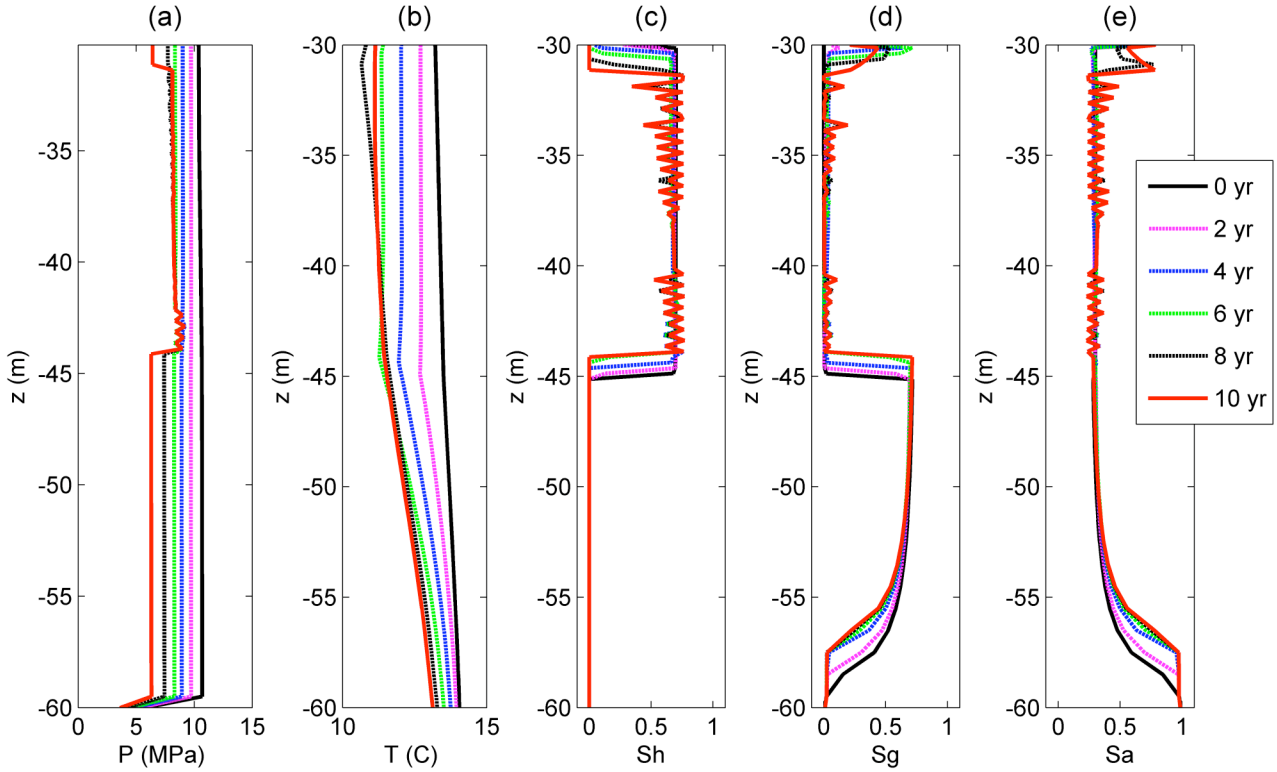

Figure 13 – Problem 1, Class 1W deposit: Evolution of the properties and conditions at r = 50 m.

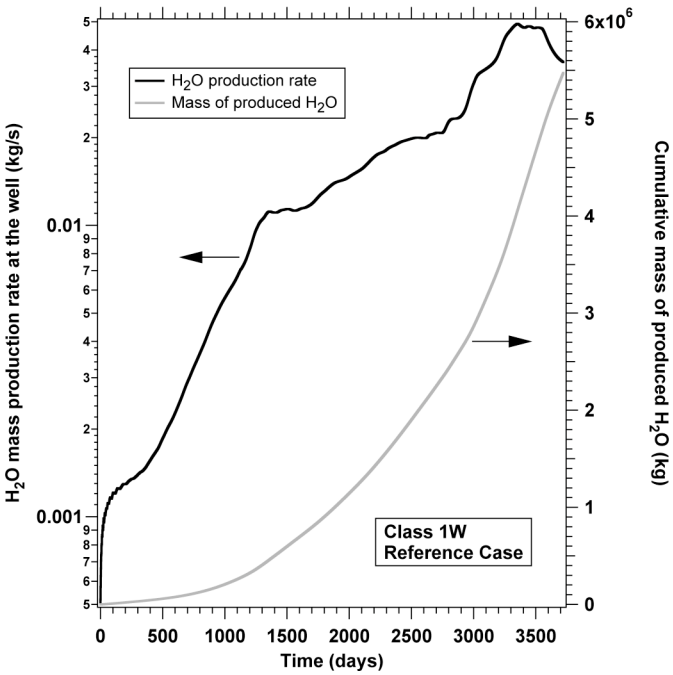

Figure 14 – Evolution of the water production rate and of the gas mass fraction in the production stream over the 30-year production period of Problem 1 (reference case).

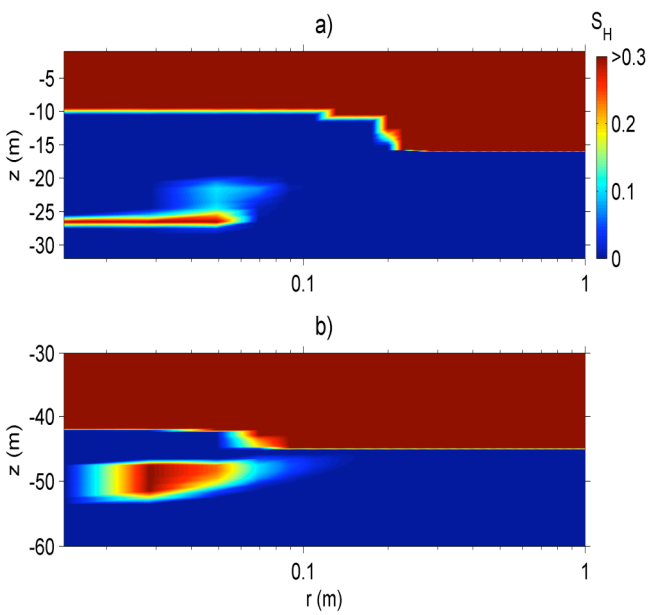

Figure 15 – Blockage of flow to the well (well "choking") caused by hydrate formation: (a) Class 1W deposit, Reference case, (b) Class 1G deposit, Case 2a.

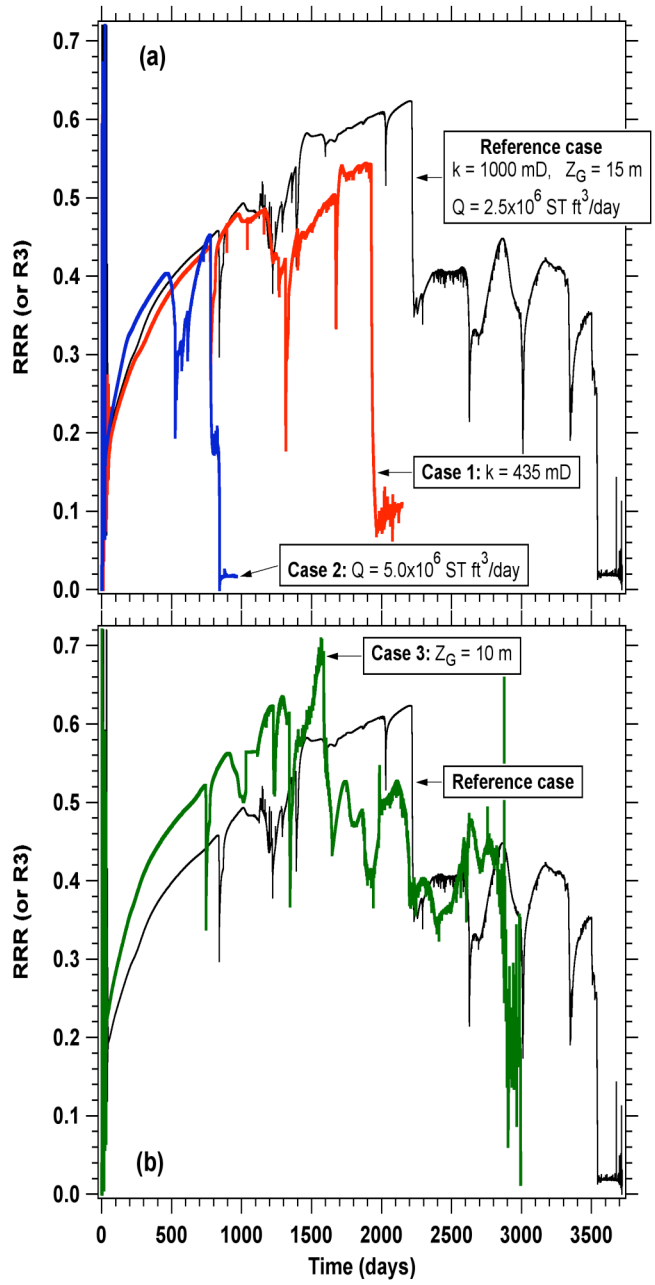

Figure 16 – Problem 1, sensitivity analysis: Effect of intrinsic permeability, production rate and thickness of the free gas zone on the RRR in a Class 1G deposit.

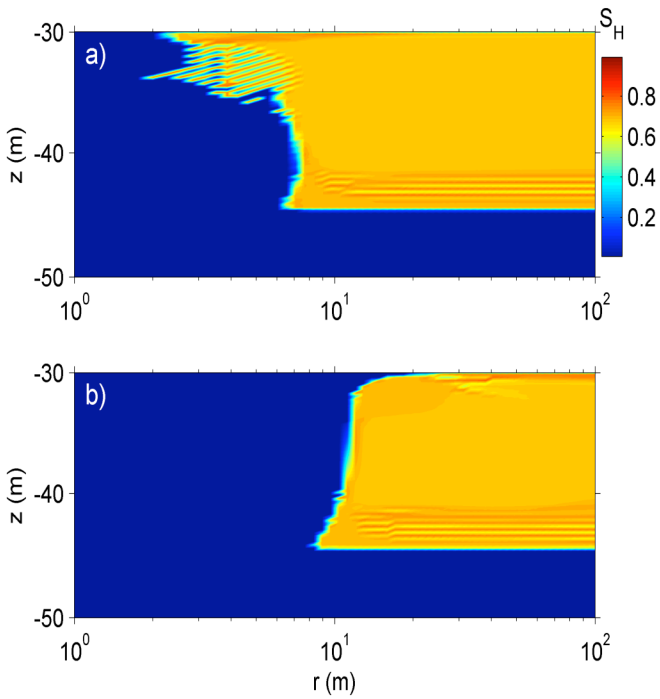

Figure 17 – Effect of intrinsic permeability on the S_H distribution at the beginning of Stage II: (a) Reference case, (b) Case 1.

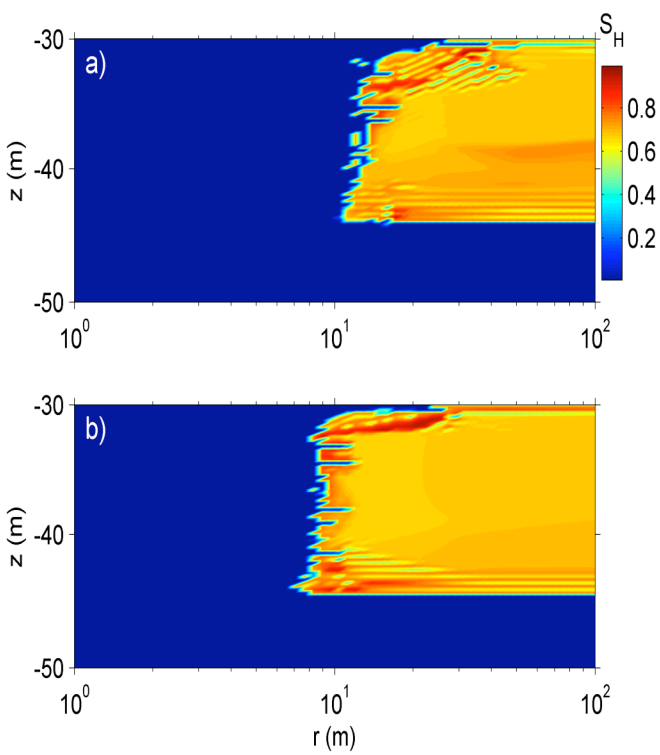

Figure 18 – Hydrate saturation distribution at the beginning of Stage IV (a) in Case 1 (lower k), and (b) in Case 2 (higher Q).

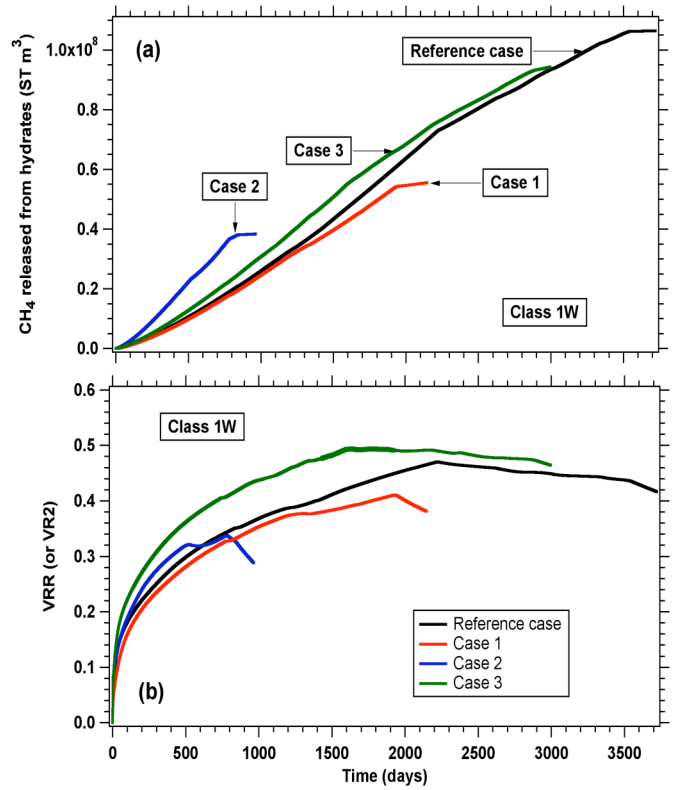

Figure 19 – Problem 1, Class 1W, sensitivity analysis: Effect of intrinsic permeability, production rate and thickness of the free gas zone on (a) the cumulative volume of CH_4 released from hydrates and (b) on the corresponding VRR.

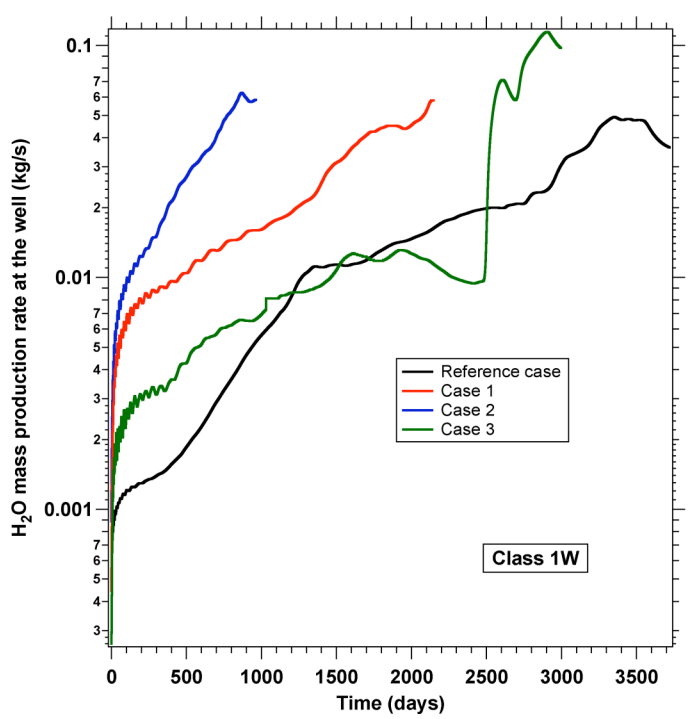

Figure 20 – Problem 1, Class 1W, sensitivity analysis: Effect of intrinsic permeability, production rate and thickness of the free gas zone on the rate of water production at the well.

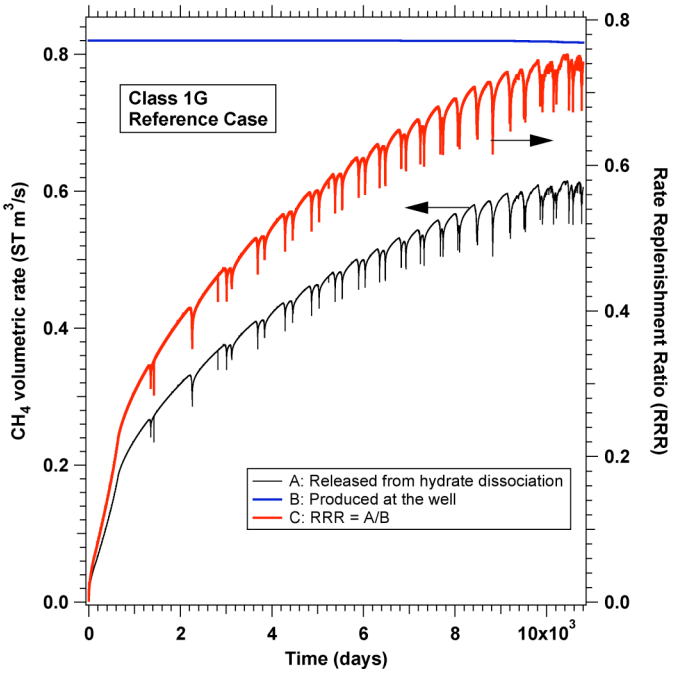

Figure 21 – Problem 2, Class 1G: Evolution of (a) the rate of CH_4 release from hydrate dissociation, (b) the rate of CH_4 production at the well, and (c) the corresponding RRR over the 30-yr production period.

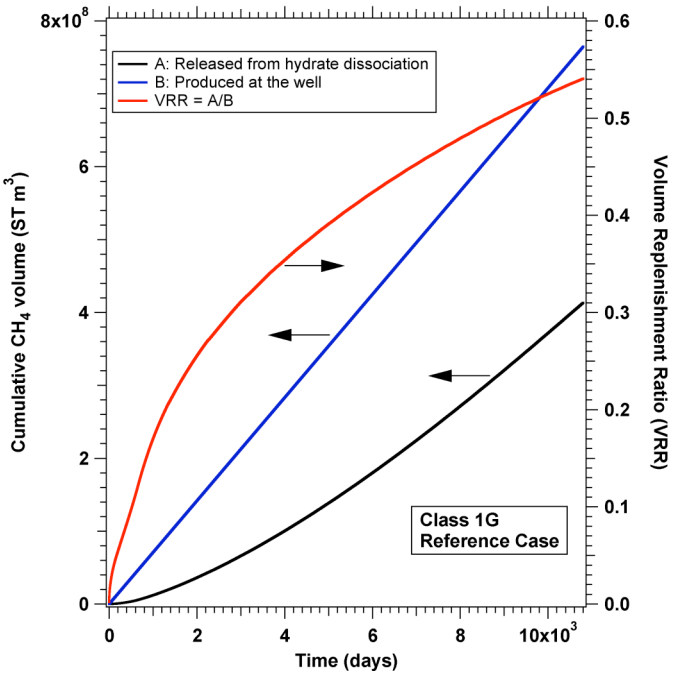

Figure 22 – Problem 2, Class 1G: Evolution of (a) the cumulative CH_4 volume released from hydrate dissociation, (b) the produced CH_4 volume at the well, and (c) the corresponding VRR over the 30-yr production period.

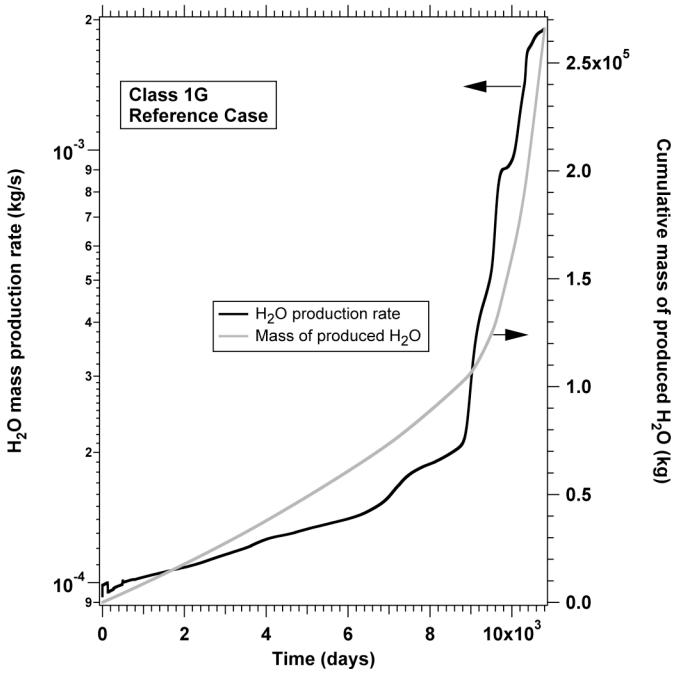

Figure 23 – Evolution of the water production rate and of the gas mass fraction in the production stream over the 30-year production period of Problem 2.

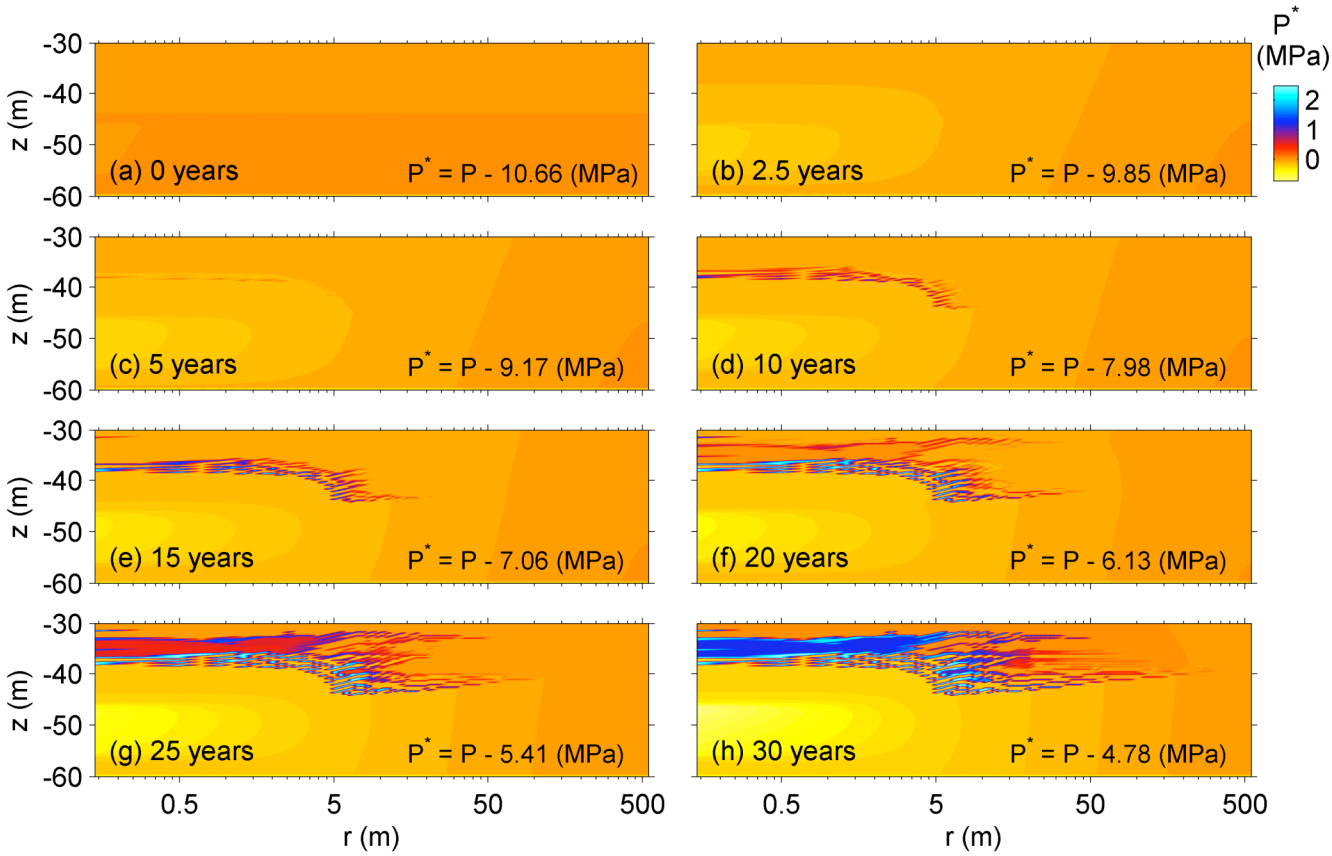

Figure 24 – Evolution of the pressure distribution in the Class 1G hydrate deposit of Problem 2 during depressurization.

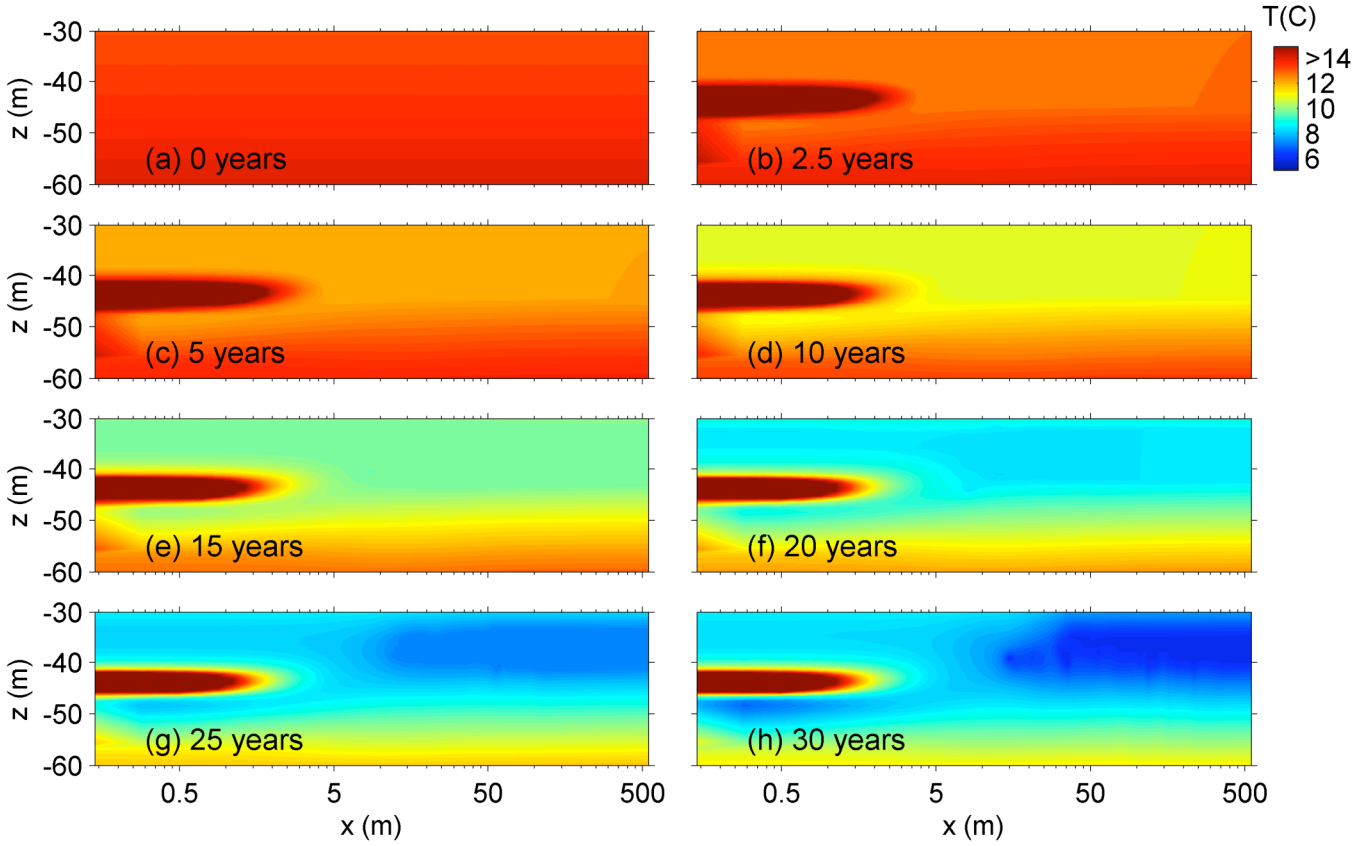

Figure 25 – Evolution of the temperature distribution in the Class 1G hydrate deposit of Problem 2 during depressurization.

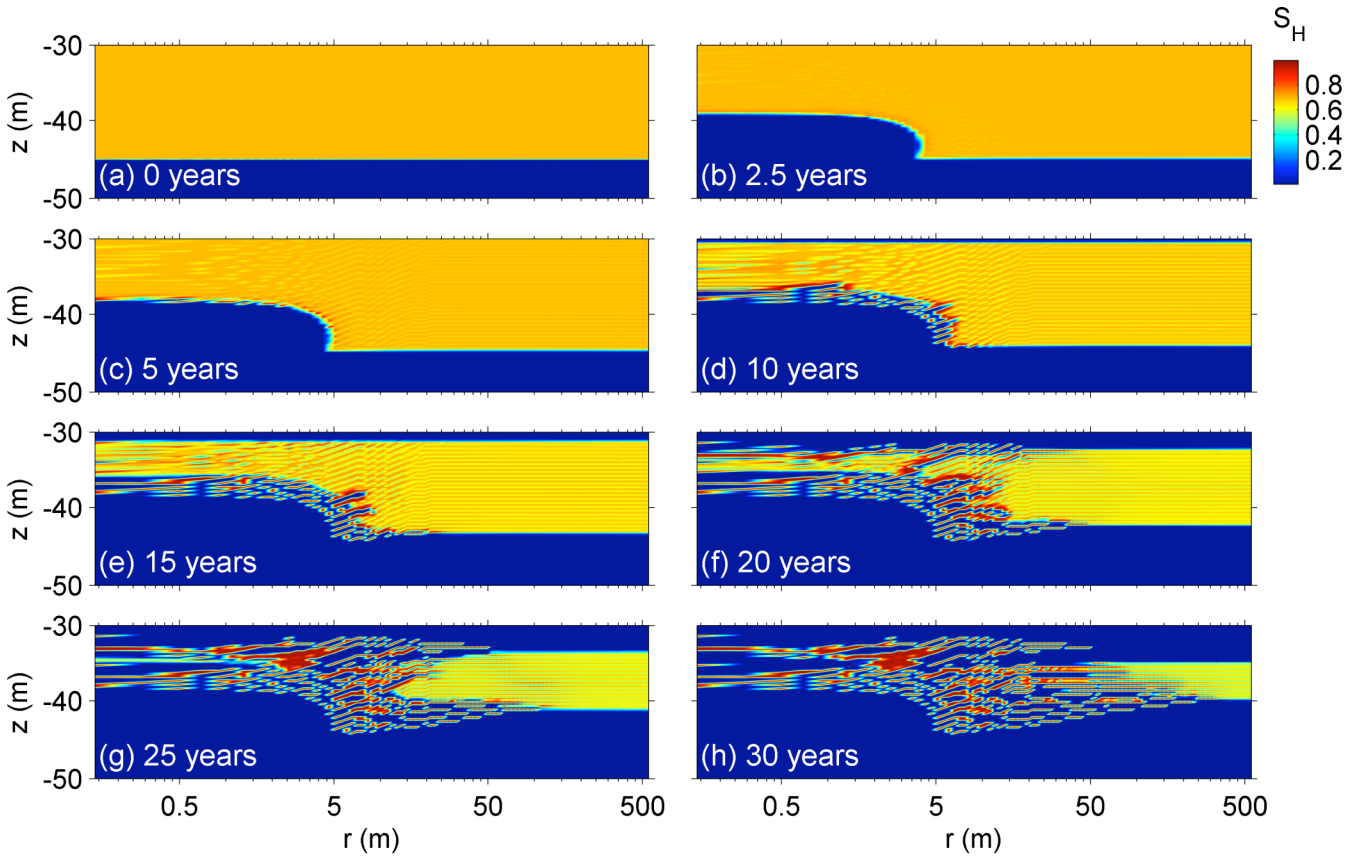

Figure 26 – Evolution of the hydrate saturation distribution in the Class 1G hydrate deposit of Problem 2 during depressurization.

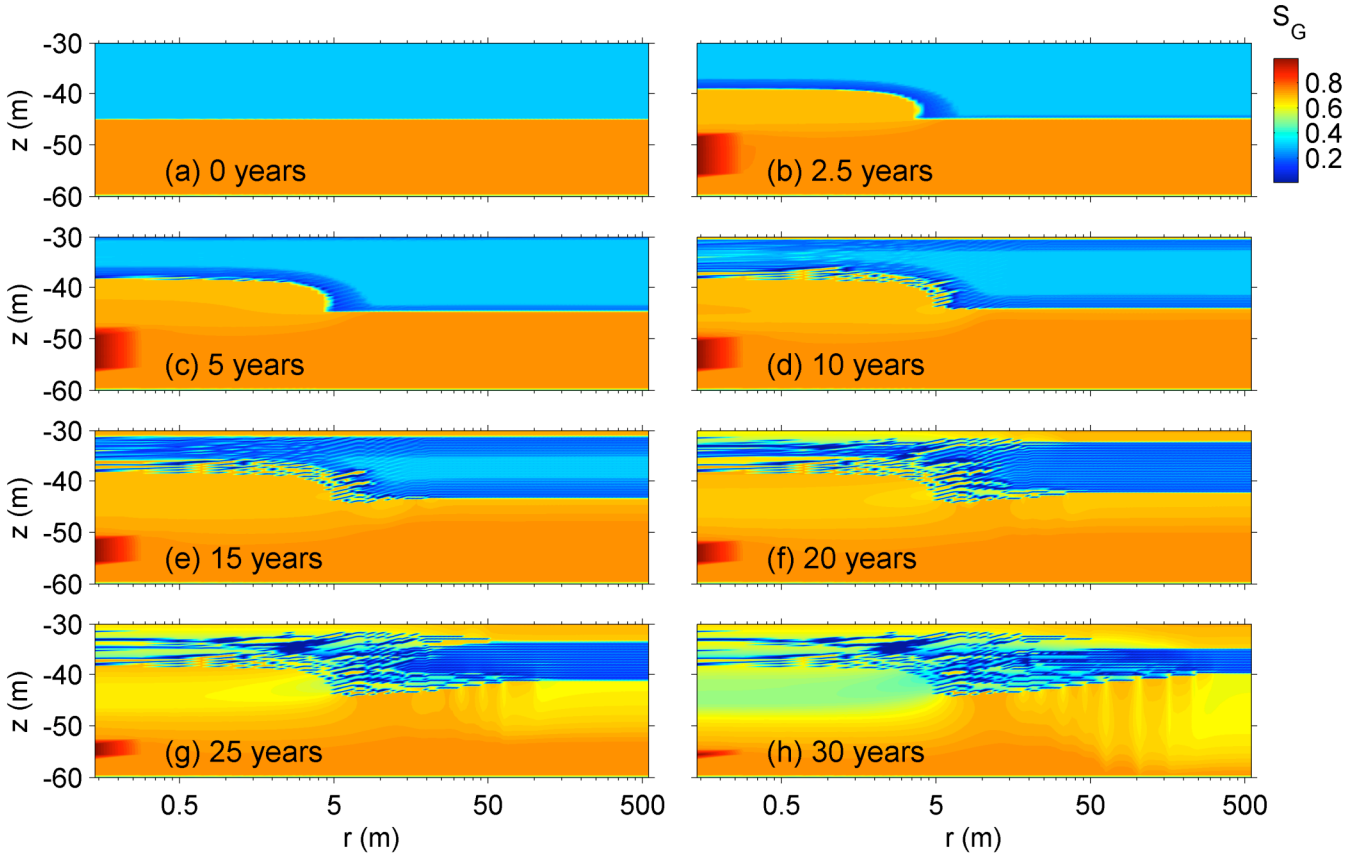

Figure 27 – Evolution of the gas saturation distribution in the Class 1G hydrate deposit of Problem 2 during depressurization.

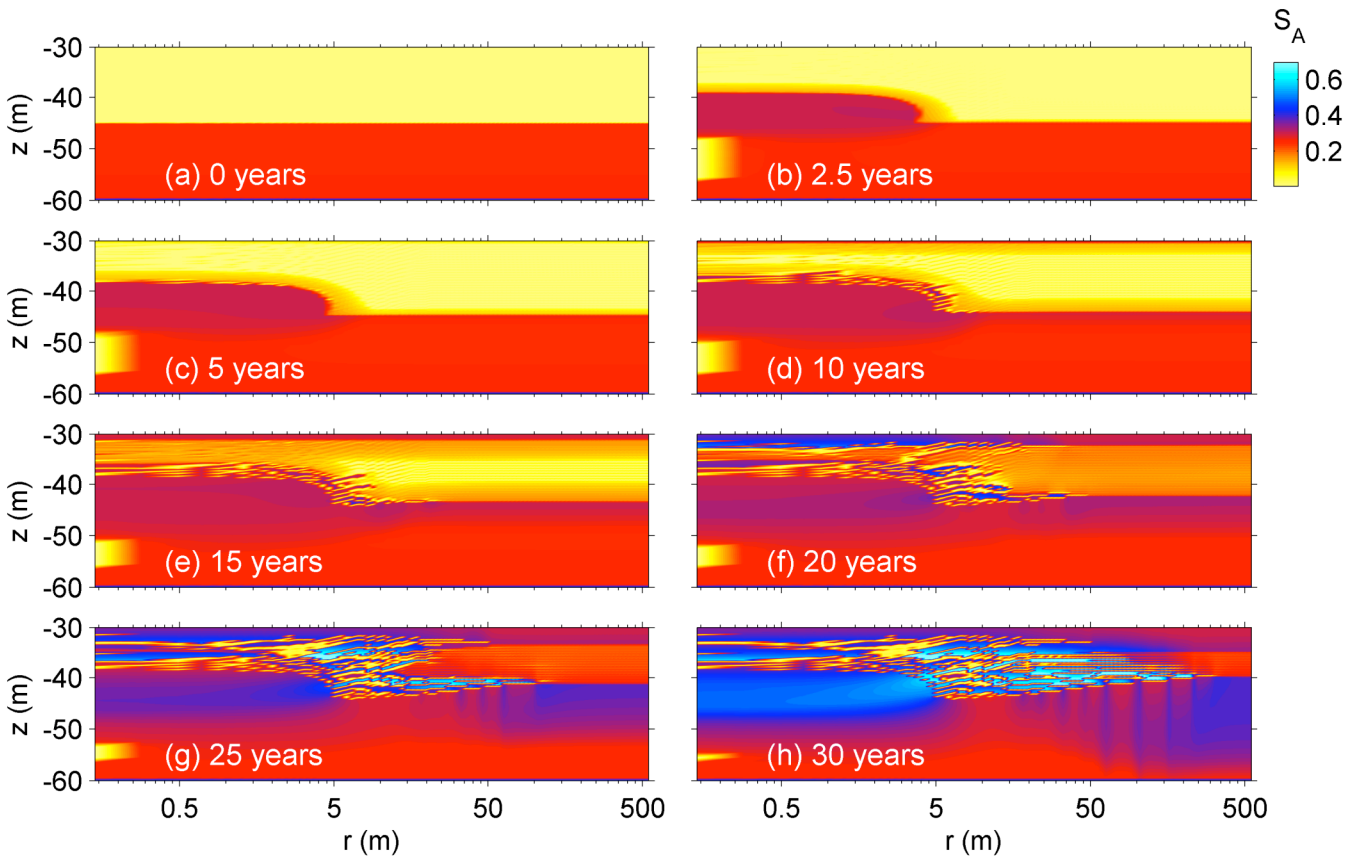

Figure 28 – Evolution of the aqueous phase saturation distribution in the Class 1G hydrate deposit of Problem 2 during depressurization.

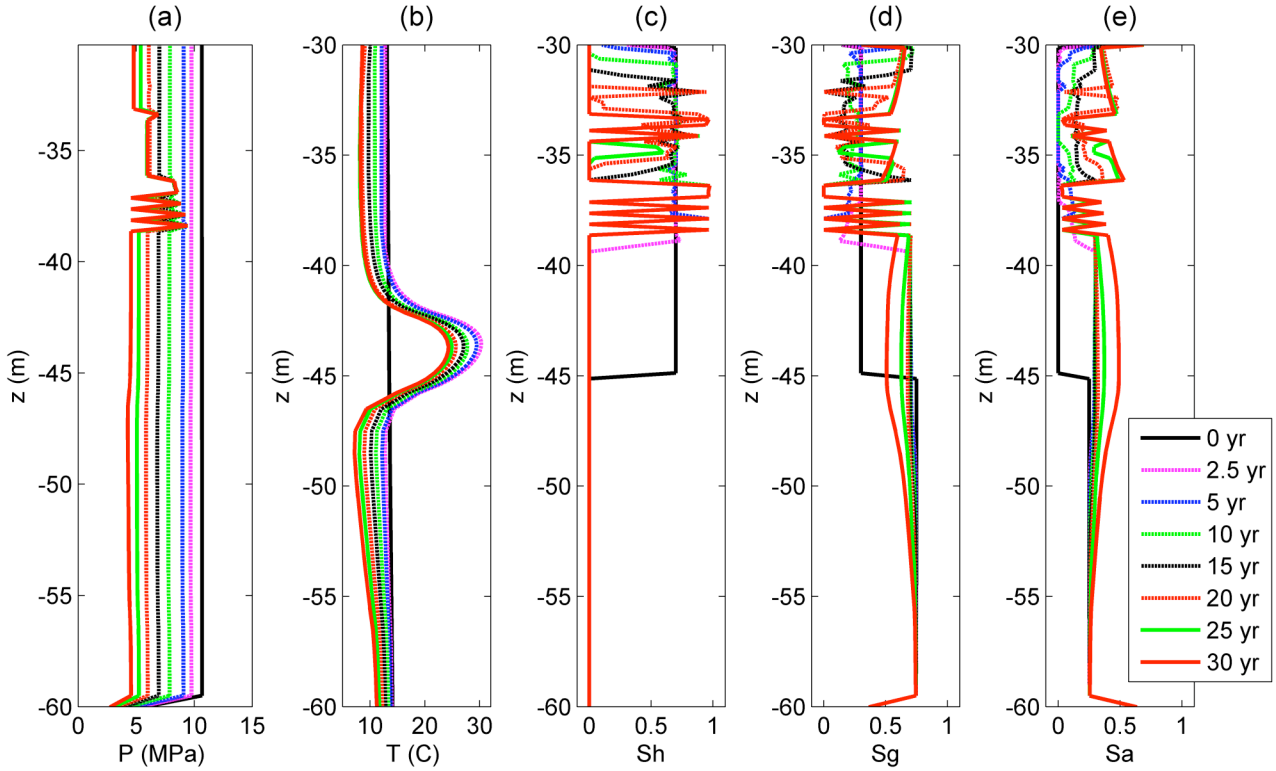

Figure 29 – Problem 2, Class 1G deposit: Evolution of the properties and conditions at r = 0.5 m.

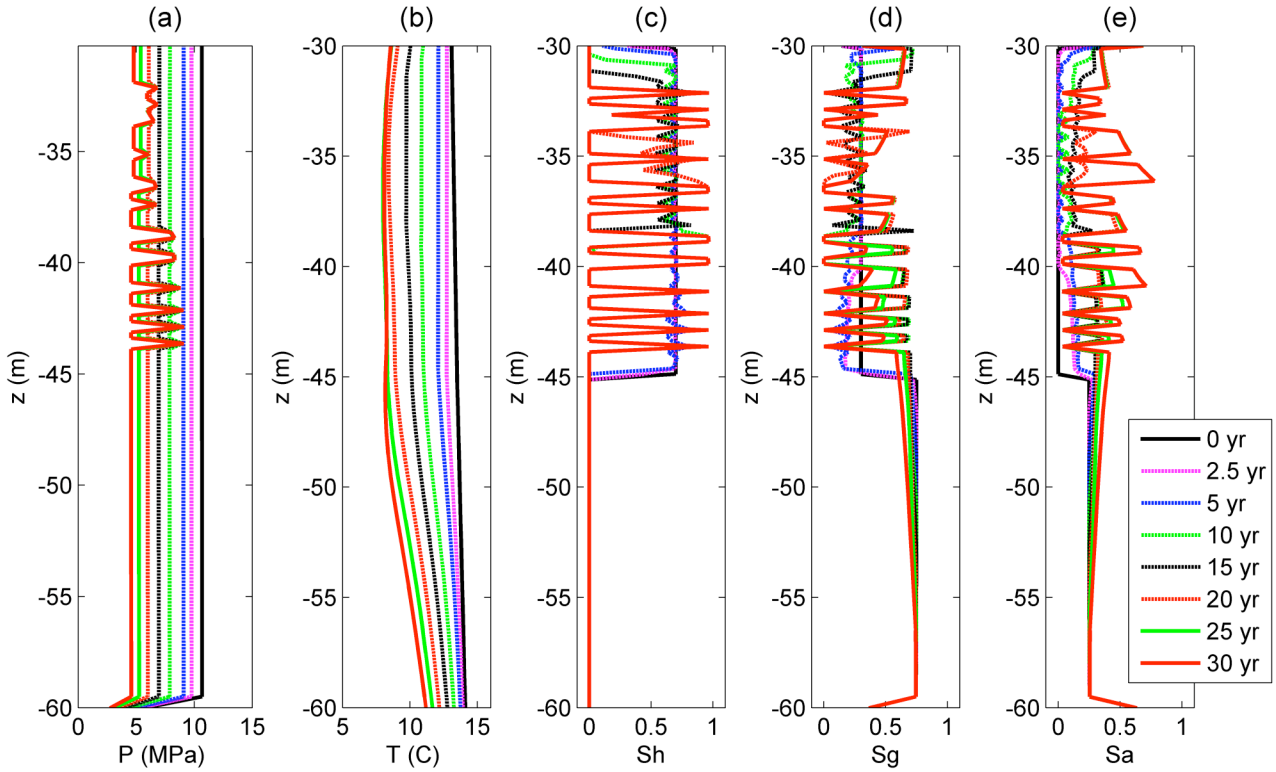

Figure 30 – Problem 2, Class 1G deposit: Evolution of the properties and conditions at r = 5 m.

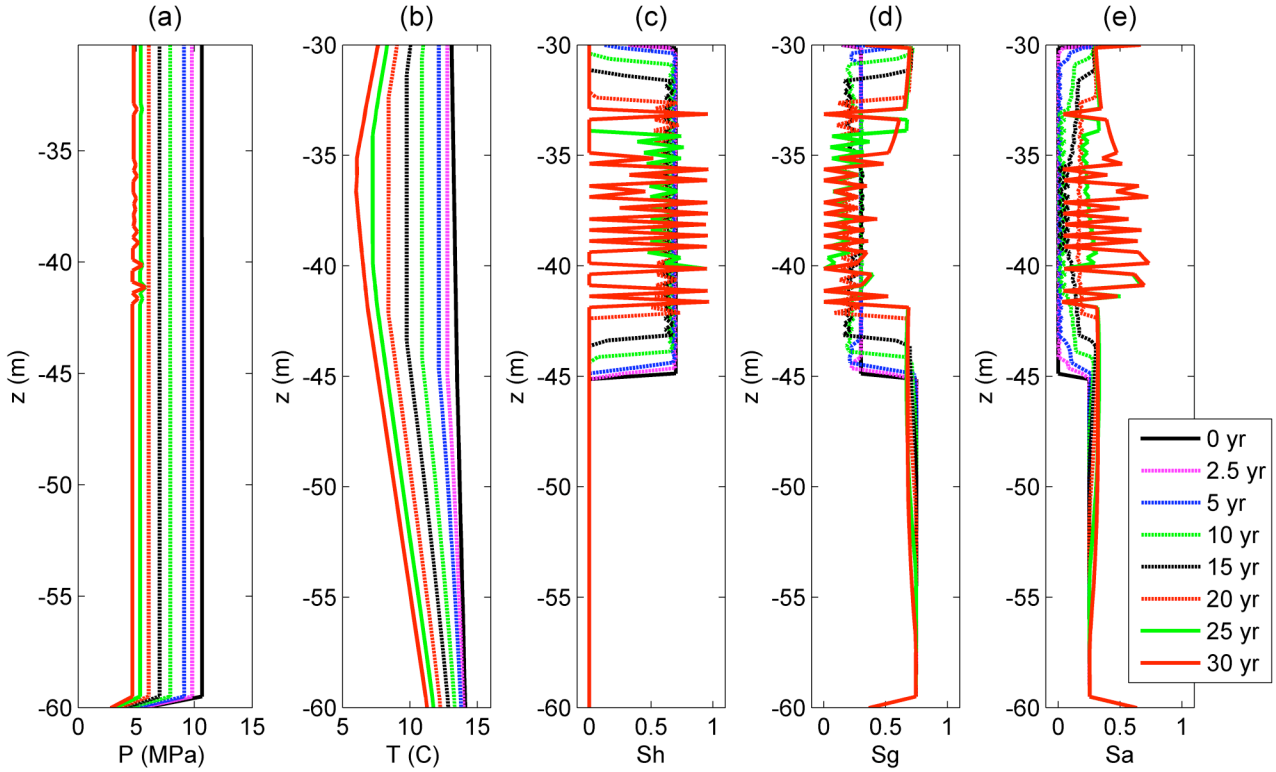

Figure 31 – Problem 2, Class 1G deposit: Evolution of the properties and conditions at r = 50 m.

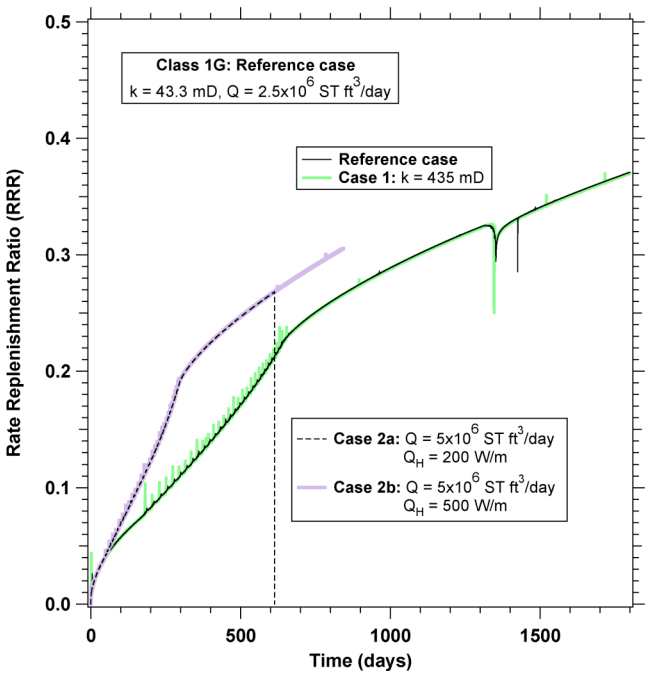

Figure 32 – Problem 2, sensitivity analysis: Effect of intrinsic permeability and production rate on the RRR in a Class 1G deposit.

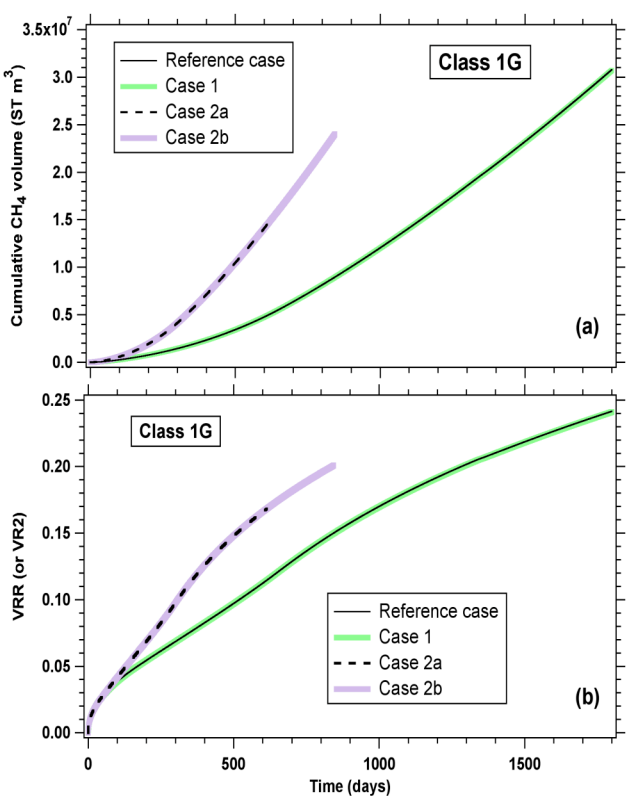

Figure 33 – Problem 2, sensitivity analysis: Effect of intrinsic permeability and production rate on (a) the volume of CH_4 released from dissociation and (b) on the VRR in a Class 1G deposit.

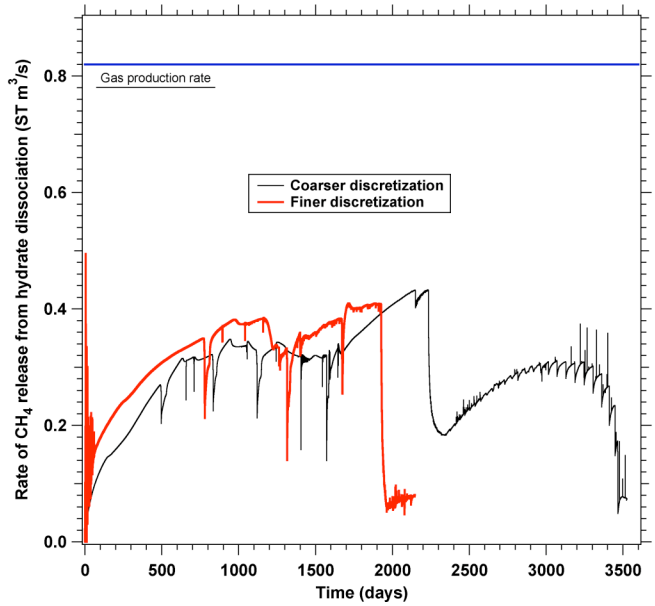

Figure 34 – Effect of grid refinement on predictions of the rate of CH_4 release from hydrate dissociation (Class 1W, reference case).

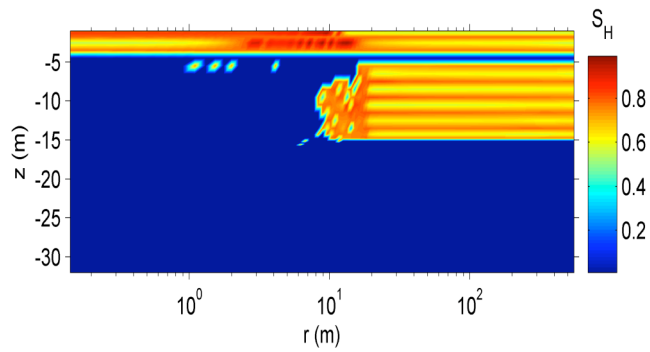

Figure 35 – Hydrate saturation distribution at the beginning of Stage IV in the case of the coarser grid.

OTC 18193

Response of Oceanic Hydrate-Bearing Sediments to Thermal Stresses

G.J. Moridis, SPE, and M. B. Kowalsky, Lawrence Berkeley National Laboratory

Copyright 2006, Offshore Technology Conference

This paper was prepared for presentation at the 2006 Offshore Technology Conference held in Houston, Texas, U.S.A., 1–4 May 2006.

This paper was selected for presentation by an OTC Program Committee following review of information contained in an abstract submitted by the author(s). Contents of the paper, as presented, have not been reviewed by the Offshore Technology Conference and are subject to correction by the author(s). The material, as presented, does not necessarily reflect any position of the Offshore Technology Conference, its officers, or members. Papers presented at OTC are subject to publication review by Sponsor Society Committees of the Offshore Technology Conference. Electronic reproduction, distribution, or storage of any part of this paper for commercial purposes without the written consent of the Offshore Technology Conference is prohibited. Permission to reproduce in print is restricted to an abstract of not more than 300 words; illustrations may not be copied. The abstract must contain conspicuous acknowledgment of where and by whom the paper was presented. Write Librarian, OTC, P.O. Box 833836, Richardson, TX 75083-3836, U.S.A., fax 01-972-952-9435.

Abstract

In this study we evaluate the response of oceanic subsurface systems to thermal stresses caused by the flow of warm fluids through non-insulated well systems crossing hydrate-bearing sediments. Heat transport from warm fluids, originating from deeper reservoirs under production, into the geologic media can cause dissociation of the gas hydrates. The objective of this study is to determine whether gas evolution from hydrate dissociation can lead to excessive pressure build-up and possibly to fracturing of hydrate-bearing formations and their confining layers, with potentially adverse consequences on the stability of the suboceanic subsurface. This study also aims to determine whether the loss of the hydrate – known to have a strong cementing effect on the porous media – in the vicinity of the well, coupled with the significant pressure increases, can undermine the structural stability of the well assembly.

Scoping 1D simulations indicated that the formation intrinsic permeability, the pore compressibility, the temperature of the produced fluids and the initial hydrate saturation are the most important factors affecting the system response, while the thermal conductivity and porosity (above a certain level) appear to have a secondary effect. Large-scale simulations of realistic systems were also conducted, involving complex well designs and multilayered geologic media with non-uniform distribution of properties and initial hydrate saturations that are typical of those expected in natural oceanic systems. The results of the 2D study indicate that although the dissociation radius remains rather limited even after long-term production, low intrinsic permeability and/or high hydrate saturation can lead to the evolution of high pressures that can threaten the formation and its boundaries with fracturing. Although lower maximum pressures are observed in the absence of bottom confining layers and in deeper (and thus warmer and more pressurized) systems, the reduction is limited. Wellbore designs with gravel packs that allow gas venting and pressure relief result in substantially lower pressures.

Introduction

Background. Gas hydrates are solid crystalline compounds in which gas molecules (referred to as guests) are lodged within the lattices of ice crystals (called hosts). Under suitable conditions of low temperature and high pressure, a gas G will react with water to form hydrates according to

$$G + N_H\, H_2O = G{\bullet}N_H\, H_2O,$$

where N_H is the hydration number. Of particular interest are hydrates formed by hydrocarbon gases when G is an alkane. Natural hydrates in geological systems also include CO_2, H_2S and N_2 as guests. Vast amounts of hydrocarbons are trapped in hydrate deposits[1]. Such deposits occur in two distinctly different geologic settings where the necessary low temperatures and high pressures exist for their formation and stability: in the permafrost and in deep ocean sediments.

The three main methods of hydrate dissociation are[1]: (1) depressurization, in which the pressure P is lowered to a level lower than the hydration pressure P_e at the prevailing temperature T, (2) thermal stimulation, in which T is raised above the hydration temperature T_e at the prevailing P, and (3) the use of inhibitors (such as salts and alcohols), which causes a shift in the P_e-T_e equilibrium through competition with the hydrate for guest and host molecules. Dissociation results in the production of gas and water, with a commensurate reduction in the saturation of the solid hydrate phase.

Gas hydrates exist in many configurations below the sea floor, including massive (thick solid zones), continuous layers, nodular, and disseminated, each of which may affect the seafloor stability differently. The hydrates in all of these configurations may be part of the solid skeleton that supports overlying sediments, which ultimately support platforms and pipelines needed for production from conventional oil and gas resources, and from hydrate accumulations (when it becomes economically and technically viable).

Objective and Problem Description. The main objective of this study is to evaluate the response of marine Hydrate-Bearing Sediments (hereafter referred to as HBS) to thermal loading. Such thermal loading occurs when heat from hot reservoir fluids (produced from deeper reservoirs) flows into the HBS through uninsulated pipes.

The resulting rise in temperature in the HBS can have serious consequences. Even before dissociation is attained, a rising temperature T is expected to affect the mechanical strength of hydrate-bearing sediments – possibly severely, given the narrow temperature range between hydrate stability and dissociation. When the temperature T reaches the hydrate equilibrium T_e temperature (see Figure 1) at the prevailing pressure P

(usually close to the hydrostatic pressure at the location), hydrate dissociation occurs by thermal stimulation. This leads to the rapid release of large amounts of gas, which can in turn result in the evolution of high pressures. This higher pressure can result in formation fracturing, with potentially serious consequences if the fracture plane crosses the confining (impermeable) top boundary of an underlying reservoir, thus allowing the escape of the reservoir fluids. It is also possible that the increased P, if sufficiently high, can have detrimental effects on the wellbore assembly, including cement fracturing and wellbore collapse.

Another problem that can be potentially caused by thermal loading is the deterioration of the structural stability of the geologic formation in the vicinity of the wellbore. Hydrates are very effective cementing agents[2], and their dissociation can lead to significant geomechanical changes in the thermally affected region (including substantial subsidence). Unless accounted for, these changes can pose a hazard to the structural stability of the wellbore assembly. The reason for the concern is demonstrated in the photograph of Figure 2, which shows a dissociating core of a marine HBS. While the more isolated inner portion of the core (where hydrate still remains) appears "solid" and structurally strong, the medium in the outer annular space (where hydrate dissociation is in progress or has already occurred) has a fluid and very weak consistency because of the loss of the cementing hydrate and shows evidence of escaping gases (bubbling). Because of its consistency, the remaining watery mud is characterized as "soupy sediment". The impact of its evolution on the structural stability of marine HBS demands evaluation, especially in the case of compressible sediments such as muds and clays. Finally, during dissociation, the basal zone of the gas hydrate becomes underconsolidated and possibly over-pressurized because of the newly released gas[3], leading to a zone of weakness akin to that indicated in Figure 2 (i.e., low shear strength, where failure could be triggered by gravitational loading or seismic disturbances), which can result in submarine landslides[4,5].

In this study, we employ numerical simulation to determine the effects of thermal loading on the behavior of marine hydrate deposits (assumed to be pure CH_4 hydrates). More specifically, we determine the evolution over a 30-year production period of important conditions and parameters in the oceanic subsurface, including P, T, phase saturations, porosity (as affected by P and T), and salt concentration (as influenced by the release of fresh water from the dissociating hydrates). We also determine the magnitude and location of the maximum pressure evolving in the dissociating HBS, and we provide estimates of the rate of gas release and of the cumulative volume of released gas. These data can be used as inputs in standard geomechanical models to determine the geomechanical and structural response of the oceanic subsurface, and to evaluate the safety and adequacy of proposed well designs.

The numerical simulation code. The numerical studies in this paper were conducted using the TOUGH-Fx/HYDRATE simulator[6], which can model the non-isothermal hydration reaction, phase behavior and flow of fluids and heat under conditions typical of natural CH_4-hydrate deposits in complex geologic media. It includes both an equilibrium and a kinetic model[7,8] of hydrate formation and dissociation. The model accounts for heat and up to four mass components (i.e., water, CH_4, hydrate, and water-soluble inhibitors such as salts or alcohols) that are partitioned among four possible phases: gas phase, liquid phase, ice phase, and hydrate phase. A total of 12 states (phase combinations) can be described by the code, which can handle any combination of hydrate dissociation mechanisms and can describe the phase changes and steep solution surfaces that are typical of hydrate problems.

Contextual analysis of simulation predictions and important assumptions. Note that the TOUGH-Fx/HYDRATE simulator[6] is a mass and heat flow and transport code, and does not include a full geomechanical component. Thus, it cannot internally estimate stresses and strains resulting from P and T changes in response to HBS heating and hydrate dissociation. As such, it cannot compute the effect of the resulting changes in stress and strain on the HBS hydraulic, thermal and geomechanical properties system, and on the overall system behavior (e.g., deformation and subsidence). However, TOUGH-Fx/HYDRATE can predict the evolution of all the other important hydraulic and thermal properties and conditions discussed earlier, which can then serve as inputs in subsequent geomechanical studies. Additionally, the code includes a simplified geomechanical model that accounts for the effect of pressure P and temperature T on porosity through the relationship[6]

$$\phi = \phi_0 \left[1 + \alpha (P - P_0) + \beta (T - T_0)\right]$$

where ϕ is the porosity, the subscript 0 indicates a reference state, and the pore compressibility α and expansivity β are defined as follows:

$$\alpha = \frac{1}{\phi}\left(\frac{\partial \phi}{\partial P}\right)_T \quad \text{and} \quad \beta = \frac{1}{\phi}\left(\frac{\partial \phi}{\partial P}\right)_P$$

As indicated earlier, the hydrates in these studies are assumed to be pure CH_4 hydrates. Although CH_4 is the dominant hydrate-forming constituent in oceanic deposits, other hydrate-forming gases are usually involved. Because of the complexity of the thermodynamics of such composite hydrates and the paucity of data on the subject, such systems cannot be currently simulated. However, the dominance of CH_4 makes the use of a pure-hydrate model a good analog.

All the simulations in this study were conducted assuming an equilibrium reaction of hydrate dissociation or formation. This is valid assumption because recent studies[9] have indicated that kinetics can be important only in very short-term processes (lasting a maximum of a few hours), while long-term processes (such as the ones discussed in this investigation) show practically no kinetic limitation.

Scoping Studies

Purpose. In this component of the study we analyze the response of a simplified, infinite-acting, 1-D radial (single-well) HBS system to heating by warm fluids rising to the surface through uninsulated tubing at the center of the domain. The purpose is to determine the sensitivity of the system response to the parameters that are most relevant in HBS systems.

System description. A domain of uniform properties and initial conditions, and consisting of a single layer (with Δz = 1 m thick) was considered (Table 1), thus allowing the estimation of the response per unit thickness of HBS. The domain radius

r_{max} = 1000 m was subdivided into 275 cells of non-uniform Δr. Because of the need to accurately describe heat transfer within and in the vicinity of the wellbore assembly, and because heat conduction (which is expected to play an important role in this study) is a slow process, a very fine discretization was used near the center of the radial grid.

Well description. The design and material properties of the wellbore assembly, along with details of the system geometry, are given in Table 2. In the discretized domain used in the simulation, the first 23 radial elements (out of the total of 275) are used to describe the well system. This fine discretization provides a high-resolution description of the critically important heat flow through the inner tubing, the five steel casings (including the outer conductor), and the corresponding cement– and brine–filled annular spaces. Note that the same well design was used in the ensuing large-scale 2-D studies of HBS heating in realistic natural hydrate accumulations. The innermost radial gridblocks in the 1-D and 2-D studies correspond to the region in which hot fluids flow through the tubing (hydraulically impermeable in the horizontal direction), and are designated as constant-conditions boundary cells. In the reference case of the scoping studies, the inner boundary cell is maintained at a T_{WF} = 90 °C (= 194 °F).

Sensitivity analysis. The properties of the reference case of the simplified 1-D problem in the scoping calculations are listed in Table 1. Note that, for reasons already discussed, this study does not aim to directly determine structural stability, but rather investigates the system sensitivity to conditions that can potentially undermine the structural stability of the HBS.

We tested the HBS system sensitivity to the following parameters: (a) the formation permeability k, (b) the formation porosity ϕ, (c) the pore compressibility α, (d) the initial hydrate saturation S_H, (e) the temperature of the fluids T_{WF} flowing through the tubing, and (f) the thermal conductivities of the saturated and dry porous medium ($k_{\Theta RW}$ and $k_{\Theta RD}$, respectively).

HBS reference system behavior. The HBS system behavior in the reference case (Table 1) is described by Figures 3, 4 and 5, which show the temporal evolution of the spatial distributions (along r) of P, T, and S_H and S_G, respectively, during a 30-year simulation period. The HBS system behavior when the values of hydraulic, thermal and operational parameters (identified in Figures 6 and 7) are modified is entirely analogous. An important observation from Figure 3 is that the maximum pressure in the domain P_{max} is observed in a subdomain that coincides roughly with the zone of complete dissociation (ZCD) defined by $0 < r < r_{d0}$, where r_{d0} is the radius r at which $S_H = 0$ (see Figure 4). P_{max} does not occur at a single location but is practically uniform within the ZCD, and decreases slowly with time as the advancing dissociation front makes a progressively larger volume available for gas storage (Figures 5a and 5b).

The two marked changes in the slope of the T curves in Figure 4 correspond to the outer radius of the well assembly r_w and r_{d0}, respectively. Consistent with expectations, the thermally disturbed zone is limited in extent because of the constant T_{WF} temperature, the decreasing (with time) thermal gradient at the well (as its vicinity becomes warmer), and the rapidly increasing volume (and, consequently, mass) as the radius of the affected zone expands. For the same reasons, r_{d0} remains limited even after 30 years of continuous heating (Figure 5a). Similarly, the width of the zone of active dissociation (ZAD), defined as the zone $r_{d0} < r < r_d$, increases with time (Figures 5a and 5b), but it also remains limited. Note that the outer radius r_d of the ZAD represents the edge of the dissociation front that occurs where $S_G > S_{G0}$ and $S_H < S_{H0}$ (Figures 5a and 5b).

Figures 6 and 7 quantify the system sensitivity by showing the observed maximum pressure deviation ΔP (= $P_{max} - P_0$) in the domain to variations in the hydraulic and thermal properties discussed earlier. Each one of the graphs in Figures 6 and 7 (as well as the corresponding ones in Figures 8 and 9, which will be described next) represents a variation in the single parameter indicated in the legend; all other parameters remain as in the reference case (Table 2). P_{max} is the maximum pressure occurring in the hydrate-bearing portion of the domain under investigation at a given time. The magnitude and the extent of the zone of P_{max} occurrence are important parameters determining the upper limit of the geomechanical response of a HBS under thermal stress.

Figures 8 and 9 show the volumetric rate Q_V of hydrate-originating CH_4 release corresponding to Figures 6 and 7, respectively. A direct correlation is expected between an increasing Q_V and a rise in P_{max}. The CH_4 release is induced by thermal stimulation caused by heat flow from the well fluids into the formation through the well assembly, and is responsible for the pressure rise in the domain. An important observation from Figures 6 through 9 is that the maximum levels of P_{max} and Q_V are invariably observed early (at t < 200 days) during the 30-year heating process.

Note that the Q_V fluctuations in Figures 8 and 9 (as well as in the subsequent Q_V curves of Figure 18) are an inevitable feature of the dissociation process[6]. Hydrate dissociation leads to an increase in the rate of CH_4 release, which results in a localized increase in pressure (caused by the evolving gas and the resistance to flow posed by the porous medium) and a drop in temperature (caused by the endothermic nature of the hydratie dissociation reaction). The increase in pressure and the temperature drop result in a subsequent reduction in Q_V until conduction and convection (of the advancing warm fluids) can raise the temperature and accelerate dissociation. The result of this sequence of events is the oscillatory appearance (of a roughly periodic nature) of the Q_V curve, which is also affected by grid discretization effects[6].

Sensitivity to k. Consistent with expectations, P_{max} increases with a decreasing k (Figure 6a) because of reduced pressure dissipation (caused by increasing impedance to flow). This occurs despite the decrease in the rate of CH_4 release Q_V with a decreasing k (Figure 8a), caused by the reduction in the advection of warmer fluids (a far more efficient mechanism of heat transport than conduction, with conduction becoming increasingly dominant in less permeable systems) outward from the well assembly. Note that the P_{max} for $k = 10^{-16}$ m^2 (0.1 mD) and $k = 10^{-17}$ m^2 (0.01 mD) correspond to pressure increases of about 13% and 59%, respectively, relative to the initial P_0, and may be sufficient to cause significant geomechanical changes to the formation (including permeability and

porosity changes, displacement, and fracturing). The low initial intrinsic permeabilities considered in these cases are not uncommon in muddy oceanic sediments rich in clays.

Sensitivity to ϕ. Counter to expectations (which would associate a lower ϕ with a limited volume for gas expansion, and, consequently, higher pressures), P_{max} increases with an increasing ϕ (Figure 6b). This is because more hydrate is available for dissociation and gas generation when the hydrate saturation is kept constant (at $S_H = 0.5$ in the reference case). This is evident in Figure 8b, which shows a decline in Q_V as ϕ decreases. Note that the effect of ϕ on P_{max} is much less pronounced for $\phi > 0.30$.

Sensitivity to α. P_{max} increases with a decreasing α (Figure 6c) because of reduced pressure dissipation caused by increasing resistance to deformation of the porous medium. The effect is non-linear, with P_{max} increasing by only about 12% when α decreases by an order of magnitude. Note that in this case Q_V is relatively unaffected because CH_4 is released at about the same rate for both values of α (Figure 8c).

Sensitivity to S_H. P_{max} increases with an increasing S_H (Figure 7a) because of the corresponding reduction in effective permeability, in a manner analogous to the effect of a decreasing k discussed earlier. In the rate of CH_4 release Q_v in Figure 9a, there are two processes in competition: the availability of hydrate (with higher S_H tending to lead to larger Q_v), and the reduced relative permeability of fluids (which would tend to reduce advective transport of warmer fluids outward from the well, thus leading to lower Q_V). It is evident from Figure 7a that the reduction in permeability outweighs the impact of the increased hydrate availability in the case of S_H = 0.75. The two processes are roughly in balance for $S_H = 0.25$ and $S_H = 0.50$. Despite the lower Q_V for $S_H = 0.75$, the reduced permeability results in a significant increase of P_{max} compared to that for the reference case.

Sensitivity to T_{WF}. An increasing temperature of the rising reservoir fluids in the tubing is expected to lead to higher heat fluxes into the HBS, and consequently, larger Q_V and higher P_{max}. The results in Figures 7b and 9b are consistent with these expectations, and show a nearly linear relationship between Q_V and ΔP.

Sensitivity to $k_{\Theta RW}$ and $k_{\Theta RD}$. A reduction in the values of the thermal conductivities of the saturated and dry porous medium ($k_{\Theta RW}$ and $k_{\Theta RD}$, respectively) leads to values of Q_V that are nearly equal to those for the reference case at early times, and are slightly lower at later times (Figure 9c). This is attributed to the slow nature of heat transfer through conduction, which results in relatively longer times before this process affects the system response. At early times, the effect of the lower thermal conductivities of the porous media are balanced by the resulting steeper temperature gradients, yielding approximately the same heat fluxes and resulting in very similar Q_V. The effect of lower $k_{\Theta RW}$ and $k_{\Theta RD}$ on P_{max} (Figure 7c) appears to be closely correlated with that on Q_V (Figure 9c), with lower thermal conductivities leading to practically the same P_{max} at earlier times (when the highest levels are observed), and slightly lower P_{max} after prolonged heating, relative to the reference case.

Analysis of Realistic 2D Marine Hydrate Systems

Geologic system description. Although the large-scale 2D problem and its three variations discussed in this section are synthetic, they involve realistic representations of the geology and conditions occurring in natural oceanic HBS. In all cases, the geological system of interest was composed of a layered sequence of five formations (A through E), confined at the top and bottom by impermeable (or nearly-impermeable) layers (designated as formations U and L, respectively).

Practically impermeable shale layers (such as the L formation) are often encountered underneath hydrates. The impermeable upper boundary U corresponds to either a shale or a calcite layer extending from the ocean floor to the top of the uppermost HBS. Such calcite layers are common in oceanic hydrate accumulations. At the seafloor above methane hydrate deposits or methane "cold vent" sites, advecting fluids transport methane upward, meeting downward-diffusing seawater containing sulfate. A collection of benthic microorganisms can anaerobically oxidize the methane to bicarbonate and sulfide, a process referred to in the benthic chemistry literature as anaerobic oxidation of methane[10] (AOM). This process increases alkalinity within the sediment and encourages the precipitation of carbonites[11] (authigenic calcite and aragonite). Studies at the Hydrate Ridge show "massive authigenic carbonate deposits" and widespread "carbonate pavements" overlying regions of intense fluid venting[10]. Cementation of surface sediments redirects fluid venting, leaving behind solid stable crusts. Numerical studies have shown that these processes can create a 1m thick carbonate layer over a 20,000 year period[11]. This layer can both entrain rising methane-laden fluids and also restrict diffusion of seawater sulfates downward into the biologically reactive benthic environment.

The five formations (A through E) had the same hydraulic properties and initial fluid saturation distributions in all the test cases of this study (see Table 3). All other properties and parameters remained as in Table 1 of the scoping study.

The thickness of the carbonate layer in the upper boundary was 50 m. There was a downward trend of the intrinsic permeability k with depth, declining from 10^{-15} m^2 (1 mD) in the shallower formation A to 5×10^{-18} m^2 (0.005 mD) in the deepest formation E. Similarly, the porosity ϕ decreased from 0.50 in formation A to 0.40 in formation E. These variations are consistent with the increased compaction of marine formations with depth. The relatively large ϕ values (generally higher than those observed in onshore reservoirs) are often observed in unconsolidated oceanic sediments[12]. Conversely, the initial hydrate saturation S_H generally increased with depth from 0.15 in formation A to 0.50 in formation E, and were within the reported range in similar systems. These variations in k, ϕ and S_H with depth were consistent with field observations.

The cases investigated in this 2D study are the following:

Case A: Reference case. The reference case for this problem involves the system and conditions described in Tables 1 and 3. Heat from the hot fluids in the inner tubing flows through the well assembly to the hydrate-bearing formations, causing a temperature rise and resulting in hydrate dissociation. The confining formations (top and bottom boundaries) are impermeable, but allow heat exchange with the overburden and the underburden. Consequently, the gas released from

dissociation cannot escape into the ocean, but remains trapped in the system and leads (inevitably) to higher pressures. The geothermal gradient in this case (as well as in cases C and D, see below) to the base of the hydrate (i.e., at the bottom of layer E) was dT/dz = 0.0332 °C/m. With this geothermal gradient, the base of the hydrate coincided with the bottom of the hydrate stability zone at the P = 12.4 MPa at that elevation.

Case B: Deeper deposit and different geothermal gradient. As can be seen in Table 3, case B involved a deeper mudline (at an elevation of –1500 m, as compared to –1000 m for all other cases). With pressures in the HBS following the hydrostatic gradient, this resulted in a higher-pressure system. The temperature at the mudline was kept at 5 °C. In case B, the geothermal gradient dT/dz = 0.0446 °C/m, resulting in (a) hydrate occurrence throughout the 5-layer (A to E) profile and (b) the bottom of Formation E coinciding with the bottom of the hydrate stability zone, at which P = 17.33 MPa. The steeper geothermal gradient results in higher temperatures in the upper parts of the profile, leading to expectations of higher rates of gas generation from hydrate dissociation and higher pressures. The reason for the consideration of this case was the evaluation of the relative performance of a deeper (and, consequently, warmer and more pressurized) system exposed to thermal stresses.

Case C: Absence of bottom confining shale layer. The geological system in Case C differs from the reference Case A in that there is no bottom shale layer (impermeable formation L, see Table 3) coinciding with the bottom of the hydrate stability zone. Thus, the shale layer is now replaced by a deep hydrate-free layer with the properties of Formation E and 300 m thick. Using the terminology of *Moridis and Collett*[13], this configuration describes a Class 2 hydrate deposit, with all other cases representing Class 3 hydrate accumulations. The absence of the lower confining impermeable layer is expected to result in lower pressures because the released gas can expand into a larger permeable volume (compared to the reference case, in which hydrate-originating gas can only move through the HBS away from the well towards the outer boundaries). The reason for the consideration of Case C is the assessment of the importance of such boundaries to the system response.

Case D: Pressure release. The only difference between Case D and the reference Case A is the inclusion of high-permeability region ($k = 10^{-11}$ m^2 = 10000 mD) that extended radially 0.1 m into the formation from the outermost cement "ring" of the well assembly. The high k in this region is attributed to a sand or gravel pack emplaced during drilling and well construction operations, which are also assumed to have caused dissociation of the hydrate originally located there. The high-permeability region extends to from the bottom of formation E to the mudline, at which point creates a constant pressure boundary (equal to the hydrostatic pressure at the bottom of the ocean).

This configuration is designed to provide pressure relief by allowing gas released from hydrate dissociation to escape into the ocean, and is expected to result in the evolution of lower pressures in the HBS. Such lower pressures are desired to prevent wellbore collapse, and/or to avoid the inadvertent fracturing of the hydrate or of the shale overburden and underurden. The reason for the consideration of Case D is the evaluation of a well design to mitigate the potentially adverse effects of higher pressure.

Simulation specifics

Domain discretization and boundary conditions. An infinite-acting single-well system (described by a cylindrical domain) was used in the simulations. The outer reservoir radius was placed at r_{max} = 1000 m, where an outer constant-conditions boundary was located. Based on scoping calculations, the domain included only 30 m of the bottom-confining layer (i.e., the no-flow but heat-exchanging lower shale boundary) when underburden was considered (Cases A, B and D). The 30-m thickness is sufficient to allow accurate heat exchange with the hydrate deposit during the 30-yr long production period. The thicknesses of the five hydrate-bearing formations (A to E) are described in Table 3.

The 2-D cylindrical domain was discretized in 194 x 100 = 19,400 gridblocks in (r,z). The uppermost and lowermost layers corresponded to constant temperature, no-flow boundaries, while the layers corresponding to the top and bottom confining layers (formations U and L, see Table 3) were impermeable but allowed heat exchange between the deposit and its surroundings.

To describe accurately the processes and phenomena occurring in the critically important vicinity of the wellbore, and because the extent of the ZCD and ZAC are expected to be limited (see Figures 3 to 5), we used a very fine discretization in the HBS along the r direction (especially in the r < 20 m zone). Using the equilibrium hydration reaction option in TOUGH-Fx/HYDRATE, the grid resulted in 77,600 coupled equations that were solved simultaneously.

Initial conditions. We determined the initial conditions in the reservoir by following the initialization process described by *Moridis et al.*[14]. The initial temperature distribution was computed from the known temperature at the mud line (reported as 5 °C) and the corresponding geothermal gradients. The pressures in the subsurface profile were assumed to follow a hydrostatic distribution. This is consistent with observations of natural hydrate accumulations in geologic media[15]. The initial pressures were computed using the water depths reported earlier, and a pressure-adjusted saline water density typical of ocean water (1003 kg/m^3 at atmospheric pressure).

Well description. The well design is the same as the one described earlier in the scoping study (see Table 2). In the discretized domain used in the 2-D simulation, the first 23 radial elements (out of a total of 194 at each elevation) are used to describe the well system (to $r = r_w$), thus providing the high resolution needed to capture the heat transfer within the well assembly. In all cases, the temperature of the rising hot fluids in the tubing was T_{WF} = 90 °C (= 194 °F).

Simulation process and outputs. The simulation period was 30 years, corresponding to the typical production life span of the deeper hot reservoir. Because the well assembly is radially impermeable, only heat is exchanged between the hot production fluids and the colder (initially) hydrate-bearing formations. As a result, T in the HBS increases, hydrate dissociation begins, gas and water are released, and the pressure rises. Dissociation is a self-limiting reaction because it is strongly endothermic (thus consuming a large portion of the

heat supplied by the wellbore), and because the rising pressure makes further dissociation progressively more difficult.

In the course of the simulation, the following conditions and parameters are monitored: Spatial distributions (at t = 1 year, 5 years, 10 years, 20 years and 30 years of (a) pressure, (b) temperature, (c) aqueous, gas and hydrate phase saturations, (d) water salinity (as affected by the evolving pressure and temperature), and (e) porosity; Location and magnitude of maximum pressure; Volumetric rate of CH_4 released from dissociation from the entire hydrate-bearing system (Q_V); and Cumulative volume of CH_4 released from dissociation (V_C). In Case D, the following variables are also monitored: volumetric rate of gas produced from the annular gravel pack Q_P, mass water production rate from the gravel pack Q_W, and cumulative gas volume and water mass produced from the gravel pack (V_C and M_W, respectively) during the 30-year period.

2D System Response to Heating in Case A

Despite their differences, the system response was consistent in pattern and similar in magnitude in all four cases. This allows us to discuss the spectrum of the results by using a basic set as an example of the general pattern of response, while using focused datasets (and the corresponding figures) to discuss differences in the system behavior caused by a variety of factors. In this section, we use the evolution of the spatial distributions of important variables in Case A (i.e., the reference case) as the basis of discussion of the system behavior.

Spatial distributions of *P*. The P distribution in the reference case in Figure 10 indicates that the region of maximum pressure P_{max} is observed in the lowermost hydrate-bearing formations (where the lowest k and ϕ, and the highest S_H occur). A very important observation from Figure 10 is that the pressure rise is very significant (about 9 MPa, i.e., a 70% increase of P_0 at the bottom of formation E), but the high-pressure region is confined to a small volume in the vicinity of the well and does not appear to extend significantly past r = 25 - 30 m (in a domain with an r_{max} = 1000 m) even after 30 years of continued heating. The high-pressure region is restricted to formations C through E (with pressure increasing with depth), and does not appear to extend to the upper formations A and B. This is because of the relatively high permeabilities and low initial hydrate saturations in formations A and B. It is evident that the bulk of significant geomechanical changes will occur in the high-pressure region. Despite their limited extent, it is reasonable to expect that the significant pressure changes we observe can have adverse effects in weak marine sediments. Because no information is currently available on the geomechanical behavior of HBS, it is not possible to predict whether these pressure changes are sufficient to effect fracturing of the HBS or of the continuing shale layers.

Spatial distributions of *T*. The T distribution in Figure 11 indicates that the temperature rise caused by the heating from the wellbore affects a narrow cylindrical zone, as is depicted by the very faint color variation over time within the r = 25 m zone of observation. In order to highlight the temperature distribution beyond r = 2 m, the color scale is saturated at 30°C. Note that, unlike the scoping studies (Figures 3 and 4), neither the P distributions in Figure 10 nor the T distributions in Figure 11 can provide a satisfactory approximation of the location of the hydrate dissociation front (see Figure 12). If the relationship of a rising T on the mechanical strength of HBS is known, comparison of the T distributions in Figure 11 and the S_H distributions in Figure 12 can provide an estimate of the extent of the region that is structurally compromised (and subject to deformation and subsidence) by weakened HBS.

Spatial distributions of S_H. The most important observation from the review of the hydrate saturation distribution in the reference case in Figure 12 is the limited extent of the hydrate dissociation zone, which decreases with depth and is barely larger than r_{d0} = 15 m at its maximum after 30 years of heating. The r_{d0} ranges from 15 m in the uppermost formation A, to 10 m in the lowermost formation E, and is very small compared to the R_{max} = 1000 m of the simulated domain. The outer radius r_d of the ZAD is also very small, decreasing with depth from about 32 m in formation A to 14 m in formation E.

The limited r_{d0} and r_d were consistent with expectations because the cylindrical configuration of the system results in rapidly increasing volumes (as the radius increases) supplied with heat by a constant-temperature boundary (the inner tubing). Thus, a progressively decreasing fraction of the released heat reaches the dissociation front, the rest being consumed to maintain the temperature of the increasing volume of the hydrate-free (after dissociation) cylindrical zone around the well. Additionally, the heat flux from the constant-temperature boundary continuously decreases because of the increasing formation temperature that leads to smaller temperature differentials, thus weakening the driving force of heat transfer.

Note the creation of a thin zone of "new" hydrate in the uppermost region of layer A, where the released gas accumulates (because of buoyancy) and where T is relatively low. Consistent with the scoping studies (Figure 5a), formation of new hydrates is also observed ahead of the dissociation fronts in the various layers (as indicated by the slightly darker color at these locations, e.g., layers B and C).

The *staircase* appearance of S_H distributions in Figure 12 is attributed to the layered pattern (Table 3) of decreasing k and increasing S_H with depth (ϕ has been shown to be insensitive in this range, see Figure 6b). While the larger S_H results in a lower composite heat capacity of the HBS (and, thus, in a faster response to heating), the effect is outweighed by the reduction in the relative permeability of fluids. Consequently, the advection of warm fluids (an effective mechanism of heat transfer) moving radially outward from the well is increasingly restricted with depth, while the contribution of the far more inefficient conduction increases. This results in heat transport, hydrate dissociation and ZAD that increase with the effective permeability of the system, hence the staircase S_H pattern.

An additional reason for r_{d0} and r_d decreasing with depth is the larger pressure that results from the gas release in the lower formations (Figure 10), which acts as an impediment to dissociation. Conversely, the higher permeability and lower hydrate saturations in the upper formations allow gas flow toward the outer radius of the reservoir, prevent pressure build-up, and result easier dissociation.

While the ZCD and ZAD may be limited, significant concerns regarding the geomechanical behavior of this system need to be alleviated if wells are to be installed under such conditions. The question that begs to be answered is whether

the ZCD (at the center of which lies the well) can provide stability by supporting the considerable weight of the wellbore assembly if a weak unconsolidated porous medium is involving, leaving "soupy sediments" (Figure 2) after the dissociation of the hydrate. The issue becomes more critical if the production system design involves close spacing of multiple wells. Lack of fundamental knowledge precludes any reliable predictions at this time.

Spatial distributions of S_G and S_A. The S_G and S_A phase saturation distributions in the reference case (Figures 13 and 14, respectively) roughly mirror the hydrate saturation distribution in Figure 12. Note that the occurrence of high S_G in the ZCD near the wellbore can have a negative impact on the structural stability of that region because of the very high compressibility of gases.

Of interest is the drainage of water (originating from the dissociating hydrate) observed in Figure 14, which is particularly evident in the upper formations. The drainage of water is also reflected in the S_G distribution in layer A of Figure 13, where it is depicted as a reduction in the gas saturation.

A feature common to all phases (Figures 12 to 14) is the wedge-like appearance of the saturations at the bottom of each formation, where the dissociation front intrudes deeper into the hydrate layer. This is caused by the preferential upward flow patterns of hydrate-originated fluids released from the underlying less permeable formations..

Spatial distribution of porosity changes $\Delta\phi = \phi - \phi_0$. As expected, the porosity deviations (from their initial levels) in the reference case in Figure 15 follow closely the pressure distributions in Figure 12, and are limited in areal extent. An increasing pressure leads to an increasing porosity, and the change appears to be substantial in this study. Note that these results were not obtained using a geomechanical model, but were predicted by the TOUGH-Fx/HYDRATE[6] simulator that accounts for the P and T effects on ϕ only (and not on permeability) using reasonable (but assumed and unverified) pore compressibility and expansivity estimates. As such, these results should be considered as indicative only. Note that if the pore changes shown in Figure 15 are correct, significant sediment displacement (although localized) is possible, the effects of which on the system structural stability is unknown because of lack of data.

Spatial distribution of salinity. The salinity distribution may have a significant effect on the shale boundaries because these would tend to swell and lose their structural integrity when exposed to fresh water released from hydrate dissociation. As expected, Figure 16 shows pervasive low-salinity water regions that roughly coincide with the ZCD, closely following the staircase patterns and extent of the phase saturation distributions (Figures 12 to 14). The low salinity is caused by the mixing of the native saline water with the fresh water released from hydrates during dissociation. The region of minimum salinity is shown to coincide with the deepest HBS in layer E, and is consistent with expectations as the location of accumulation of the fresh water draining from higher elevations.

Additionally, the locations of formation of new hydrate are clearly depicted in Figure 16 as regions of elevated salinity and help to identify the upper boundaries of the ZAD. These are observed in the uppermost reaches of layer A, and as wedges at the bottom of each of the formations following the advancing gas front along the bottom boundary of the system. An area of elevated salinity is also observed, coinciding with the location of hydrate formation. There is currently no quantitative information on the mechanical properties of swelling marine shales to evaluate whether the predicted salinity distribution will be a cause for concern during similar production operations.

Sensitivity Analysis of the 2D System

Evolution of maximum pressure. The maximum pressure attained within the hydrate-bearing layers of the simulated system, as well as the corresponding location, are of critical importance because they determine the potential for fracturing the HBS and/or the confining impermeable layers, in addition to providing a measure of the damage hazard to the wellbore assembly. Based on anecdotal evidence, because of the unconsolidated, unlithified nature of such waterlogged media and their very high porosity (see Figure 2), the fracture pressure of the formations can be quite low and not significantly larger than the initial pressure.

Figure 17 shows the evolution of maximum pressure in Cases A through D. Review of the maximum pressure evolution in Case A indicates that the maximum pressure increase $\Delta P = P_{max} - P_0$ increases rapidly during the early stages of thermal loading (starting at $t < 1$ day), rises to $\Delta P = 8.0$ MPa in about 30 days, and reaches a maximum level of 8.8 MPa (i.e., about 70% higher than the initial pressure) after about 280 days, after which time it begins to decline very slowly (dropping to $\Delta P = 7.6$ MPa at t = 30 years). This indicates that, after a short initial period (during which heat from the wellbore reaches a rapidly expanding zone and the released gas causes the pressure to rise fast), the maximum pressure remains practically stable as the hydrate dissociation front (i.e., the locus of P_{max}) advances. This is attributed to (a) the slowing rate of advance of the dissociation front (because the cylindrical volume of the thermally affected zone increases fast as a function of the square of the radius), and (b) an approximate balance between the rate of heat addition (originating from the hot fluids flowing in the inner tubing) through the wellbore assembly and the rate of heat consumption needed to sustain the strongly endothermic hydrate dissociation reaction.

The evolution of ΔP in Cases B and C is remarkably similar in pattern to that in Case A. The onset of the rapid P_{max} rise practically coincides in the isolated domains of Cases A, B and C. However, counter to expectations, Figure 17 indicates that the absence of a lower impermeable boundary (Case C) does not have a significant moderating effect on ΔP, the maximum level of which is lowered only slightly to $\Delta P = 8.1$ MPa (observed at about $t = 100$ days). Additionally, the ΔP in Cases A and C coincide until about t = 10 days (when over 90% of the maximum ΔP has already been attained), after which time the absence of the lower confining boundary is reflected by the lower ΔP.

The evolution of ΔP in the case of the deeper system of Case B was also unexpected. The anticipation was that the higher temperature of the deeper formation would lead to a

larger max{ΔP}, given the decrease in the heat of dissociation at n elevated T. However, ΔP in Case B is consistently lower than in Case A, and reaches a max{ΔP}= 7.7MPa at about t = 300 days (corresponding to about a 45% increase over P_0). Given the fact that P_0 is significantly higher in Case B (= 17.33 MPa at the base of formation E, as opposed to 12.40 MPa at the same location in Case A), it appears that the impact of thermal loading is relatively less pronounced in deeper formations. This is attributed to increased gas solubility at the higher pressures of the deeper formation of Case B, which outweighs the relatively mild (and opposite) effect of elevated T on CH_4 solubility.

ΔP increase in Case D (in which pressure relief is provided through gas venting) is consistently and significantly lower than in all other case. This was expected because of the high-permeability zone in the annular gravel pack and the constant-pressure boundary, through which gas evolving from the hydrate dissociation can escape into the ocean (thus preventing a pressure build-up). The max{ΔP}= 6.0MPa (corresponding to about a 48% increase over P_0) is reached much later than in all other cases at about t = 1500 days. While the P_{max} observed in Case D is substantially lower than in all other cases, it is unknown (given the lack of information on the mechanical behavior of HBS) if it is at a level that can be considered safe for the prevention of formation fracturing at that location.

Review of the locations of P_{max} during the simulation period indicates that these are always confined in the lowermost regions of the system (the bottom gridblock layers corresponding to the hydrate-bearing formation E). This was expected because at these locations (a) the initial temperature is higher because of the deeper formation (thus allowing easier dissociation after heating by the wellbore), (b) the permeability is lower, while (c) the hydrate saturation is higher, as is the composite thermal conductivity (the main heat transfer mechanism from the wellbore). Consequently, the large amounts of available hydrates can dissociate easily and fast, while the hydrate-originating gas is released into a smaller "free" pore volume and cannot flow easily away from the dissociation front. Note that P_{max} occurs within the bottom 10 m in cases A and B, while its range of occurrence extends to the bottom 23 m in Case C, and narrows considerably to the bottom 5 m in Case D.

Evolution of volumetric rates of gas release. Figure 18 shows the evolution of the volumetric rate Q_V of gas released from hydrates in the entire simulated domain in Cases A to D. The Q_V increases rapidly in all cases during the early phase of dissociation (to t = 10 days). Because of the higher T and the corresponding lower heat of dissociation, Q_V is higher in case B than in the reference case. The absence of a confining structure next to the site of early dissociation in Case C leads initially to a lower (than in case A) Q_V. A lower initial Q_V is also observed in Case D, caused by the assumption of a hydrate-free annular gravel pack at the location of early dissociation.

The evolution of Q_V in Case B is of particular interest. Figure 18 indicates a distinct tendency for a large gas release, which becomes apparent at about t = 40 days, culminates in a very rapid gas release starting at about 500 days, is followed by a period of hydrate reformation and re-dissociation in the 1200< t <3000 period, and concludes with a gradual and consistent Q_V decrease for t > 3000 days. Repeating the simulation with different grids (first half as coarse, and then twice as fine as the one used in these simulations) produced the same results, indicating that this process is not a numerical artifact related to grid discretization. Our current hypothesis is that the deeper (and warmer) formation is more sensitive to external thermal stresses than shallower colder ones, leading to violent phase transitions and reversals in response to small changes in P and T. This sensitivity appears to occur very close to hydration equilibrium and to be related almost exclusively to phase composition. The fact that the corresponding ΔP in Cases B (see Figure 17) appears relatively smooth without any of the violent swings that Q_V exhibits lends credence to this hypothesis.

A comparison between the ΔP and Q_V in Cases A and B (Figures 17 and 18, respectively) indicates that although Q_V in Case B is larger than in Case A, ΔP is lower. This observation provides further support to the thesis that increase gas dissolution is the reason for the lower P_{max}.

The absence of a confining structure in Case C allows the flow of warm fluids into the hydrate-free formation underneath layer E, thus depriving the HBS of their dissociation-fueling heat. This leads to a reduced overall dissociation and a lower Q_V.

Finally, the Q_V in case D is consistently higher than in the reference case because the continuous pressure relief lowers the pressure in the HBS and enhances dissociation. It is obvious that loss of warm fluids into the ocean through the highly permeable gravel pack is not sufficient to counter the effect of venting. The reason for the lower P_{max} in Case C (see Figure 17) despite the larger Q_V is demonstrated in Figures 19 and 20, which show the (a) volumetric rate Q_P of gas production (venting) and (b) the mass flow rate of water production into the ocean through the gravel pack, respectively. Figures 19 and 20 show that in addition to considerable amounts of water, about 20-30% of the gas released from hydrate dissociation escapes into the ocean, thus alleviating pressure build-up.

No gas is vented in the first 12 days (Figure 19). During this early period, dissociation begins, the pressure in the system gradually increases, and the hydrate-originating gas establishes a mobile gas phase and slowly rises through the gravel pack toward the ocean floor. During the same period, water is expelled at increasingly higher rates Q_W (Figure 20), which reach a maximum when a continuous gas phase is established in the gravel pack from the bottom of the system to the ocean floor and the first gas is vented into the ocean (Figure 19). The sudden pressure release leads to a significant pressure lowering, which allows water to rush back into the gravel pack and reduce Q_P. Continuous gas release from dissociation rebuilds the pressure, a second release follows, and the process is repeated (leading to the oscillations in Figures 19 and 20) until the gas phase is continuous and fully established. When the two-phase flow regime is stable in the gravel pack, the water flow rate Q_W (Figure 20) drops to a significantly lower level and exhibits a very slow decline during the 30-year simulation period. Conversely, Q_P shows no similar

drop upon the establishment of a steady flow regime, but is characterized instead by a continuous decline.

Evolution of cumulative volumes rates of released gas. The cumulative volumes V_C of CH_4 released from hydrate dissociation (corresponding to the Q_V in Figure 18) appear in Figure 21. The log-log scale of Figure 21 makes the V_C appear similar in all cases, although slight differences are evident: with the exception of very early times (t < 10 days), the relative size of the V_C is as follows: Case D > Case B > Case A > Case C. This holds true until about t = 1000 days, when the sudden gas release in the deeper and warmer system of Case B (Figure 18) leads to a quantum (step) increase in the corresponding V_C.

The cumulative volumes of gas V_P and the cumulative mass of water M_W that escape into the ocean are shown in Figures 19 and 20, respectively. Comparison of V_P to the V_C in Figure 21 shows that, at the end of the 30-year production period, 10^6 m^3 of CH_4 will have been vented into the ocean. This very significant volume represents about 30% of the total gas released from hydrate dissociation, and is sufficiently large to require appropriate actions for the collection or disposal of the released gas.

Conclusions

(1) During heating of an HBS by warm reservoir fluids rising through a well, the highest pressure P_{max} that develops in the domain is practically uniform in the zone between the well radius r_w and the radius r_{d0} of the zone of complete dissociation (ZCD). The thermally disturbed zone is limited even after prolonged heating, as is the dissociation radius. The extent of the zone of active dissociation (ZAD, $r_{d0} < r < r_d$) increases with time, but this also remains limited.

(2) During heating of an HBS by warm reservoir fluids rising through a well, P_{max} increases with (a) a decreasing k and α, and (b) with an increasing S_H, T_{WF}, and ϕ (below a certain level). The sensitivity of P_{max} to $k_{\Theta RW}$ and $k_{\Theta RD}$ is limited, and becomes significant only at later times.

(3) In addition to studying a reference case involving a large realistic hydrate-bearing system in the oceanic subsurface, three variations of the problem considered (a) the influence of depth and of the geothermal gradient, (b) the effect of boundaries, and (c) well designs and configurations for pressure release. In all four cases, the response to thermal loading (caused by warm reservoir fluids rising to the surface through unisulated pipes that cross the HBS) is similar in pattern, though not in magnitude.

(4) In all cases, the maximum pressure P_{max} occurs consistently at the deepest hydrate-bearing layers. In enclosed systems with no pressure release (Cases A, B and C), P_{max} increases rapidly during the early stages of thermal loading (starting at t = 1 day), rises to a maximum within 100-300 days, and then decreases consistently (but very slowly) over the remainder of the 30-year simulation period. In case D (involving pressure release to the ocean through an annular gravel pack), the maximum P_{max} was much lower, and occurred much later (i.e., at t = 1000 days).

(5) The maximum pressure changes $\Delta P = P_{max} - P_0$ represented increases between 45% and over 70% over the initial P_0. Without any information on the geomechanical properties and behavior of HBS, it is unknown if such pressures are above the safety threshold for formation fracturing and wellbore collapse.

(6) Compared to the reference Case A, ΔP in Case B is lower (despite higher rates Q_V of gas release from hydrate dissociation) because of increased solubility at the higher pressures of the deeper system.

(7) ΔP in Case C is slightly lower than in the reference Case A (and higher than in Case B), because of lower rates Q_V of gas release from hydrate dissociation (as warm fluids into the hydrate-free formation underneath the HBS, thus depriving the hydrates of their dissociation-fueling heat). Thus, the absence of a lower impermeable boundary does not appear to have a significant moderating effect on ΔP.

(8) The lowest ΔP is observed in Case D. This is caused by the continuous escape of gas and water into the ocean through the annular gravel pack, which is sufficient large to negate the effects of the larger Q_V in this case. Thus, about 30% of the gas released from dissociation is vented into the ocean. The magnitude of the vented volume (10^6 m^3 over 30 years) is sufficiently large to require collection and commercial exploitation (if feasible) or safe disposal to avoid environmental degradation.

(9) In the large 2D systems, the high-pressure region (developed in response to gas release from hydrate dissociation) increases with depth, is confined to a small volume in the vicinity of the well (not extending significantly past r = 30 m after 30 years of continuing heating), and is restricted to the lowermost formation.

(10) The temperature rise (caused by heating from the wellbore) is limited to a very narrow cylindrical zone, which is not a good indicator of the ZCD or ZAC of the HBS.

(11) The extent of the hydrate dissociation zone is limited, and does not extend past r = 10 - 15 m at its widest point after 30 years of continuous heating. The radii of the ZCD and ZAD increase with an increasing k and a decreasing S_H. It is not known if the formation is weakened to the point of being unable to support the considerable weight of the wellbore assembly after the loss of the cementing hydrate through dissociation.

(12) The S_G and S_A distributions of mirror the S_G distributions over time. The occurrence of a high S_G in the ZCD can adversely affect the wellbore stability after the hydrate dissociation if soft, compressible and unconsolidated porous media are involved.

(13) The salinity distribution may have a significant effect on the shale boundaries because these would tend to swell and lose their structural integrity when exposed to fresh water released from hydrate dissociation.

Nomenclature

Δr = Radial increment (m)
Δt = Timestep size (s)
Δz = Vertical discretization, i.e., in the z-direction (m)

C = specific heat (J/kg/K)
k = intrinsic permeability (m^2)
k_Θ = thermal conductivity (W/m/K)
$k_{\Theta RD}$ = thermal conductivity of dry porous medium (W/m/K)
$k_{\Theta RW}$ = thermal conductivity of fully saturated porous medium (W/m/K)
M_W = cumulative mass of water released into the ocean through the annular gravel pack (kg)
N_H = hydration number
P = pressure (Pa)
P_0 = initial pressure in hydrate-bearing sediments (Pa)
P_{max} = maximum pressure in the domain at any given time (Pa)
ΔP = P_{max} - P_0 (Pa)
Q_P = volumetric rate of gas release into the ocean through the annular gravel pack (ST m^3/s)
Q_W = mass rate of water release into the ocean through the annular gravel pack (kg/s)
Q_V = rate of CH_4 release from hydrate dissociation (ST m^3/s)
r,z = coordinates (m)
r_w = radius of the well assembly (m)
r_{d0} = radius of the zone of complete dissociation (m)
r_d = outer radius of the zone of complete dissociation (m)
r_{max} = maximum radius of the simulation domain (m)
S = phase saturation
t = time (s)
T = temperature (K or ^{0}C)
V_C = cumulative volume of CH_4 released from hydrate dissociation (ST m^3)
V_P = cumulative volume of CH_4 released into the ocean through the annular gravel pack (ST m^3)

Greek Symbols

α = pore compressibility (Pa^{-1})
β = pore expansivity (Pa^{-1})
λ = van Genuchten exponent – Table 1
ϕ = porosity

Subscripts and Superscripts

0 = denotes initial state
β = denotes phase
A = aqueous phase
e = equilibrium conditions
cap = capillary
G = gas phase
$G0$ = initial gas phase
H = solid hydrate phase
$H0$ = initial solid hydrate phase
irG = irreducible gas
irW = irreducible aqueous phase
n = permeability reduction exponent – Table 1
R = rock
WF = well fluids

Acknowledgment

This work was supported by the Assistant Secretary for Fossil Energy, Office of Natural Gas and Petroleum Technology, through the National Energy Technology Laboratory, under the U.S. Department of Energy, Contract No. DE-AC03-76SF00098. The authors are indebted to Stefan Finsterle, John Apps and Dan Hawkes for their thorough review and their insightful comments. Charlie Paull of the Monterey Bay Aquarium Research Institute, who contributed the photograph in Figure 2, is also gratefully acknowledged. Thanks are extended to Matt Reagan for his help in describing the process of calcite formation above hydrate deposits at the ocean floor.

References

1. Sloan, E.D.: *Clathrate Hydrates of Natural Gases*, Marcel Dekker, Inc., New York, NY (1998).
2. Durham, W.B., Kirby, S.H., Stern, L.A. and Zhang, W.: "The Strength and Rheology of Methane Clathrate Hydrate", *J. Geophys. Research*, **108**(B4), 2182, doi:10.10292002JB001872 (2003).
3. Schmuck, E.A., and Paull, C.K.: "Evidence for Gas Accumulation Associated With Diapirism and Gas Hydrates at the Head of the Cape Fear Slide", *Geo-Marine Letters*, **13**,145 (1993).
4. McIver, R.D: Hydrates of natural gas–an important agent in geologic processes, in: *Abstracts with Programs*, 1089, Geological Society of America (1977).
5. Paull, C.K., Buelow, W.J., Ussler W., and Borowski, W.S.: "Increased Continental Margin Slumping Frequency During Sea-Level Low Stands Above Gas Hydrate-Bearing Sediments, *Geology*, **24**, 143 (1996).
6. Moridis, G.J., Kowalsky, M.B., and K. Pruess: "TOUGH-Fx/HYDRATE v1.0 User's Manual: A Code for the Simulation of System Behavior in Hydrate-Bearing Geologic Media", Report LBNL-58950, Lawrence Berkeley National Laboratory, Berkeley, CA (2005).
7. Kim, H.C., Bishnoi, P.R., Heidemann, R.A., and Rizvi, S.S.H.: "Kinetics of Methane Hydrate Decomposition", *Chem. Eng. Sci.*, **42**(7), 1645 (1987).
8. Clarke, M.A., and Bishnoi, P.R.: "Determination of the Intrinsic Rate of Methane Gas Hydrate Decomposition", *Chem. Eng. Sci.*, **55**, 4869 (2000).
9. Kowalsky, M.B., and Moridis, G.J.: "Comparison of Kinetic and Equilibrium Reaction Models in Simulating the Behavior of Gas Hydrates in Porous Media", in press, *J. Energy Cons. Management* (LBNL-60361, 2006)
10. Luff, R., Greinert, J., Wallmann, K., Klaucke, I., and Suess, E.: "Simulation of Long-Term Feedbacks From Authigenic Carbonate Crust Formation at Cold Vent Sites", *Chem. Geology*, **216**, 157, (2005).
11. Luff, R. and Wallman, K.: "Fluid Flow, Methane Fluxes, Carbonate Precipitation, and Biogeochemical Turnover in Gas Hydrate-Bearing Sediments at Hydrate Ridge, Cascadia Margin: Numerical Modeling And Mass Balances", *Geochimica et Cosmochimica Acta*, **67**(18), 3403 (2003).
12. Aoki, Y., Shimizu, S., Yamane, T., Tanaka, T., Nakayama, K., Hayashi, T., and Okuda, Y: "Methane Hydrate Accumulation Along the Western Nankai Trough", in *Gas Hydrates: Challenges for the Future*. Holder, G.D., and Bishnoi, P.R., Eds., Annals of the New York Academy of Sciences, **912**, 136 (2000).
13. Moridis, G.J., and Collett, T.S.: "Strategies for Gas Production From Hydrate Accumulations Under Various Geologic Conditions", Report LBNL-52568, Lawrence Berkeley Laboratory, Berkeley, CA (2003).

14. Moridis, G.J., Kowalsky, M.B., and Pruess, K.: "Depressurization-Induced Gas Production From Class 1 Hydrate Deposits", SPE 97266, 2005 SPE Annual Technical Conference and Exhibition, Dallas, Texas, U.S.A., 9 – 12 October 2005b.
15. Wright, J.F., Dallimore, S.R., and Nixon, F.M.: "Influences of Grain Size and Salinity on Pressure-Temperature Thresholds for Methane Hydrate Stability in JAPEX/JNOC/GSC Mallik 2L-38 Gas Hydrate Research-Well Sediments", in *Scientific Results from JAPEX/JNOC/GSC Mallik 2L-38 Gas hydrate research-well, Mackenzie Delta, Northwest Territories, Canada*. Dallimore, S.R., Uchida, T., and Collett, T.S., Eds., Geological Survey of Canada Bulletin 544, 229 (1999).
16. Moridis, G.J., Seol, Y., and T. Kneafsey: "Studies of Reaction Kinetics of Methane Hydrate Dissociation in Porous Media", Report LBNL-57298, Lawrence Berkeley National Laboratory, Berkeley, CA (2005).
17. van Genuchten, M.Th.: "A Closed-Form Equation for Predicting the Hydraulic Conductivity of Unsaturated Soils", *Soil Sci. Soc.*, **44**, 892 (1980).

Table 1 – Properties in the Reference Case of the Scoping Study

Parameter	Value
HBS layer thickness Δz	1 m
Initial pressure P	1.195×10^7 Pa
Initial temperature T	12.9 °C
Initial saturations	$S_H = S_A = 0.5$
Water salinity (mass fraction)	0.03
Hydrate-forming gas composition	100% CH_4
Permeability k_r	10^{-15} m^2 (= 1 m D)
Porosity ϕ	0.30
Pore compressibility α	10^{-8} Pa^{-1}
Pore expansivity β	0 K^{-1}
Temperature of fluids at well T_{WF}	90 °C
Grain desnity ρ_R	2750 kg/m^3
Dry thermal conductivity $k_{\Theta RD}$	1.0 W/m/K
Wet thermal conductivity $k_{\Theta RW}$	3.3 W/m/K
Composite thermal conductivity model[16]	$k_{\Theta C} = k_{\Theta RD} + (S_A^{1/2} + S_H^{1/2})(k_{\Theta RW} - k_{\Theta RD}) + \phi S_I k_{\Theta I}$
Capillary pressure model[6,17]	$P_{cap} = -P_0\left[\left(S^*\right)^{-1/\lambda} - 1\right]^{-\lambda}$ $S^* = \frac{(S_A - S_{irA})}{(S_{mxA} - S_{irA})}$
S_{mxA}	1
λ	0.45
P_0	2000
Relative permeability model[6]	$k_{rA} = (S_A^*)^n$ $k_{rG} = (S_G^*)^n$ $S_A^* = (S_A - S_{irA})/(1 - S_{irA})$ $S_G^* = (S_G - S_{irG})/(1 - S_{irA})$ OPM model[6]
Relative permeability exponent[6] n	4
S_{irG}	0.02
S_{irA}	0.20

Table 2 – Well design, description and properties

Component	OD radius (in)	ID radius (in)	Density (kg/m^3)	k_θ (W/m/K)	C (J/kg/K)
Conductor	18	17	7850	45.35	461
Cement 1	17	10	1561	0.66	2100
Casing 1	10	9.365	7850	45.35	461
Cement 2	9.365	8	1561	0.66	2100
Casing 2	8	7.505	7850	45.35	461
Brine 1	7.505	6.6875	1250	0.55	4800
Casing 3	6.6875	6.2075	7850	45.35	461
Brine 2	6.2075	5.375	1250	0.55	4800
Casing 4	5.375	4.88	7850	45.35	461
Brine 3	4.88	2.75	1250	0.55	4800
Tubing	2.75	2.389	7850	45.35	461
Hot fluids	2.389	–	–	–	–

Table 3 – System description (Cases A, B, C, D)

Formation	Depth (Mbml)	ϕ	k (mD)	S_H	S_A
U	0–50	0	0	0	0
A	50–90	0.5	10^{-15}	0.20	0.80
B	90–130	0.475	10^{-16}	0.30	0.70
C	130–170	0.45	5×10^{-17}	0.40	0.60
D	170–210	0.425	10^{-17}	0.45	0.55
E	210–250	0.40	5×10^{-18}	0.50	0.50
L	250–280 (A,B,D) 250–550 (C)	0 (A,B,D) 0.40 (C)	0 (A,B,D) 5×10^{-18}(C)	0	0

Mbml: meters below mudline
Mudline elevation: -1000 m in Cases A,C,D; -1500 m in Case B

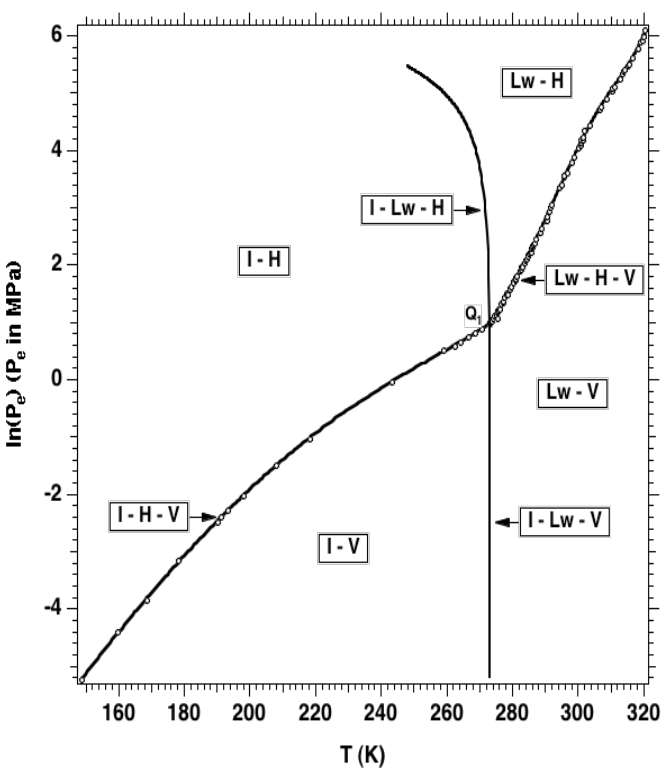

Figure 1 - Pressure-temperature equilibrium relationship in the phase diagram of the water--CH_4--hydrate system (Moridis et al.[6]).

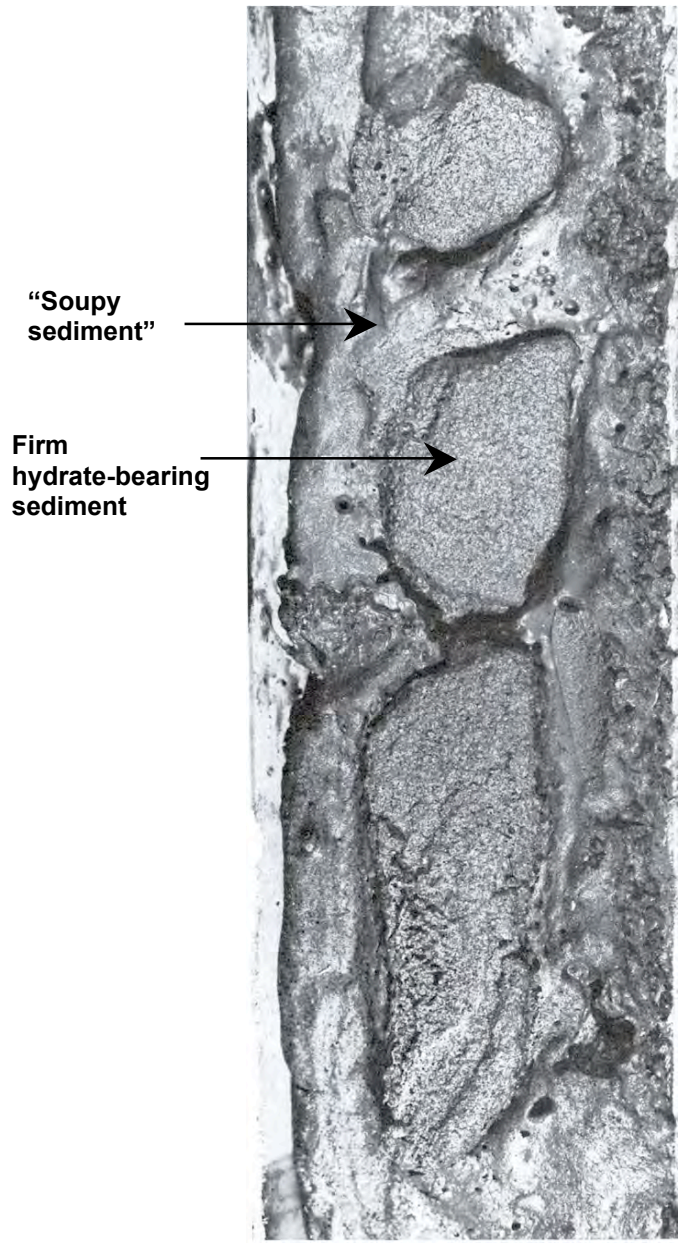

Figure 2 – Dissociating sample of a marine HBS core. Note the firm appearance of the hydrate-bearing inner core, as opposed to the "soupy sediment" (soft mud of fluid consistency with evidence of bubbling gas) in the dissociating outer annulus (source: Deep Sea Drilling Program, Leg 67, courtesy of C.K Paull of the Monterey Bay Aquarium Research Institute).

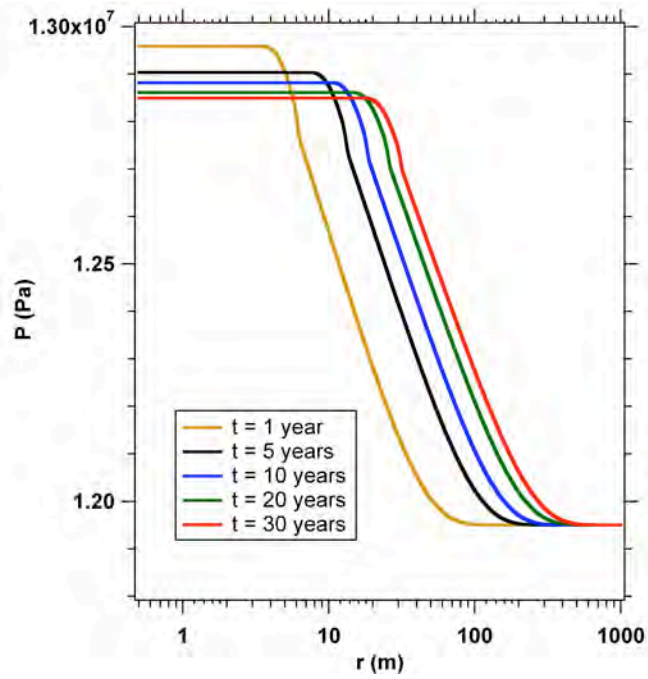

Figure 3 – Spatial distribution of pressure P in the reference case of the 1D scoping studies.

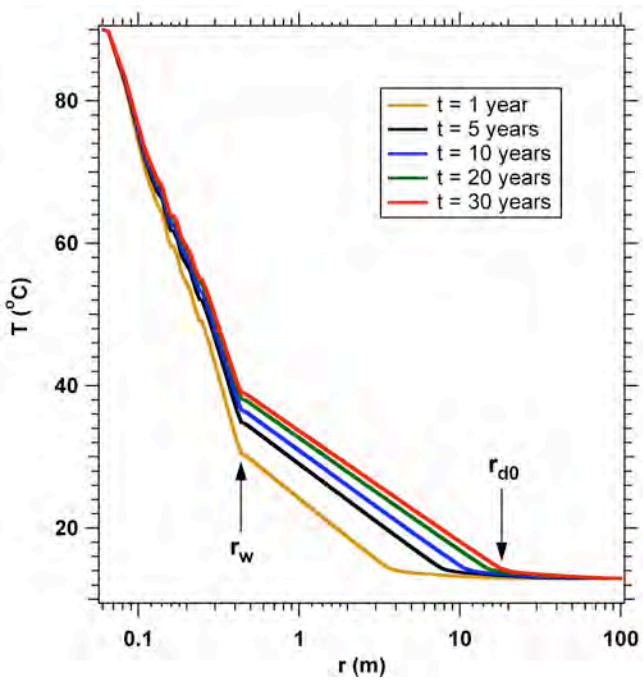

Figure 4 – Spatial distributions of temperature T in the reference case of the 1D scoping studies. Note that (a) the radius of the wellbore assembly (r_w - static) and (b) the radius of the zone of complete dissociation (r_{d0} – evolving with time) are identified by the abrupt change in slope of the T distribution.

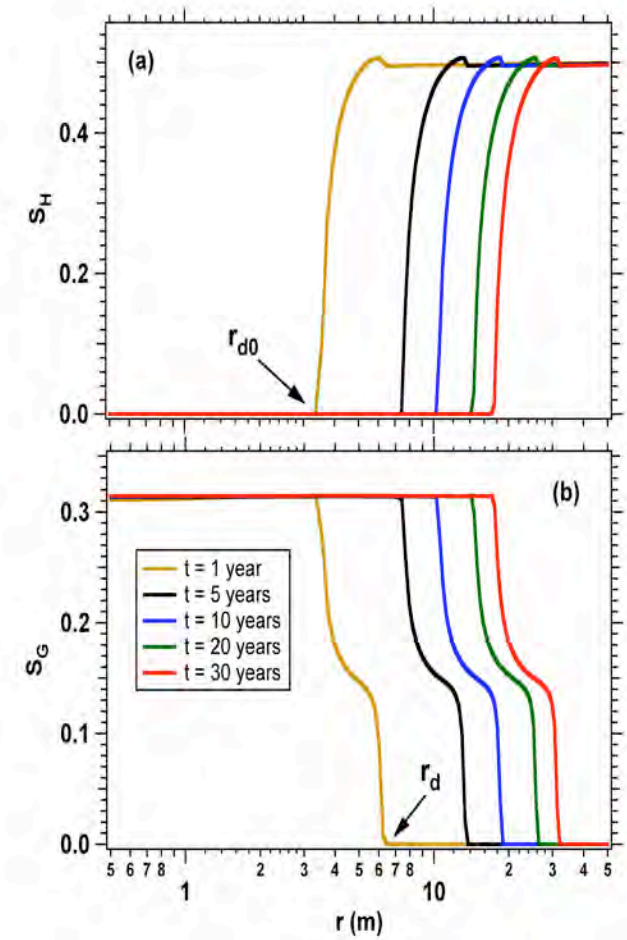

Figure 5 – Spatial distributions of (a) S_H, and (b) S_G in the reference case of the 1D scoping studies. The radius of the zone of complete dissociation (r_{d0}) and the radius of the active zone of dissociation (r_d) are identified (they evolve with time).

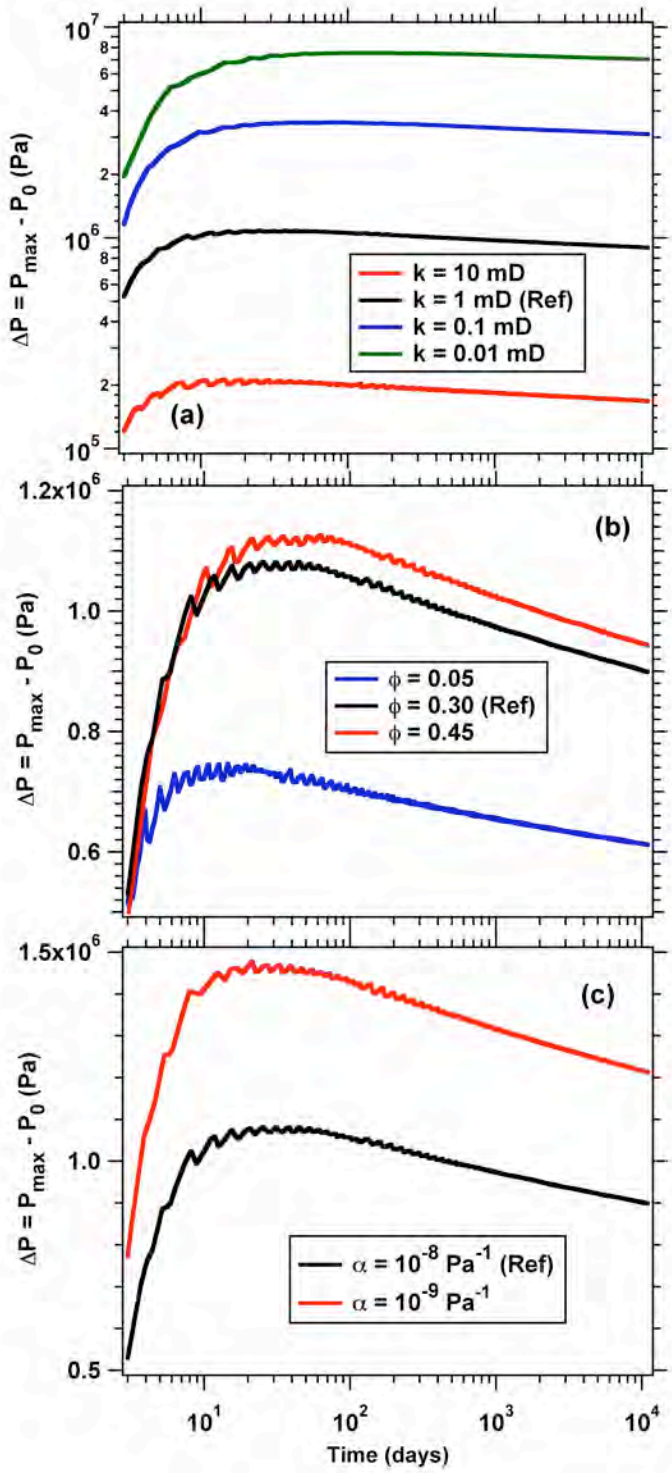

Figure 6 – Scoping studies: sensitivity of P_{max} (described as $\Delta P = P_{max} - P_0$) to variations in (a) intrinsic permeability k, (b) porosity ϕ, and (c) pore compressibility α.

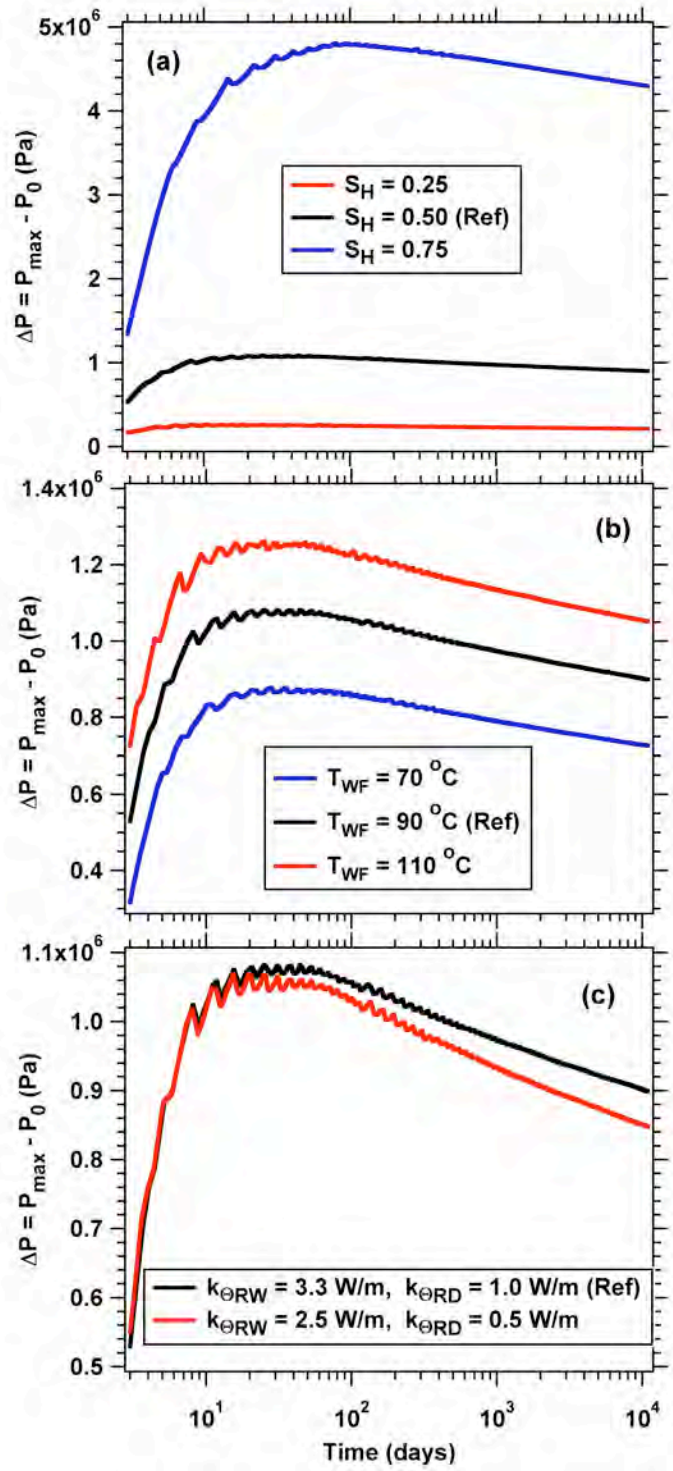

Figure 7 – Scoping studies: sensitivity of P_{max} (described as $\Delta P = P_{max} - P_0$) to variations in (a) the hydrate saturation S_H, (b) the temperature of well fluids T_{WF}, and (c) the medium thermal conductivities.

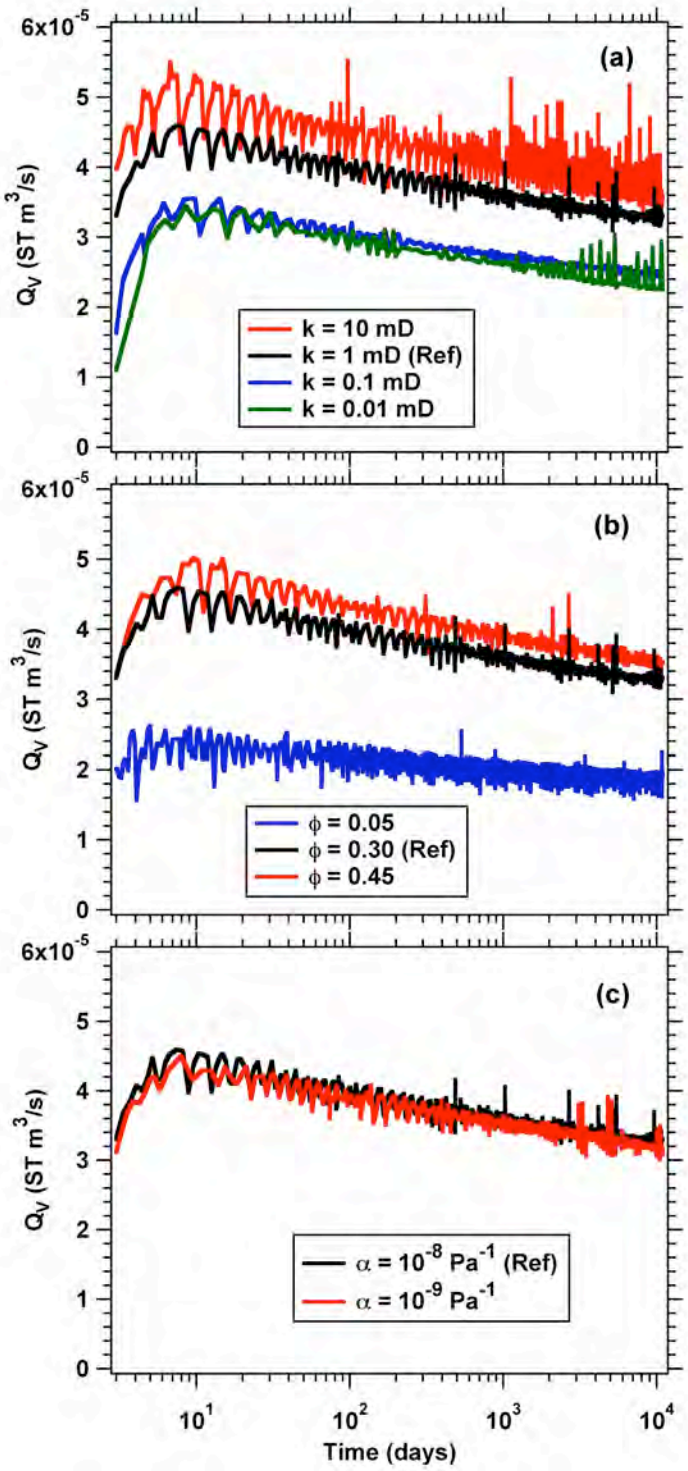

Figure 8 – Scoping studies: sensitivity of the rate of gas release from hydrate dissociation Q_V to variations in (a) intrinsic permeability k, (b) porosity ϕ, and (c) pore compressibility α.

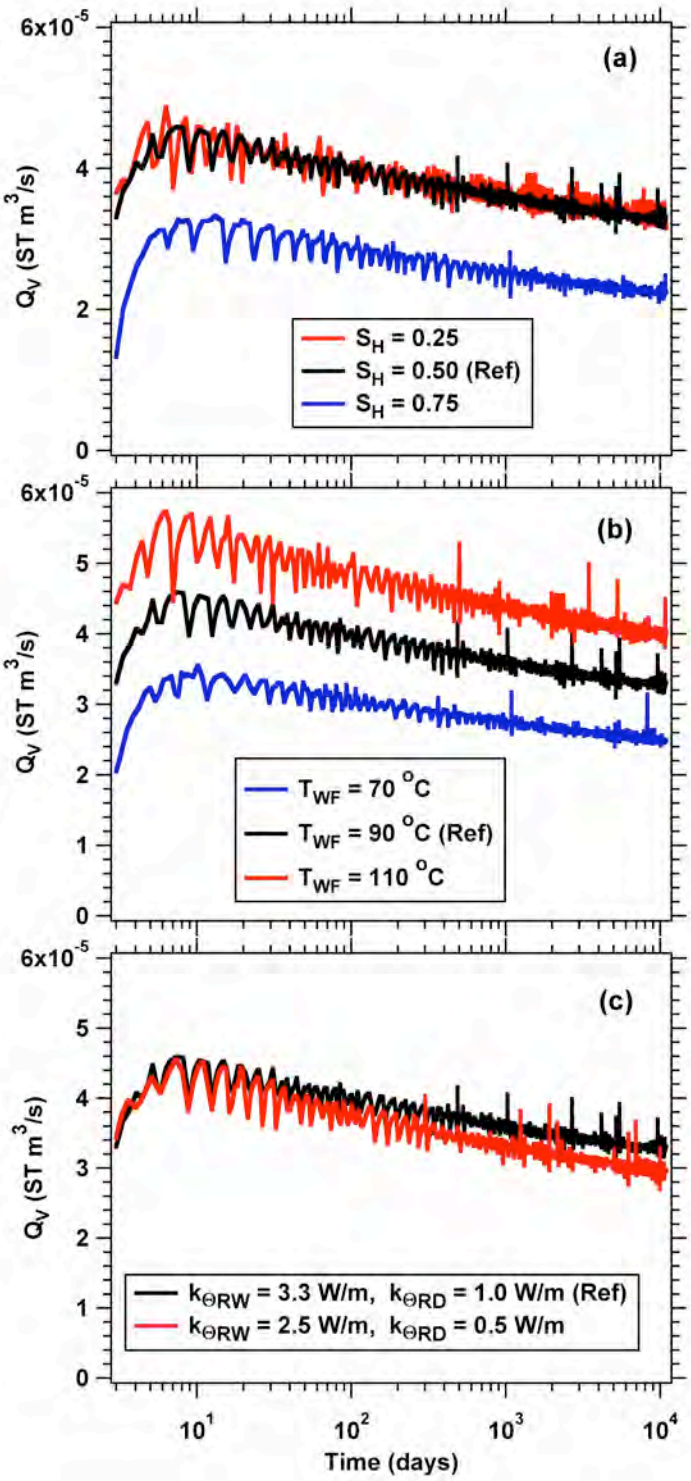

Figure 9 – Scoping studies: sensitivity of the rate of gas release from hydrate dissociation Q_V to variations in (a) the hydrate saturation S_H, (b) the temperature of well fluids T_{WF}, and (c) the medium thermal conductivities.

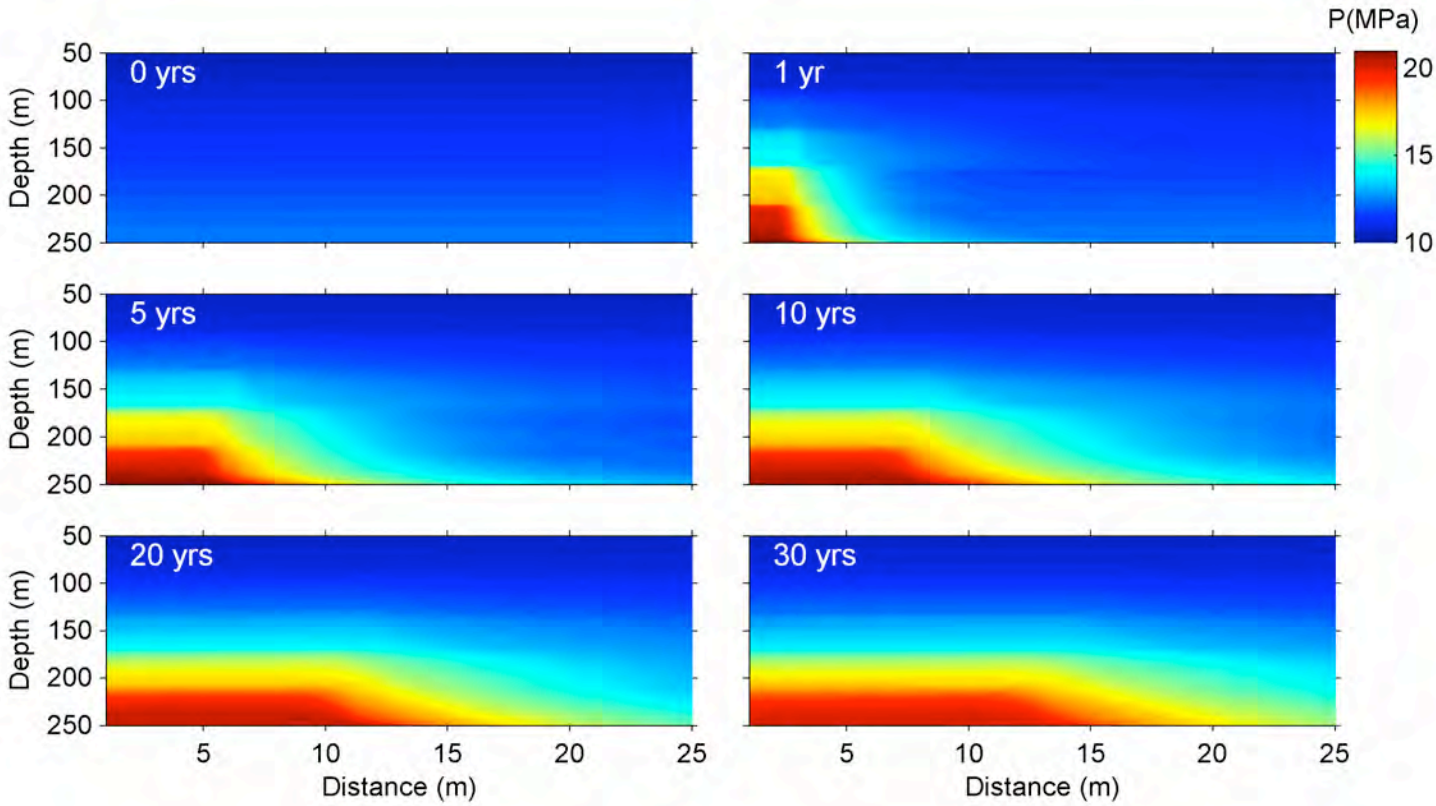

Figure 10. Evolution of spatial distribution of pressure in the HBS of Case A (reference case).

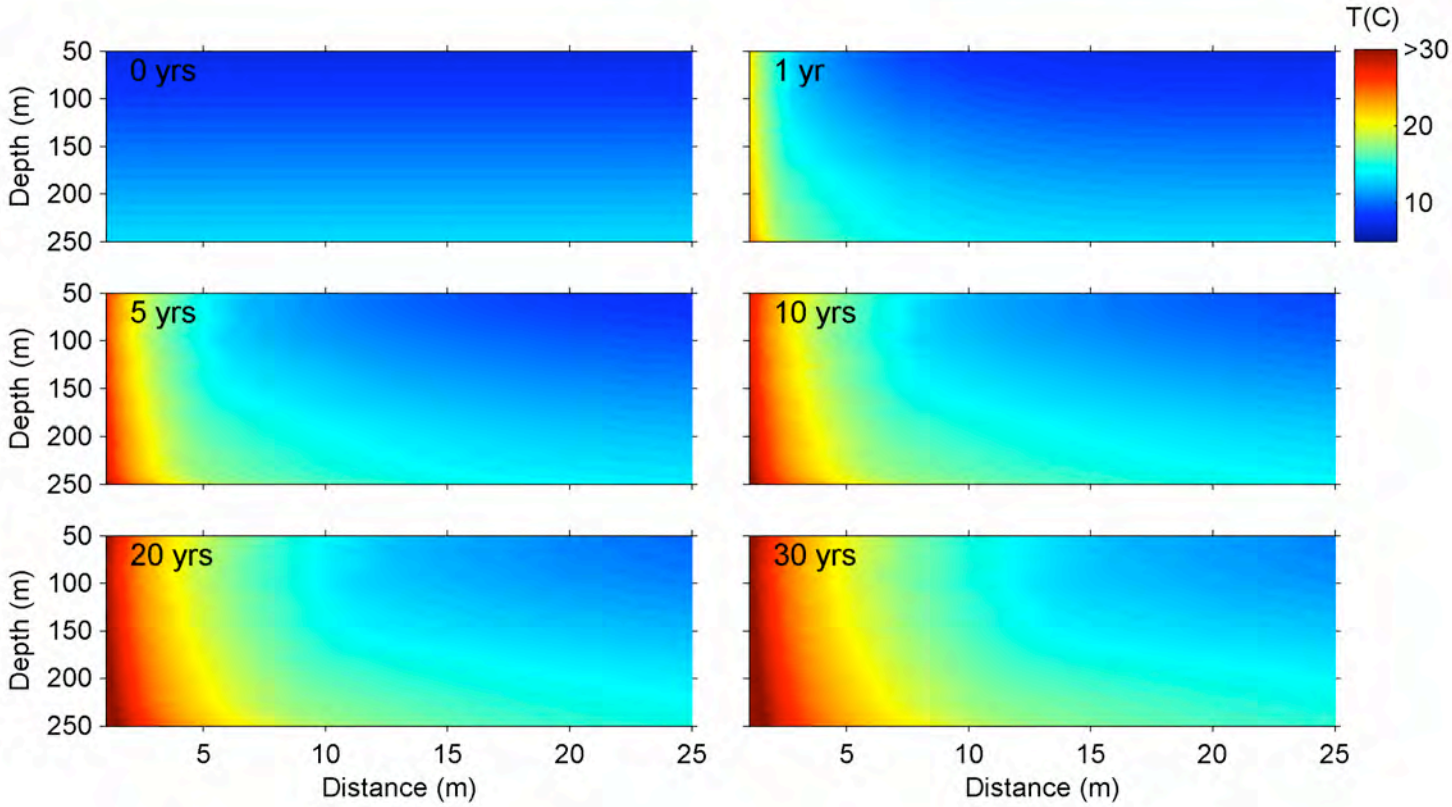

Figure 11. Evolution of spatial distribution of temperature in the HBS of Case A (reference case).

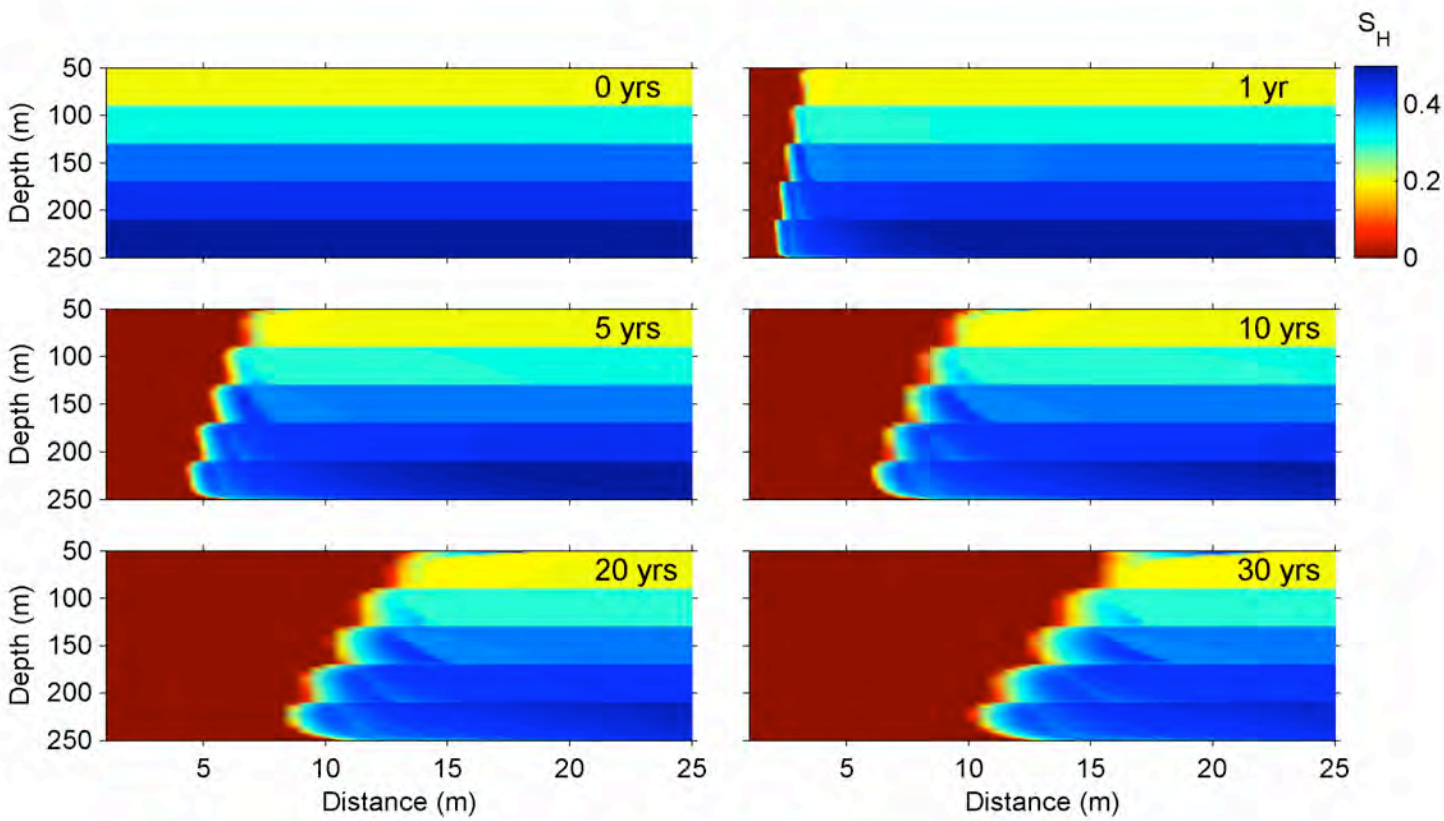

Figure 12. Evolution of spatial distribution of S_H in the HBS of Case A (reference case).

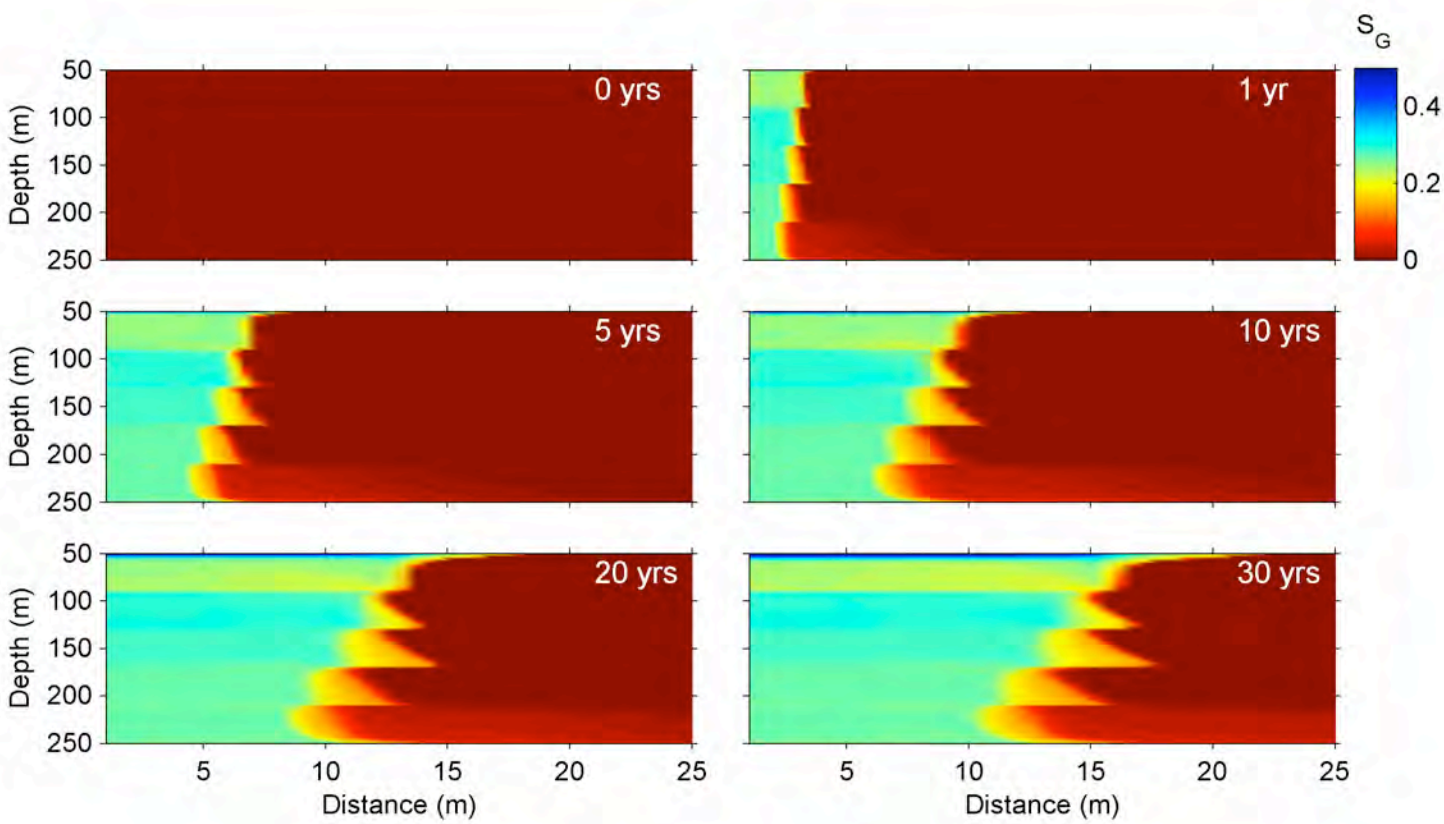

Figure 13. Evolution of spatial distribution of S_G in the HBS of Case A (reference case).

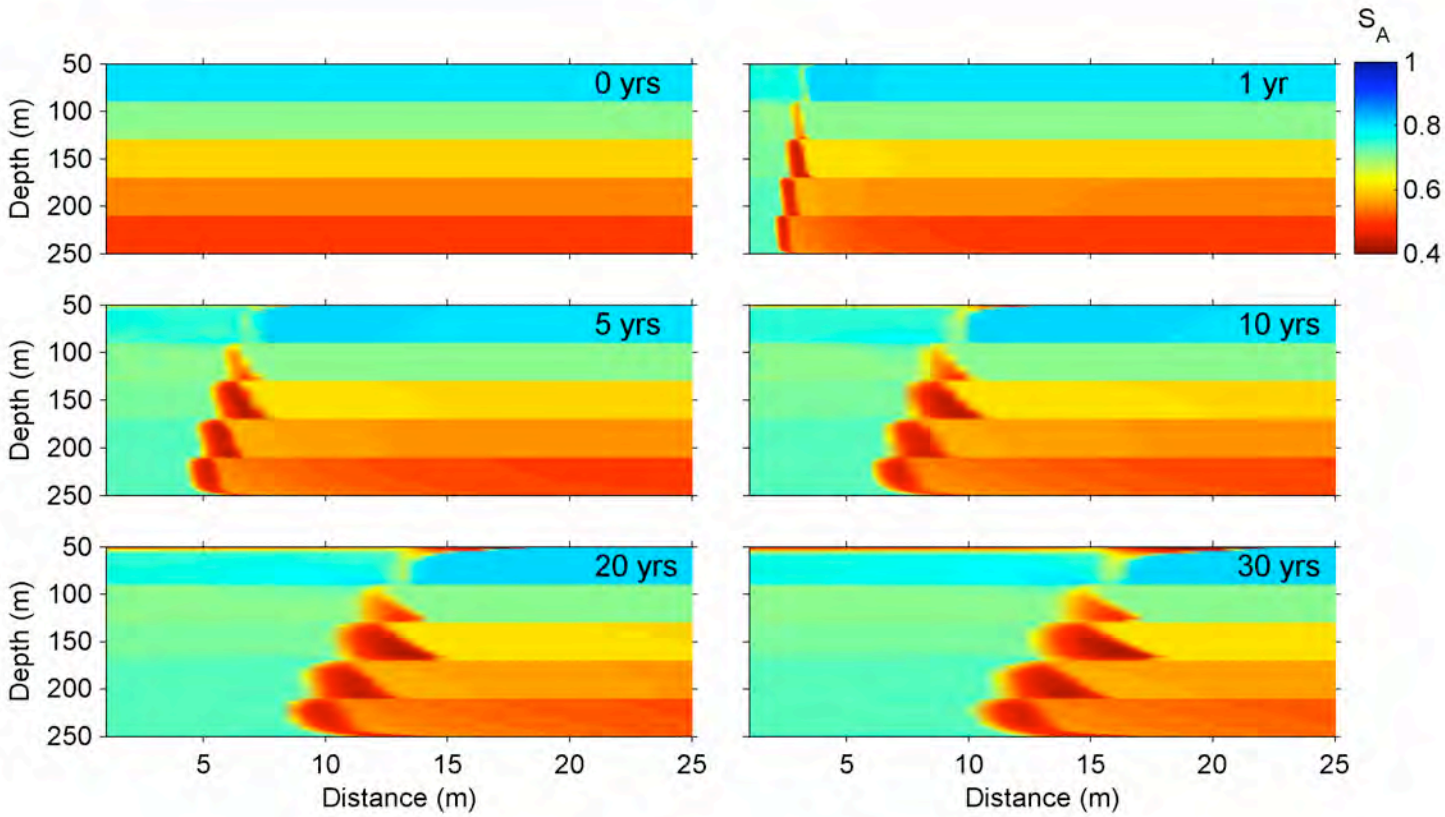

Figure 14. Evolution of spatial distribution of S_A in the HBS of Case A (reference case).

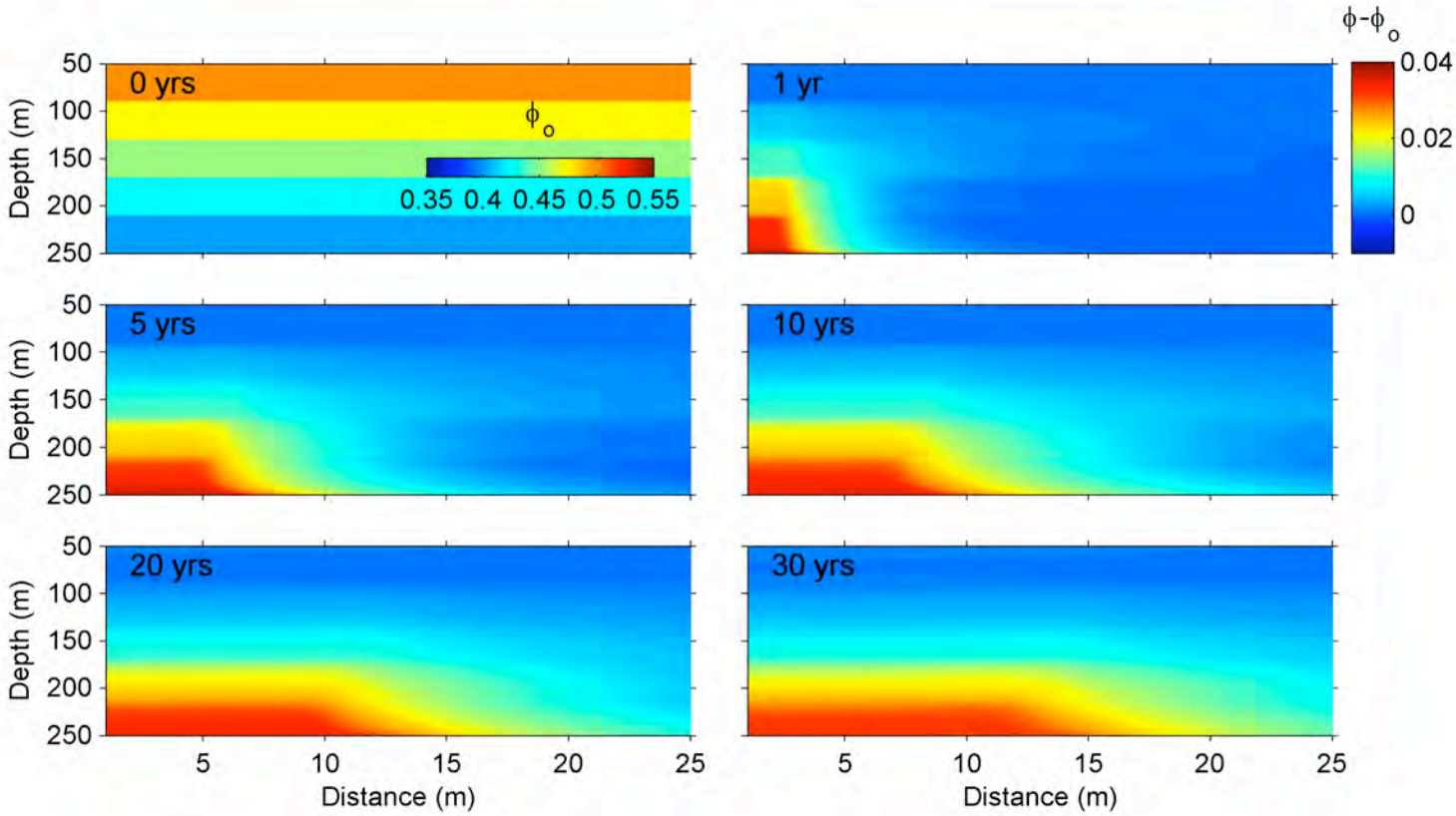

Figure 15. Evolution of spatial distribution of porosity deviation $\Delta\phi = \phi - \phi_0$ in the HBS of Case A (reference case).

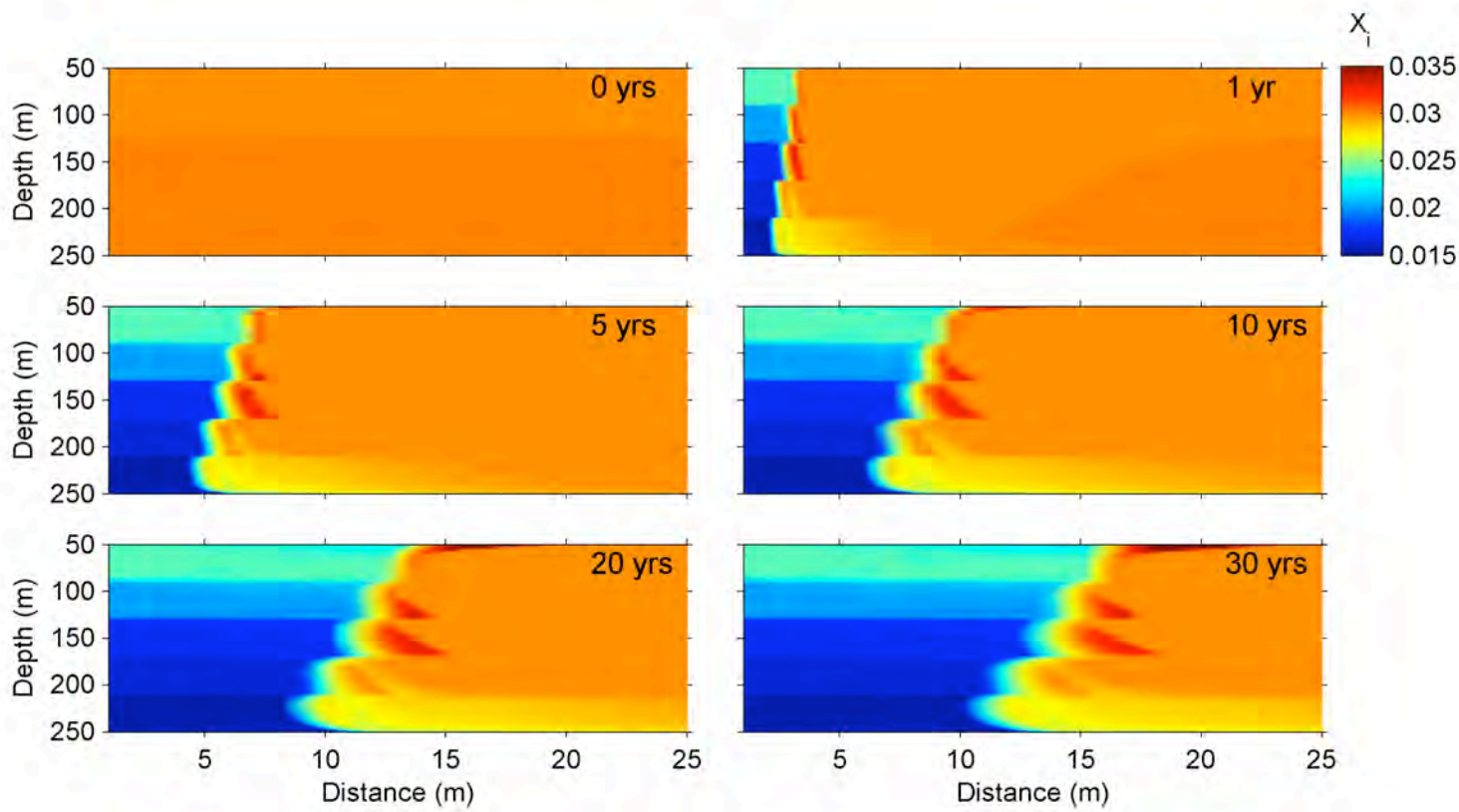

Figure 16. Evolution of spatial distribution of the salt mass fraction in the aqueous phase in the HBS of Case A (reference case).

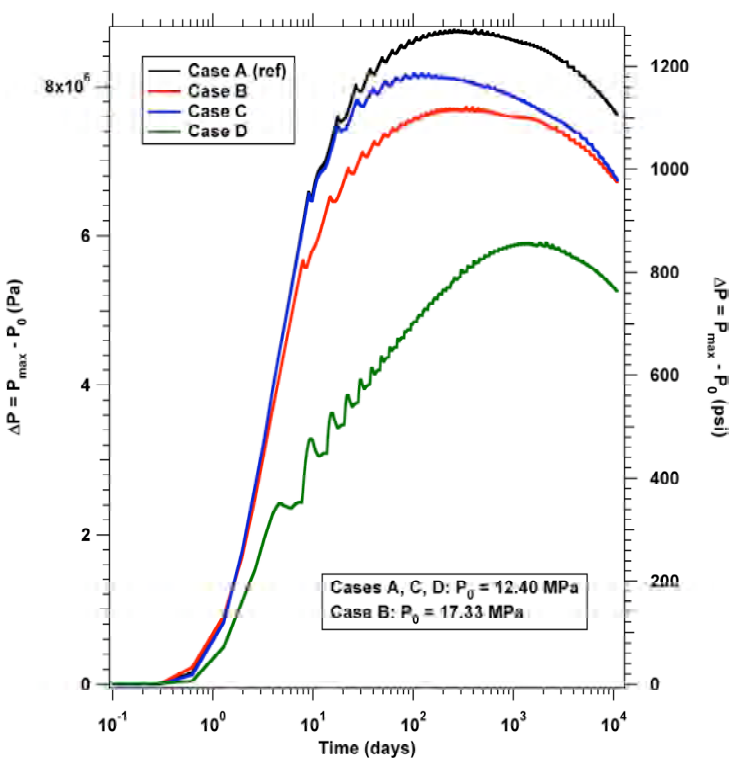

Figure 17. Evolution of maximum pressure in the hydrate-bearing sediments in Cases A through D.

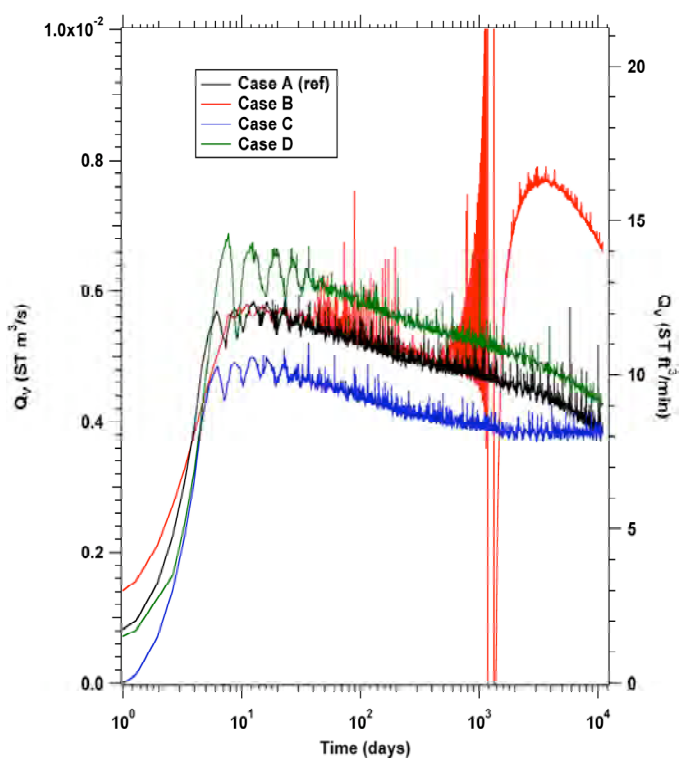

Figure 18. Volumetric rate Q_V of release of CH_4 originating from hydrate dissociation (Cases A through D).

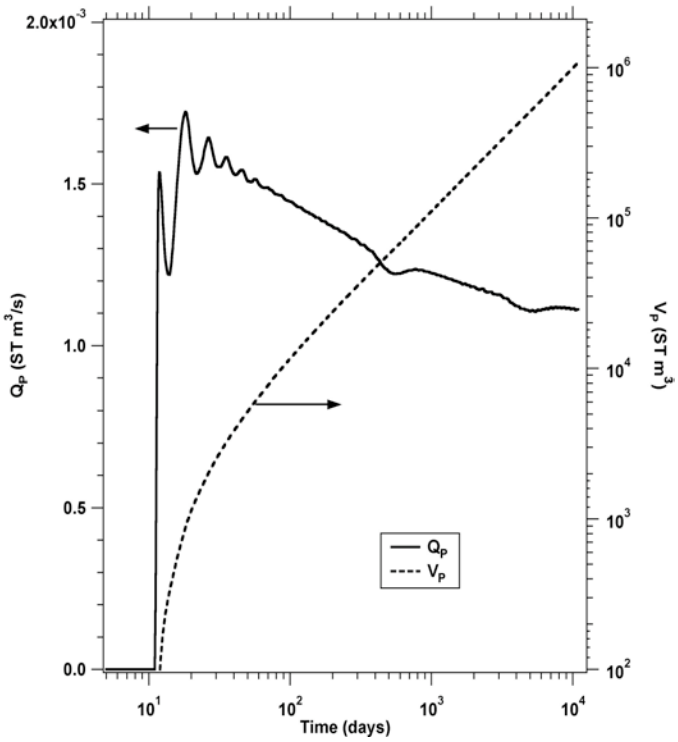

Figure 19. Case D: Evolution of volumetric rate of gas production (Q_P), and cumulative volume of gas produced from the gravel pack (V_P).

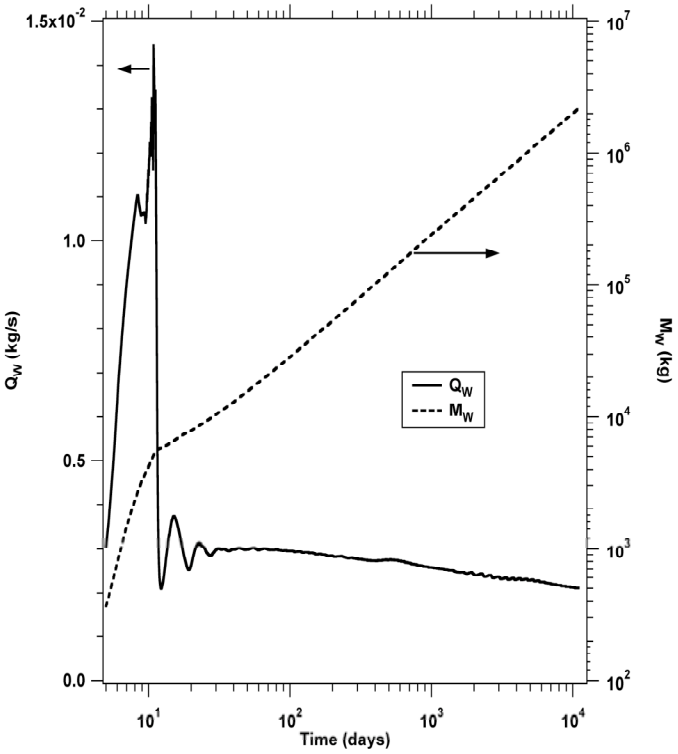

Figure 20. Case D: Evolution of mass rate of water production (Q_W), and cumulative mass of water produced from the gravel pack (M_W).

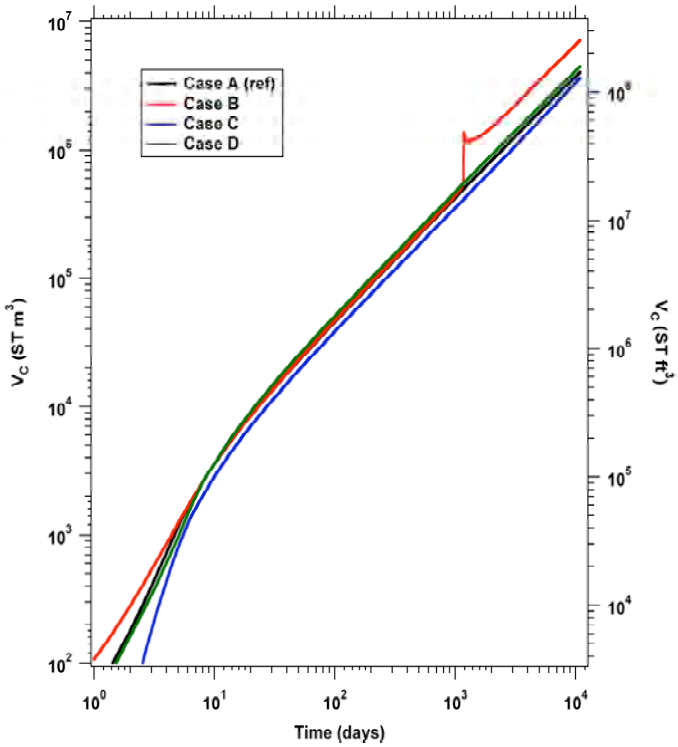

Figure 21. Cumulative volume of CH_4 released from hydrate dissociation in Cases A through D.

Gas Production from Unconfined Class 2 Hydrate Accumulations in the Oceanic Subsurface

George J. Moridis and Michael Kowalsky

Lawrence Berkeley National Laboratory, Earth Sciences Division, 1 Cyclotron Rd., Berkeley, CA 94720, U.S.A.
GJMoridis@lbl.gov

Keywords: gas hydrate, production, depressurization, thermal stimulation

Abstract

Unconfined Class 2 hydrate accumulations in the oceanic subsurface are characterized by mobile saline water zones enveloping the hydrate-bearing formation and by the absence of impermeable layers to vertical flow. In this paper, we evaluate the gas production potential of such deposits using both single-well and five-spot well configurations. Single-well production is based on depressurization-induced dissociation of the hydrates, whereas the five-spot configuration involves both depressurization at the production wells and thermal stimulation at the injection wells. The results of the study indicate that unconfined Class 2 hydrate accumulations are among the most challenging targets for gas production because (a) the absence of confining boundaries limits the effectiveness of depressurization, (b) gas production is accompanied by the production of very large volumes of water, and (c) thermal stimulation, when employed, requires substantial energy inputs. The amount of produced gas is limited in both the single-well and the five-spot configurations, and is significantly smaller than the total volume of gas released in the formation. For the five-spot configuration, hydrate dissociation releases relatively large amounts of gas into the reservoir, but these are not readily recoverable. Gas production is also significantly affected by the initial hydrate saturation in the hydrate-bearing sediment.

Introduction

Background

Gas hydrates are solid crystalline compounds in which gas molecules are lodged within the lattices of ice crystals. Vast amounts of hydrocarbons are trapped in hydrate deposits [Sloan, 1998]. Such deposits occur in two distinctly different geologic settings where the necessary low temperatures and high pressures exist for their formation and stability: in the permafrost and in deep ocean sediments.

Current estimates of the worldwide quantity of hydrocarbon gas hydrates vary widely, and a range between 10^{15} to 10^{18} m^3 has been reported [Sloan, 1998]. These estimates are not the result of a systematic attempt to evaluate hydrate reserves, but are based mainly on data obtained while investigating conventional hydrocarbon resources. Even by the most conservative estimates, the total quantity of gas in hydrates may surpass, by a factor of two, the energy content of the total fuel fossil reserves recoverable by conventional methods [Sloan, 1998]. The magnitude of this resource commands attention because it could make hydrate reservoirs a substantial future energy resource. The potential importance of hydrates is further augmented by the environmental

attractiveness of natural gas (as opposed to solid and liquid) fuels. Although the current energy economics cannot support gas production from hydrate accumulations by conventional means, their potential clearly demands further evaluation.

The three main methods of hydrate dissociation for gas production are: (1) depressurization, in which the pressure is lowered to a level lower than the hydration pressure P_H at the prevailing temperature, (2) thermal stimulation, in which the temperature is raised above the hydration temperature T_H at the prevailing pressure, and (3) the use of inhibitors (such as salts and alcohols), which causes a shift in the P_H-T_H equilibrium through competition with the hydrate for guest and host molecules [Sloan, 1998].

The numerical studies of gas production in this paper were conducted using the TOUGH-Fx/HYDRATE model [Moridis et al., 2005a], the successor to the earlier EOSHYDR2 code [Moridis, 2003] for the simulation of the system behavior in hydrate-bearing geologic media. TOUGH-Fx/HYDRATE can model the non-isothermal hydration reaction, phase behavior and flow of fluids and heat under conditions typical of common natural CH_4-hydrate deposits (i.e., in the permafrost and in deep ocean sediments) in complex formations. TOUGH-Fx/HYDRATE includes both an equilibrium and a kinetic model [Kim et al., 1987; Clarke and Bishnoi, 2001] of hydrate formation and dissociation. The model accounts for heat and up to four mass components, i.e., water, CH_4, hydrate, and water-soluble inhibitors such as salts or alcohols. These are partitioned among four possible phases: gas phase, liquid phase, ice phase and hydrate phase. By solving simultaneously the coupled equations of mass and heat balance, hydrate dissociation or formation, phase changes and the corresponding thermal effects are fully described, as are the effects of inhibitors. The model can describe all possible hydrate dissociation mechanisms, i.e., depressurization, thermal stimulation, salting-out effects and inhibitor-induced effects.

Description of the Geologic System

Moridis and Collett [2004] have developed a simple classification system for naturally occurring gas hydrate deposits, describing three classes on the basis of the phase distributions in the immediate vicinity of the hydrate-bearing layer. Class 1 and Class 2 hydrate deposits are characterized, respectively, by a hydrate-bearing layer (hereafter referred to as the HBL) underlain by (a) a two-phase zone involving mobile gas and water, and (b) a single-phase zone of mobile water. Class 3 accumulations are composed of a single zone, the HBL, and are characterized by the absence of an underlying zone of mobile fluids.

In terms of gas production, Class 1 is the most desirable exploitation target because of the favorable relative permeability regime and the thermodynamic proximity to the hydration equilibrium at the highest possible T_H (necessitating only small changes in pressure and temperature to induce dissociation). The desirability of Class 2 and 3 accumulations as gas production targets is less well defined than for Class 1 deposits, and can be a complex function of several factors, including economic considerations, thermodynamic proximity to hydration equilibrium, initial conditions, and environmental concerns [Moridis et al., 2004; Moridis, 2004].

Production from Class 1, Class 2 and Class 3 hydrates from confined permafrost accumulations has been discussed by Moridis and Collett [2004], Moridis et al. [2004], and Moridis [2004]. In this paper, we focus on gas production from a Class 2 hydrate deposit in the oceanic subsurface.

A particular feature of this gas hydrate accumulation is the absence of confining geologic formations. Thus, the HBL is enveloped by permeable sediments that are fully saturated with ocean water. Such a gas hydrate accumulation (hereafter referred to as a Class 2-OU deposit, with the 'O' denoting the oceanic environment and the 'U' the unconfined type of the deposit) can be formed from supersaturation in dissolved CH_4 (emanating from deeper in the oceanic subsurface), and its evolution can be facilitated by the presence of a lower permeability layer, which causes gas to accumulate and to begin forming hydrates. Generally, the bottom of such deposits coincides with the bottom of the hydrate stability zone at the prevailing pressure and temperature.

Class 2-OU hydrate deposits appear to be challenging targets for gas production because the absence of barriers to vertical flow can severely limit the effectiveness of depressurization, the fastest and most efficient method of hydrate dissociation. An additional complication in such deposits is the difficulty in focusing and directing flow through the hydrate (thus allowing an appropriate pressure drop to develop) because the low-permeability HBL can be bypassed if faster flow pathways (through the more permeable bounding layers) are available. If permeability is not a limiting factor (otherwise, cavitation may occur), the production efficiency appears to be adversely affected by the ready availability of practically limitless amounts of water. This condition requires very large (and potentially uneconomical) water production rates to effect a pressure drawdown sufficient to induce hydrate dissociation at an acceptable rate, while the flow of the evolving gas is hampered by an unfavorable relative permeability regime. Note that, in Class 2-OU deposits, the permeability and extent of the water-saturated formation underlying the HBL are generally more important than those of the overlying one because of the low permeability in the HBL. This limits the amount of water that flows to the well from the upper boundary and through the HBL (at least during the initial stages of production), especially when the hydrate saturation and the thickness of the HBL are large.

Although clearly a disadvantage, there is a potential advantage in the availability of large amounts of water during gas production from Class 2-OU hydrate deposits. Because permeability within the hydrate-bearing layer is generally limited, the large proportion of water in the production stream flows toward the producing well mainly from further and deeper in the underlying formation. By appropriate placement of producing wells, this water (which has a high heat capacity and relatively high temperature by virtue of its large flow rate) can provide some of the heat needed to fuel the strongly endothermic hydrate dissociation reaction. An additional potential advantage is that disposal of the produced water in an oceanic environment is expected to pose far less of an environmental challenge than in the sensitive arctic environment. The produced water need not be brought to the ocean surface, but can be safely released above the ocean floor, thus reducing the cost of production.

Objectives

The aim of this study is not to develop a design for efficient gas production from Class 2-OU hydrate deposits. Instead, the main objectives are to provide a first-level estimate of the production potential of such deposits using conventional technologies, to identify the major issues and limitations affecting production, and to obtain a measure of their relative appeal against other hydrate deposit classes.

Case 1: Gas Production from a Single-Well System

Geometry and Conditions of the System

The schematic in Figure 1 describes the geometry of the single-well gas production from a Class 2-OU hydrate accumulation. The thickness of the HBL is a uniform $H = 50$ m over the footprint of the reservoir. The absolute (intrinsic) permeability of the HBL and of the underlying water-saturated stratum is $k = 10^{-12}$ m^2 (1 Darcy), while the absolute permeability of the overlying layer is $k = 10^{-14}$ m^2. The porosity of all three strata is $\phi = 0.38$. The pressure follows a hydrostatic distribution, and is $P = 10.24$ MPa at the bottom of the HBL. The temperature follows the geothermal gradient, and is $T = 11.25$ ^{o}C at the bottom of the HBL. The top boundary (i.e., at $z < 0$, immediately above the HBL) and the bottom boundary (at $z \leq -350$ m) were maintained at constant temperature, pressure, and salinity conditions. The HBL has an areal extent of 1 km^2. In the HBL, the hydrate is pure CH_4-hydrate, and the initial hydrate and water saturations are $S_H = 0.75$ and $S_w = 0.25$, respectively.

Fluids are produced from a single well at a rate of $Q = 36.8$ kg/s (corresponding to an initial rate of 20,000 BPD of water), and are distributed according to their mobilities at the well. The well is completed in the –45 m to –55 m interval. The initial conditions in the HBL and its enveloping layers, as well as the basic pertinent hydraulic and operational parameters, are listed in Figure 1.

The water released during dissociation continuously dilutes the salinity of the native reservoir water. Because this is a localized phenomenon concentrated where flow (and, under the conditions of the proposed scheme, maximum dissociation) occurs, salinity could not be ignored in this analysis. Note that the salinity level in the native pore water of an oceanic hydrate accumulation can be significant, causing a 1.4 ^{o}C decrease in the dissociation temperature [Dallimore et al.,1999] at the prevailing pressure of 10.24 MPa.

Domain Discretization and Simulation Specifics

To describe this single-well problem, a cylindrical system was used, extending to an outer impermeable boundary at $R_b = 564.19$ m, which corresponds to an area of 1 km^2. The domain was discretized in 38 x 36 subdomains in (r, z), resulting in a total of 1214 gridblocks. Because the hydrate dissociation reaction was assumed to occur at equilibrium, the four equations per cell (mass balance equations of H_2O, CH_4 and salt, plus the heat balance equation) resulted in a system of 4856 equations.

The well is represented as a domain of porosity $\phi = 1$, very high vertical permeability ($k_z = 10^{-8}$ m^2), and of horizontal permeability equal to that of the formation in the completed section of the well and zero elsewhere. The distribution of fluid production along the completed section of the well is determined by the phase permeability regimes in the vicinity of the wellbore when fluids are withdrawn at a mass flow rate Q applied at the well cell immediately above the completed section of the well. The production period is 4 years.

The phase relative permeabilities follow a modification [Moridis et al., 2005a] of the model of Stone [1970], with an irreducible water saturation of $S_{wr} = 0.2$, irreducible gas saturation $S_{gr} = 0.02$, and an exponent $n = 3.572$. The capillary pressure was computed using the method of Parker et al. (1987) with $S_{wr} = 0.2$, $\alpha = 3$ m^{-1}, and $n = 1.65$. These values were based on data

obtained during the Mallik field test of gas production from a permafrost hydrate deposit [Moridis et al., 2005b].

Results of the Single Well Study

The fluid production from the single well leads to depressurization-induced hydrate dissociation. Figure 2 shows the evolution over time of the rate of CH_4 release into the reservoir and the rate of CH_4 production at the well, expressed as ST m^3/day. The gas production rate at the well exhibits oscillations, but the average remains roughly constant during the entire production period. The gas release rate into the reservoir is marked by an initial steep increase, followed by a decline and eventual stabilization. The oscillations in both curves are caused by discretization effects and heat transfer limitations affecting the dissociation reaction. Dissociation is followed by a pressure increase (caused by the gas release) and a drop in temperature (due to the strongly endothermic nature of the dissociation reaction), and results in the steep drop in the release rate and the production rate because of a shift in the dissociation P_H-T_H relationship (see Figure 3). As more heat becomes available (through conduction and fluid advection), the dissociation rate begins increasing. The oscillations are exacerbated by the finite size of the elements into which the simulation domain is subdivided.

Figure 4 shows the cumulative volumes (expressed as ST m^3) of hydrate-originating CH_4 released during the depressurization-induced dissociation and the cumulative gas volume produced from the well over the four-year duration of the study. A comparison of these curves to the ones of the corresponding rates in Figure 2 indicates that the rate fluctuations are attenuated in the cumulative volume curves, which appear remarkably smooth.

Review of Figures 2 and 4 indicates that the amount of produced gas represents a small fraction (about 1/8th) of the amount of gas released from dissociation. In essence, this means that gas continuously accumulates into the reservoir during the four-year production period. Despite the gas accumulation, the gas reaching the well does not increase over time (because of an adverse gas relative permeability regime) but remains constant (as demonstrated by the practically linear appearance of the cumulative CH_4 volume curve). This is an undesirable scenario, and indicates that simple depressurization in the lower part of and immediately below the HBL do not appear to be a very promising production method. This observation is clearly supported by the magnitude of the CH_4 production rate (about 100 ST m^3/day), which is very low compared to the roughly 3,150 m^3/day of water produced in the process. The lack of appeal of gas production from the single-well depressurization of a Class 2-OU deposit would persist even if the production rate equaled the entire CH_4 release rate in the reservoir.

Effect of the Initial S_H in the HBL

Figure 5 shows the evolution of the cumulative volumes (expressed as ST m^3) of produced CH_4 and of the CH_4 released in the reservoir over the four-year production period when the initial S_H = 0.375, i.e., half of that in the base simulations of Figures 2 and 4. Comparison of Figures 4 and 5 indicate that production from a Class 2-OU deposit with a lower initial S_H is even less appealing. The cumulative gas production decreases with S_H. In this case, the lower initial S_H leads to higher S_w, and, consequently higher water permeability, which allows more flow through the HBL (most of which is bypassed in the higher S_H case), and more effective depressurization of the hydrate. The increase in gas production (as a larger HBL volume becomes available for gas release) is countered by the smaller amount of hydrate (i.e., the CH_4 source) and the increasingly limited flow through the HBL as the hydrate near the well dissociates. As in the

case of higher initial S_H, the produced CH_4 volume represents a rather small fraction of the released volume, and increases roughly linearly with time.

Note that, because of differences in the formation process (and the fact that the presence of hydrates in oceanic porous media limits mass transfer and further hydrate formation), low hydrate saturations are far more common (and probably the norm) in ocean deposits. This further limits the attractiveness of the Class 2-OU deposits,

Case 2: Gas Production from a Five-Spot Well System

Geometry and Conditions of the System

In Case 2, the geology, geometry, properties and initial saturations distribution of the Class 2-OU hydrate accumulation and its boundary formations remain as in Case 1. The stencil in Figure 6 represents the five-spot well configuration, which involves production and injection wells. The injected fluid was hot water at a temperature of 41 ^{o}C. Hot water was chosen over steam because the parametric study of McGuire [1981] indicated that the amount of produced gas is less than the estimated fuel consumption when steam is employed. Hot water was injected into the center-well of the five-spot pattern, and reservoir fluids were produced from the four production wells. The obvious advantage of this scheme is that it combines the two most important mechanisms of hydrate dissociation, i.e., depressurization at the production well, and thermal stimulation at the injection well.

In an effort to focus the thermal stimulation and depressurization effects in the vicinity of the hydrate interface, the production well was completed in the 0 to –55 m interval, and the injection well in the 0 to –50 m interval. This configuration offered the advantage of limiting mixing of the injected hot water with the colder native reservoir water, while maximizing the thermal advantages of buoyancy that tends to concentrate the warmer water immediately below (and in contact with) the hydrate interface. Additionally, the completion of the wells in the entire hydrate interval took advantage of the gas buoyancy and the maximized contact with the receding hydrate interface in its vicinity. However, the upper parts of the well intervals did not contribute practically any fluids in the early stages of gas production because of adverse relative permeability conditions.

Domain Discretization and Simulation Specifics

Because of symmetry, only a quarter of the domain was simulated using a 3-D Cartesian system. The side of the simulated quadrant was 100 m. The domain was discretized in 15x15x25 unequally spaced subdivisions in (x,y,z), resulting in a total of 5,625 elements. Assuming equilibrium dissociation, four equations (i.e., components) were considered (CH_4, H_2O, salt, and heat) in each element, leading to a system of 22,500 simultaneous equations. The large size and the complexity of the simulated system made the solution of this problem very computationally demanding.

The well representation, as well as the relative permeability and capillary pressure models and parameters remained as in Case 1. Because only a quadrant of the five-spot pattern in Figure 6 (corresponding to 1/4th of the rates in the full system) is simulated, and each five-spot configuration occupies 1/25th of the 1 km^2 area of the footprint of the hydrate deposit, the initial mass production rate was Q = 36.8/(4x25) = 0.368 kg/s, but the water injection rate was equal to

the rate of water withdrawal from the production well. Thus, the total production rate from the entire hydrate deposit was equal to that in the single-well system of Case 1. The gas and aqueous phase production rates were determined by the phase relative permeabilities in the production well elements. The simulation was allowed to continue for 4,000 timesteps, at which time the results were to be evaluated and a decision made regarding further continuation of the simulation.

Results of the Five-Spot Study

After 4000 timesteps, the simulation had lasted over three days of continuous execution and had covered a production period of 212 days. Because the results and their pattern were rather well defined, and because the execution time requirements of this problem were very substantial, we decided to terminate the simulation at that point.

Figure 7 shows the evolution over time of the rate of CH_4 release into the reservoir and the rate of CH_4 production at the well, expressed as ST m^3/day. These results correspond to the entire 1 km^2 hydrate accumulation. Comparison to the rates from the single-well production in Case 1 leads to the obvious conclusion that, while the rate of gas release in the reservoir is substantially larger than that in Case 1, the rate of CH_4 production at the well is much lower. Additionally, although the rate of gas release continues increasing (albeit slowly) over the 212-day period of the study, the rate of CH_4 production at the well is either constant or declines slightly.

The lower production rate and the difference in the long-term trend are attributed to two reasons. The first is that the injection and production rates are roughly equal during this period (as evidenced by the very low gas production). This rate parity does not allow significant depressurization at the production well because of the relatively short distance between the injection and production wells, and the speed at which the pressure front advances. Thus, the warm water re-injection prevents a significant pressure drop at the production well, leading to lower hydrate dissociation and a lower CH_4 production rate at the well. Moreover, after a maximum pressure imbalance early in the production period, the pressure tends to a steady-state distribution (though continuously disrupted by the gas release from hydrate dissociation), leading to the constant (or slight decline of) the production rate of CH_4 that originating almost exclusively from depressurization-induced hydrate dissociation near the production well.

The second reason for the low gas production rate (and for the increasing release rate trend) is because gas from the thermally induced dissociation in the vicinity of the injection well has not yet reached the production well because of adverse relative permeability conditions. Thus, most of the gas released in the reservoir is expected to be by thermal dissociation. The slowly and continuously expanding thermal front leads to the slowly increasing (over time) release rate observed in Figure 7. The disparity between CH_4 release (in the reservoir) and production rates, brought about by low depressurization and the limited mobility of the gas from thermal dissociation, are expected to lead to a significant gas accumulation in the reservoir.

The differences in the fluctuations of the rate curves in Figure 7 stem from the origin of gas they represent, and from the different impact of discretization effects. Thus, the release rate curve is expected to affect a relatively large number of elements as the warm water front advances toward the production well, as indicated by the large number of oscillations (denoting finite element size). Conversely, because of the limited impact of depressurization, dissociation is expected to

occur in a limited number of elements, as implied by the few and distinct oscillations in the production rate curve.

The expectations from Figure 7 are confirmed in Figure 8, which shows the evolution over time of the cumulative volume (in ST m^3) of produced CH_4 and of CH_4 released in the entire 1 km^2 deposit. The curves in Figure 8 point to a very substantial gas accumulation in the reservoir, which is not accompanied by a commensurate increase in gas production during the 212 days of simulation. If the reason for this disparity is that the gas from thermal dissociation has not reached the production well during that period, then it is almost inevitable that this will happen at a later time, and will be accompanied by a surge in production. However, the question that has to be asked before further pursuing this venue is whether such an approach holds any appeal, as it tends to indicate over 0.6 of a year of continuous water production, heating and circulation with practically no gas production. Note that, as in Case 1, the cumulative volume curves attenuate the oscillations in the corresponding rate curves, and have a remarkably smooth appearance.

Further consideration of Figures 7 and 8 indicates that the rate of CH_4 release in the reservoir and the corresponding cumulative volume are large and within the range of commercial viability. The obvious issue is whether an appropriate production system can be designed that enables the early access to, and production of, the majority of the released gas. Such a system may involve asymmetric production and injection rates (with injection rate being a fraction of the production rate) or horizontal wells, and are likely to require higher levels of management. Although these studies can hold substantial scientific interest, their appeal is eclipsed by far more promising hydrate targets for gas production, e.g., Class 1 deposits.

Figure 9 shows the pressure distribution in the (a) 3-D five-spot quadrant and (b) along the $x = y$ plane, i.e., the plane passing from the injection and production wells. As expected, the highest pressures are observed in the vicinity of the injection well, and the lowest in the immediate neighborhood of the production well. The temperature distribution in Figure 10 exhibits high temperatures at the injection well, and low temperatures (below the initial $T = 11.25$ ^{o}C) near the production well, where some depressurization-induced dissociation occurs (see Figure 7).

The gas and hydrate saturations in Figures 11 and 12, respectively, are consistent with each other, with the pressure and temperature distributions of Figures 9 and 10, and with the rates and cumulative volumes of Figures 7 and 8. Minor hydrate dissociation is observed along the bottom of the HBL, consistent with the limited depressurization to which this region is exposed. The highest gas saturation corresponds to the location of maximum hydrate dissociation, and is located near the well of warm water injection. This is consistent with the expectations and deductions from Figures 7 and 8. The main body of the gas saturation front in Figure 11 has not reached the production well after 212 days of production (actually, it has covered less than half the distance between the wells), thus explaining the reason for the low production rate and confirming the source of the majority of the released gas. The maximum pressure is observed at a location above the hydrate interface and of the location of the highest temperature, and is caused by the resistance to flow of the CH_4 (released from thermal dissociation of hydrate) into the low permeability HBL. The increased pressure shifts the equilibrium T_H, and results in hydrate persistence despite the higher temperatures.

Summary and Conclusions

This paper focuses on the study of gas production from Class 2-OU hydrate accumulation, i.e., oceanic deposits characterized by a HBL enveloped by permeable geologic media fully saturated with mobile water. The objectives of this study were to provide a measure of the production potential of such deposits using conventional technologies and to identify the factors limiting production, thus developing the knowledge base for meaningful comparisons of the relative value of such deposits as production targets against those from other hydrate accumulations.

Using a Class 2-OU deposit with an areal footprint of 1 km^2 and a HBL of pure CH_4-hydrate and 50 m thick, two production strategies were investigated. In the first, fluid production from a single well at the center of the reservoir effected depressurization, which led to gas production by inducing hydrate dissociation. The second strategy employed combinations of injection and production wells in a five-spot pattern, and involved both depressurization (at the production wells) and thermal stimulation near the injection wells, through which the produced water (heated to 40 ^oC) was re-injected.

The results of these studies lead to the following conclusions:

(1) In both cases, the CH_4 production rates were practically constant over time, and significantly lower than the rate of gas release into the reservoir. At no time during the simulation period do the release and production curves show any tendency toward convergence or even constant deviation. This indicates that gas accumulates in the reservoir at a rate that increases with time, but the adverse relative permeability regime does not allow ready gas recovery.

(2) As indicated by the trend in the rates, in both cases, the cumulative volumes of produced CH_4 were significantly lower than cumulative volumes of CH_4 released into the reservoir.

(3) Gas production decreases with a decreasing hydrate saturation of the HBL because of reduced availability of hydrate.

(4) The production rate was higher in the case of single-well production because, in the five-spot pattern, the (a) gas produced from the thermal dissociation of hydrate caused by the warm water re-injection is very slow to reach the production well, and (b) the water re-injection does not allow a significant pressure drop, thus reducing the driving force of the depressurization-induced dissociation near the production well.

(5) Conversely, the CH_4 release rate into the reservoir was significantly higher in the five-spot well pattern because of the large volumes of re-injected water as an agent of thermal dissociation. The rather spatially uniform injection of the warm water (a result of the small footprint of the five-spot stencil) increases the effectiveness of thermal dissociation.

(6) Although the volume of CH_4 released from dissociation is large (and within the realm of economic viability) in the case of the five-spot well system, this volume is not readily recoverable using the vertical wells of this conventional configuration. A higher-level of management and/or different well systems (e.g., horizontal wells) may be needed to achieve a more efficient (and economically attractive) recovery from such hydrate deposits.

(7) The production rates in both well configurations are very low, and cannot justify considering Class 2-OU hydrate accumulations as economically viable targets for gas

production. Further study will be needed to develop appropriate production strategies if such deposits are to be targeted for gas recovery.

(8) For all the aforementioned reasons, Class 2-OU hydrate accumulations do not appear to be appealing targets for gas production using conventional technologies, especially when considered against far more promising candidates such as Class 1 deposits.

(9) The main reasons for the limited potential of Class 2-OU hydrate deposits as a gas source are (a) the ineffectiveness of depressurization as the driving force of dissociation in the absence of confining layers, (b) the availability of practically limitless amounts of water in the vicinity of the HBL, necessitating large water production rates for an effective pressure drop, (c) the challenge of focusing and directing water flow through the HBL (easily bypassed if higher permeability pathways through the enveloping boundary layers are available), and (d) the adverse relative permeability to gas flow, as gas attempts to emerge as a mobile free phase in a fast-flowing water-saturated geologic medium.

Acknowledgments

This work was supported by the Assistant Secretary for Fossil Energy, Office of Natural Gas and Petroleum Technology, through the National Energy Technology Laboratory, under the U.S. Department of Energy, Contract No. DE-AC03-76SF00098. The authors are indebted to Timothy Kneafsey and John Apps of LBNL for their insightful review comments.

References

Clarke, M. and P.R. Bishnoi, *Determination of Activation Energy and Intrinsic Rate Constant of Methane Gas Hydrate Decomposition*, **Canadian Journal of Chemical Engineering**, 79(1), 143-147, 2001.

Dallimore, S.R., T. Uchida and T.S. Collett, Eds., Scientific Results from JAPEX/JNOC/GSC Mallik 2L-38 Gas Hydrate Research Well, Mackenzie Delta, Northwest Territories, Canada; Geological Survey of Canada Bulletin 544, 1999.

Kim, H.C., P.R. Bishnoi, R.A. Heideman, and S.S.H. Rizvi, *Kinetics of Methane Hydrate Decomposition,* **Chemical Engineering Science**, 42(7), 1645-1653, 1987.

McGuire, P.L., Methane hydrate gas production: An assessment of conventional production technology as applied to hydrate recovery, Report LA-9102-MS, Los Alamos National Laboratory, Los Alamos, NM, 1981.

Moridis, G.J., M. Kowalsky and K. Pruess, TOUGH-Fx/HYDRATE: A code for the simulation of system behavior in hydrate-bearing geologic media, Lawrence Berkeley National Laboratory, 2005 (LBNL Report No. pending).

Moridis, G.J., T.S. Collett, S.R. Dallimore, T. Inoue, and T. Mroz, *Analysis and Interpretation of the Thermal Test of Gas Hydrate Dissociation in the Mallik 5L-38 Research Well, Mackenzie Delta, Canada*; in **Scientific Results from the Mallik 2002 Gas Hydrate Production Research Well Program, Mackenzie Delta, Northwest Territories, Canada**, (ed.) S.R. Dallimore and T.S. Collett; Geological Survey of Canada, Bulletin 585, 2005.

Moridis, G.J., *Numerical Studies of Gas Production from Class 2 and Class 3 Hydrate Accumulations at the Mallik Site, Mackenzie Delta, Canada*, **SPE Reservoir Evaluation and Engineering,** 7(3), 175-183, 2004.

Moridis, G.J. and T. Collett, *Gas Production from Class 1 Hydrate Accumulations*, in ***Recent Advances in the Study of Gas Hydrates***, C. Taylor and J. Qwan, Editors, Kluwer Academic/Plenum Publishers (Section I, Chapter 6, 75-88), 2004.

Moridis, G.J., T. Collett, S. Dallimore, T. Satoh, S. Hancock and B. Weatherhill, *Numerical Studies Of Gas Production From Several Methane Hydrate Zones At The Mallik Site, Mackenzie Delta, Canada*, **Journal of Petroleum Science and Engineering,** 43, 219-239, 2004.

Moridis, G.J., *Numerical Studies of Gas Production From Methane Hydrates*, **SPE Journal**, 32(8), 359-370, 2003.

Parker, J.C., R.J. Lenhard, and T. Kuppusamy, *A Parametric Model for Constitutive Properties Governing Multiphase Flow in Porous Media***, Water Resources Research**, 23(4), 618-624, 1987.

Sloan, E.D., *Clathrate Hydrates of Natural Gases*, Marcel Dekker, Inc.: New York, NY, 1998.

Stone, H.L., *Probability Model for Estimating Three-Phase Relative Permeability*, **Transactions of the SPE of AIME**, 249, 214-218, 1970.

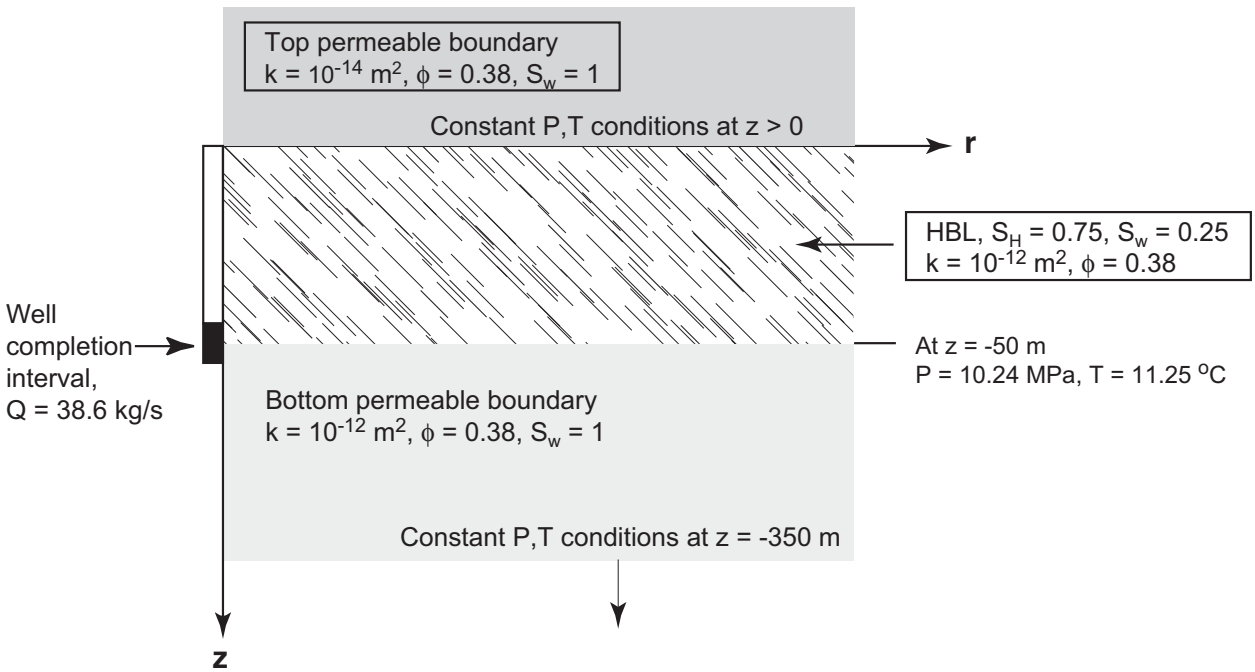

Figure 1. The characteristics and properties of the Class 2-OU formation studied in Case 1.

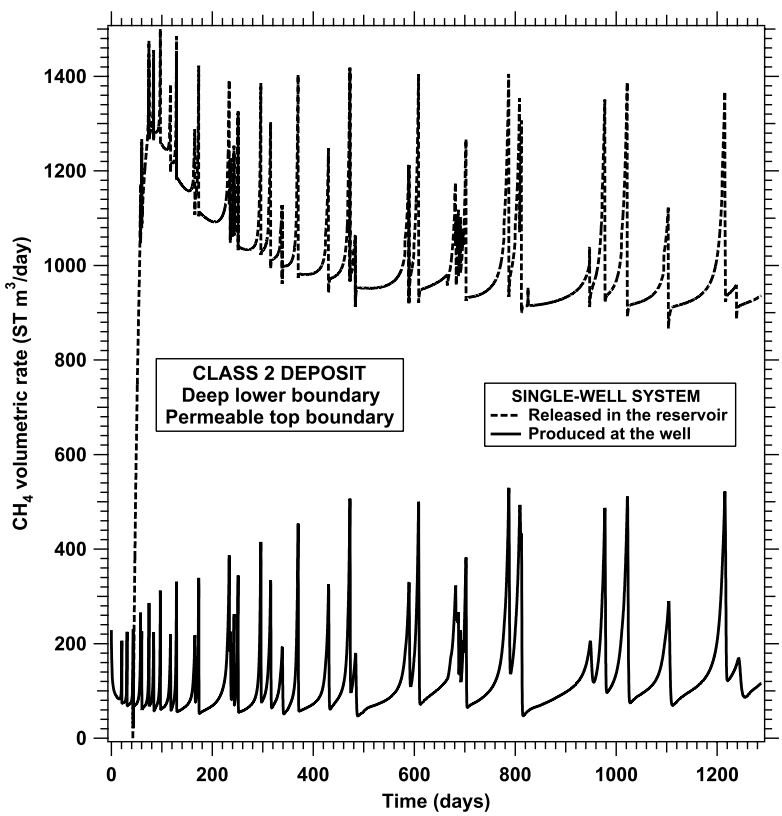

Figure 2. Evolution of the CH_4 production rate and of the rate of CH_4 release (from depressurization-induced hydrate dissociation) into the reservoir during production from a single well in Case 1 ($S_H = 0.75$).

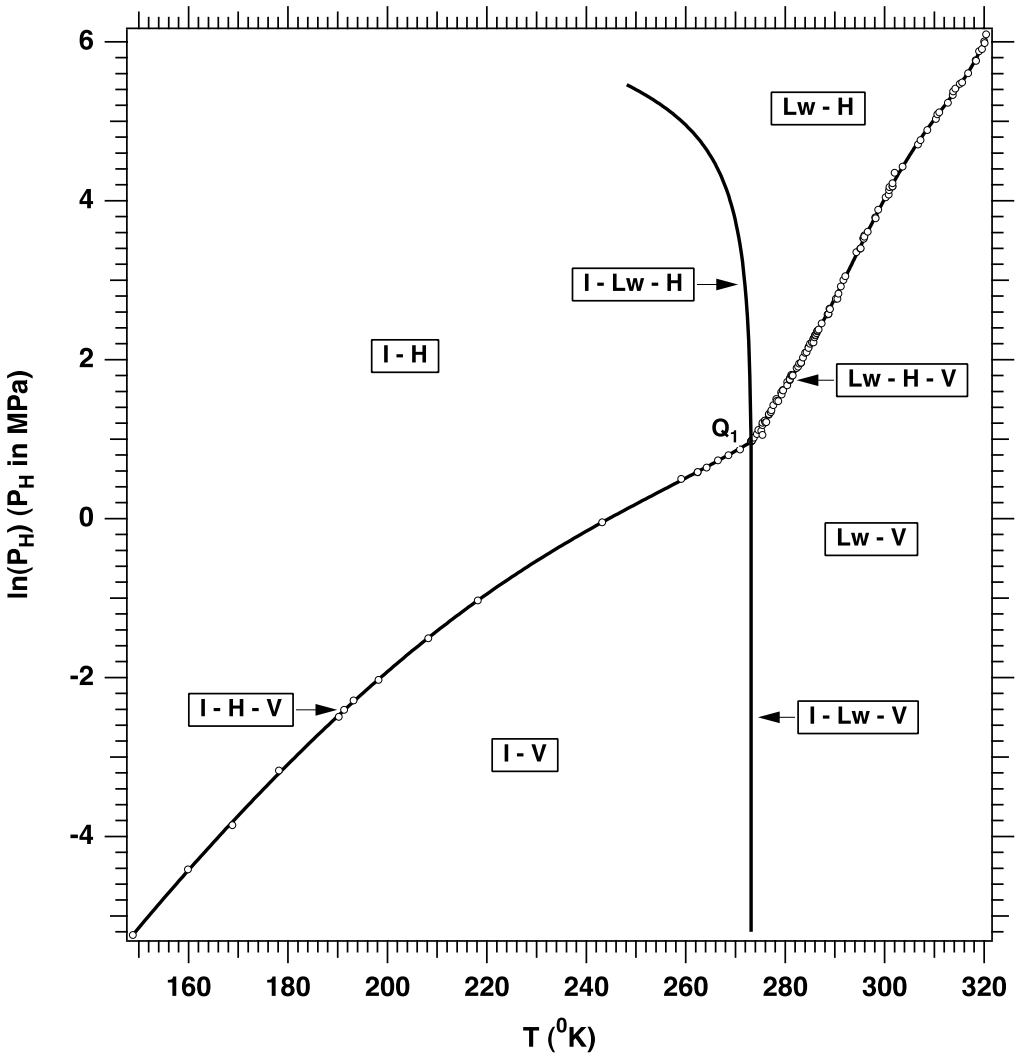

Figure 3. Pressure-temperature equilibrium of the simple methane hydrate [Moridis, 2003].

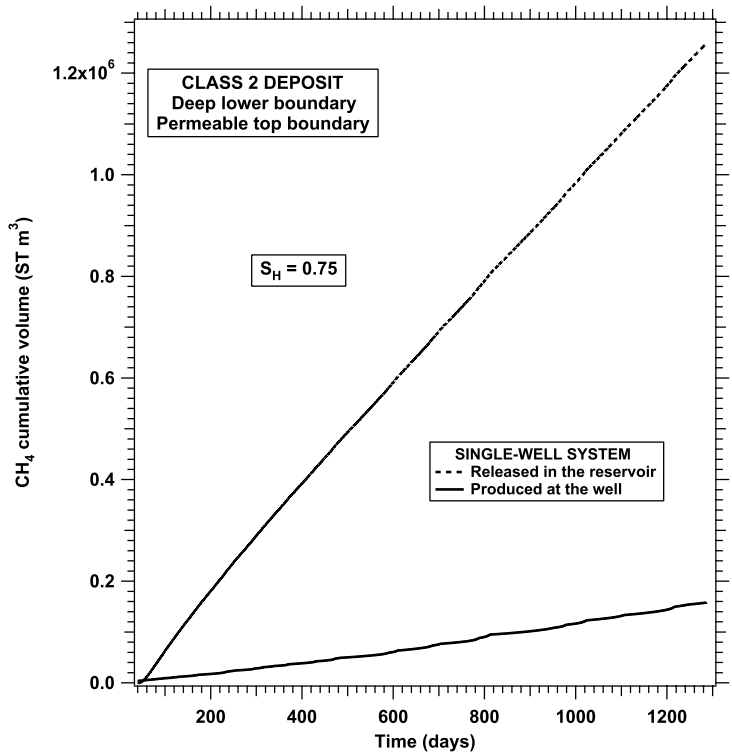

Figure 4. Evolution of the cumulative volumes of produced CH_4 and of CH_4 released into the reservoir during production from a single well in Case 1 (S_H = 0.75).

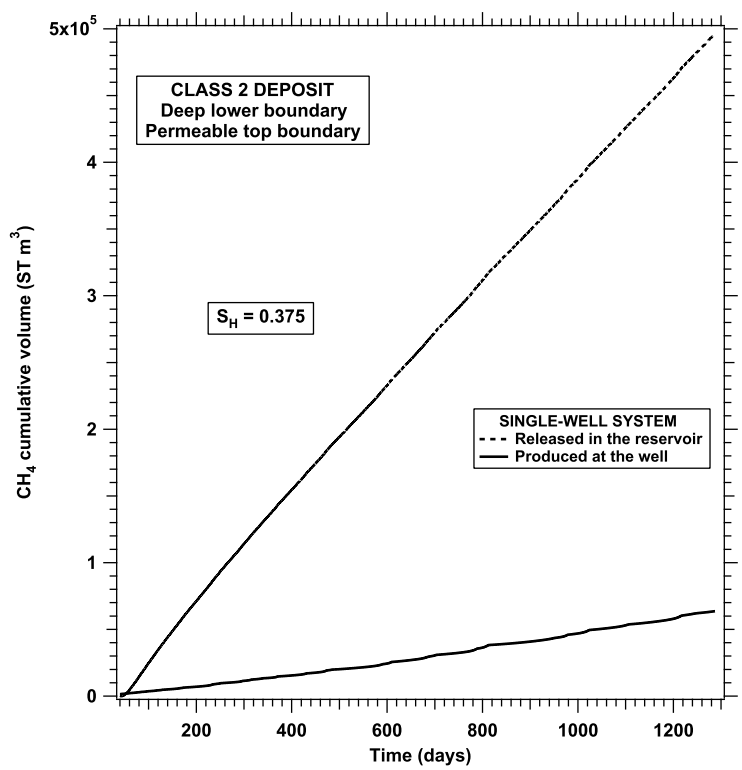

Figure 5. Evolution of the cumulative volumes of produced CH_4 and of CH_4 released into the reservoir during production from a single well in Case 1 (S_H = 0.375).

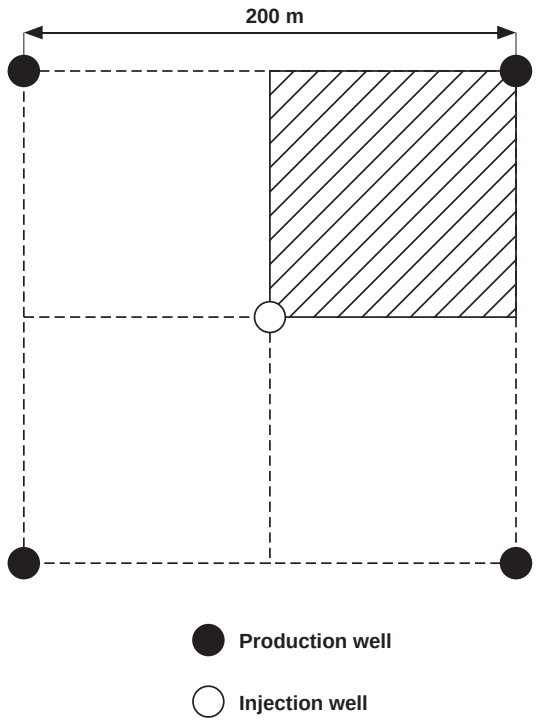

Figure 6 - Five-spot well stencil (pattern) for modeling a 1/4 symmetry subdomain (shaded) in the simulations of Case 2.

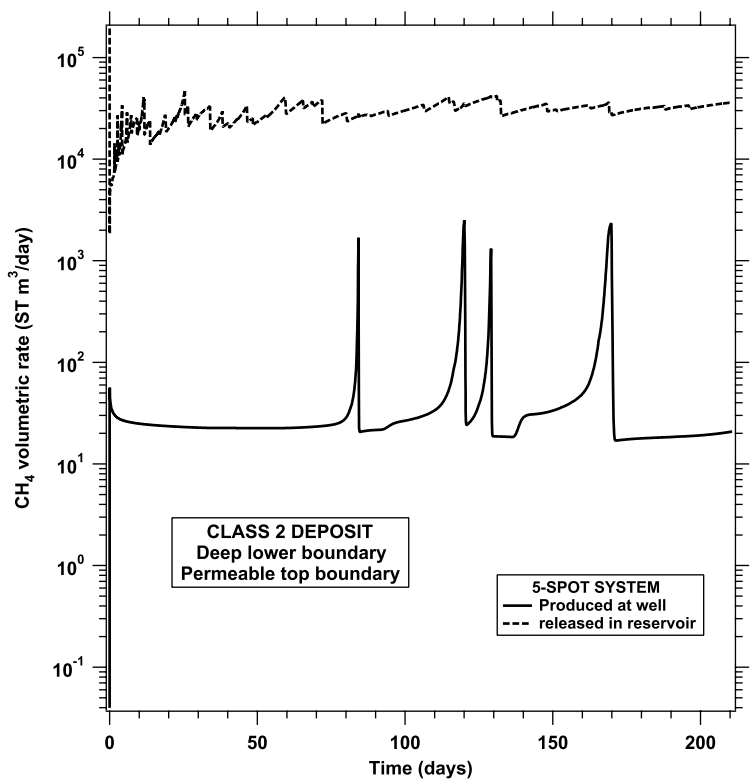

Figure 7. Evolution of the CH_4 production rate and of the rate of CH_4 release into the reservoir during production from a five-spot well system in Case 2 ($S_H = 0.75$).

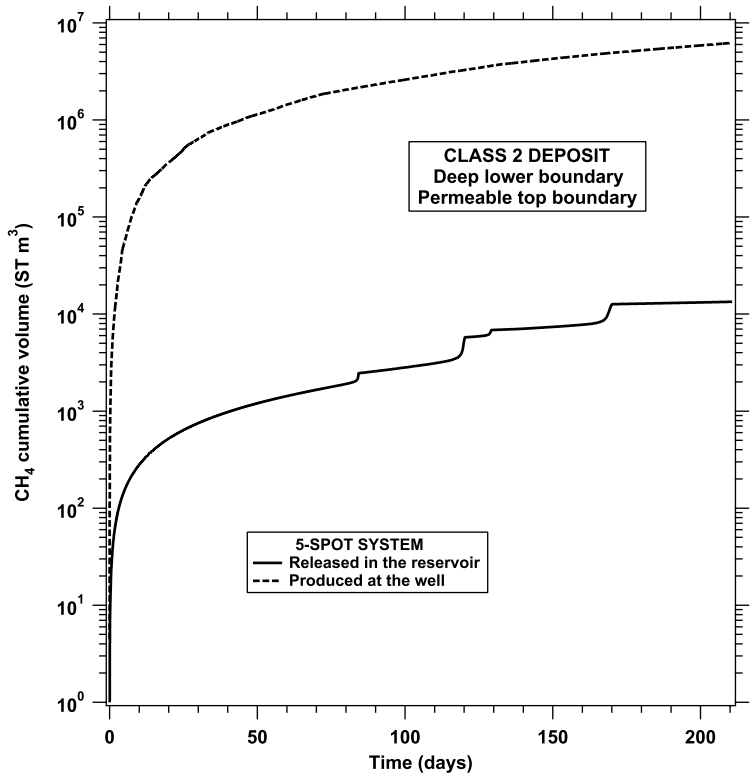

Figure 8. Evolution of the cumulative volumes of produced CH_4 and of CH_4 released into the reservoir during production from a five-spot well system in Case 2 ($S_H = 0.75$).

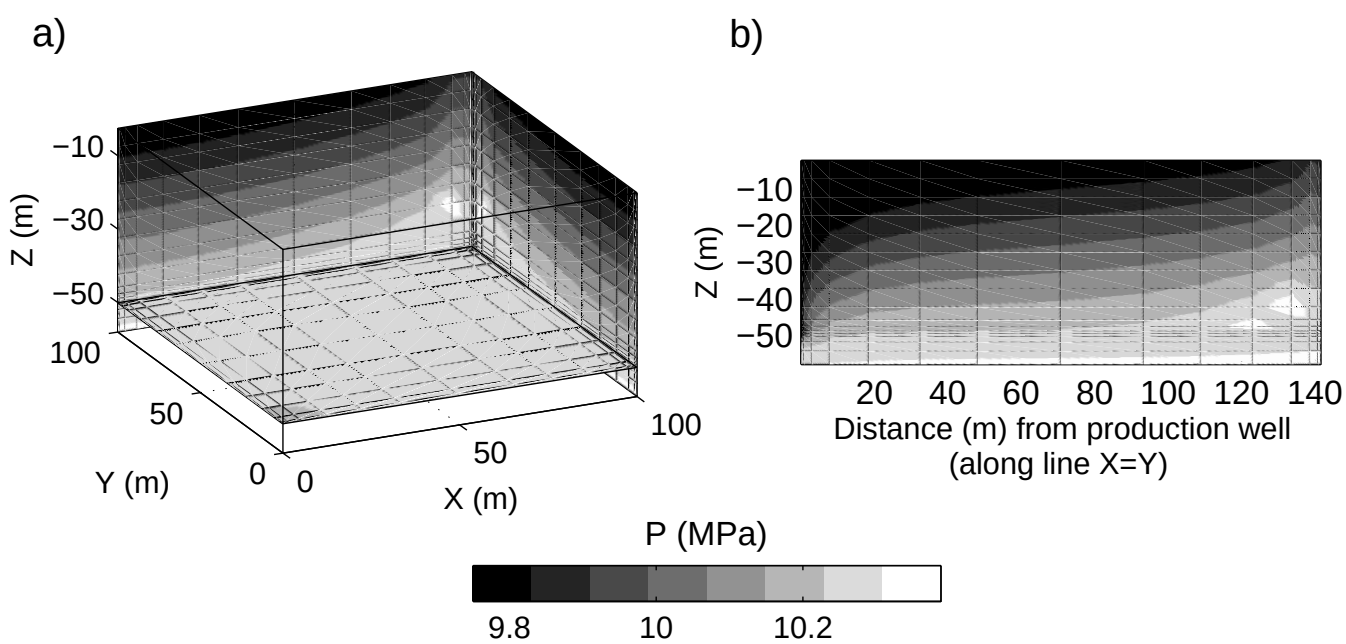

Figure 9. Pressure distributions (a) in the simulated 3-D domain and (b) in the plane defined by the injection and production wells in Case 2.

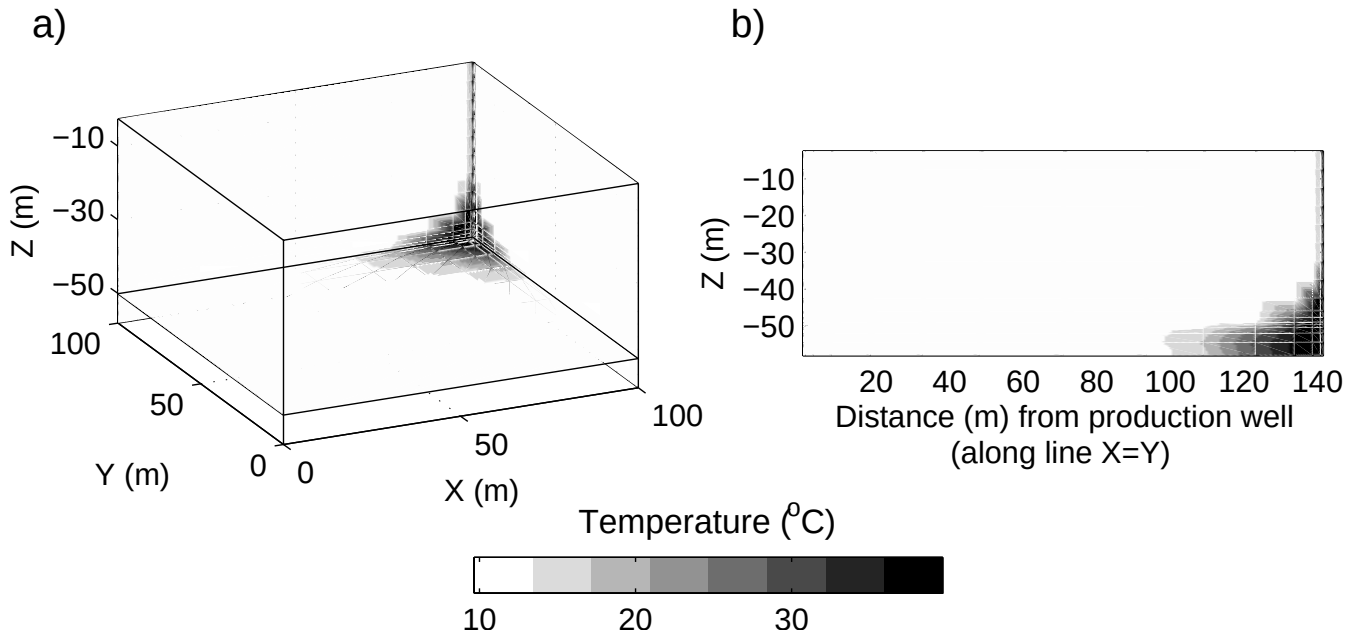

Figure 10. Temperature distributions (a) in the simulated 3-D domain and (b) in the plane defined by the injection and production wells in Case 2.

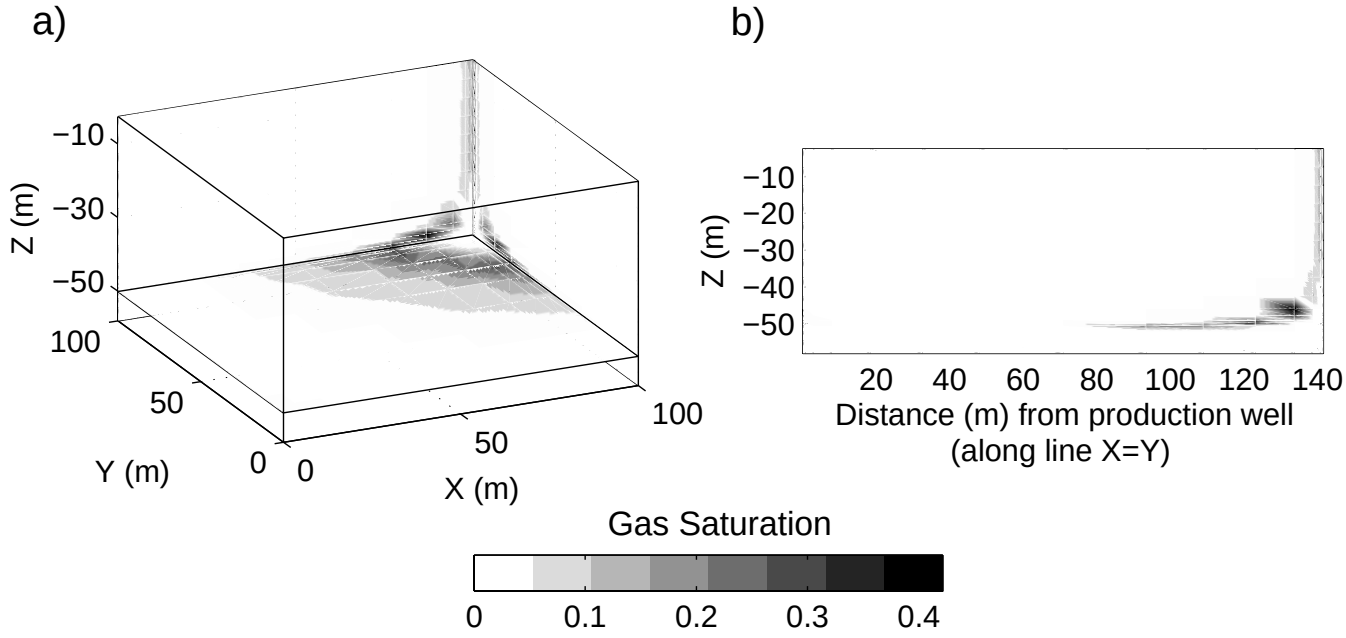

Figure 11. Gas saturation distributions (a) in the simulated 3-D domain and (b) in the plane defined by the injection and production wells in Case 2.

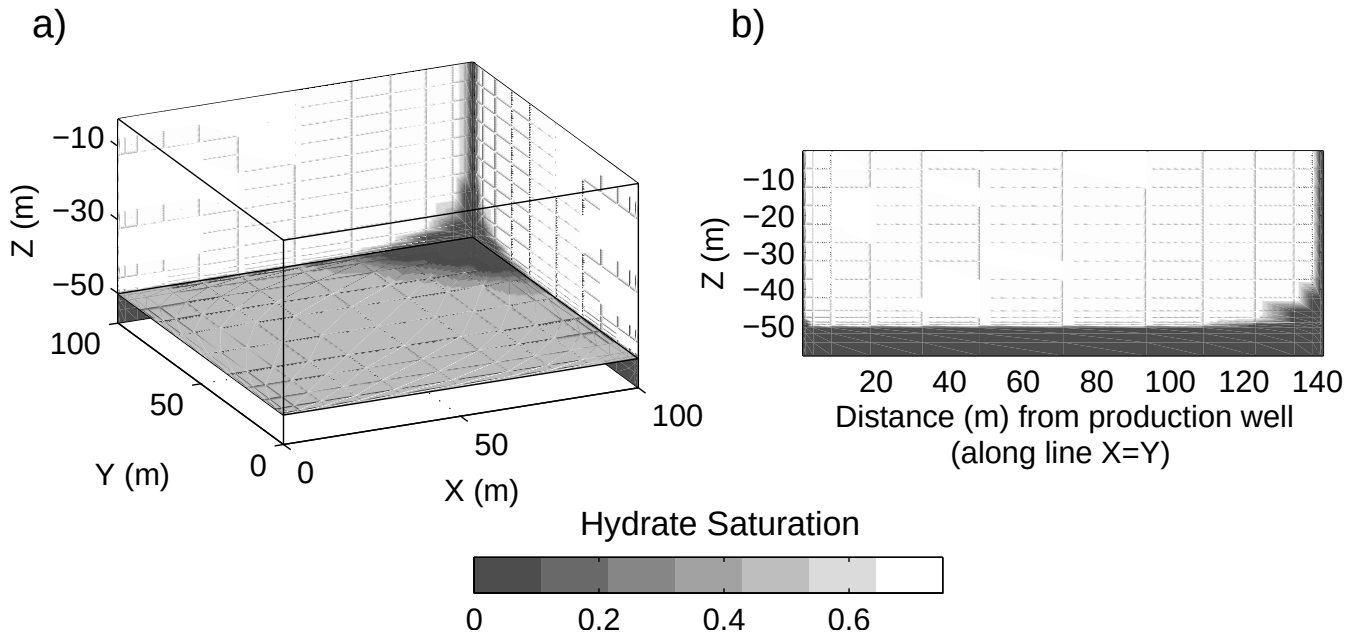

Figure 12. Saturation distributions of the gas hydrate (a) in the simulated 3-D domain and (b) in the plane defined by the injection and production wells in Case 2.

2007 R&D 100 AWARDS
ENTRY—TOUGH+HYDRATE (Berkeley Lab)

Appendix D

Selected Press Coverage

"Gas Hydrate Resource: Smaller But Sooner," Science, February 13, 2004

"From Athens to Mallik—In the Name of Science," NETL Methane Hydrate Newsletter, Winter 2004.

"Model Evaluates Production Potential of Methane Hydrates," Energy & Petrochem Engineering Standards News, April 21, 2006

"The National Methane Hydrates R&D Program," DOE/NETL Projects, August, 2006.

"TOUGH-Fx/HYDRATE V2.4 Announcement," NETL Methane Hydrate Newsletter, Spring 2005.

"Workshop on Integrating Modeling and USGS Laboratory Studies of Gas Hydrates," USGS Sound Waves Monthly Newsletter, September 2005.

at least two animal species, they concluded, and they should run long enough to pick up enhancement even if it happens many months after vaccination. Some said they would like to see such trials completed before the start of phase I clinical testing—small-scale safety testing in, say, a few dozen humans. But the meeting participants eventually accepted the fact that China—at greater risk of a repeat outbreak and under political pressure to push ahead—will start phase I ahead of the rest of the world. Wei He insists that safety will not suffer, saying his team is committed to studying disease enhancement before it expands its studies to include a large number of vaccinees.

Although Fauci thinks that "individual cases" of SARS may continue to appear from time to time, he expects that China's increased vigilance and greater willingness to share data with outside experts will prevent a new epidemic this year. For now, he says, as drug and vaccine development move along, standard infection-control measures should be stressed "more than anything else." But if public health measures do succeed in suppressing the virus, as everyone hopes, that poses another obstacle to testing a SARS vaccine. In effect it is "impossible" to do clinical tests of efficacy without "many, many cases somewhere in the world," says Chiron's Rappuoli.

There is one other possibility for testing vaccines without an outbreak. Faced with the prospect of rare bioterrorism diseases, the U.S. Food and Drug Administration (FDA) in 2002 adopted the so-called animal rule, which states that drugs and vaccines can be approved based on animal data alone. The FDA rule has stringent conditions, however. For instance, the animal model's pathology has to resemble that of the human disease.

Whether a SARS vaccine could meet those conditions remains to be seen, FDA's Mark Abdy told meeting participants. But vaccine developers say they're counting on FDA being somewhat flexible when it comes to fighting SARS.

–ELIOT MARSHALL AND MARTIN ENSERINK

With reporting by Dennis Normile in Tokyo and Ding Yimin in Beijing.

Energy

Gas Hydrate Resource: Smaller But Sooner

Although methane trapped in a peculiar subterranean ice is no energy panacea, new tests in the Arctic show that the first commercial production of gas hydrates may not be that far off

The yellow gas flame lighting the high-Arctic night back in early 2002 may have looked like just another sign of industrialization in the far north. But it was the first flicker of a potential new energy source: methane trapped molecule by molecule in subsurface ice.

The flare came from the first effort to produce a controlled stream of gas from these strange hydrates—an energy source perhaps twice as abundant as all the world's known oil, gas, and coal combined. The results, released late last year, indicate that it will be at least feasible to produce energy from these sources. Indeed, all that drillers need in order to start drawing on gas hydrates as an energy supply, say many observers, is a gas pipeline into the Canadian or Alaskan Arctic.

At the same time, geologists are adding a dose of realism to the good news: Recent surveys indicate that all but a few percent of the great vastness of gas hydrates will likely remain beyond reach indefinitely. Most deposits are simply spread too thinly for economical recovery. And even the small proportion concentrated in the most geologically and economically propitious locations faces a decades-long road before it will make a significant contribution to any one country's energy needs. An energy bonanza of gas hydrates now seems unlikely, but a modest new energy source is closer to reality.

Known to be on both land and sea since the 1970s from chance encounters while drilling for oil and conventional gas, gas hydrate—"the ice that burns"—is by far the most exotic of energy deposits. It forms when methane from organic decomposition comes together with water at low enough temperatures and high enough pressures to trap individual gas molecules within atomic-scale crystalline cages of water ice. It has been found as layers, nodules, and pore infillings on and beneath the sea floor in deeper waters around the world and in the permafrost areas of the Arctic.

A light of hope. Burning methane in the Canadian Arctic is the first ever produced from subsurface gas-containing ice called hydrate.

CREDIT: GEOLOGICAL SURVEY OF CANADA

No one knows how much gas hydrate there is in the world within an order of magnitude or so, but everyone's numbers are big. Paleoceanographer Gerald Dickens of Rice University in Houston, Texas, considered what reasonable uncertainties might be attached to the more central of the wide range of estimates and came up with a likely range of 10,500 to 42,000 trillion cubic meters (tcm). That global estimate compares with the 368 tcm of natural gas thought to be recoverable from all of the world's natural gas deposits. If just 1% of that hydrate could be made to give up its gas, the world would be awash in a clean-burning fuel that yields the least greenhouse gas of any fossil fuel.

Such best guesses by geologists have been enough to excite growing interest in gas hydrates as an energy source, but even as world hydrate research budgets ramped up toward $75 million per year, scientists didn't know if it would ever be possible to get any gas out of hydrates on a commercial scale. Whenever drillers brought a chunk of hydrate-laden sediment to the surface, it would sizzle with escaping gas as the reduced pressure and higher temperature destabilized the hydrate. You could even ignite the gas. But could hydrates be made to give up their gas in situ so that the methane could be piped to the surface?

Conventional gas simply gushes out of the cracks and pores of "solid" rock when a well is drilled through it. But it wasn't clear that hydrate de-

posits would be permeable enough for the required heat or reduced pressure to permeate them from a borehole. Nor was it clear whether they would be permeable enough to let any released gas out. So an international consortium of six countries, led by Japan and Canada, drilled a test well in the Mackenzie delta in far northwest Canada, where a rich gas hydrate deposit had been discovered in 1972 during drilling for deeper, conventional gas. The $22.5 million Mallik project would scientifically characterize the hydrate deposit and then try to produce a small amount of gas.

As announced at a December meeting* and discussed at this week's annual meeting of AAAS (the publisher of *Science*), the first controlled attempt to produce gas from a hydrate well was a success. "We weren't even sure if we'd produce gas, but we did," says Scott Dallimore of the Geological Survey of Canada in Sidney, British Columbia, a principal investigator (PI) on the project. When he and his team reduced the pressure on meter-long sections of well penetrating hydrate-rich sand and gravel, gas came out of the hydrate and flowed up the well. When they circulated warm water through the well, gas came up with the recirculating water.

The Mallik tests "have shown us that gas can be produced from hydrates," says chemical engineer E. Dendy Sloan of the Colorado School of Mines in Golden. "We just have to be smart about how we do it." The success comes in large part because the Mallik hydrates "are more permeable than we expected," says co-PI Timothy Collett of the U.S. Geological Survey (USGS) in Denver. Enough open pore space remained after hydrates formed between the sand grains that the reduced pressure was felt far into the hydrate deposit, allowing the gas to escape. The deposits even contain natural fractures that help conduct gas, the researchers found, and new fractures can be created by pressurizing the well.

The amounts of hydrate gas produced at Mallik were, by design, tiny. But the findings, plugged into simulations of hydrate production under a variety of geologic conditions, indicate that "you can get very high production rates," says Collett. So far, the most productive case simulated in computer models considered a well-known gas field on the North Slope of Alaska. There, as at Mallik, deep, conventional gas deposits that formed from heat-generated methane have been slowly leaking gas that rises to form hydrates at shallow depths.

In computer simulations using the Mallik results, says Collett, producing gas from the underlying conventional reservoir eventually drops the pressure on the hydrates, releasing gas from them that follows the conventional gas up the well. Simulated flow rates reach a competitive multimillions of cubic meters per day. In the first 20 years of simulated production, half the gas produced is from the hydrates.

Although these observation-based simulations are a major milestone, the Mallik results are "one step forward with a long way to go," says Collett. "The tests were all short duration." And there was an abrupt decrease in gas production during the thermal test that is not yet understood. "We're still a significant ways from having a full understanding of the economics" of gas hydrates, he says. Among the remaining questions, he adds, is how many deposits are as rich as Mallik.

The mother lode. Sand and gravel from a kilometer beneath the Arctic surface is laced with gas-charged hydrate (white infilling).

CREDIT: TOM MROZ/GEOLOGICAL SURVEY OF CANADA

Not many, it seems. Mallik was chosen for the first production test precisely because it is one of the richest hydrate deposits known. Between depths of 890 meters and 1106 meters, there are at least 10 hydrate-rich layers, averaging 10 meters thick, in which hydrate fills 80% to 90% of the commodious space between sand grains. Most hydrate deposits are not as well endowed. USGS has estimated that the U.S. offshore contains 10,200 tcm of gas in hydrates, but "a very high percentage of that" is found at concentrations of 2% to 3%, says Collett. And even that dispersed hydrate is locked up in low-permeability clays rather than sands. "When we look at the economics [of such deposits], it's very minimal," he says.

Drillers looking for economically attractive hydrates turn first to the Arctic. As part of the U.S. Department of Energy's (DOE's) $9.5-million-per-year gas hydrate program, drillers late last month began extending a well into the hydrates of the Tarn gas field on the North Slope of Alaska. Production tests there must await thorough characterization of the deposits, but Collett estimates that the hydrates of this field and others like it in Alaska could ultimately add about 1 tcm of gas to the United States' 6.2 tcm of gas thought to remain to be recovered. All Alaska lacks "is a gas pipeline to bring it to market," says Arthur Johnson of Hydrate Energy International in New Orleans, chair of DOE's hydrate advisory committee.

No Alaska gas pipeline is in the offing—hydrate gas has not yet changed the perceived economics there—but prospects for one from Canada's Mackenzie delta "are very good," says Dallimore. The lure of abundant conventional gas could bring a pipeline to gas hydrates there in 5 to 10 years, he adds; hydrate production might follow in another 5 to 10 years. Pipelines to hydrate-only regions are unlikely, given today's relatively low natural gas prices and likely higher costs of extracting hydrate gas.

Japanese researchers and drillers hope to be producing gas from hydrates even sooner, and from a tougher target. Prompted by Japan's need to import 99% of the oil and gas it consumes, they are in the third year of their 16-year Methane Hydrate Exploitation Program, which is funded at $50 million this year. Much of that money is going toward the current drilling of 30 exploratory holes in the Nankai trough just off southeast Japan. Earlier drilling had found 20% hydrate in a Nankai borehole that pierced sand—the sort of coarse-grained sediment required to accommodate lots of hydrate. Seismic surveying suggests that the current drilling will confirm an abundance of gas hydrates in the same area.

Although the first commercial production of gas from hydrates may begin within 10 or 15 years, hydrates will probably not make a significant contribution for at least 30 years, says Collett. He cites the example of the methane trapped in coal beds. The first wells dedicated to extracting coal-bed methane were drilled 30 years ago, also with substantial DOE support. Now coal-bed methane is accounting for 8% of total U.S. natural gas production. Eight percent may not sound like a lot, but "if we didn't have that 8% this winter, we'd feel it," says Johnson. On a 30-year time scale, "I could see hydrates being commercially viable and one component of America's gas supply—not the dominant one, but without it we'd be in a lot of trouble."

–RICHARD A. KERR

With reporting by Dennis Normile.

* "From Mallik to the Future," 8–10 December 2003, Chiba, Japan. www.mh21japan.gr.jp/english/index.html

GEORGE MORIDIS

Staff Geological Scientist
Hydrogeology & Reservoir Dynamics Department
Lawrence Berkeley National Laboratory, Earth Sciences Division
Berkeley, CA
gjmoridis@lbl.gov

George Moridis is currently the Research Area Leader of the Transport Dynamics Group and a Principal Investigator in charge of gas hydrate studies. He is also responsible for the radionuclide transport studies of the proposed Yucca Mountain High Level Waste Repository, and for the development of the next generation of models for the simulation of subsurface processes. He is the author or co-author of 26 refereed publications, and of over 100 reports.

Spotlight on Research

From Athens to Mallik–In the Name of Science

George Moridis began his academic studies at the National Metsovion Technical University in Athens in his native Greece. He graduated with a B.S. (1979) and an M.S. (1980), both in chemical engineering.

George was fascinated by the subject of modeling physical systems, and had a chance to pursue this interest in his graduate studies for a second M.S. (1982) in agricultural engineering at Texas A&M University, where he worked on a model of water flow in a soil-plant system. His expanding interest in mathematical models and numerical simulation led him to pursue a PhD in reservoir engineering from Texas A&M.

Upon graduation in 1986, he joined the Food and Agriculture Organization of the United Nations (U.N.) where he was responsible for groundwater development in south and southeast Asia. In 1989 he returned to the United States and joined the faculty of the Civil Engineering Department at Texas A&M.

While at Texas A&M, he was responsible for the design and development of the largest dual-gamma attenuation system in the world (6ft x 6ft x 0.5 ft), designed for non-destructive studies of multiphase fluids in porous media while evaluating aggressive decontamination methods (such as hydraulic controls, steam injection, and the use of surfactants). In addition, he developed the Laplace Transform Finite Difference method, a new numerical method for solving of the equations of flow and transport in the subsurface.

George joined the Berkeley Lab in 1991. He has developed new analytical, semi-analytical, and numerical methods and new solvers for matrix equations that arise in numerical analysis. He has worked on geothermal and environmental restoration problems, and he has developed new technologies to isolate contaminants in the subsurface using a new generation of barrier fluids.

He received a patent for his Liquid Barrier Technology. This technology won the 1996 Best of What is New award in environmental technology (organized by *Popular Science* magazine). The technology was used to isolate radionuclides in the subsurface at Brookhaven National Laboratory. He received another patent for the development and use of magnetic fluids to guide and emplace liquids in the subsurface.

George has been working on hydrates since 1998, using a numerical model he developed (1) to evaluate a wide range of natural hydrate deposits in geologic systems, and (2) to develop appropriate production strategies.

He has used this numerical model for scoping calculations and the design of the first field test of gas production from hydrates at the Mallik site well (see "Mallik Partners…" story, this issue). The numerical model has also been used to design planned field experiments in the North Slope, Alaska, in DOE-funded projects led by Maurer/Anadarko and British Petroleum. He is using the field data from a North Slope test, conducted in early 2002, to validate the numerical model and to determine the values of important parameters. Along with colleagues Barry Freifeld, Tim Kneafsey, Liviu Tomutsa, and Yongkoo Seol, George is also involved in laboratory projects focusing on new techniques for the preparation of large-scale samples of hydrates (both pure and produced in situ within porous media), and on the use of X-ray computed tomography to non-destructively study hydrate dissociation and flow processes under controlled conditions.

George cannot hide his excitement about the opportunity to work on the cutting edge of hydrate research, and to be involved in the study of this challenging frontier resource.

Standards Store

Search for Standards by document number, titles and keywords.

Go

Include Title/Keyword

Search Help

Petrochemical Resources

Industry Home Page
Products & Solutions
Industry News
Newsletter
Literature
Web Seminars
Request a Price Quote

Top Documents

API STD 1104 - Welding Of Pipelines And Related Facilities
API SPEC 5L - Spec For Line Pipe
API STD 650 - Welded Steel Tanks For Oil Storage
API RP 14C - Recommended Practice For Analysis, Design, Installation, And Testing Of Basic Surface Safety Systems For Offshore Production Platforms
API STD 653 - Tank Inspection, Repair, Alteration, And Reconstruction

Worldwide Locations

Model Evaluates Production Potential of Methane Hydrates

April 21, 2006

The U.S. Department of Energy (DOE) developed the TOUGH-Fx/Hydrate program to help researchers and industry partners better understand an emerging natural gas resource: methane hydrates - frozen compounds of flammable methane gas trapped inside water molecules.

Purchase Standards, Codes & Regulations

Individual **Documents** from the Standards Store
For help, call
1-877-413-5184
Outside US/Canada call 303-792-2181

Complete **Collections** from IHS Specs & Standards
For help, call
1-888-752-0334
Outside US/Canada call 303-397-2892

Quote Request

"Small amounts of gas have been extracted from methane hydrate reservoirs in the past. However, obtaining quantities large enough for commercial production requires significant technological advances and additional research to further our fundamental understanding of these reservoirs," explained Kelly Rose, a project manager at DOE's National Energy Technology Laboratory (NETL). "Using an advanced tool like the TOUGH-Fx/Hydrate simulator to understand how methane hydrates behave in the natural environment is one way to overcome these obstacles."

TOUGH-FX/Hydrate simulates the behavior of hydrate-bearing geologic systems and evaluates appropriate hydrate production strategies for both permafrost and marine environments, including thermal stimulation, depressurization and dissociation induced and/or enhanced by inhibitors (such as brines and alcohols).

Since its public release in 2005, there has been considerable interest in the program, both domestically and abroad. Program licenses have been granted to 25 non-commercial organizations in 11 countries. Two major oil and gas companies have also purchased licenses - the first steps toward industry application. In all, DOE estimates that nearly 80 researchers now have access to the TOUGH-Fx/Hydrate program.

According to DOE, the program's strength lies in its wide-ranging scope, scale and applicability. The model can be used by laboratory scientists for fundamental research from the molecular to the reservoir level. It can also be run by industrial operators to conduct large-scale production studies using actual field data.

Once believed to exist only in the outer reaches of the solar system, large deposits of methane hydrates have been found in deepwater marine and permafrost sediment around the globe. If produced on a larger scale, the compound known as "fire ice" could more than double the U.S. natural gas resource base. Moving from concept to commercial production, however, will require ongoing investigation of this vast but complex natural resource.

"Continued academic inquiry and growing commercial use of the TOUGH-Fx/Hydrate program will help identify knowledge and technology gaps, evaluate different production scenarios and anticipate potential hazards for oil and natural gas operators," said Rose. "With this simulation program, researchers from around the world can better understand the future production potential of methane hydrate reservoirs and determine next steps in the overall R&D effort."

Source: U.S. Department of Energy (DOE).

ENERGY & PETROCHEM ENGINEERING STANDARDS NEWS

NRC Issues Letter on Inaccessible or Underground Electric Cables Feb 13, 2007
The Nuclear Regulatory Commission (NRC) issued a generic letter asking all operators of U.S. nuclear power plants for information on how they inspect or monitor a plant's buried or otherwise inaccessible electrical cables to ensure safe operation.

ASTM Int'l Offers Interlaboratory Crosscheck Program on Fuel Ethanol Feb 12, 2007
A new interlaboratory crosscheck program (ILCP) on fuel ethanol will be offered by the ASTM International Proficiency Testing Center starting in August 2007.

NRC Approves Final Rule Amending Security Requirements Feb 5, 2007
The U.S. Nuclear Regulatory Commission (NRC) approved a final rule that enhances its security regulations governing the design basis threat (DBT) - the latest in a series of actions addressing security at nuclear power plants.

ABOUT NETL

KEY ISSUES & MANDATES

ONSITE RESEARCH

TECHNOLOGIES

Oil & Natural Gas Supply
- E&P Technologies
- Future Supply
- T&D and Refining
- Contacts

Coal & Power Systems
Carbon Sequestration
Hydrogen & Clean Fuels
Technology Transfer

ENERGY ANALYSES

SOLICITATIONS & BUSINESS

CAREERS & FELLOWSHIPS

NEWSROOM

CONTACT NETL

The National Methane Hydrates R&D Program

DOE/NETL Methane Hydrate Projects

TOUGH+/HYDRATE - Hydrate Reservoir Simulator Development

FWP-G308 formerly ESD00-021 and FWP-G302

Project Goal

The primary objective of this project is to develop and maintain a reservoir model that simulates the behavior of hydrate-bearing geologic systems and evaluates appropriate hydrate production strategies for both permafrost and marine environments, including thermal stimulation, depressurization and dissociation induced and/or enhanced by inhibitors (such as brines and alcohols).

Background

TOUGH+/HYDRATE, the most recent implementation of the TOUGH-Fx/HYDRATE code, is a new code, developed by LBNL that simulates the behavior of hydrate-bearing geologic systems. By solving coupled equations of mass and heat balance, TOUGH+/HYDRATE can model the non-isothermal gas release, phase behavior and flow of fluids and heat under conditions typical of common, natural CH4-hydrate bearing deposits (i.e., in the permafrost and in the deep ocean sediments) in complex formations.

TOUGH+/HYDRATE v1.0 includes both an equilibrium and kinetic model of hydrate formation and dissociation. The model accounts for heat and up to four mass components, i.e., water, CH4, hydrate, and water-soluble inhibitors such as salts or alcohols. These are portioned among four possible phases (gas phase, liquid phase, ice phase, and hydrate phase) and up to five components (heat, hydrate, water, CH4, and water-soluble inhibitors). Hydrate dissociation or formation, phase changes and the corresponding thermal effects are fully described, as are the effects of inhibitors. The model can describe all possible hydrate dissociation mechanisms, i.e., depressurization, thermal stimulation, salting-out effects, and inhibitor-induced effects.

TOUGH+/HYDRATE is the first member of TOUGH+, the successor to the TOUGH2 family of codes for multi-component, multiphase fluid and heat flow developed at the Lawrence Berkeley National Laboratory. It is written in standard FORTRAN 95, and can be run on any computational platform (workstation, PC, Macintosh) for which such compilers are available. TOUGH+/HYDRATE is fully backward compatible with the formats of the input files of conventional TOUGH2.

During this project, different mechanisms and strategies for gas production from hydrate reservoirs were explored. The results tend to indicate that methane production from methane hydrates is technically feasible and has significant potential. Both depressurization and thermal stimulation appear to be mechanisms that are capable of producing substantial amounts of methane gas, and that their effectiveness can be further enhanced by inhibitors.

It is not possible to reach a definitive judgment on the relative advantages of these methods, however, due to the lack of information on the properties of hydrate reservoirs and their thermodynamic behavior under field conditions. Further modeling efforts will be possible once data is available on permeability, porosity and saturation of natural methane deposits, kinetic behavior of hydrates, type of formation/dissociation reactions in natural hydrate accumulations (equilibrium vs. kinetic), hysteretic behavior of formation and dissociation curves, relative permeability of hydrate formations, hydrocarbon solubility near the hydration point, and hydrate thermal properties. While the available data allow a determination of model sensitivity and the relative importance of various reservoir and production parameters, data representative of actual reservoir conditions must be obtained for predictive applications.

Performer

Lawrence Berkeley National Lab – model modifications and runs, project management

Location

Berkeley, CA 94720

Potential Impact

TOUGH+/Hydrate is designed exclusively to model hydrate reservoir behavior and production potential. This allows users to more accurately predict the behavior of hydrates and hydrate-bearing geologic systems, in the laboratory or field, from the pore to regional scale. The model simulates both kinetic and equilibrium hydrate formation & dissociation and uses state of the art, underlying principles, physics & thermodynamics.

This model will allow commercial operators to assess, identify, and predict reservoir performance/production for various prospects and provide data for detailed economic assessment of potential plays. The model will also help operators identify uncertainties and risks for a particular prospect or project.

Accomplishments:

TOUGH+/HYDRATE is the most recent implementation of the TOUGH-Fx/HYDRATE code which was formerly released during the spring 2005. This simulator replaces, updates, and modifies the hydrate reservoir simulator work conducted previously on the EOSHYDR module for TOUGH2.

- Previously developed EOSHYDR2, an extended version of the EOSHYDR module for the TOUGH2 general-purpose simulator.
- Previously explored different mechanisms and strategies for gas production from methane hydrate reservoirs via a set of test problems.

TOUGH+/Hydrate is available from LBNL[external site] for commercial and non-commercial users. Non-commercial licenses are available at no cost to academic and research institutions, and for use on U.S. Government-sponsored research projects. For more information on obtaining a license for TOUGH+/Hydrate please see the "additional information" section below.

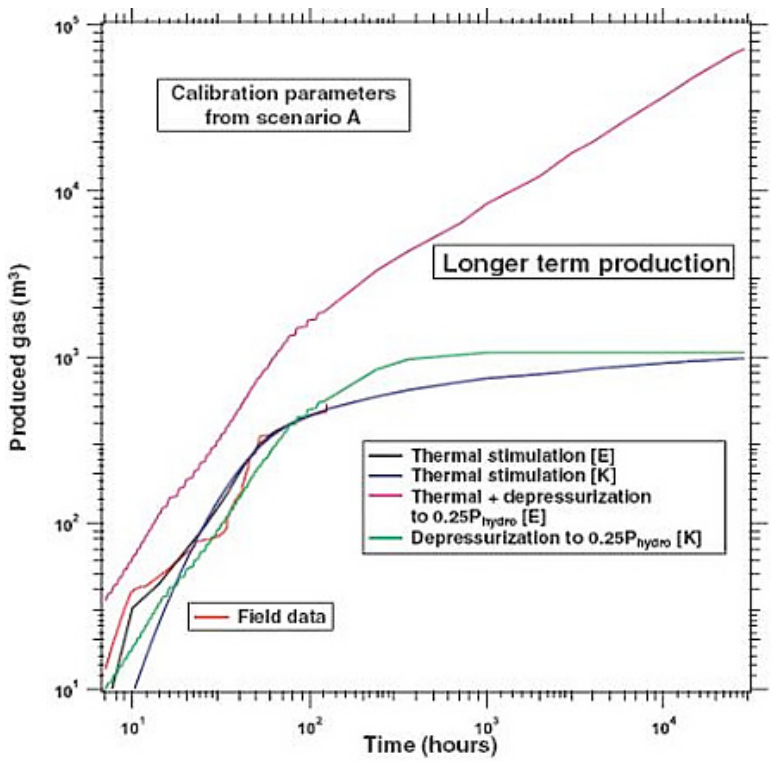

Predictions of long-term production for the JAPEX/JNOC/GSC et al. Mallik 5L-38 gas hydrate production research well (from Moridis et al. March 2005)

Current Status and Remaining Tasks

Ongoing work includes:

- Modification and finalization of the freeware version of TOUGH+/Hydrate, called HydrateResSim and the associated User's Manual
- Participation in the NETL-led code hydrate reservoir simulator code comparison study
- Laboratory Studies To Quantify Hydrate Processes in Reservoirs

Project Start: June 30, 2000
Project End: September 30, 2006

DOE Contribution: $839,000
Performer Contribution: $0

Contact Information:
NETL – Kelly Rose (Kelly.Rose@netl.doe.gov or 304-285-4157)
LBNL – George Moridis (gjmoridis@lbl.gov or 510-486-4746)

Additional Information:
Project Report August 2006: Gas Production Potential of Disperse Low-Saturation Hydrate Accumulations in Oceanic Sediments [PDF-1.05MB]

Licensing information for TOUGH+/HYDRATE and PetraSim, a pre/post processor for use with the model.

Freeware version of TOUGH+/Hydrate, called HydrateResSim and the associated User's Manual

Project Factsheet [PDF-1605KB]

Topical Report - Numerical Studies of Gas Production from Several CH4-Hydrate Zones at the Mallik Site [PDF-185KB]

Pertinent Publications:
Moridis, G.J. and M. Kowalsky, Gas Production from Unconfined Class 2 Hydrate Accumulations in the Oceanic Subsurface, in Economic Geology of Natural Gas Hydrates, M. Max, A.H. Johnson, W.P. Dillon and T. Collett, Editors, Kluwer Academic/Plenum Publishers, In Press (LBNL-57299, 2005).

Moridis, G.J. , T.S. Collett, S.R. Dallimore, T. Inoue and T. Mroz, Analysis and Interpretation of the Thermal Test of Gas Hydrate Dissociation in the JAPEX/JNOC/GSC et al. Mallik 5L-38 Gas Hydrate Production Research Well, in Geological Survey of Canada, Bulletin 585, S.R. Dallimore and T. Collett, Editors, In Press (LBNL-57296, 2005).

Moridis, G.J., Y. Seol and T. Kneafsey, Studies of Reaction Kinetics of Methane Hydrate Dissociation in Porous Media, LBNL-57298, 2005 (to appear in the Proceedings of the 5th International Conference on Gas Hydrates, Trondheim, Norway, June 13-16, 2005).

T. Kneafsey, L. Tomutsa, G.J. Moridis, Y. Seol, B. Freifeld, C.E. Taylor and A. Gupta, Methane Hydrate Formation and Dissociation in Partially Saturated Sand – Measurements and Observations, LBNL-57300, 2005 (to appear in the Proceedings of the 5th International Conference on Gas Hydrates, Trondheim, Norway, June 13-16, 2005).

Gupta, A., E.D. Sloan, T. Kneafsey, L. Tomutsa and G.J. Moridis, Modeling Methane Hydrate Dissociation X-Ray CT Data Using a Heat Transfer Model, (to appear in the Proceedings of the 5th International Conference on Gas Hydrates, Trondheim, Norway, June 13-16, 2005).

G.J. Moridis, Numerical Simulation Studies for the Hot Ice Well, project completion report, 2004 (LBNL number pending)

G.J. Moridis, Numerical Studies of Gas Production from Oceanic Hydrate Accumulations, paper presented at the AAPG 2004 Hedberg Conference, Vancouver, Canada, September 12-16, 2004 (LBNL number pending)

Kneafsey, T.J., B.M. Freifeld, L. Tomutsa, Y. Seol, H. Elsen, "Measurements on laboratory core-scale sediment/hydrate samples to predict reservoir behavior," AAPG Hedberg Conference, Gas Hydrates: Energy Resource Potential and Associated Geological Hazards, September 12-16, 2004, Vancouver, BC, Canada, LBNL-54863

S. Hancock, T. Collett, S. Dallimore, T. Satoh, T. Inoue, B. Weatherill, G. Moridis, E. Huenges, J. Henninges, D. Carle, Overview of Production Test Results from the Japex/JNOC/GSC Mallik 5L-38 Gas Hydrate Research Well, paper presented at the AAPG 2004 Hedberg Conference, Vancouver, Canada, September 12-16, 2004.

Freifeld, B. M., Kneafsey, T.J., and Rack, F., On-Site Geologic Core Analysis Using a Portable X-ray Computed Tomographic System. Journal of the Geological Society, LBNL-55698, 2004.

S. Hancock, T. Collett, M. Pooladi-Darvish, S. Gerami, G. Moridis, T. Okazawa, K. Osadetz, S. Dallimore, B. Weatherill, A Preliminary Investigation on the Economics of Onshore Gas Hydrate Production Based on the Mallik Field Discovery, paper presented at the AAPG 2004 Hedberg Conference, Vancouver, Canada, September 12-16, 2004.

Moridis, G.J., T. Collett, S. Dallimore, T. Satoh, S. Hancock and B. Weatherhill, Numerical Studies Of Gas Production From Several Methane Hydrate Zones At The Mallik Site, Mackenzie Delta, Canada, Journal of Petroleum Science and Engineering, 43, 219-239, 2004.

Moridis, G.J., Numerical Studies of Gas Production from Class 2 and Class 3 Hydrate Accumulations at the Mallik Site, Mackenzie Delta, Canada, SPE Reservoir Evaluation and Engineering, 7(3), 175-183, 2004.

Moridis, G.J. and T. Collett, Gas Production from Class 1 Hydrate Accumulations, in Recent Advances in the Study of Gas Hydrates, C. Taylor and J. Qwan, Editors, Kluwer Academic/Plenum Publishers (publication date: October 2004).

G.J. Moridis, Y. Seol, T.S. Collett, S.R. Dallimore, T. Inoue, T. Mroz, and J.Henninges, Thermal Properties of Hydrates from Temperature Data Analysis of an Isolated Formation Interval in the 5L-28 Mallik Research Well, Mallik Consortium Scientific Meeting, Chiba, Japan, December 2003 (in review for publication in proceedings, LBNL number pending).

G.J. Moridis, Y. Seol, T.S. Collett, S.R. Dallimore, T. Inoue, T. Mroz, and J.Henninges, Analysis and Interpretation of the Thermal Test of Hydrate Dissociation in the 5L-28 Mallik Research Well, Mallik Consortium Scientific Meeting, Chiba, Japan, December 2003 (in review for publication in proceedings, LBNL number pending).

Moridis, G.J., Numerical Studies of Gas Production From Methane Hydrates, SPE Journal, 32(8), 359-370, 2003 (SPE paper 87330 - LBNL-49765).

Freifeld, B. M. and T.J. Kneafsey, Development of a Portable X-ray Computed Tomography Imaging System, presented to the Joint Industrial Partnership, 2003.

Moridis, G.J. and T. Collett, Strategies for Gas Production From Hydrate Accumulations Under Various Geologic Conditions, LBNL-52568, presented at the TOUGH Symposium 2003, Berkeley, CA, May 12-14, 2002.

Moridis, G.J. and J. Qwan, Numerical Studies of Hydrate Preservation in Cores and of Gas Production from Permafrost Hydrate Accumulations, LBNL-52828, June 2003.

Moridis, G.J., and T. Collett, Evaluation of Gas Production From Class 1 Deposits of Hydrates, LBNL-52827.

Freifeld, B., T. Kneafsey, J. Pruess, P. Reiter, L. Tomutsa, X-ray Scanner for ODP Leg 204: Drilling Gas Hydrates on Hydrate Ridge, Cascadia Continental Margin, July 31, 2002 Progress Report, LBNL-51327

Moridis, G.J., Numerical Studies of Gas Production From Methane Hydrates, presented at the SPE 2002 Gas Technology Symposium, April 29-May 2, 2002, Calgary, Alberta, Canada (SPE paper 75691 - LBNL-49765).

Tomutsa, L., B. Freifeld, T.J. Kneafsey, and L.A. Stern, X-ray Computed Tomography Observation of Methane Hydrate Dissociation, SPE Gas Technology Symposium held in Calgary, Alberta, Canada, 30 April–2 May 2002, SPE 75533, LBNL-49580

Moridis, G.J., T. Collett, S. Dallimore, T. Satoh, S. Hancock and B. Weatherhill, Numerical Studies Of Gas Production Scenarios Hydrate Accumulations at the Mallik Site, Mackenzie Delta, Canada, 4th International Conference on Gas Hydrates, Yokohama, Japan, May 19-23, 2002, Proceedings, Vol. 1, pp. 239-244 (LBNL -49764).

Freifeld, B.M., T.J. Kneafsey, L. Tomutsa, L.A. Stern, and S.H. Kirby, “Use of X-Ray Computed Tomographic Data for Analyzing the Thermodynamics of a Dissociating Porous Sand/Hydrate Mixture,” Proceedings of the Fourth International Conference on Gas Hydrates, Yokohama, May 19-23, 2002, pp. 750-755, LBNL-49859

Moridis, G.J., Numerical Simulation Studies of Thermally-Induced Gas Production From Hydrate Accumulations With No Free Gas Zones at the Mallik Site, Mackenzie Delta, Canada, presented at the SPE 2002 Asia Pacific Oil and Gas Conference and Exhibition, Melbourne, Australia, October 8-10, 2002 (SPE paper 77861 – LBNL-50256).

Moridis, G.J., T. Collett, S. Dallimore, T. Satoh, S. Hancock and B. Weatherhill, Numerical Studies Of Gas Production From Several Methane Hydrate Zones At The Mallik Site, Mackenzie Delta, Canada, LBNL-50257, November 2002.

Moridis, G. J., Numerical Simulation of Gas Production From Hydrate Accumulations, LBNL Report No. 47998, May 2001.

Moridis, G. J., Analysis of Gas Production Scenarios From Hydrate Zones A through C of the Mallik Fields, LBNL Report No. 47999, May 2001.

Moridis, G. J., Analysis of Gas Production Scenarios From Hydrate Target Zones 1 and 2 of the Mallik Field, LBNL Report No. 48000, May 2001.

Moridis, G.J., 2002. Numerical Studies of Gas Production from Methane Hydrates, paper presented at the SPE Gas Technology Symposium, Calgary, Alberta, April 30 - May 2, SPE 75691.

Moridis, G.J., 2002. Numerical Simulation of Thermally-Induced Gas Production from Hydrate Accumulations with No Free Gas Zones at the Mallik Site, Mackenzie Delta, Canada, paper presented at the SPE Asia Pacific Oil and Gas Conference and Exhibition, Melbourne, Australia, Oct 8 - 10, SPE 77861.

Norway ICGH Meeting

The Fifth International Conference on Gas Hydrates (ICGH 5) will take place at the Royal Garden Hotel in Trondheim, Norway, on June 13-16. It is expected that more than 300 flow assurance and gas hydrate specialists from around the world will be in attendance to witness 24 oral presentations and 220 poster presentations. The conference is organized around the following five topical sessions: Kinetics and Transport Phenomena; Structure and Physical Properties; Exploration, Resources and Environment; Industrial Applications and; Thermodynamic Aspects. Details and registration are available on the Conference website at http://www.icgh.org/.

Reservoir Simulator Publicly Released

LBNL's hydrate reservoir simulator (TOUGH-Fx/HYDRATE v1.0) is now publicly available for licensing. TOUGH-Fx/HYDRATE models non-isothermal gas release, phase behavior and flow of fluids and heat in complex geologic media. The code can simulate production from natural methane hydrate deposits in permafrost and in deep ocean sediments, as well as laboratory experiments of hydrate dissociation/formation in porous/fractured media. TOUGH-Fx/HYDRATE v1.0 includes both an equilibrium and a kinetic model of hydrate formation and dissociation. For more information about the model and how to obtain a license, please visit http://www.netl.doe.gov/scngo/Natural%20Gas/hydrates/index.html and select "FWP-G308" from the lefthand menu "DOE Projects" list or contact: Seth Rosen, Senior Licensing Associate, Technology Transfer Department, Lawrence Berkeley National Laboratory, Phone (510) 486-4303 or vial e-mail (SBRosen@lbl.gov).

PetraSim V2.4 for TOUGH-Fx/HYDRATE

PetraSim Version 2.4 - is an interactive preprocessor and postprocessor tool to rapidly develop models and view results for TOUGH-Fx/HYDRATE. PetraSim Version 2.4 can be downloaded for a free 30 day trial at: www.petrasim.com. Example input, output, and manual files can be downloaded at: http://www.thunderheadeng.com/petrasim/help/tough/examples.htm . For additional information please contact Thunderhead Engineering at: Thunderhead Engineering Consultants, Inc., 1006 Poyntz Ave., Manhattan, KS 66502-5459, Phone (785) 770-8511 (or via e-mail at sales@thunderheadeng.com).

Committee to Meet During AAPG Convention

During this year's annual AAPG convention in Calgary, a meeting of the Energy Minerals Division's Gas Hydrate Committee has been scheduled for Tuesday evening, June 21, from 5:30 to 8:00 pm at the Hyatt Regency (Imperial Rooms 1 and 2). Several presentations are planned that focus on recent developments in the gas hydrate field. In addition, plans will be made for additional activities by the committee and its members. Individuals interested in attending shuld contact Committee Chair Art Johnson at art_johnson@hydrate-energy.com/.

Meetings

Workshop on Integrating Modeling and USGS Laboratory Studies of Gas Hydrates

By Debbie Hutchinson
September 2005

in this issue:
previous story | next story

Above: Fred Wright (Geological Survey of Canada) presents his thought-provoking ideas summarizing the issues and linkages between gas-hydrate modeling and laboratory research. The workshop took place at the USGS Energy Resources Team Conference Room at the Federal Center in Lakewood, CO. Photograph by **Bill Winters**. [larger version]

On August 2-3, the U.S. Geological Survey (USGS) hosted a workshop in Denver, CO, to determine how its gas-hydrate laboratory studies could be more closely aligned with a growing number of modeling studies that simulate gas hydrates within geologic and petroleum systems. This strategic focus on specific models is a response to several gas-hydrate-related computer-modeling codes currently being used in the hydrate community (for example, TOUGH-Fx/hydrate from Lawrence Berkeley National Laboratory; CGM STARS from commercial hydrocarbon exploration; MH21 from the University of Tokyo, Japan; and STOMP-HYD from the Pacific Northwest National Laboratory). The workshop was intended not to suggest that laboratory results are relevant only to constraining or validating these types of models, but rather to identify those key parameters that USGS laboratory experiments could provide to help further our understanding of gas hydrates in the natural environment.

The workshop was convened by USGS scientists **Debbie Hutchinson** (Coastal and Marine Geology, Woods Hole, MA) and **Tim Collett** (Energy Resources, Denver). Twenty-nine scientists representing the USGS, the Geological Survey of Canada, the U.S. National Laboratories, industry, academia, the U.S. Department of Energy (DOE), and the Minerals Management Service (MMS) participated in the meeting. Covering a broad range of expertise, they included laboratory experimentalists, numerical modelers, field scientists, and Federal research managers.

The day-and-a-half meeting began with a day of presentations and

Sound Waves
September 2005

Mailing List:
Sign up to receive monthly email updates:
your email address
Sign Up

print this issue

in this issue:
Fieldwork
Cover Story:
USGS Provides Aid in the Aftermath of Hurricane Katrina
Coastal Impacts of Hurricane Katrina
Hydrologic Impacts of Hurricane Dennis
ATRIS Used to Survey Sea Floor in Dry Tortugas National Park
Research
Using Genetic Modeling to Assess the Health and Status of Manatee Populations
Outreach
USGS Activities Rock the Waquoit Bay Watershed Block Party
Balancing Wildlife Needs and Wetland Restoration in San Francisco Bay
Journalism Interns Help Get the USGS Word Out
Meetings
2005 Meeting of the Digital

discussions about modeling approaches, laboratory knowledge, and how laboratory and modeling studies are linked. Here is a sampling of some of the key themes that emerged from these indepth discussions:

- Confidence in current modeling results is constrained by an incomplete understanding of some key processes and uncertainties regarding appropriate values for model inputs.
- Heterogeneity is rarely adequately modeled (at micro-to-macro spatial scales and short-to-long temporal scales).
- Understanding transport properties is a critical need (especially fluid-flow characteristics, the role of fractures, changing permeability, and so on).
- Despite years of study, the research community still cannot reliably quantify gas-hydrate saturations from seismic data.
- Scaling between millimeter-to-centimeter laboratory sizes (with simple, well-characterized experiments) and hundreds of meter-to-kilometer model results (with large heterogeneity and complexity) remains a major challenge.
- A newly developing research challenge is to understand the biogeochemical processes in sediment associated with gas hydrate (that is, linking physics, biology, and chemistry).

The last half-day of the workshop involved brainstorming and synthesis, in which all participants identified the five highest-priority hydrate-research topics they felt were required to advance laboratory, field, and modeling studies, within the context of understanding the natural gas-hydrate system. The priorities generally followed the major themes summarized above.

Of particular note is that the primary knowledge gap that repeatedly arose was in characterizing transport and transient phenomena in the gas-hydrate system. The nature of this gap shows that, in the 45 years since gas hydrates have been recognized in the natural environment, the study of natural gas hydrates has finally matured from characterizing the simple, static situation (that is, how to identify and characterize gas hydrates in the Earth) to understanding the time-dependent processes that control their formation and dissociation. A better understanding of these transport and transient phenomena will go a long way toward clarifying and refining the role of gas hydrates as a potential future energy resource, as a hazard within the shallow sea floor, and as an agent of climate change.

Library for Earth System Education

Workshop on Integrating Modeling and Laboratory Gas Hydrate Studies

Staff & Center News

Steven Schwarzbach Appointed Director of USGS Western Ecological Research Center

Woods Hole Science Center Hosts Visitor from India

Publications

September Publications List

Related *SOUND WAVES* Stories

USGS and WHOI Investigate Gas-Hydrate Mounds on the Gulf of Mexico Sea Floor
August 2004

Special Sessions on Gas-Hydrate Systems at Fall 2003 AGU Meeting Showcase USGS Work
February 2004

USGS Scientists Discover Gas Hydrate in Southern California During Cruise to Study Offshore Landslides, Earthquake